UNIVERSITÉ DE LORRAINE | BIBLIOTHÈQUES UNIVERSITAIRES

AVERTISSEMENT
DROIT D'AUTEUR

Ce document est le fruit d'un long travail approuvé par le jury de soutenance et mis à disposition de l'ensemble de la communauté universitaire élargie.

Il est soumis à la propriété intellectuelle de l'auteur. Ceci implique une obligation de citation et de référencement lors de l'utilisation de ce document. Toute contrefaçon, plagiat ou reproduction illicite encourt une poursuite pénale.

Contact bibliothèque : ddoc-theses-contact@univ-lorraine.fr
(Cette adresse ne permet pas de contacter les auteurs)

Code de la Propriété Intellectuelle. articles L 122. 4
Code de la Propriété Intellectuelle. articles L 335.2- L 335.10

UNIVERSITÉ DE LORRAINE
34 COURS LÉOPOLD — CS 25233
54052 NANCY CEDEX
TÉL : 03 54 50 54 00
CONTACT@UNIV-LORRAINE.FR
WWW.UNIV-LORRAINE.FR

Université de Lorraine, Collégium Sciences et Technologies
Ecole Doctorale SIRENA – Sciences et Ingénierie des Ressources Naturelles

THESE

Présentée pour l'obtention du grade de
Docteur de l'Université de Lorraine
Mention « Géosciences »

par **Naila MEZOUED**

L'analyse portable, rapide, quantitative et minéralogique dans les roches felsiques à métaux rares : application au leucogranite de Beauvoir

Soutenance publique le 25/06/2025

Membres du jury

Directeurs de thèse:	Mme Cécile Fabre	Professeure HDR, Université de Lorraine
	M. Jean Cauzid	Maître de conférences HDR, Université de Lorraine
Président du jury et rapporteur :	M. Olivier Musset	Professeur, Université de Bourgogne
Rapporteur:	M. Jean-Marc Baele	Professeur, Université de Mons
Examinatarice:	Mme Bijal Chudasama	Senior scientist, Geological Survey of Finland

Faculté des Sciences et Technologies – Campus des Aiguillettes – 54506 Vandoeuvre-lès-Nancy

Résumé

Les méthodes géochimiques sont indispensables à l'exploration des ressources minérales. Cependant, l'acquisition des données géochimiques, à l'aide des méthodes analytiques conventionnelles, est un processus long et coûteux, de moins en moins compatible avec les défis actuels de l'industrie minière. Dans ce contexte, les outils d'analyse spectroscopique portables, dont la technique LIBS, représentent une solution innovante pour l'acquisition rapide de données géochimiques sur le terrain. À travers les travaux présentés dans ce manuscrit, nous explorons le potentiel de l'outil portable LIBS pour acquérir des données quantitatives et minéralogiques sur des échantillons de roche directement sur le site d'exploitation, lors de campagnes d'exploration minières.

Pour l'analyse quantitative, des courbes de calibration ont été développées à l'aide d'analyses LIBS afin de prédire les concentrations d'éléments critiques, Li et Rb, dans des échantillons de carottes brutes, dans le cadre de l'exploration du granite à métaux rares de Beauvoir, un gisement de lithium stratégique pour la France. L'objectif était d'élaborer un protocole analytique adapté aux conditions de terrain, permettant de réduire le délai d'accès aux données géochimiques quantitatives, passant de plusieurs mois à quelques heures. De plus, la capacité de généraliser ces modèles à des gisements similaires mais géographiquement éloignés a été étudiée.

La deuxième partie de cette thèse s'est focalisée sur la capacité à automatiser l'identification minérale, particulièrement lorsque l'identification macroscopique s'avère difficile, en combinant le signal élémentaire LIBS et des méthodes d'apprentissage automatique (ANN, SVM, Random Forest, PLS-DA et LDA). Cela a impliqué l'acquisition et l'organisation d'une base de données spectrale de référence, l'identification des signatures spectrales caractéristiques de chaque phase minérale représentée, ainsi que l'évaluation des différents modèles de classification testés. Une fois entrainés, ces modèles permettent de déterminer la composition minéralogique d'un échantillon et de quantifier l'abondance relative de chaque phase identifiée.

Bien qu'ils ne remplacent pas les techniques de laboratoire, les outils d'analyse spectroscopique portables, dont la LIBS, apportent une nouvelle dimension à l'exploration géochimique sur le terrain en facilitant la caractérisation des objets géologiques étudiés, ce qui permet d'argumenter la prise de décision stratégique lors de missions de terrain, qu'elles soient à visée économique ou scientifique.

Abstract

Geochemical exploration is widely used for ore exploration. However, conventional methods to acquire geochemical data, based on sampling, transport, and laboratory analytical techniques, are resource-intensive and time-consuming. These limitations are increasingly incompatible with the current demands of the mining industry, which faces the challenge of exploring deeper and less accessible regions. Consequently, there is a need for faster, more efficient, and automated exploration strategies to improve resource management and operational efficiency during field operations. Portable spectroscopic techniques, including handheld LIBS, represent innovative solutions to acquire rapid, on-site, geochemical data. This study investigates the potential of handheld LIBS to provide reliable quantitative and mineralogical data to facilitate rock sample characterization during mining operations.

Handheld LIBS was applied to predict critical element, Li and Rb, concentrations in unprepared core samples from the Beauvoir rare-metal granite, a lithium deposit of regional significance. The analytical protocol was designed for field conditions, reducing the time required to obtain ore values from months to hours. The methodology, including sample selection, spectral parameter optimization, and statistical model evaluation, is outlined. Additionally, the ability to transfer the LIBS models developed to similar geological settings is assessed, as it represents a critical factor for the wider adoption of handheld LIBS in the mining sector.

In the second part of this thesis, we explore the application of handheld LIBS for automated mineral identification by processing LIBS data using machine learning algorithms. This involves building a LIBS database of mineral samples, identifying spectral signatures, and determining key spectral parameters to train the algorithms selected in classifying LIBS spectra in different mineral classes. Once trained, the models can determine the mineral composition of a rock sample and quantify the relative abundance of each phase. Handheld LIBS offers a new dimension to field operations by providing real-time geochemical data, facilitating the assessment of geological samples to support informed decision-making during field investigations, for both economic and scientific applications.

Remerciement

Nous arrivons à la fin de ce périple de 3 ans qu'a été cette thèse. Ces années m'ont parfois semblé s'étirer à l'infini, tandis qu'à d'autres moments, elles ont filé à la vitesse de la lumière. À cette occasion, je tiens à remercier toutes les personnes qui, de près ou de loin, ont contribué à la réalisation de ce projet.

Il me tient à cœur de remercier mes directeurs de thèse, Cécile Fabre et Jean Cauzid, sans qui ce travail n'aurait jamais vu le jour. Ils m'ont transmis le goût de la recherche dès mon stage de Master II, et accepter cette thèse était avant tout une opportunité de continuer à travailler avec eux. Je leur suis profondément reconnaissante pour le temps et l'énergie qu'ils m'ont consacrés. Je garde en mémoire nos discussions, jamais très sérieuses mais toujours drôles. Merci pour votre patience infinie, du début à la fin, et plus que tout, pour votre bienveillance, car vous n'avez jamais fait passer cette thèse avant mon bien-être.

Je tiens à remercier chaleureusement les membres du jury d'avoir accepté, malgré leurs emplois du temps chargés, d'évaluer ce travail : Bijal Chudasama, Jean-Marc Baele, et Olivier Musset. Je souhaite également exprimer ma gratitude aux membres de mon comité de suivi, Ludovic Duponchel et Yan Foucaud, pour leurs retours précieux qui ont contribué à l'amélioration de ce travail. I would also like to sincerely thank Bijal Chudasama and Johanna Torppa, who welcomed me with open arms in Finland and made me feel right at home. I'll always remember our daily coffee breaks and that amazing trip to the little island in the middle of a Scandinavian lake. Meeting you has truly been one of the most beautiful experiences of this journey.

Je tiens à remercier l'équipe Imerys du projet d'exploitation du granite de Beauvoir, notamment Patrick Fullenwarth, Benjamin Barré, et Alyson Bargain pour leur accueil chaleureux lors de nos missions de terrain et pour tous les échanges enrichissants que nous avons pu avoir, que ce soit à Nancy ou à Beauvoir. Je les remercie également pour nous avoir toujours facilité l'accès aux échantillons et aux données. Leur disponibilité et leur réactivité, répondant à nos questions et apportant leurs retours, ont été particulièrement précieuses.

Je souhaite remercier l'ensemble du personnel du laboratoire GeoRessources, pour leur accompagnement et leur disponibilité. Je pense notamment à Michel Cathelineau, Steven Zia Kahou, Christophe Ballouard, Marie-Camille Caumon, Julien Mercadie, et Anne-Sylvie Andre-Mayer. Je remercie Odile Barès, qui m'a généreusement permis de m'installer dans la salle infrarouge aussi souvent que

nécessaire. Enfin, je tiens à exprimer ma gratitude à toutes les personnes qui font fonctionner GeoRessources au quotidien et qui nous ont permis de travailler dans d'excellentes conditions.

À ma famille, loin des yeux mais toujours près du cœur. À mes grands-parents, Louisa et Kader, qui ne comprennent pas toujours ce que je fais mais qui sont tellement fiers de moi. À ma mère, mon père, et mes deux frères, que j'appelle pour un rien, car leur parler me fait me sentir à la maison, peu importe où je me trouve. À mon chat Bouboula, qui n'a absolument rien fait mais qui mérite d'avoir son nom dans ma thèse.

Si cette page de ma vie se tourne, j'espère que les liens tissés durant ces années perdureront. À Océane et Baptiste, mes collègues de bureau (à mi-temps ?), qui m'ont supportée alors que je me plaignais de la météo, de Nancy, de ma thèse et de bien d'autres choses. Je repense à cette première journée de thèse, je revois Océane s'installer dans son bureau, puis toutes nos soirées improvisées, nos fous rires, nos galères. Je repars de cette expérience avec un diplôme de docteur et une amie pour la vie. A Caroline avec qui j'ai partagé l'un des plus beaux voyages de ma vie et Marjolaine pour nos séances potins. Merci à Saïd, Alix, Célestine, Quentin, Yonghwi, Bastien, et à tous ceux que j'ai côtoyé durant ces années, pour tout ce que nous avons partagé : nos voyages, nos rires, nos discussions et nos galères.

À mes amis, Jouda, Sara et Alaa, pour nos sorties mémorables, nos ateliers de cuisine animés et nos longues discussions qui ont si souvent apaisé mon mal du pays. Nancy nous a réunis et j'espère qu'aucune distance ne pourra nous éloigner. Issaadi, merci d'avoir été là, avant et pendant la thèse, pour toutes les fois où je n'ai cessé de me plaindre. Merci de m'avoir encouragée, aidée et soutenue.

Résumé élargi

L'acquisition des données géochimiques durant une campagne d'exploration minière implique la collecte des échantillons sur le terrain, leur transport et enfin leur analyse dans des laboratoires spécialisés. Un processus, souvent, long et coûteux qui devient de moins en moins compatible avec les défis actuels de l'industrie minière. La nécessité d'explorer des régions plus reculées et moins accessibles rend l'évolution des stratégies d'exploration géochimique essentielle pour optimiser la gestion des ressources déployées et augmenter l'efficacité opérationnelle durant les missions de terrain. Les outils d'analyse spectroscopique portables (XRF, VNIR-SWIR, RAMAN), et en particulier l'outil d'analyse portable LIBS, représentent une solution rapide et innovante pour l'acquisition *in situ* de données géochimiques. Dans ce contexte, nous explorons le potentiel de la LIBS portable pour caractériser les échantillons géologiques, en fournissant des valeurs quantitatives et des informations minéralogiques, pour faciliter la prise de décision rapide et adaptée lors de campagnes d'exploration de gisements miniers. Cette thèse répond à deux problématiques principales:

- Comment quantifier de manière fiable des éléments chimiques d'intérêt économique dans des échantillons de carottes non traitées, directement sur le site d'exploitation d'un gisement minier, à l'aide de l'outil portable LIBS ?
- Comment identifier la composition minéralogique d'échantillons rocheux, et déterminer l'abondance relative de chaque phase, à partir d'analyses élémentaires acquises à l'aide de l'outil portable LIBS ?

Pour l'analyse quantitative, la LIBS portable a été appliquée pour prédire les concentrations du Li et Rb dans des échantillons de carottes brutes extraites lors de l'exploration du granite à métaux rares de Beauvoir, un gisement de lithium situé dans le nord du Massif Central, d'importance stratégique pour la France. Le protocole analytique développé, adapté aux contraintes rencontrées sur le terrain, permet de réduire le temps nécessaire pour accéder à des données géochimiques quantitatives sur les éléments ciblés, de plusieurs mois à seulement quelques heures. Les étapes successives mises en place pour le développement des modèles quantitatifs sont décrites, dont la sélection d'échantillons de référence représentatifs du gisement, l'optimisation des paramètres spectraux et l'utilisation d'approches statistiques pour déterminer le modèle le plus approprié pour chaque élément. De plus, nous évaluons la capacité de ces modèles, développés dans le contexte du granite de Beauvoir, à être transférés à des gisements similaires mais géographiquement éloignées. Comprendre dans quelle mesure des modèles LIBS préétablis peuvent être généralisés à un type de

gisement particuliers, est un point clé pour augmenter l'attractivité de la technique LIBS portable dans le secteur minier.

La deuxième partie de cette thèse est axée sur la reconnaissance automatique des minéraux à l'aide de l'outil portable LIBS, associé à des algorithmes d'apprentissage automatique. Pour cela, une base de données spectrale a été constituée, regroupant des spectres LIBS de référence de minéraux afin d'identifier les signatures spectrales caractéristiques de chaque phase. Ces données ont été utilisées pour entraîner divers modèles d'apprentissage automatique (ANN, SVM, Random Forest, PLS-DA et LDA), visant à classer des spectres LIBS en différentes classes minérales. Les outils d'analyse spectroscopique portables, et en particulier la technique LIBS, apportent une nouvelle dimension dans l'exploration géochimique en offrant un accès immédiat à des données quantitatives et minéralogiques sur des échantillons bruts, directement sur le site d'exploitation, et ce, dans des délais considérablement réduits. Bien que ces outils ne viennent pas encore remplacer les méthodes conventionnelles, ils contribuent de manière significative à une meilleure compréhension des objets géologiques étudiés, facilitant ainsi la prise de décisions stratégiques lors des campagnes d'exploration géologique, qu'elles soient menées dans un objectif économique ou scientifique.

Les méthodologies développées sont détaillées dans sept chapitres principaux. Les sections supplémentaires correspondent à l'introduction, la discussion générale, et la conclusion.

Chapitre (I) La technique d'analyse spectroscopique portable LIBS. Le Chapitre I synthétise les connaissances existantes sur la principale technique analytique sur laquelle repose ce travail de thèse : la LIBS portable. Il présente son évolution technologique, ses capacités analytiques et les diverses applications en géosciences explorées au cours de ces dernières années.

La technique a évolué, des premiers systèmes mobiles des années 1990, pesant plus de 13 kg, aux analyseurs compacts et portables commercialisés actuellement, d'un poids compris entre 2 et 3 kg et dotés d'une plage spectrale étendue (UV-NIR). L'analyseur utilisé dans cette thèse est le modèle Z-300 (SciAps), qui propose deux modes opératoires : Element Pro pour les analyses ponctuelles, et Geochem Pro pour la cartographie élémentaire. L'évolution des modèles récents de LIBS portables semble indiquer qu'un plateau est atteint en termes de miniaturisation. Les développements récents concernant la technique et notamment son application aux géosciences se concentrent désormais sur le traitement des données pour décrypter la géochimie des objets étudiés au-delà des informations purement élémentaires. C'est d'ailleurs l'un des aspects traités dans la deuxième partie de cette thèse (chapitres V - VI - VII), qui retrace le traitement des données élémentaires LIBS par des algorithmes

d'apprentissage automatique pour traduire les spectres élémentaires obtenus sur des roches en données minéralogiques.

La capacité de la LIBS à détecter le lithium, élément léger inaccessible à d'autres techniques d'analyse spectroscopique portables, constitue également un avantage décisif dans le contexte de l'utilisation de la LIBS pour l'exploration minière. Environ 50 % des études quantitatives LIBS en géosciences recensées dans ce chapitre portent sur le lithium, principalement sur poudres et pastilles ; les études sur carottes brutes, davantage représentatives des contraintes opérationnelles réelles des campagnes d'exploration minière, restent minoritaires dans la littérature. Le chapitre identifie deux principaux obstacles à la démocratisation de la méthode dans le secteur minier : d'une part, des modèles souvent élaborés à partir d'échantillons fortement transformés, et d'autre part, la nécessité de développer des modèles de calibration quantitative individuelles pour chaque gisement ciblé, ce qui remet en question l'avantage fondamental des dispositifs de terrain, conçus pour être rapides et pratiques. En réponse, cette thèse explore deux approches complémentaires : le développement de modèles quantitatifs pour l'analyse de carottes dans le cadre de l'exploration du granite de Beauvoir (chapitre III) et l'évaluation de leur transférabilité à des gisements géographiquement éloignés mais de composition similaire (chapitre IV).

Chapitre (II) Le granite à métaux rares de Beauvoir. Le chapitre II présente le contexte géologique du granite de Beauvoir, site d'exploration minière sélectionné comme cas d'étude pour cette thèse. Le granite de Beauvoir est un pluton leucogranitique peralumineux ultra différencié, situé à 70 km au nord-nord-ouest de Clermont-Ferrand, au sein du complexe magmatique d'Échassières. Associé au magmatisme tardi- à post-collisionnel varisque, il constitue l'un des sites clés pour l'étude des granites à métaux rares en Europe.

Le gisement est enrichi en lithium, étain, niobium, tantale et béryllium, ces éléments critiques étant incorporés dans des phases minérales spécifiques : la lépidolite, principal minéral porteur de lithium, tandis que la cassitérite, le columbite et la tantalite concentrent respectivement l'étain, le niobium et le tantale. Cette concentration exceptionnelle en métaux stratégiques en fait une cible minière de premier intérêt. Le projet EMILI (Exploitation du Lithium Mica par Imerys), lancé en 2021, a conduit une campagne de forage multiphases jusqu'à 2024. Les analyses géochimiques ont confirmé des ressources en lithium significatives, avec une concentration moyenne en oxyde de lithium (Li_2O) de 0,9 %, l'une des plus élevées rapportées pour les gisements de lithium à base de mica en Europe. Le programme cible particulièrement le faciès B1, l'unité magmatique superficielle du granite qui s'organise en trois niveaux successifs (B1, B2, et B3), dont la composition minéralogique est dominée par les micas lithinifères (lépidolite), l'albite et le quartz, dans une texture hololeucocrate, équigranulaire non

orientée. La distribution du lithium est hétérogène : les concentrations varient de moins de 1 000 à plus de 7 000 ppm, avec les valeurs les plus faibles dans les zones altérées des premiers mètres (kaolin).

L'analyse approfondie de données issues de 28 forages, révèle que l'altération hydrothermale, kaolinisation dans les 100 premiers mètres et greisenisation plus uniformément répartie en profondeur, affecte significativement le gisement. Sur la base d'indicateur géochimique, 63 % des forages présentent moins de 25 % d'intervalles greisenisés, 27 % un degré d'altération modéré, et 10 % des sections fortement greisenisées. Ces caractéristiques (variabilité géochimique, hétérogénéité texturale et altération hydrothermale) a conditionné directement les stratégies méthodologiques développées dans les chapitres suivants.

Chapitre (III) L'analyse quantitative du lithium et du rubidium à l'aide de l'outil portable LIBS. Le chapitre III constitue le cœur méthodologique de l'axe quantitatif de la thèse, publié dans le Journal of Geochemical Exploration (Mezoued et al., 2025). Il présente le protocole analytique développé pour prédire in situ les concentrations de lithium et de rubidium dans des sections de carottes brutes sans préparation préalable, sur le site d'exploitation du granite de Beauvoir. L'objectif central est de réduire le délai d'accès aux données géochimiques quantitatives, passant de plusieurs mois à quelques heures, afin de faciliter la prise de décision lors de l'exploration ou l'exploitation du gisement, tout en respectant les contraintes opérationnelles d'un site minier.

L'analyse quantitative LIBS sur des matériaux rocheux bruts implique une contrainte fondamentale : représenter une composition de roche totale, alors que le cratère d'ablation laser, d'une taille moyenne de 50 µm, signifie que chaque point d'analyse correspond davantage à un minéral individuel qu'à une composition de roche totale. La stratégie développée consiste à maximiser la zone d'analyse en acquérant un grand nombre de points le long d'un profil vertical couvrant la longueur totale des échantillons de carottes — entre 200 et 400 points par section de 2 à 4 mètres. Chaque point correspond à 36 zones organisées en grille (6×6), avec 4 tirs laser moyennés par zone et un tir de nettoyage initial. Onze échantillons manuels et quatre segments de carottes ont constitué les données d'entraînement, les concentrations en Li couvrant un intervalle de 120 à 9360 ppm, soit l'intervalle de concentration observé dans le gisement.

Douze modèles quantitatifs pour le lithium et neuf pour le rubidium ont été construits en variant trois facteurs : le prétraitement spectral (spectres bruts, normalisation SNV, normalisation à l'aire totale), les paramètres univariés (signal d'une raie d'émission, somme ou rapport de signaux) et les approches multivariées par régression PLS sur intervalles spectraux (iPLS). Ces dernières intègrent les signaux du silicium (288,05 nm), aluminium (309,15 nm),

potassium (766,33 nm), sodium (589,14 nm), césium (852,20 nm), manganèse (259,25 nm) et béryllium (312,98 nm) comme variables matricielles. La sélection du modèle optimal s'est basée sur la comparaison statistique de deux paramètres (Biais et Erreur Standard de Prédiction, Duponchel et al., 2023), appliqué à un jeu de données test indépendant. La reproductibilité des prédictions a été confirmée par un test de Student apparié (p-values > 0,05). La réduction de la proportion des données LIBS utilisées pour calculer le signal moyen jusqu'à 10 % des données initiales ne produit pas de différence statistiquement significative sur la MAE, en raison de la texture équigranulaire isotrope du faciès B1. Ces résultats confirment la possibilité d'acquérir un signal représentatif en ne couvrant que 1,8 % de la surface totale de la carotte.

Plusieurs sources de biais ont été identifiées durant la phase test sur des échantillons non impliqués dans la conception des modèles. Les anomalies texturales, telles que les veines de quartz diagonales observées dans certains échantillons, affectent localement le ratio Si/Al utilisé dans le modèle lithium et peuvent engendrer des surestimations. Les variations géochimiques verticales documentées le long du forage GPF (diminution de rubidium, césium et aluminium du toit à la base, augmentation de silicium) constituent une limite à la généralisation des modèles quantitatifs impliquant le signal d'autres éléments chimiques au-delà du faciès B1. Si les valeurs prédites demeurent dans les marges d'erreur acceptables pour guider la prise de décision sur le terrain, La technique LIBS portable est donc explicitement positionnée en tant qu'outil complémentaire aux méthodes d'analyse conventionnelles en laboratoire, sans prétendre s'y substituer

Chapitre (IV) Généralisation de modèles de LIBS pour l'analyse quantitative. Le chapitre IV aborde l'une des problématiques clés pour la démocratisation de l'utilisation de la LIBS portable dans le secteur minier : dans quelle mesure un modèle de calibration développé pour un gisement spécifique, en l'occurrence le granite de Beauvoir, peut-il être généralisé à des échantillons rocheux de composition similaire, mais provenant de sites géographiques différents ? Cette étude constitue la première évaluation systématique de la transférabilité inter-dépôts de modèles LIBS quantitatifs dans le contexte des granites à métaux rares.

Le modèle de calibration du lithium, développé pour le granite de Beauvoir (chapitre III), a été appliqué à des échantillons du massif du Blond, un pluton magmatique situé à environ 30 km au nord-ouest de Limoges. Ce massif présente une composition minéralogique dominante (quartz, micas lithinifères et feldspaths) analogue à celle du granite de Beauvoir. Les concentrations en lithium des échantillons du massif du Blond testés (1 205 à 3 870 ppm) correspondent à l'intervalle compositionnel le mieux représenté dans les données d'entraînement du modèle Beauvoir. Les résultats du modèle montrent une corrélation

satisfaisante (R^2 = 0,92), mais révèlent un biais systématique de surestimation (MAE = 1 966 ppm, contre 815 ppm pour Beauvoir). L'analyse de la distribution des erreurs met en évidence une relation marquée avec la texture des échantillons : le faciès microgranulaire (MAE = 870 ppm) performe significativement mieux que le faciès rhyolitique dévitrifié du dyke de Richemont (MAE = 2 697 ppm). Cette différence est attribuée à l'impact des propriétés physiques d'un échantillon sur le signal LIBS : la texture dévitrifiée, résultant d'un refroidissement rapide en surface, moins consolidée que les textures microgrenues équigranulaires et plus sensible à l'altération, ce qui favorise une ablation accrue et des intensités de signal LIBS systématiquement plus élevées à concentration équivalente. Une réduction du nombre de tirs laser par zone, de 4 à 1, réduit le MAE rhyolitique de 52 % (passant de 2 697 à 1 264 ppm). Cependant, cette approche d'ajustement paramétrique présente ses propres limites méthodologiques, qu'il faudrait définir à l'aide d'un plus grand nombre d'échantillons.

Le chapitre établit ainsi que la cohérence texturale entre les échantillons cibles et les échantillons de référence constitue une condition essentielle, mais non unique, à la transférabilité de modèles LIBS quantitatifs. L'intégration de paramètres texturaux comme variables d'entrée dans les modèles de calibration, ainsi que le recours à l'apprentissage automatique pour modéliser les relations non linéaires entre texture, signal et concentration, ont été identifiés comme des voies d'amélioration potentielles.

Chapitre (V) Base de données spectrales LIBS pour différentes phases minérales. Le chapitre V marque la transition de la thèse vers son second axe scientifique : l'identification minéralogique automatisée à l'aide des données spectrales LIBS. La constitution d'une base de données spectrales LIBS, publiée dans la revue Data (Mezoued et al., 2025), a été une étape méthodologique nécessaire avant la mise en œuvre des modèles d'apprentissage automatique. En effet, l'application de ces modèles repose sur l'utilisation de données de référence de haute qualité, représentatives de la diversité géochimique naturelle des phases minérales observées dans les roches étudiées, pour entraîner et paramétrer les algorithmes construits.

La base de données spectrale regroupe l'analyse de 171 échantillons minéraux purs à l'aide de l'analyseur portable LIBS : 127 spécimens cristallins, 25 phénocristaux inclus dans des matrices rocheuses, et 19 pastilles de poudre compressées à une pression de 7 tonnes dans un moule cylindrique de 13 mm de diamètre. L'acquisition suit un protocole constant : quatre points d'analyse moyennés par échantillon, organisés en grilles (3×3, 5×5 ou 6×6 zones), avec au moins deux tirs laser par zone après un tir de nettoyage préliminaire. La distance entre deux zones est maintenue entre 100 et 200 µm pour minimiser l'interférence des plasmas. Le

résultat obtenu correspond à une base de plus de 12 000 spectres LIBS portable de référence couvrant 55 espèces minérales : silicates (albite, béryl, micas, spodumène, vésuvianite), carbonates (dolomite, magnésite, aragonite), phosphates (amblygonite, apatite, topaze), oxydes (hématite, magnétite, rutile, chromite, wolframite), sulfates (baryte, gypse), sulfures (chalcopyrite, pyrite, pyrrhotite), halogénures (fluorite) et éléments natifs (soufre, cuivre). Les micas riches en lithium constituent la classe la plus représentée, avec 2 550 spectres issus de 22 échantillons. Cette base est mise à disposition en libre accès sur la plateforme ORDaR (doi : 10.24396/ORDAR-165, licence CC-BY-NC-SA), sans post-traitement, afin de préserver la compatibilité avec différentes voies d'applications.

Le nombre et la diversité des spectres obtenus ont permis de documenter plusieurs caractéristiques spectrales déterminantes sur les minéraux analysés. La ligne de base varie significativement selon la composition chimique du minéral : les minéraux riches en éléments métalliques (pyrite, chromite, arsénopyrite) présentent un fond élevé dans les domaines UV et visible, attribué à la haute conductivité thermique, qui affecte la densité et la température du plasma ; à l'inverse, les minéraux comme le quartz ou les micas lithinifères affichent une ligne de base plate. L'intensité du signal dépend également de la nature physique de l'échantillon, les poudres présentant des intensités substantiellement supérieures à celles des cristaux, en raison d'un taux d'ablation plus élevé, et du potentiel d'ionisation des éléments : le lithium (~5,39 eV) génère des signaux très intenses, tandis que le silicium (~8,15 eV), pourtant majeur dans de nombreux minéraux, produit des signaux comparativement plus faibles.

Chapitre (VI) Reconnaissance automatique de minéraux à l'aide d'algorithmes d'apprentissage automatique supervisé. Le chapitre VI explore les modèles d'apprentissage automatique supervisé pour automatiser la reconnaissance minéralogique sur des échantillons rocheux bruts provenant du granite de Beauvoir. La problématique spécifique du cas d'étude est la suivante : dans le facies B1 du granite de Beauvoir ciblé pour l'exploitation minière, la lépidolite (principal minéral porteur de lithium) est visuellement difficile à distinguer des phases de la matrice composée principalement d'albite et de quartz, car elle se présente principalement translucide, rendant les estimations de terrain approximatives et incertaines.

Pour automatiser cette tâche et apporter une solution analytique lorsque les critères texturaux altèrent l'identification visuelle, quatre algorithmes de classification ont été comparés pour le traitement des données élémentaires LIBS : l'Analyse Discriminante Linéaire (LDA), les Machines à Vecteurs de Support (SVM), la Forêt Aléatoire (Random Forest) et l'Analyse Discriminante par Moindres Carrés Partiels (PLS-DA). Le jeu d'entraînement représente la composition simplifiée du granite de Beauvoir : albite, lépidolite, quartz, muscovite, topaze, orthose et phosphates (apatite et amblygonite), avec 300 spectres par classe dans la mesure

du possible. Afin de réduire la dimensionnalité des spectres (chaque spectre contenant plus de 24 000 variables), une extraction des raies d'émission de 20 éléments chimiques a été réalisée à partir d'intervalles spectraux précisément définis. Des normalisations SNV et des réductions dimensionnelles supplémentaires par ACP et régression PLS ont été testées en combinaison, générant au total 14 itérations de modèles entrainés.

L'application aux échantillons de granite a porté sur quatre dalles rectangulaires (12 × 5 × 0,5 cm) issues du forage EMILI (C42, C52, C112, C117), analysées à 10 localisations par dalle en grilles de 90 points espacés de 30 µm, soit 900 spectres par échantillon acquis en 20 minutes. Les prédictions minéralogiques ont été comparées à des valeurs de référence obtenues par cartographie µXRF et analyse pétrographique.

Sur le jeu de test issu des minéraux purs, tous les modèles atteignent des métriques supérieures à 0,8. Le SVM obtient la précision la plus élevée (0,99), tandis que la Forêt Aléatoire affiche les performances les plus faibles (0,81). Les jeux SNV améliorent légèrement les résultats pour LDA, SVM et PLS-DA. Appliqués au granite, les résultats se dégradent sensiblement. Pour la classification multi-classes, le PLS-DA avec normalisation SNV est le plus performant (MAE = 9,2 %), devant SVM (12,2 %), Random Forest (17,0 %) et LDA (18,8 %). Pour la lépidolite spécifiquement, le SVM est le plus précis (MAE = 11,7 %), devant PLS-DA (14,7 %), Random Forest (15,4 %) et LDA (28,6 %).

Plusieurs sources d'erreur systématique ont été identifiées. Le quartz est majoritairement sous-estimé, car les mesures LIBS réalisées sur le granite captent des spectres mixtes intégrant le signal des minéraux riches en lithium adjacents, orientant la classification vers la lépidolite. Le degré d'altération influence fortement les performances : l'échantillon de granite sain C52 (indice F'(K-Na) = −150,5) présente les erreurs les plus faibles, tandis que l'échantillon le plus greisénisé, C117 (F' = +121,5), génère des erreurs atteignant 60 % pour certaines classes. Cette corrélation entre altération et erreur souligne l'importance de prendre en compte les effets de matrice physique dans toute stratégie de classification impliquant des données LIBS.

Chapitre (VII) Reconnaissance automatique de minéraux à l'aide d'algorithmes d'apprentissage automatique non supervisé. Le chapitre VII explore l'identification minéralogique automatisée à travers des modèles de type réseau de neurones artificiels (ANN), sélectionnés pour leur capacité à capturer des relations non linéaires dans les données à haute dimensionnalité.

Douze modèles ANN ont été évalués en variant différents paramètres structuraux : la fonction d'activation (tangente hyperbolique TanH ou linéaire Lin), le nombre de couches internes (une ou deux) et le nombre de neurones par couche (30, 60 ou 100). Six jeux de données de

référence, issus de la base de données spectrale LIBS de minéraux purs (chapitre VI), ont été utilisés en données d'entrée. Lors de la phase de test, les modèles ont ensuite été évalués systématiquement sur des échantillons de granite sain pour identifier la configuration la plus adaptée au contexte d'application du granite de Beauvoir. Il ressort qu'aucune tendance claire n'émerge concernant l'influence de la fonction d'activation ou du nombre de couches total. Le modèle 1 (TanH, une couche, 30 neurones, données brutes) obtient les meilleures performances globales : erreur absolue de 3,08 % pour la lépidolite et 7,72 % pour la classification multi-classes comprenant les autres phases minérales de la matrice. Plusieurs modèles atteignent une erreur de 0,42 % pour la lépidolite seule, au prix d'une dégradation importante pour la classification multi-classes (17–21 %). Ce résultat illustre la nécessité de prendre en considération l'objectif opérationnel lors du développement de ce type de modèles. Les données brutes et les données optimisées par ACP constituent les meilleures méthodes de prétraitement, tandis que la normalisation SNV dégrade les performances des différents modèles. Les variations du taux d'apprentissage n'ont pas eu d'effet significatif sur la précision finale. Sur les échantillons de validation, le modèle 1 atteint une MAE de 9,14 % pour la lépidolite et une MAE moyenne de 11,20 % pour la classification multi-classes. Le modèle 2, optimisé pour la lépidolite, réduit l'erreur sur cette phase à 6,28 %, soit une réduction de 30 % par rapport au modèle 1. Ces performances, comparées aux taux d'erreur obtenus par identification visuelle, surpassent significativement cette dernière, dont les erreurs typiques s'échelonnent entre 10 et 24 % sur des carottes brutes pour les échantillons de granite de Beauvoir. Le quartz demeure la classe la plus difficile à prédire, avec des erreurs dépassant 50 % pour des échantillons comportant des veines.

Ce chapitre conclut que même une architecture d'ANN relativement simple, une seule couche interne, permet tout à fait de décrypter des données LIBS non labélisé en information minéralogique pertinentes avec une précision supérieure à l'évaluation visuelle, lorsque cette dernière fait face à des difficultés liées à des critères texturaux.

Table of Content

Résumé i
Abstract ii
Remercîment iii
Résumé élargi v
Introduction 1
1.General context 1
3.Organization of the thesis 2
References 5
Chapter I. The handheld LIBS technique 6
Introduction 6
1.Handheld LIBS development and current market 6
2.Handheld LIBS analyzer 7
3.Application in geology 10
3.1.Quantitative analysis 10
3.2.Discriminant analysis 12
4.Discussion and conclusion 14
References 16
Chapter II. Case study: The Beauvoir granite 20
Introduction 20
1.Historical context 20
2.Geological context 21
3.Lithium exploration 23
4.Geochemistry 23
4.1.Mineral composition 23
4.2.Geochemical composition (EMILI data) 25
Conclusion 26
Facies nomenclature 30
References 30

Chapter III. Handheld LIBS contribution to quantify critical elements during mining operations: The Beauvoir granite case study 34
Introduction 34
1.Background 35
2.Case study 36
2.1.Geological setting 36
2.2.Geochemistry 36
3.Methodology 37
3.1.Sample description 37
3.2.Handheld LIBS analysis 37
3.3.Signal acquisition 37
3.4.Quantitative models 37
4.Results 39
4.1.Element detection 39
4.2.Quantification models 40
4.3.Statistical comparison 40
4.4.Reproducibility 43
4.5.Acquisition time 44
5.Discussion 44
Conclusion 47
References 48
Supplementary data 51
Chapter IV. Quantitative Analysis Using Handheld LIBS: Assessing Model Transferability Across Similar Deposits 59
Introduction 60
2.Methodlogy 60
2.1.Handheld LIBS 60
2.2.Data acquisition 61
2.3.Qauntitative model 61
2.4.Sample 63
3.Results and discussion 65
Conclusion 73
References 74
Supplementary data 77
Chapter V. Analysis of Minerals Using Handheld Laser-Induced Breakdown Spectroscopy Technology 79

1.Summary …….. 79
2.Data description …… 81
2.1.Spectra files ……. 81

2.2.LIBS signal …… 82
2.3.Element detection …….. 82
3.Methods …… 84
3.1.Samples …….. 84
3.2.LIBS technique …… 84
3.3.LIBS analyzer …….. 84
3.4.Data acquisition …… 85
3.5.Spectra visualization ……. 85
References …… 86
Chapter VI. Automated Mineral Recognition combining LIBS Spectra and Machine Learning: Assessing Ore Mineral Abundance in the Beauvoir granite 89
Introduction …… 90
1.Methodology …….. 91
1.1.Samples ……. 91
1.2.Handheld LIBS …… 92
1.3.Data acquisition …… 92
1.4.Tarining data ……. 94
1.5.Workflow ……. 97
2.Results …….. 100
2.1.Principal component analysis (PCA) ……. 100
2.2.Partial least square (PLS) …… 100
2.3.Machine learning models ……. 101
2.4.Beauvoir granite application …… 104
3.Discussion …….. 109
Conclusion …… 112
References …… 114
Supplementary data …… 120
Chapter VII. Artificial neural network for handheld LIBS data processing: application to automated mineral identification in granite samples …….. 125
Introduction …… 126
1.Methodlogy …….. 127
1.1.Neural network …….. 127

1.2.Handheld LIBS …… 127
1.3.Beauvoir data …… 128
1.4.Training data …… 129
1.5.Preprocessing ……. 129
2.Results ……... 130
2.1.2.ANN models …….. 130
2.2. Beauvoir granite application ……. 132
Conclusion …… 137
References …… 138
General discussion …… 142
Conclusion and perspectives …….. 144
1.Conclusion ……. 144
2.Perspectives …….. 146
References ……... 147
List of figures ……. 148
List of tables ……. 155
Appendix ……. 156

Introduction

1 General context

Geochemistry plays a key role in ore exploitation (5,6). Historically, mineral deposits were discovered through visual observations of surface clues (e.g., outcrops, specific minerals), traditional techniques (e.g., panning), and indigenous knowledge. However, the emergence of geochemical exploration in the 20th century, along with advancements in analytical methods (e.g., ICP-MS, XRF, etc.), enabled the detection of chemical signatures in soils, sediments, and rock outcrops, for more deliberate and systematic ore prospecting. Today geochemical exploration, combined with complementary methods, dominates the mining industry with approximately 70% of new mineral deposit discoveries (7)

Accessing geochemical data in geology has always been a matter of time and resources. Conventionally, following field observations, samples considered relevant to the specific research problem are collected, transported, and analyzed using various analytical techniques in specialized laboratories. This process is often time-consuming and resource-intensive. During drilling campaigns, the large volumes of samples analyzed and the economic constraints of such projects often result in significant delays, ranging from weeks to several months, between the drilling phase and the receipt of chemical analysis results. These delays pose challenges, as geochemical data is critical for modeling ore distribution and planning extraction. Extended timelines increase both operational costs and decision-making uncertainty. Meanwhile, the mining companies face new challenges, including the decreasing number of large surface deposits leading to target deeper formations (8), and inaccessible locations (9), the industry has developed new expectations for geochemical exploration strategies, prioritizing faster, efficient, and automated solutions to optimize resources management during field-operations (10,11). In this context, this thesis aligns with previous research projects at the Georessources Laboratory (University of Lorraine, France), which were focused on developing rapid, in situ methods for onsite geochemical data acquisition on geological samples using portable spectroscopic analysis devices (12–14).

The emergence of portable analytical instruments revolutionized geochemical data acquisition during field exploration, effectively transposing laboratory capabilities to the sample location. By enabling real-time data collection, these devices overcome the logistical constraints due to samples enhancing operational efficiency. Portable spectroscopic devices determine the chemical composition of a sample by examining how it interacts with light. The acquired signal can be used to generate qualitative, quantitative, and mineralogical information. The devices are specifically designed to address the challenges of fieldwork, with a focus on: i) Enhancing robustness and stability to withstand shocks and uncontrolled environmental conditions; ii)

Simplifying operational protocols, enabling operation by non-experts in spectroscopic techniques; iii) Integrating preprocessing features to provide immediate analytical results, such as element concentration estimates (XRF) or elemental abundance measurements (LIBS); iv) Developing software to simplify data visualization and interpretation.

In this thesis, handheld Laser-Induced Breakdown Spectroscopy (LIBS) was applied as a solution to provide reliable predictions of critical element concentrations in unprepared core samples during the exploration of the Beauvoir granite rare-metal deposit. The objective was to develop an analytical protocol suited for field conditions, while also evaluating the limitations of these models for broader applications in similar geological contexts. While the use of quantitative LIBS is expanding, many existing studies are predominantly designed for laboratory settings, emphasizing the importance of adapting the methodology for in situ applications. This study contributes to bridge the gap between quantitative LIBS analysis and the practical needs of field operations. While the application of quantitative LIBS continues to expand, most existing studies are primarily conducted under controlled laboratory conditions, highlighting the need to adapt methodologies for in situ applications. In this context, the present study advances the integration of quantitative LIBS analysis with the practical demands of field operations.

Additionally, machine learning algorithms, including Artificial Neural Networks (ANN), Support Vector Machines (SVM), Random Forests (RF), Partial Least Squares Discriminant Analysis (PLS-DA), and Linear Discriminant Analysis (LDA), were trained using reference mineral spectra to automate mineral identification in rock samples. Due to its wide spectral coverage, the handheld LIBS analyzer generates spectra that accurately reflect the detailed chemical composition of minerals, encompassing both major and trace elements. These chemical signatures were used as input variables for the classification models, allowing LIBS spectra to be systematically assigned to specific mineral classes and thus enabling the mineralogical composition of rock samples to be inferred. This strategy is intended to support preliminary mineralogical characterization, particularly the identification of ore phases and their relative abundances, during drill core logging operations, especially when visual identification is limited or ambiguous

Handheld spectroscopic devices, specifically LIBS, have the potential to significantly transform the way geologists conduct field operations. A deeper understanding of the targeted geological object allows for more informed and adaptive decision-making.

2 Organization of the Thesis

This manuscript is organized to address two primary questions:

- How can onsite quantitative analyses acquired on unprepared rock samples be sufficiently reliable to support strategic decision-making during ore exploration?
- How to automate mineral identification in geological samples by combining LIBS spectral data with machine learning techniques?

To address these questions, the methodologies developed are detailed in seven main chapters, complemented by additional sections that provide contextual background, a general discussion, and a conclusion (**Fig.1**).

Chapter (I) Laser-induced breakdown spectroscopy (LIBS). Focuses on the handheld technique, history, current market, and applications in geological settings for quantitative, and mineralogical challenges, to contextualize and highlight key methodological gaps addressed in this thesis.

Chapter (II) The Beauvoir granite. Introduces the case study: the Beauvoir deposit, a rare metal granite in France. The site is characterized by high concentrations of rare metals (Li, Rb, Cs, Nb, Ta, Sn) and is currently being explored for lithium extraction. This chapter covers the preliminary analysis of the geochemical database, obtained through the extensive drilling campaigns EMILI, aimed at understanding the chemical characteristics of the targeted lithology for lithium extraction. This analysis represents a critical step in selecting representative reference samples and developing LIBS models to characterize the targeted samples effectively.

Chapter (III) The quantitative analysis of Li, and Rb using handheld LIBS. Outlines the analytical protocol developed for on-site quantitative analyses of Li and Rb in unprepared drill core sections during the Beauvoir granite exploration. The chapter describes the successive steps implemented, including the selection of representative reference samples, the "try and test" approach adopted to establish quantification models, the statistical protocol used to select the optimal option for ensuring reliable and consistent predictions, and finally, an optimization section designed to repond to the needs and feedback of the company.

Chapter (IV) Transferability of LIBS quantitative models. Investigates the ability to transfer LIBS quantitative models initially developed within the context of the Beauvoir granite, to similar deposits in different locations. The LIBS technique is highly sensitive to physical and chemical matrix effects, often requiring unique and individualized calibration curves for each targeted deposit which challenges the broader application of the technique in the mining sector.

Chapter (V) LIBS spectral database of minerals. Presents the LIBS spectral data acquired on mineral samples throughout this research project, along with data from additional

collaborative efforts. This chapter outlines the data acquisition process, details the samples analyzed, and describes the data processing techniques used to establish a spectral database containing over 12,000 reference spectra for 56 mineral species using 176 reference samples. This work constituted a critical preliminary step, to gather reliable input data for training the machine learning models for automated mineral recognition using handheld LIBS.

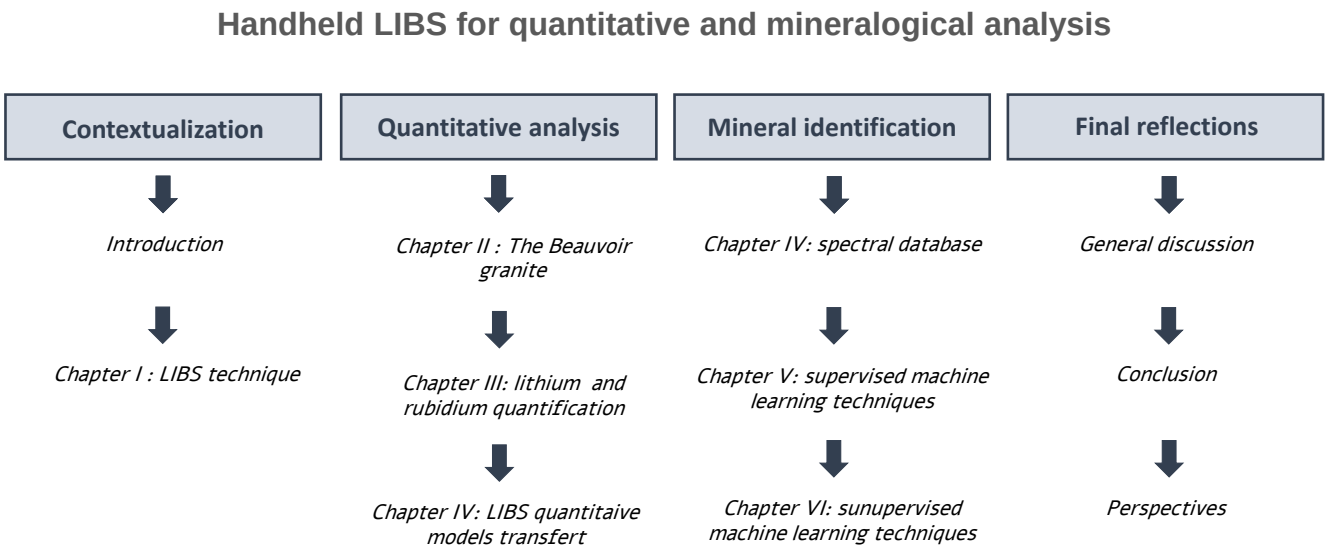

Figure.1. Organization of the Ph.D. thesis.

Chapter (VI) Automated mineral identification using machine learning methods part I. Presents the results of the machine learning algorithms including Partial Least Squares Discriminant Analysis (PLS-DA), Self-Organizing Maps (SOM), and Linear Discriminant Analysis (LDA) developed to automate mineral identification in the Beauvoir granite samples.

Chapter (VII) Automated mineral identification using machine learning methods part II. Presents the results of Artificial Neural Networks (ANN), trained to match unknown LIBS spectra with specific mineral groups, to determine the mineral composition of rock samples using elemental LIBS analysis.

References

1. Gohau G. A History of Geology. Rutgers University Press; 1990. 284 p.

2. Gohau G. Les Sciences de la Terre. Albin Michel; 1990. 420 p.

3. Manten AA. Historical foundations of chemical geology and geochemistry. Chemical Geology. 1966 Jan 1;1:5–31.

4. Govett GJS. Rock Geochemistry in Mineral Exploration. Elsevier; 2013. 474 p.

5. Govett GJS. Chapter 11 - The Development of Geochemical Exploration Methods and Techniques. In: Govett GJS, Govett MH, editors. Developments in Economic Geology [Internet]. Elsevier; 1976 [cited 2025 Jan 16]. p. 343–76. (World Mineral Supplies; vol. 3). Available from: https://www.sciencedirect.com/science/article/pii/B9780444425775500186

6. Zuo R, Wang J, Xiong Y, Wang Z. The processing methods of geochemical exploration data: past, present, and future. Applied Geochemistry. 2021 Sep 1;132:105072.

7. Haldar SK. Chapter 5 - Exploration Geochemistry. In: Haldar SK, editor. Mineral Exploration (Second Edition) [Internet]. Elsevier; 2018 [cited 2025 Apr 25]. p. 85–101. Available from: https://www.sciencedirect.com/science/article/pii/B9780128140222000058

8. Ghorbani Y, Nwaila GT, Zhang SE, Bourdeau JE, Cánovas M, Arzua J, et al. Moving towards deep underground mineral resources: Drivers, challenges and potential solutions. Resources Policy. 2023 Jan 1;80:103222.

9. Scott SD. Deep Ocean Mining. Geoscience Canada [Internet]. 2001 Jun 6 [cited 2025 Apr 25]; Available from: https://journals.lib.unb.ca/index.php/GC/article/view/4078

10. Bourdeau JE, Zhang SE, Nwaila GT, Ghorbani Y. Data generation for exploration geochemistry: Past, present and future. Applied Geochemistry. 2024 Oct 1;172:106124.

11. Cohen DR, Kelley DL, Anand R, Coker WB. Major advances in exploration geochemistry, 1998–2007. Geochemistry: Exploration, Environment, Analysis. 2010 Feb 1;10(1):3–16.

12. Fabre C, Ourti NE, Mercadier J, Cardoso-Fernandes J, Dias F, Perrotta M, et al. Analyses of Li-Rich Minerals Using Handheld LIBS Tool. Data. 2021 Jun;6(6):68.

13. Kim Y, Fabre C, Cauzid J. Access to quantitative analysis of carbonates using a portable LIBS instrument: First applications to single minerals and mineral mixtures. Spectrochimica Acta Part B: Atomic Spectroscopy. 2022 May 1;191:106397.

14. Fabre C, Ourti NE, Ballouard C, Mercadier J, Cauzid J. Handheld LIBS analysis for in situ quantification of Li and detection of the trace elements (Be, Rb and Cs). Journal of Geochemical Exploration. 2022 May 1;236:106979.

15. The EMILI project | EMILI [Internet]. 2025 [cited 2025 Apr 18]. Available from: https://emili.imerys.com/en/emili-project

Chapitre I.
The handheld LIBS technique

Chapter I. The handheld LIBS technique

Introduction

When mining companies develop new projects, the scale of investments often reflects the fluctuations in the mineral commodity market and the global financial system stability. In 2016, exploration budgets declined by 35% in average in north america and australia (1), due to global macroeconomic slowdowns, particularly in Asia, and successive financial crises, including the commodity price collapse (2). To guarantee investment returns, mining companies have gradually shifted towards cost-control strategies, focusing on methodological efficiency and innovative approaches to optimize prospecting (3). In this context, handheld spectroscopic techniques (i.e., XRF, VNIR-SWIR, Raman, and LIBS) (4) are redefining geochemical data acquisition by reducing reliance on extensive laboratory procedures (sampling, transport, processing, and analysis) and facilitating rapid access to qualitative, quantitative, and mineralogical information, to support fast and strategic decisions during mining operations.

This chapter explores handheld LIBS, from its technical evolution to the current market trends, and the different applications for quantitative and discriminant analysis in geoscience. The contribution of LIBS to these questions will be discussed to provide a context to the methodologies developed in this study. Handheld LIBS was chosen based on key advantages of the technique over alternative onsite analytical techniques: i) light elements detection, especially Li, ii) high data-acquisition speed well-suited to the volume of rock generated during a drilling campaign, and iii) Multi-scale analytical capabilities, from mineral to rock.

1 Handheld LIBS development and current market

The evolution of LIBS technique from fixed laboratory systems to field devices has followed three major stages (5). First, LIBS components were organized to fit a suitcase format, the device was transportable but with limited mobility. Next the backpack-mounted systems, offered improved flexibility and better access to rock and soil samples. The versions currently available on the market are handheld, compact units.

The first field-based LIBS systems (6,7), developed in the 1990s, consisted of two connected units: a suitcase containing the spectrometer, detector, power supply, and data acquisition system, and a handheld probe equipped with a laser, lenses, and fiber optics for plasma emission collection, with a total weight exceeding 13 kg (6,7). In early 2000s, a second generation of man-portable LIBS emerged, offering greater mobility and operational practicality (8–11). Relocating the main dispositif from a suitcase to a backpack improved accessibility to samples in challenging environments (e.g., hazardous material, geological fieldwork, and soil) (8,10–12). These models carried Li-ion batteries for extended autonomy and incorporated real-

time spectral analysis and remote control (8). Subsequent efforts focused on developing robust, compact handheld devices, integrating all optical components into a single, lightweight unit (13). These systems eliminated the external probe simplifying manipulation during data acquisition, as well as, user-friendly interfaces and extended battery life-span (up to 10 hours)(14). The success of early prototypes led to the first commercialized models, including StellarNet's Porta-LIBS-2000, the EasyLIBS system, and the LIBSCAN 25, launched by Applied Photonics. The market for handheld LIBS has since expanded significantly (**Table.1**), largely driven by the success of LIBS analyzers in the metallurgy sector. The currently available models, summarized in **Table.1**, weight between 2 - 3 kg, a spectral range either limited or extended from UV to NIR, and a spatial resolution ranging from moderate (0.3 mm) to high (0.03 mm). Larger models (LIBS M-Trace - Trioptics France) provide enhanced detection capabilities.

Even if the potential of field-based LIBS for geoscience was recognized early (15), it is the growing demand for lithium that has significantly contributed to the broader adoption of handheld LIBS in mineral resources exploration. SciAps has emerged as a leader in this sector with its Z-series analyzers, designed to capture the heterogeneous and complex chemical composition of geological materials, adopted both in industrial and academic contexts. If the evolution in handheld LIBS analyzers was first focused on reducing the size and increasing autonomy, it now appears that a plateau has been reached in terms of enhancing miniaturization (**Fig.1**), battery life, and optical parameters. Recent developments have shifted from size reduction to optimizing data processing capabilities, user interface, and overall functionality. For example, the Z-900 series, compared to the previous Z-300 model used in this thesis, incorporates advanced calibration curves for lithium, including new deposit types that were previously underrepresented, as well as dedicated reference samples to ensure prediction consistency. This suggests that, having optimized the physical design, the future evolution of handheld LIBS devices will be driven by improvements in data management, eventually closing the gap toward standardized routines, such as pXRF.

2 Handheld LIBS analyzer

Critical design considerations for Handheld LIBS systems include compact size, optical performance and mechanical durability. The instrument must also be suitable for handheld manipulation, and a production cost aligned with the portable spectroscopy market. The model used in this study is the Z-300 (SciAps), which can operate in two different modes :

Element Pro: operates individual analysis points based on several parameters: number of analysis zones per point, shots per location, distance between locations, number of cleaning

Table.1. Summary of the Design Characteristics, Analytical Capabilities, and elemental detection of Handheld LIBS analyzers currently available (2024).

Manufacturer	Models available	Analytical features	Dimensions (cm)	Weight (Kg)	Element detected
Torontech	a. alloys b. Li-model	a. 190 - 705 b. 450 – 705nm	25.5x29.4x8	a. 1.65 b. 2.0	a. Mg - U b. H, Li, Na, Zn, Sr, Ag, Ba
Hitachi HighTech	a. Vulcan Spart+ b. Vulcan Optimum+ c. Vulcan Expert+	-	24x30x9	2.2	Metals
SciAps	Z-901 Z-901 CSi Z-901 Li Z-902 Carbon Z-902 + Z-903 Carbon Z-903	200 – 420nm 190 – 260nm 380 – 680nm 190 – 420nm 190 – 625nm 190 – 625nm 190 – 950nm	21.9x27.3x6.0	1.65 1.75 1.75 1.97 1.60 1.97 1.97	a. Metals b. C, Si c. Li, Na, H, Al, Ba d. H - U
ThermoFisher	Niton-Apollo	200 – 400nm	30.4x33.0x10.1	2.9	C, Al, Si, Ti, V, Cr, Mn, Co, Ni, Cu, Nb, Mo, W
OceanOptics	OA-100S	-	24.0x25.7x8.4	1.5	Li - Au
Trioptics France	LIBS M-trace	190 – 750nm	63x30x60	30	H-U



Figure.1. Handheld LIBS analyzers: from early commercialized models (LIBSCAN 25+ and StellarCASE-LIBS) to recent designs (Z-300 and Z900).

shots, X/Y coordinates of the first analysis point, focal length, number of spectra averaged per location, and the averaging method used. Reference emission lines are automatically identified in the acquired spectrum. When an element's characteristic lines are detected, the element is listed in function of presence probability and assigned an estimated relative abundance, representing its proportion in the sample compared to other detected elements.

Geochem Pro : generates elemental maps by performing raster scans (4x4, 6x6, or 12x12 zones) across the sample surface to capture the spatial distribution of an element. At each map pixel, the signal intensity for a specific element is normalized to the highest signal detected across the grid producing elemental "heat maps" with a color gradient for high and low concentrations. The resulting data includes an image of the analyzed area, individual spectra for each location, an averaged spectrum for the entire grid, and a heat map for each detected element.

The analyzer features a user-friendly software interface, ProfileBuilder, for analysis acquisition, parameter control, and spectra visualization. The reference database included helps to identify elements emission lines, while the calibration mode facilitates the creation of internal calibration curves. LIBS data can be exported in two formats: i) raw pixel data, in a CSV file with "pixel," "wavelength," and "intensity"; and ii) wavelength-calibrated spectra as artificial pixels are added through interpolation to correct spectrometer distortions, resulting in a "wavelength," - "intensity" format. The number of spectra per analysis point corresponds to the number of analyzed locations, averaged shots per location, and the average spectrum of the total area analyzed.

3 Application in geology

3.1 Quantitative analysis

Quantitative analysis using handheld LIBS can be achieved through two main approaches: building a calibration curve or using a calibration-free modelization (16). For the calibration curve method, reference samples of the targeted material are analyzed to correlate the LIBS signal intensity to the elemental concentrations (17). However, the LIBS signal intensity is not only related to elemental concentration but is also influenced by several matrix-related factors that must be carefully considered when developing quantitative models. Surface texture, flatness, moisture content, and chemical variations, can affect LIBS signal (18–20). Additionally, data acquisition must ensure a sufficient number of data points to capture a representative signal, particularly when analyzing heterogeneous materials (21,22). In the context of lithium exploration, Several studies have demonstrated the potential of handheld LIBS to generate quantitative geochemical information at different spatial scales. In Cardoso-Fernandes et al. (2022)(23), handheld LIBS was used to confirm mineralized zones identified

through a geochemical survey. Li-enriched areas were initially located based on stream sediment analysis and mineral pathfinders. The selected pegmatite outcrops were then analyzed onsite to confirm whether a zone was correctly predicted as a potential lithium resource. In Wise et al. (2022)(24), pulverized pegmatite samples were analyzed to build a LIBS calibration curve for quantitative elemental analysis in the context of the Carolina Tin-Spodumene Belt to discriminate fertile from barren pegmatites. Similarly, in the study by Ferreira et al. (2022)(25), various data analysis methods were tested to measure lithium in pegmatite samples obtained through drilling using both linear and non-linear models, addressing issues such as signal saturation and matrix effects. Both studies emphasized the importance of physical matrix matching to ensure representative models for accurate lithium prediction. At the mineral scale, Fabre et al. (2022)(21), developed a calibration curve to quantify lithium content in Li-rich minerals (spodumene, lepidolite, and petalite) associated with rare-metal pegmatites and granites. The predicted lithium concentrations were consistent with reference values obtained through conventional laboratory methods. The study emphasizes the importance of appropriate LIBS acquisition and processing protocol, including analysis point distribution and spectra normalization for optimal results. Korbel et al. (2024)(26), and Foucaud et al. (2019)(27) evaluate handheld LIBS in post-extraction stage, to monitor ore recovery throughout the mineral processing chain. Korbel et al. (2024)(26), focused on the Beauvoir granite deposit, analyzing powdered pellets derived from processing (flotation concentrates). In Foucaud et al. (2019)(27), fluorine content was measured in flotation samples from tungsten-skarn ore. The study demonstrated that combining the two CaF emission bands in a multivariate model significantly improved analytical accuracy. In both studies, particular attention was given to ensuring pellet uniformity in terms of grain size, surface texture, and density, as these physical characteristics were reported to significantly impact LIBS signal quality and affect quantitative models reliability.

Besides light elements, the multi-elemental detection capability of LIBS offers remarkable versatility. Fontana et al. (2023)(22) explored the use of a benchtop LIBS prototype for automated whole-rock geochemical analysis (Al, Ca, Fe, K, Mg, Na, Si, and Ti) during drilling operations. Rock segments from different lithofacies (basalt, breccia, conglomerate, dolostone, granite, microgranite, orthogneiss, pegmatite, rhyolite, sandstone, and schist) were used to build linear regression models. The influence of mineralogical diversity, element distribution, and surface roughness on prediction accuracy is discussed. While In a broader context, Ytsma et al. (2020)(28) assessed calibration performance using over 2,000 rock standards for both major oxides (SiO_2, Al_2O_3, CaO, TiO_2, K_2O, MgO, MnO, Na_2O, P_2O_3) and trace elements (Ba, Cr, Li, Cu, Ni, Pb, S, Zn). The results demonstrated the superiority of multivariate approaches (e.g., PLS) over univariate models, especially for trace and minor elements. Custom

calibrations built using rock-specific standards outperformed the default industrial models, reinforcing the importance of tailored approaches for LIBS quantitative analysis. Brinkmann et al. (2023)(29) targeted copper grades in two deposit types: a volcanogenic massive sulfide deposit and a stratiform sedimentary copper deposit. Both univariate and multivariate modeling were tested, comparing synthetic and field samples, preprocessing and raw data, as well as handheld and laboratory LIBS systems to identify the most accurate method for copper prediction. The results exhibited lower accuracy for field samples due to factors like matrix inhomogeneity, weathering, and spectral interference. The use of multivariate regression significantly improved the prediction accuracy, especially when synthetic data were complemented with field samples. In the context of Elvira Volcanogenic Massive Sulfide exploration, Kim et al. (2022)(30) developed and optimized a methodology for quantifying major elements (Ca, Mg, Fe, Mn) in a set of carbonate-mineral standards within the Ca-Mg-Fe-Mn system. The analysis revealed strong linear correlations and high prediction accuracy for Ca, Fe, and Mn. While Mg performance was inconsistent.

Developing quantitative LIBS models, particularly for geoscience, is not a straightforward process. The chemical and textural heterogeneity of geological samples, coupled with the complexity of laser-plasma interactions, often implies a trial-and-error approach, building multiple predictive models to identify the most suitable option, depending on the specific analytical context. Numerous factors influence the performance of the models and must be considered to align with the targeted samples. The effect of the training dataset size has been shown to impact the accuracy and robustness of predictions (31). Similarly, the choice of spectra normalization (total signal intensity, internal standardization, or background correction) can enhance both prediction accuracy and limit of quantification (32). An equally important step is assessing models performances. While model are often evaluated based on standard metrics (R^2, RMSE, or MAE), statistical comparison is strongly recommended to determine whether observed differences are statistically significant (33). A model exhibiting better metrics may not be statistically superior and could be overfitted to the training data. Therefore, model selection should prioritize not only predictive accuracy but also robustness and generalization potential, while avoiding unnecessary complexity that could decrease applicability in field conditions.

3.2 Discriminant analysis

The substantial amount of information contained within a single handheld LIBS spectrum, combined with the flexibility in spatial resolution, extend the range of application of handheld LIBS beyond element detection and quantification.

In Wójcik et al. (2020)(34), a set of 60 different copper minerals was used to train a linear

regression to classify unknown mineral samples. To address the challenges of analyzing natural geological samples, including textural inconsistency and chemical variation, the collected LIBS spectra were processed using Non-negative Tensor Factorisation to isolate the spectral signature of each mineral from background noise and interference, ensuring more reliable predictions. In the context of ethical sourcing, Hark et al. (2012) (35) applied handheld LIBS to determine the geographic origin of columbite-tantalite, a critical mineral associated with conflict regions. Over 50 samples from 37 locations were analyzed. Major and trace elements, including rare earth elements (REEs), were examined to implement PLS-DA to detemrine sample origin. The model achieved high geographic classification accuracy (90% - 100%). In the work of Lawley et al. (2021)(36), automated mineral identification was applied using LIBS elemental maps to determine the composition and the spatial distribution of mineral phases in a rock samples. A drill core section representing mantle xenoliths was analyzed at various locations using 3×3 mm LIBS maps, which were then combined to create cm-scale geochemical images. LIBS analysis detected trace elements, including light elements (Na and Li), enabling the mapping of alteration and metasomatic patterns. Advanced analytical techniques (PCA) and clustering methods, were employed to enhance mineral interpretation by grouping LIBS data points according to mineral class and illustrating both primary and secondary mineral phases in color-coded images.

One interesting aspect of mineral classification using handheld LIBS is that the complexity of a mineral sample is so effectively captured, from major constituents to trace elements, that even simple signal processing techniques, such as signal ratio analysis, can demonstrate successful results. In Kim et al. (2022)(30) Correlations between specific LIBS emission-line ratios, including Mg/Ca, Mg/Mn, and Fe/Ca, were established for the discrimination of carbonate minerals: ankerite, magnesite, siderite, calcite, rhodochrosite, and dolomite. LIBS analysis revealed clear spectral changes, effectively distinguishing between different mixtures, including calcite-ankerite, calcite-dolomite, and ankerite-dolomite, hardly identifiable at the macroscopic scale. Similarly, Fabre et al (2022)(21) and Wise et al. (2022)(24,37) used signal ratio of Si, Al, K, and Rb to discriminate ore minerals in the context of lithium deposit. In Fabre's study, the Si/Al signal ratio proved effective in discriminating Li-rich ore phases (spodumene, lepidolite, and petalite). While in Wise et al.'s work, a single mineral phase, muscovite, was targeted to differentiate mineralized from barren pegmatite using the K/Rb ratio.

At the rock scale, LIBS analysis classification can facilitate automated lithological logging, rock sample source identification, and rock characterization. In Fontana et al. (2021)(38) the LIBS signal of major elements (Al, Ca, Fe, Mg, Si, Na, and K) from 22 magmatic and metamorphic rock samples, were used to train a clustering algorithm (k-means) to predict lithological facies in drill core sections and create pseudologs representing geological stratigraphy. LIBS analysis

spatial resolution facilitates meticulous lithogeochemical interpretations, including textural and mineralogical zonation. In Senesi et al. (2023)(39), a solution for the classification of cherts, a silica-rich sedimentary rock, visually similar to silica polymorphs, is proposed. The signal of Al, Ti, Fe, Ca, Mn, and Mg from five chert mining sites in the Gargano promontory (Apulia, Italy) constituted input data for machine learning algorithms (LDA, SVM). This approach successfully distinguished different chert samples and helped identify potential archaeological sources. In Roux et al. (2015)(40), a lab-made handheld LIBS system was developed for classifying 21 volcanic rocks from various magmatic series in Iceland. The emission lines of Al, Ba, Ca, Cr, Cu, Fe, Mg, Mn, Na, Si, Sr, and Ti were used as key parameters to categorize the rock samples analyzed in the field into alkalic, transitional alkalic, and tholeiitic magmatic series, using discriminant analysis.

The performance of classification algorithms in predicting unknown samples is highly dependent on the quality of the input data, emphasizing the need for reliable geological spectral data to effectively implement these solutions. In this context, studies have focused on providing reference LIBS spectra acquired from known geological samples (41–43), which can be used to identify key spectral features and train machine learning models for advanced applications

4 Discussion and Conclusion

The applications reported in the literature highlight the broad analytical potential of handheld LIBS in geological environments, from precise element quantification to minerals and rocks identification. A key strength of handheld LIBS is the ability to perform multi-scale analysis. The small laser spot size (~50 µm) allows detailed measurements of individual mineral grains (44) and broader whole-rock characterization by averaging multiple data points (40). The spatial resolution of LIBS measurement can therefore be adapted, for both quantitative and identification purposes, to generate geochemical data either at mineral or rock scale.

In the context of quantitative analysis, although approximately 50% of the reviewed studies center on lithium (**Fig.2a**), handheld LIBS has also proven effective for the detection of different major and trace elements (22,29,45). The multi-elemental capabilities of geoscience-oriented LIBS analyzers not only address the detection gap for light elements but offer high analytical flexibility opening substantial possibilities in terms of target and deposit types. Therefore, from an operational perspective, handheld LIBS represents a strategic and highly adaptable solution for mining companies with potential to address evolving operational needs throughout the different stages of a mining project, from exploration to production. While successful applications of handheld LIBS have been demonstrated on outcrops, individual minerals, and solid rock samples, the use of powder pellets is often prioritized (**Fig.2b**). Typically, LIBS

measurements are limited to the surface, ablating only a few tens of microns of material at each spot, whereas reference values for whole-rock analysis result from bulk analytical methods. The homogenization of the heterogeneous composition of geological samples facilitates the acquisition of a representative signal, particularly in the context of whole-rock analysis, and guarantees signal consistency and replicability. The studies conducted on rock fragments and drill core sections (22), align more closely with the operational realities of mining activities, reflecting the practical constraints, including limited time for sample preparation and the need for high sample throughput, during field operations. The LIBS calibration models, often developed in a research setting (**Fig.2c**) are challenging to implement in field workflows due to limited on-site resources. The analytical protocol for the Beauvoir granite samples was specifically designed for application to unprocessed drill core sections, ensuring that the LIBS calibrations were developed to address both the operational requirements, reliable Li predictions, and the practical constraints of an exploration drilling campaign.

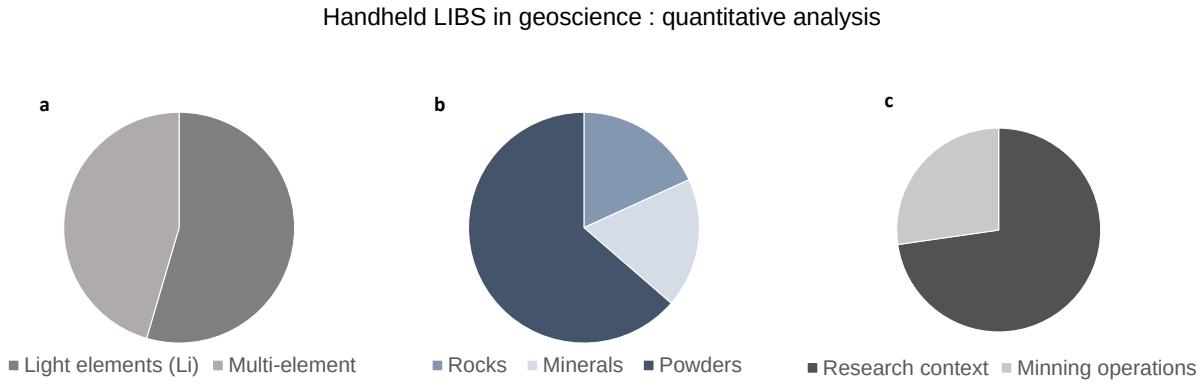

Figure.2. Handheld LIBS in geological applications for quantitative analysis: a) distribution of target elements, b) sample types, and c) development contexts.

Additionally, although operating a handheld LIBS device is relatively straightforward, the development of reliable calibration models requires skills, matrix-specific reference samples, and a minimum of understanding of the geological object. The need to create individual calibrations for each case, as current on-device quantitative models often show limited accuracy (23), is a major challenge for the wider adoption of LIBS in the mining sector, especially when compared to standardized methods (XRF).To address this aspect, the potential to transfer LIBS quantitative models by assessing whether pre-calibrated models could be applied to deposits that are geographically distant but geochemically similar was investigated.

In the second part of this thesis, we investigate the potential of LIBS to generate mineralogical data from elemental analysis. Previous studies have demonstrated that the high resolution of

LIBS is capable of capturing enough chemical complexity to distinguish minerals by their unique spectral signatures (41). In this context, we explore the integration of machine learning models with LIBS data to automate mineral recognition, for: i) identify the mineralogical composition of granite samples, and ii) determine the relative proportions of the ore phase, in the context of mineral resources exploration.

References

1. Bonakdarpour M, Hoffman F, Rajan K. Mine development times: The US in perspective.

2. Zhang D, Broadstock DC. Global financial crisis and rising connectedness in the international commodity markets. International Review of Financial Analysis. 2020 Mar 1;68:101239.

3. Okada K. Breakthrough technologies for mineral exploration. Miner Econ. 2022 Dec 1;35(3):429–54.

4. Harmon RS. Laser-Induced Breakdown Spectroscopy in Mineral Exploration and Ore Processing. Minerals. 2024 Jul 1;14:731.

5. Senesi GS, Harmon RS, Hark RR. Field-portable and handheld laser-induced breakdown spectroscopy: Historical review, current status and future prospects. Spectrochimica Acta Part B: Atomic Spectroscopy. 2021 Jan 1;175:106013.

6. Castle BC, Knight AK, Visser K, W.smith B, Winefordner JD. Battery powered laser-induced plasma spectrometer for elemental determinations. J Anal At Spectrom. 1998 Jan 1;13(7):589–95.

7. Yamamoto KY, Cremers DA, Ferris MJ, Foster LE. Detection of Metals in the Environment Using a Portable Laser-Induced Breakdown Spectroscopy Instrument. Appl Spectrosc. 1996 Feb 1;50(2):222–33.

8. Fortes FJ, Cuñat J, Cabalín LM, Laserna JJ. In Situ Analytical Assessment and Chemical Imaging of Historical Buildings Using a Man-Portable Laser System. Appl Spectrosc. 2007 May 1;61(5):558–64.

9. Cuñat J, Fortes FJ, Laserna JJ. Real time and in situ determination of lead in road sediments using a man-portable laser-induced breakdown spectroscopy analyzer. Analytica Chimica Acta. 2009 Feb 2;633(1):38–42.

10. Cuñat J, Fortes FJ, Cabalín LM, Carrasco F, Simón MD, Laserna JJ. Man-Portable Laser-Induced Breakdown Spectroscopy System for in Situ Characterization of Karstic Formations. Appl Spectrosc. 2008 Nov 1;62(11):1250–5.

11. Harmon RS, Lucia FCD, LaPointe A, Miziolek AW. Man-portable LIBS for landmine detection. In: Detection and Remediation Technologies for Mines and Minelike Targets XI [Internet]. SPIE; 2006 [cited 2024 Aug 16]. p. 154–60. Available from: https://www.spiedigitallibrary.org/conference-proceedings-of-spie/6217/62170I/Man-portable-LIBS-for-landmine-detection/10.1117/12.667564.full

12. Bousquet B, Travaillé G, Ismaël A, Canioni L, Michel-Le Pierrès K, Brasseur E, et al. Development of a mobile system based on laser-induced breakdown spectroscopy and

dedicated to in situ analysis of polluted soils. Spectrochimica Acta Part B: Atomic Spectroscopy. 2008 Oct 1;63(10):1085–90.

13. Roux C. Etude et développement d'un système LIBS portable hautes performances de nouvelle génération et d'une source de marquage UV à faible durée d'impulsion [Internet] [These de doctorat]. Dijon; 2016 [cited 2025 Apr 25]. Available from: https://theses.fr/2016DIJOS047

14. Goujon J, Giakoumaki A, Piñon V, Musset O, Anglos D, Georgiou E, et al. A compact and portable laser-induced breakdown spectroscopy instrument for single and double pulse applications. Spectrochimica Acta Part B: Atomic Spectroscopy. 2008 Oct 1;63(10):1091–6.

15. Harmon RS, Lawley CJM, Watts J, Harraden CL, Somers AM, Hark RR. Laser-Induced Breakdown Spectroscopy—An Emerging Analytical Tool for Mineral Exploration. Minerals. 2019 Dec;9(12):718.

16. Tognoni E, Cristoforetti G, Legnaioli S, Palleschi V. Calibration-Free Laser-Induced Breakdown Spectroscopy: State of the art. Spectrochimica Acta Part B: Atomic Spectroscopy. 2010 Jan 1;65(1):1–14.

17. El Haddad J, Canioni L, Bousquet B. Good practices in LIBS analysis: Review and advices. Spectrochimica Acta Part B: Atomic Spectroscopy. 2014 Nov 1;101:171–82.

18. Xu W, Sun C, Tan Y, Gao L, Zhang Y, Yue Z, et al. Total alkali silica classification of rocks with LIBS: influences of the chemical and physical matrix effects. J Anal At Spectrom. 2020;35(8):1641–53.

19. Wangeci A, Adén D, Greve MH, Knadel M. Effect of sample pretreatment on pelletization and performance of laser-induced breakdown spectroscopy for predicting key soil properties. Spectrochimica Acta Part B: Atomic Spectroscopy. 2023 Aug 1;206:106712.

20. Chen M, Yuan T, Hou Z, Wang Z, Wang Y. Effects of moisture content on coal analysis using laser-induced breakdown spectroscopy. Spectrochimica Acta Part B: Atomic Spectroscopy. 2015 Oct 1;112:23–33.

21. Fabre C, Ourti NE, Ballouard C, Mercadier J, Cauzid J. Handheld LIBS analysis for in situ quantification of Li and detection of the trace elements (Be, Rb and Cs). Journal of Geochemical Exploration. 2022 May 1;236:106979.

22. Fontana FF, van der Hoek B, Tassios S, Tiddy C, Stromberg J, Francis N, et al. Laser Induced Breakdown Spectroscopy (LIBS) for whole rock geochemistry. Journal of Geochemical Exploration. 2023 Mar;246:107160.

23. Cardoso-Fernandes J, Lima J, Lima A, Roda-Robles E, Köhler M, Schaefer S, et al. Stream sediment analysis for Lithium (Li) exploration in the Douro region (Portugal): A comparative study of the spatial interpolation and catchment basin approaches. Journal of Geochemical Exploration. 2022 May 1;236:106978.

24. Wise MA, Harmon RS, Curry A, Jennings M, Grimac Z, Khashchevskaya D. Handheld LIBS for Li Exploration: An Example from the Carolina Tin-Spodumene Belt, USA. Minerals. 2022 Jan;12(1):77.

25. Ferreira MFS, Capela D, Silva NA, Gonçalves F, Lima A, Guimarães D, et al. Comprehensive comparison of linear and non-linear methodologies for lithium quantification

in geological samples using LIBS. Spectrochimica Acta Part B: Atomic Spectroscopy. 2022 Sep 1;195:106504.

26. Korbel C, Mezoued N, Demeusy B, Fabre C, Cauzid J, Filippova IV, et al. Quantification of lithium using handheld instruments: application of LIBS and XRF spectroscopy to assay the lithium content of mineral processing products. J Anal At Spectrom. 2024 Jul 3;39(7):1838–53.

27. Foucaud Y, Fabre C, Demeusy B, Filippova IV, Filippov LO. Optimisation of fast quantification of fluorine content using handheld laser induced breakdown spectroscopy. Spectrochimica Acta Part B: Atomic Spectroscopy. 2019 Aug 1;158:105628.

28. Ytsma CR, Knudson CA, Dyar MD, McAdam AC, Michaud DD, Rollosson LM. Accuracies and detection limits of major, minor, and trace element quantification in rocks by portable laser-induced breakdown spectroscopy. Spectrochimica Acta Part B: Atomic Spectroscopy. 2020 Sep 1;171:105946.

29. Brinkmann P, Köllner N, Merk S, Beitz T, Altenberger U, Löhmannsröben HG. Comparison of Handheld and Echelle Spectrometer to Assess Copper in Ores by Means of Laser-Induced Breakdown Spectroscopy (LIBS). Minerals. 2023 Jan;13(1):113.

30. Kim Y, Fabre C, Cauzid J. Access to quantitative analysis of carbonates using a portable LIBS instrument: First applications to single minerals and mineral mixtures. Spectrochimica Acta Part B: Atomic Spectroscopy. 2022 May 1;191:106397.

31. Dyar MD, Ytsma CR. Effect of data set size on geochemical quantification accuracy with laser-induced breakdown spectroscopy. Spectrochimica Acta Part B: Atomic Spectroscopy. 2021 Mar 1;177:106073.

32. Guezenoc J, Gallet-Budynek A, Bousquet B. Critical review and advices on spectral-based normalization methods for LIBS quantitative analysis. Spectroc Acta Pt B-Atom Spectr. 2019 Oct;160:105688.

33. Duponchel L, Fabre C, Bousquet B, Motto-Ros V. Statistical comparison of predictive models for quantitative analysis and classification in the framework of LIBS spectroscopy: A tutorial. Spectrochimica Acta Part B: Atomic Spectroscopy. 2023 Oct 1;208:106776.

34. Wójcik M, Brinkmann P, Zdunek R, Riebe D, Beitz T, Merk S, et al. Classification of Copper Minerals by Handheld Laser-Induced Breakdown Spectroscopy and Nonnegative Tensor Factorisation. Sensors. 2020 Jan;20(18):5152.

35. Hark RR, Remus JJ, East LJ, Harmon RS, Wise MA, Tansi BM, et al. Geographical analysis of “conflict minerals” utilizing laser-induced breakdown spectroscopy. Spectrochimica Acta Part B: Atomic Spectroscopy. 2012 Aug 1;74–75:131–6.

36. Lawley CJM, Somers AM, Kjarsgaard BA. Rapid geochemical imaging of rocks and minerals with handheld laser induced breakdown spectroscopy (LIBS). Journal of Geochemical Exploration. 2021 Mar 1;222:106694.

37. Harmon RS, Wise MA, Curry AC, Mistele JS, Mason MS, Grimac Z. Rapid Analysis of Muscovites on a Lithium Pegmatite Prospect by Handheld LIBS. Minerals. 2023 May;13(5):697.

38. Fontana FF, Tassios S, Stromberg J, Tiddy C, van der Hoek B, Uvarova YA. Integrated Laser-Induced Breakdown Spectroscopy (LIBS) and Multivariate Wavelet Tessellation: A

New, Rapid Approach for Lithogeochemical Analysis and Interpretation. Minerals. 2021 Mar;11(3):312.

39. Senesi GS, Allegretta I, Marangoni BS, Ribeiro MCS, Porfido C, Terzano R, et al. Geochemical identification and classification of cherts using handheld laser induced breakdown spectroscopy (LIBS) supported by supervised machine learning algorithms. Applied Geochemistry. 2023 Apr 1;151:105625.

40. Roux CPM, Rakovský J, Musset O, Monna F, Buoncristiani JF, Pellenard P, et al. In situ Laser Induced Breakdown Spectroscopy as a tool to discriminate volcanic rocks and magmatic series, Iceland. Spectrochimica Acta Part B: Atomic Spectroscopy. 2015 Jan 1;103–104:63–9.

41. Fabre C, Ourti NE, Mercadier J, Cardoso-Fernandes J, Dias F, Perrotta M, et al. Analyses of Li-Rich Minerals Using Handheld LIBS Tool. Data. 2021 Jun;6(6):68.

42. Mezoued N, Fabre C, Cauzid J, Kim Y, Jatteau M. Analysis of Minerals Using Handheld Laser-Induced Breakdown Spectroscopy Technology. Data. 2025 Mar;10(3):40.

43. Jatteau M, Cauzid J, Fabre C, Voudouris P, Soulamidis G, Tarantola A. Portable Analyses of Strategic Metal-Rich Minerals Using pXRF and pLIBS: Methodology and Database Development. Data. 2025 Feb;10(2):12.

44. Defnet PA, Wise MA, Harmon RS, Hark RR, Hilferding K. Analysis of Garnet by Laser-Induced Breakdown Spectroscopy—Two Practical Applications. Minerals. 2021 Jul;11(7):705.

45. Zhou X, Yi G, Bhagwat NP. Synergic identification of heavy metal contaminants in mining tailings, waste rocks, and soil using laser-induced breakdown spectroscopy and x-ray fluorescence spectroscopy. 2020 Dec 1;2020:H089-0009.

Chapitre II.
Case study: The Beauvoir granite

Chapter II. Case study: The Beauvoir granite

Introduction

The methodologies developed were specifically applied to samples sourced from the Beauvoir granite, addressing practical challenges faced during the lithium exploration campaign of the deposit as part of a scientific collaboration with the mining company Imerys (Échassières, France).

This chapter provides an overview of the Beauvoir granite deposit, including historical and geological contexts, a presentation of the ongoing lithium mining project (EMILI), and a preliminary analysis of the resulting geochemical data (1). A detailed understanding of the deposit characteristics is essential, particularly when using the LIBS technique, a highly sensitive technique to chemical and physical matrix effects (2). This process guided the selection of reference samples to build representative models, for quantitative and mineralogical analyses (3), while defining the limitations of the models once generalized to the entire deposit based on the chemical and textural variations reported.

1 Historical context

The Beauvoir granite has been the focus of numerous scientific studies due to its highly evolved nature and the associated mineralizations (4–6). The site was first geologically investigated by Rosen (1963) (7,8) and Aubert (1966) (9) as part of studies on the Massif des Collettes. A detailed study of the Beauvoir intrusion was conducted in 1985 during the first drilling campaign of the Géologie Profonde de la France (GPF) project (10). The GPF was a national initiative (1982 -1994) to explore the french subsurface through deep drilling campaigns across different geological formations that were difficult to access from outcrops, contributing to both fundamental research and mineral prospecting. The Beauvoir granite was selected as a case study for the thematic peraluminous leucogranitic complexes, one of the twelve themes chosen for the program, supported by several considerations: i) The economic significant of this type of magmatic systems commonly associated spatially and genetically with metals concentrations ii) The substantial pre-existing data available at the time resulting from past mining activities, and iii) the broad range of mineralizations reported in previous studies, increasing the atractivity of the Beauvoir deposit as a regional deposit.

The project resulted in a vertical borehole intersecting the Beauvoir granite over 800 m (**Fig.1b**), providing continuous rock samples from the roof to the base of the intrusion. The geophysical studies (including borehole logging, gravimetry, and magnetic susceptibility)(11), Modelisation (heat flow measurements and thermal conductivity modeling of the massif) (12), as well as the mineralogical observations (13,14), and geochemical analyses for both whole-rock samples (15,16) and individual minerals (17,18) contributed to elaborate a 2D geological

model (**Fig.1b**) and define the textural and chemical characteristics of the three main units (B1, B2, and B3). Additionally, the findings obtained on the magmatic processes and fluid interactions associated with the emplacement of such highly evolved granitic apex, enhanced the general understanding and modelisation of element transport mechanisms within the continental crust, particularly in the context of late to post-orogenic magmatisme (19), providing valuable clues for the exploration of critical mineral resources in similar geological settings (20).

2 Geological context

The Beauvoir granite is located 70 km (NNW) from Clermont-Ferrand (Puy-de-Dôme, France) in the northeastern part of the French Massif Central (FMC) (**Fig.1a**), as part of the Echassières magmatic complex. Rare-metal granites crystallize from highly differentiated magmas and are characterized by a distinctive geochemical signature, typically enriched in volatiles (F, Li, P, and B), and critical metals (Li, Sn, Nb, and Ta) disseminated in specific ore mineral phases (21). Their composition varies from peralkaline to peraluminous, depending on the geodynamic context, the protolith, and hydrothermal interactions. Rare-metal granites crystallize generally at shallow crustal levels (1–2 km), display subvolcanic textures, and are relatively small, with a few hundred meters in diameter and volumes between 0.02 and 0.2 km^3 (21).

The Echassières granitic massif includes three magmatic bodies: The largest unit (40 km^2) is the Colettes biotite-muscovite-cordierite granite, the second unit, smaller in surface (0.014 km^2) (19), is the Beauvoir topaz-lepidolite-albite granite, while a third unit, has no outcrops but is thought to be at depths. The plutons intrude the parautochthonous basement known as the Sioule metamorphic series (**Fig.1c**), consisting of a high-grade metamorphic unit (biotite-sillimanite gneisses and migmatites) positioned over a medium-grade metamorphic unit (staurolite-garnet-sillimanite micas schist) (4,22) that are part of a broader nappe system formed during major compressive events resulting in large masses of rocks displaced through folding and faulting during the Variscan orogeny (23,24). The Beauvoir granite is associated with late- to post-collisional magmatism (25), resulting from the thermal relaxation that followed crustal thickening during the last stage of Variscan orogeny. The convergence and collision of lithospheric plates generate intense crustal shortening and large-scale thrusting, leading to significant lithospheric thickening. This process elevated pressure-temperature conditions in the lower crust leading to partial melting of crustal rocks. In the Échassières massif, the magmatic system evolved from cordierite-bearing microgranite (Colettes), formed under moderate to high pressure–temperature conditions, to the intrusion of the Beauvoir granite between 308 and 317 Ma (26,27), marking the terminal stage of magmatic activity in the region.

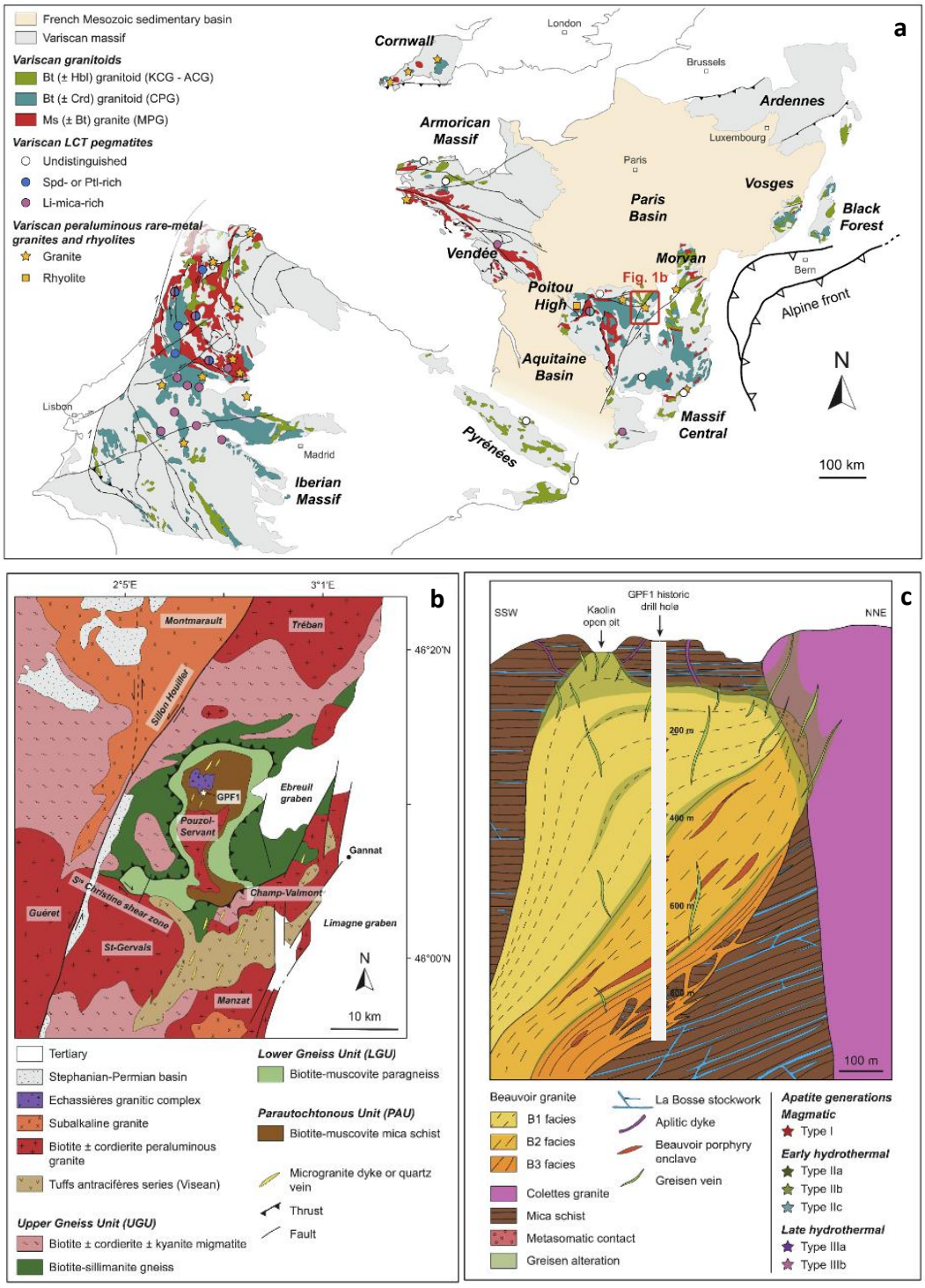

Figure.1. a) The western european variscan belt including variscan granitoids, LCT pegmatites, rare-metal granites and rhyolites outcrops (from Rocher et al. (2024) modified from Ballouard et al. (2024)). MPG: muscovite-bearing peraluminous granites; CPG: cordierite-bearing peraluminous granitoids; KCG: K-rich and K-feldspar porphyritic calc-alkaline granitoids. ACG: amphibole-rich calc-alkaline granitoids. Barbarin (1999). b) The geological context of the Echassieres granitic complex (from Rocher et al. (2024) modified from Cuney et al. (1992) and Harlaux et al. (2017)). c) 2D model of the Beauvoir granite (from Rocher et al. (2024) modified from Cuney et al. (1992) and Monnier et al. (2018)).(28)

3 Lithium exploration

The Beauvoir granite is currently exploited for kaolin (**Fig.2a**), a secondary mineral phase resulting from the hydrothermal alteration of feldspar. In parallel, the deposit mining potential for metals has been investigated through several exploration campaigns, including (i) the GPF project; (ii) The 2018 campaign resulting in three exploratory drill holes (north, south, and center); and (iii) The exploration project launched in 2021 (EMILI), with a primary focus on lithium.

Classified as a critical raw material by the EU in 2020 (29), lithium has experienced an exponential rise in demand, mainly driven by the rapid growth of the electric vehicle market. In response, the EU, a global automotive leader (accounting for 25% of the global market) and a major advocate of the green transition, has set ambitious goals to become a major producer of lithium batteries (30), especially considering the dependency of the sector on external imports from limited geographical areas, potentially exposed to geopolitical risks posing a threat to EU industrial supply chains and economic stability. Currently, lithium battery and electric vehicle production are largely based in Asia (i.e., China, South Korea, and Japan) (31), while most lithium extraction, from the two primary deposit types, brine and hard-rock mineralizations, is dominated by Chile, Argentina, Australia, and China (32). To address its reliance on imports, the EU is investing substantially in developing domestic lithium projects and strengthening regional supply chains for raw materials extraction and end-product manufacturing. In this context, Imerys, the operating company of the Echassières site, launched a large-scale lithium exploration initiative (1), the Exploitation of Lithium Mica by Imerys (EMILI) project (**Fig.2**). The multi-phase drilling campaign launched in 2021 was conducted in three successive phases, extending through 2024. Over 80 drill holes were organized across the area. The total drilling length reached around 25,000 meters, with boreholes up to 500 meters deep. The program focused on the first magmatic unit of the Beauvoir pluton (Facies B1), previously identified as the most Li-enriched zone (15). The aims were to delineate the spatial distribution of Li-enriched zones to strategically position the underground mine, develop a comprehensive 3D model of the deposit by collecting structural, geophysical, and geochemical data to support the planning of subsequent phases (33). Geochemical analyses confirmed a significant lithium resource, with an estimated 116.7 million tonnes of mineralized rock containing an average Li-oxide (Li_2O) concentration of 0.9%, one of the highest reported for mica-based lithium deposits (34).

4 Geochemistry

4.1 Mineral composition

The mineralogical composition across the B1 unit is largely consistent in terms of major phases

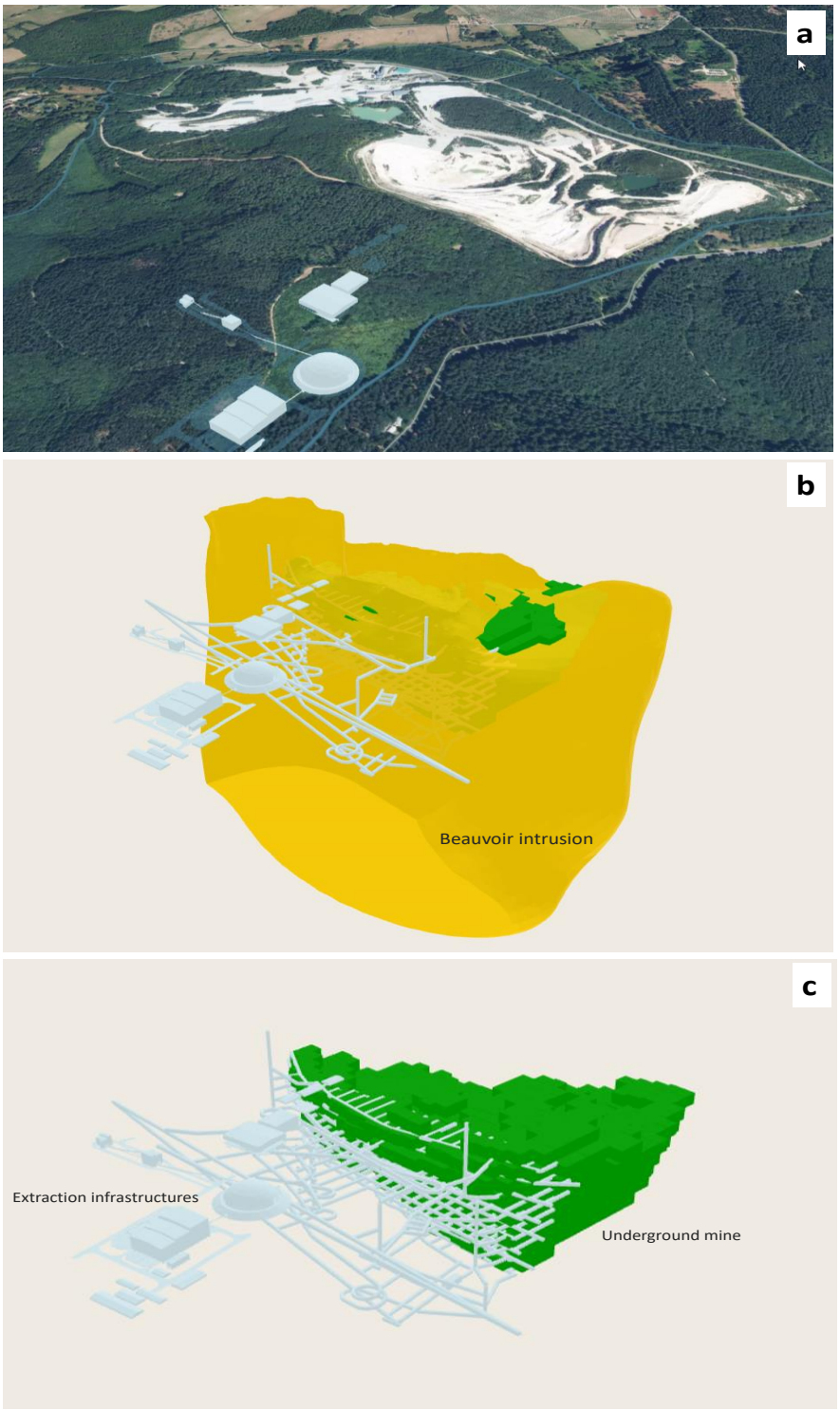

Figure.2. a) Satellite view of the Echassières mining site, highlighting the visible open-pit kaolin mine. b) 3D representation of the Beauvoir granite magmatic body. c) Schematic illustration of the underground mine (B1) and associated infrastructure planned for lithium extraction. Modified from Imerys documentation.

(13). The Beauvoir granite matrix is composed mainly of micas, feldspar, and quartz. Accessory minerals such as topaz, apatite, fluorite, zircon, kaolinite, and Fe-oxides have also been reported (13). Mineralization is mainly associated with Li-micas and Li-phosphates for Li, and cassiterite for Sn, while columbite-tantalite constitutes the Nb and Ta stock (17). Lepidolite, the dominant Li-bearing mineral (34), typically appears as fine-grained aggregates or rosette structures (18). Feldspars are mostly albite in B1, with a highly pure composition (XAn < 0.01), while K-feldspars proportions increase with depth (13). The fresh granite is hololeucocratic, ranging from white to grey, and displays a homogeneous equigranular, non-oriented texture throughout the pluton. However, local variations can be observed in mineral proportions, chemical composition of specific phases, and accessory minerals. Grain size and texture can also vary locally, especially at contacts with the host rock (aplitic texture), or in massive quartz veins (pegmatitic texture).

4.2 Geochemical composition (EMILI data)

Geochemical analyses, and logging data were made available to the research team. Although the complete dataset will not be discussed in this report due to confidentiality agreements, the general findings are presented in **Fig.3** and **Fig.4**. The logging data included visual descriptors of alteration type, lithological facies, color, visual estimation of mica content, texture, rock strength, grain size, and observed anomalies.

The logging data from 28 drillholes were analyzed to assess the homogeneity of the deposit in terms of alteration, hardness, and lithlogical facies (**Fig.3**). The rock sections are primarily fresh Beauvoir granite (GB), composing 69% of the logged intervals (**Fig.3b**). Other commonly observed facies include S (7%), GBG (6%), GBK (6%), M (5%), and AL (4%). Less common facies such as MQZ, GT, OGC, and OVB were also identified, but each represents less than 1% of the total logged sections. The depth distribution of kaolinized and greisenized facies (**Fig.3c** and **Fig.3d**) show that hydrothermal alteration is widespread throughout the deposit. The kaolinized granite is mostly concentrated in the upper 100 meters (65%), although isolated occurrences were recorded at depths up to 300 meters (8%) (**Fig.3c**). In contrast, greisen alteration appears to be more evenly distributed across all depths, even present in zones deeper than 300 meters (5%) (**Fig.3d**). Since alteration type is not directly correlated with rock strength, and the dataset does not differentiate between alteration intensities (e.g., low, moderate, or intense), rock hardness was evaluated separately (**Fig.3a** and **Fig.3e**), as it can significantly affect the laser ablation rate during LIBS analysis. The K/Na ratio was calculated for all available drillholes (n = 84) as a proxy for greisenization processes (35). The results indicate that 63% of the drillholes contained less than 25% greisen-logged intervals, 27% exhibited a moderate degree of alteration with 25–50% greisen intervals, and 10%

corresponded to highly altered drillholes, where greisenized zones accounted for more than 50% of the logged intervals (**Fig.3f**).

The geochemical data from different boreholes were plotted to study the distribution of major elements (Al, K, Na, Si, and Li) (**Fig.4**). The drillholes (n=10) were selected based on their minimal proportion of greisenized intervals, less than 10% of the total logged depth in each borehole, ensuring that the conclusions were coherent with the traget facies, the unaltered Beauvoir granite. Understanding the behavior of these elements at the deposit scale served: i) to assess the suitability of each element as an internal standard for normalizing the LIBS signal in the development of quantitative models, as an internal standard should exhibit stable concentrations or, at a minimum, a narrow, homogeneous range of values, and ii) to identify the full range of observed concentrations, from low to high values, to representative reference samples. Lithium exhibits considerable variability, ranging from low concentrations (< 1,000 ppm) to values exceeding 7,000 ppm. However, a cluster of values can be observed between 2,000 and 6,000 ppm, representing the dominant compositional interval for Li. Lower Li concentrations are generally observed in the upper sections of the boreholes, correlating with the high proportion of greisen and kaolinized portions (**Fig.3c** and **Fig.3d**). Additionally, the vertical distribution of Li is not uniform across boreholes, with concentrations at a given depth varying significantly between locations, highlighting the asymmetrical organization of the mineralization within the deposit, with distinct zones of enrichment interspersed within less mineralized area. Major elements (Al, Si, K, and Na) exhibits different patterns (**Fig.4**). The distribution of SiO2 is predominantly consistent, with an average concentration of approximately 70 wt.%. Localized positive anomalies in Si may be attributed to Massive Quartz Zones (MQZ). In contrast, Al_2O_3, Na_2O, and K_2O display pronounced fluctuations, likely reflecting hydrothermal alteration. Zones of Al depletion are especially evident in the uppermost 100 meters, with negative anomalies suggesting redistribution due to feldspar alteration or leaching. Sodium and potassium show highly irregular profiles, characterized by sharp concentration shifts; notably, low Na values are consistent with greisen alteration.

5 Conclusion

The Beauvoir granite provided an advantageous case study for developing innovative, field-adapted geochemical approaches for mining operations using handheld LIBS. The availability of extensive geochemical analyses significantly improved the geological understanding of the system and facilitated the development of representative models for both quantitative analysis and mineralogical characterization. In addition, this work offered the opportunity to test handheld LIBS method on a rare-metal granite deposit, an unconventional lithium source often less represented in favor of more established deposit types such as LCT pegmatites (36–39)

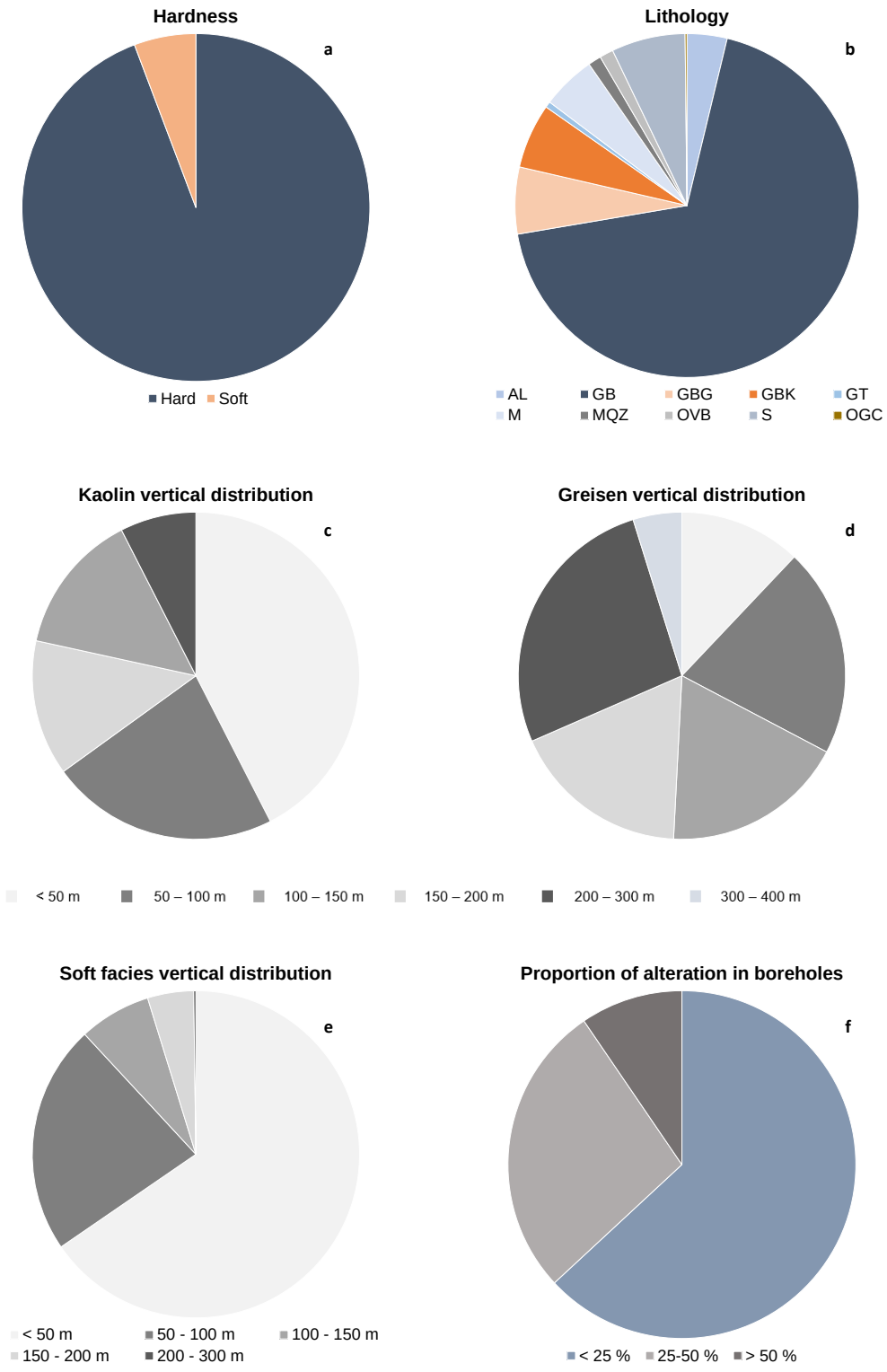

Figure.3. Logging data analysis: (a) Distribution of soft and hard rock facies; (b) Repartition of observed lithological facies, with facies abbreviations following Imerys nomenclature; (c, d) Vertical distribution of altered zones (kaolin and greisen); (e) Vertical distribution of soft rock (highly altered material); (f) Proportion of fresh, moderately altered, and highly altered boreholes based on logging descriptions, categorized by the percentage of altered intervals within each borehole (<25%, 25–50%, and >50%).

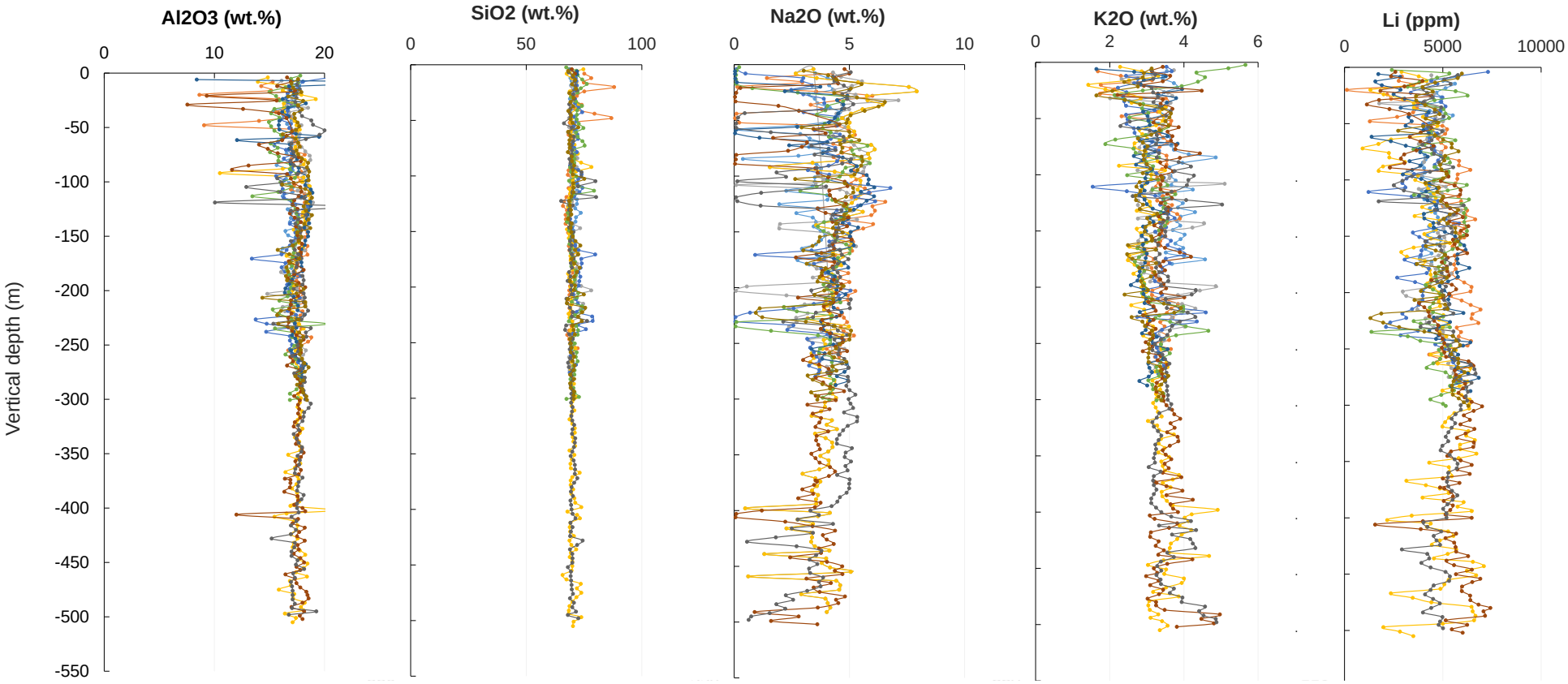

Figure.4. Vertical evolution of major elements (Al, Si, K, Na, and Li) composing the primary mineral matrix in the Beauvoir granite. The graph shows the variation in their concentrations as a function of depth, reflecting changes in lithology and alteration state. The colors correspond to the different drill holes selected.

or Li-rich brines (40), when developing LIBS quantitative models for Li. Participating to a large-scale exploration campaign also offered practical insights into the operational constraints and challenges associated with LIBS deployment in mining sites. These included considerations of sample variability, field logistics, and time efficiency. Such insights helped refine analytical protocols to ensure they were both technically robust and suited to the scale of material processed, balancing between prediction quality and analytical constrains. Discussing the results with the mining teams contributed to adressing the protocols developped in an industrial context, ensuring that the models and analytical strategies developed responded to actual operational needs and could support decision-making in future projects.

The unaltered Beauvoir granite (B1) facies, the primary target for lithium extraction was prioritized in the selection process of reference samples. However, even with drillholes positioned exclusively within the B1 unit of the Beauvoir intrusion (50 - 450 m) geochemical data and logging descriptions revealed considerable local variability (**Fig.3** and **Fig.4**). Lithological, geochemical, and textural variations are critical considerations when considering how to generalize LIBS-based models at the scale of an entire deposit. The LIBS models are developed and validated using a limited set of reference samples which, despite being sourced directly from the site, capture only a portion of the deposit broader geological heterogeneity. Parameters such as rock hardness, degree of hydrothermal alteration, and lithological diversity can significantly influence the LIBS signal and, consequently, the performances of the predictive models. In this context, the evaluation of the Beauvoir granite chemical and textural characteristics lead to several key questions: Which types of variability should be accounted for? To what extent should this variability be integrated? And what are the limitations of facies-based models in representing when applied under operational conditions.

Facies nomenclature

AL = albitized zone.

GB = unaltered Beauvoir Granite.

GBG = greisenized Beauvoir Granite.

GBK = kaolinized Beauvoir Granite.

GT = two micas Granite.

M = micaschist; the metamorphic host rock.

MQZ = massive quartz zone.

OVB = overburden; stracturally affected material above bedrock.

S = sediments.

OGC = granite colettes.

References

1. EMILI : Beauvoir Lithium Mining Project [Internet]. [cited 2024 Jan 10]. Available from: https://emili.imerys.com/en

2. El Haddad J, Canioni L, Bousquet B. Good practices in LIBS analysis: Review and advices. Spectrochimica Acta Part B: Atomic Spectroscopy. 2014 Nov 1;101:171–82.

3. Mezoued N, Fabre C, Cauzid J, Kim Y, Jatteau M. Analysis of Minerals Using Handheld Laser-Induced Breakdown Spectroscopy Technology. Data. 2025 Mar;10(3):40.

4. Cuney M, Marignac C, Weisbrod A. The Beauvoir topaz-lepidolite albite granite (Massif Central, France); the disseminated magmatic Sn-Li-Ta-Nb-Be mineralization. Economic Geology. 1992 Nov 1;87(7):1766–94.

5. Harlaux M, Mercadier J, Marignac C, Peiffert C, Cloquet C, Cuney M. Tracing metal sources in peribatholitic hydrothermal W deposits based on the chemical composition of wolframite: The example of the Variscan French Massif Central. Chemical Geology. 2018 Feb 20;479:58–85.

6. Monnier L, Salvi S, Melleton J, Bailly L, Béziat D, de Parseval P, et al. Multiple Generations of Wolframite Mineralization in the Echassieres District (Massif Central, France). Minerals. 2019 Oct;9(10):637.

7. Rosen A de. Évolution continue d'un massif granitique et succession minérale : le massif des Colettes (Échassières, Allier). Première partie : granites et micaschistes. Bulletin de Minéralogie. 1965;88(4):678–87.

8. Nicolas J, Rosen A de. Le massif granitique des Colettes (Allier) et ses minéralisations. Bulletin de Minéralogie. 1963;86(2):126–8.

9. Aubert G. Les coupoles granitiques de Monte- bras et d'Echassi&res (Massif Central frangais) et la gen&e de leurs min4ralisations en &ain, lithium, tungst~ne er b~ryllium. Thèse Fac Sc Clermont-Ferrand, et M6moire BRGM 46, 326 p. 1966;

10. M Cuney, A Autran. Objectifs généraux du projet GPF Echassières n°1 et résultats essentiels aquis par le forage de 900 m du granite albitique à topaze-lépidolite micas. 1987.

11. J. L. Vigneresse. Organisation tridimensionnelle du massif d'Echassières et bilan des mesures géophysiques de surface. Géologie profonde de la France. 1987;27–32.

12. Royer JJ, Danis M. Mise en evidence d'un phénomène de refraction thermique entre le granite de Beauvoir et son encaissant : mesures et modélisation. Géologie de la France. 1987;1(2–3):87.

13. Ph.Rossi, A.Autran. Log pétrographique et géochimique du granite de Beauvoir dans le sondage "Echassière I" Minéralogie ete géochimie comparées. Géologie de la France. n°2-3. 1987;111–35.

14. C.Gagny et T.Jacquot. Contribution de la pétrologie structurale à la connaissance des conditions de mise en place et de structuration complexe du granite des Colettes (massif d'Échassières). 1987;

15. L.Raimbault -C.Azencott. Géochimie des éléments majeurs et traces du granite à métaux rares de Beauvoir (sondage GPF, Echassières). Géologie de la france. 1987;189–98.

16. J.L. Duthou, C. Pin. Étude isotopique Rb-Sr de l'apex granitique d'Échassières (Granite des Colettes, granite de Beauvoir). 1987;

17. D. Ohnenstetter, P. Piantone. Caractérisation et étude des substitutions dans les minéraux du groupe des columbo-tantalites et des pyrochlores du granite de Beauvoir. 1987.

18. G.Monnier, B.Charoy, M.Cuney, D.Ohnenstetter, J.L.Robert. Evolution spatiale et temporelle de la composition des micas du granite albitique à topaze-lépidolite de Beauvoir. Géologie de la france. n°2-3. 1987;179–88.

19. Pichavant M. Experimental Crystallization of the Beauvoir Granite as a Model for the Evolution of Variscan Rare Metal Magmas. Journal of Petrology. 2022 Dec 1;63(12):egac120.

20. Harlaux M. Tungsten and rare-metal (Nb, Ta, Sn) hydrothermal metallogenic systems in the late-variscan orogenic context: example of the French Massif Central.

21. Michaud J. Les granites à métaux rares: origine, mise en place et mécanismes de la transition magmatique-hydrothermale. 2019;366.

22. C.Gagny. Organisation s´equentielle ´evolutive des intrusions successives du Granite de Beauvoir dans son caisson: Arguments g´eochimiques. G´eol Fr 2-3,. 1987;

23. Fréville K, Trap P, Faure M, Melleton J, Li XH, Lin W, et al. Structural, metamorphic and geochronological insights on the Variscan evolution of the Alpine basement in the Belledonne Massif (France). Tectonophysics. 2018 Feb 15;726:14–42.

24. J.L.Feybesse et M.Tegyey. Évolution tectonométamorphique dévonienne et carbonifère de la série de la Sioule. 1987;

25. Sylvester PJ. Post-collisional strongly peraluminous granites. Lithos. 1998 Dec 1;45(1):29–44.

26. Melleton J, Gloaguen E, Frei D. Rare-Elements (Li-Be-Ta-Sn-Nb) Magmatism in the European Variscan Belt, a Review. . Proceedings. 2015;2:5.

27. Cheilletz A, Cuney M, Charoy B, Archibald DA. 40 Ar/39 Ar ages of the Beauvoir topaze-lepidolite leucogranite and the Chedeville sodolithic pegmatite (North French Massif Central) Petrologic and geodynamic signification. Comptes Rendus de l'Academie des Sciences Serie 2. 1992 Jul;315(3):329–36.

28. Unravelling the magmatic and hydrothermal evolution of rare-metal granites through apatite geochemistry and geochronology: The Variscan Beauvoir granite (French Massif Central). Chemical Geology. 2024 Dec 20;670:122400.

29. Critical raw materials - European Commission [Internet]. [cited 2025 Apr 18]. Available from: https://single-market-economy.ec.europa.eu/sectors/raw-materials/areas-specific-interest/critical-raw-materials_en

30. Talens Peiró L, Villalba Méndez G, Ayres RU. Lithium: Sources, Production, Uses, and Recovery Outlook. JOM. 2013 Aug 1;65(8):986–96.

31. Kavanagh L, Keohane J, Garcia Cabellos G, Lloyd A, Cleary J. Global Lithium Sources—Industrial Use and Future in the Electric Vehicle Industry: A Review. Resources. 2018 Sep;7(3):57.

32. Mohr SH, Mudd GM, Giurco D. Lithium Resources and Production: Critical Assessment and Global Projections. Minerals. 2012 Mar;2(1):65–84.

33. DeepLime I x. EMILI - Lithium. [cited 2025 Apr 18]. EMILI : Projet d'exploitation du Lithium de Beauvoir. Available from: https://emili.imerys.com/accueil

34. Korbel C, Demeusy B, Kahou ZS, Filippova IV, Dehaine Q, Filippov LO. Flowsheet development for the selective flotation of lepidolite from the Beauvoir granite from mineralogical insights. Minerals Engineering. 2025 Jun 1;225:109207.

35. Cathelineau M, Kahou ZS. Discrimination of Muscovitisation Processes Using a Modified Quartz–Feldspar Diagram: Application to Beauvoir Greisens. Minerals. 2024 Aug;14(8):746.

36. Wise MA, Harmon RS, Curry A, Jennings M, Grimac Z, Khashchevskaya D. Handheld LIBS for Li Exploration: An Example from the Carolina Tin-Spodumene Belt, USA. Minerals. 2022 Jan;12(1):77.

37. Harmon RS, Wise MA, Curry AC, Mistele JS, Mason MS, Grimac Z. Rapid Analysis of Muscovites on a Lithium Pegmatite Prospect by Handheld LIBS. Minerals. 2023 May;13(5):697.

38. Dias F, Ribeiro R, Gonçalves F, Lima A, Roda-Robles E, Martins T. Calibrating a Handheld LIBS for Li Exploration in the Barroso–Alvão Aplite-Pegmatite Field, Northern Portugal: Textural Precautions and Procedures When Analyzing Spodumene and Petalite. Minerals. 2023 Apr;13(4):470.

39. Ferreira MFS, Capela D, Silva NA, Gonçalves F, Lima A, Guimarães D, et al. Comprehensive comparison of linear and non-linear methodologies for lithium quantification in geological samples using LIBS. Spectrochimica Acta Part B: Atomic Spectroscopy. 2022 Sep 1;195:106504.

40. Xing P, Dong J, Yu P, Zheng H, Liu X, Hu S, et al. Quantitative analysis of lithium in brine by laser-induced breakdown spectroscopy based on convolutional neural network. Analytica Chimica Acta. 2021 Sep 15;1178:338799.

Chapitre III.

The quantitative analysis of Li, and Rb using handheld

Journal of Geochemical Exploration 271 (2025) 107689

Contents lists available at ScienceDirect

Journal of Geochemical Exploration

journal homepage: www.elsevier.com/locate/gexplo

Handheld LIBS contribution to quantify critical elements during mining operations: The Beauvoir granite case study

Naila Mezoued *, Cécile Fabre, Jean Cauzid, Zia Steven Kahou, Océane Rocher

CNRS, GeoRessources Laboratory, Universit´e de Lorraine, Nancy F54000, France

ARTICLE INFO

Keywords:
Laser-induced breakdown spectroscopy
Quantitative analysis
Mining
Rare-metal granite
Lithium
Rubidium

ABSTRACT

Developing innovative methodologies has become essential for mining companies to optimize resource management and achieve economic sustainability. The spectroscopic techniques such as laser-induced breakdown spectroscopy (LIBS), used for on-site analyses, have great potential to provide reliable qualitative and quanti- tative geochemical data to support rapid decision-making. In this context, handheld LIBS was used to predict the concentrations of the main targeted elements lithium (Li), and rubidium (Rb), on unprepared core samples from the Beauvoir granite, a rare-metal granite currently studied to achieve lithium exploitation by 2028. The models were built using different spectral parameters and statistical approaches. A comprehensive comparative analysis was conducted to determine the optimal protocol for each element. Signal variation over successive measure- ments, as well as the minimum number of analyses required to maintain a representative LIBS signal of the whole rock composition, were investigated. The predicted concentrations are consistent with the reference geochemical analyses confirming the ability of handheld LIBS to provide relevant analytical results, in a short period, directly at the exploitation site.

1. Introduction

Mineral resources consumption has increased greatly during the last century (Lusty and Gunn, 2015). Meanwhile, the number of accessible high-grade mineral deposits decreased significantly, leading mining companies to consider more complex deposits resulting in substantial technological investments and higher production costs. As a result, the mining industry is facing new challenges to ensure a stable supply of mineral resources while maintaining economic viability and profitability.

The development of innovative geochemical methods is one solution to enhance operational efficiency and cost management. The use of handheld analytical devices such as LIBS (Laser Induced Breakdown Spectroscopy), XRF (X-ray Fluorescence), VNIR-SWIR (Visible-Near Infrared-Short-Wave Infrared), or RAMAN instrument have show great potential for geological materials analysis (Lemi`ere and Harmon, 2021; Young et al., 2016; Lemi`ere and Uvarova, 2019; Jehli˘cka and Culka, 2022). The spectral signal obtained can provide qualitative, quantitative, and mineralogical information directly on-site and in a short time compared to conventional laboratory analysis. Thus, beyond field observations, geologists can evaluate elemental composition and mineral occurrence to support cost and time-effective decision-making during the exploration or exploitation process.

LIBS, in particular, has seen growing interest in the geosciences community (Jolivet et al., 2019; Harmon et al., 2019; Harmon and Senesi, 2021; McMillan et al., 2014; Senesi and Harmon, 2023; Fabre, 2020). The potential to detect a wide range of elements simultaneously appeals to a scientific field where sample compositions are complex and chemical analyses using conventional procedures are expensive and time-consuming. The LIBS technique has been successfully applied to discriminate between minerals (Fabre et al., 2002; Fabre et al., 2021a; Romppanen et al., 2023; Khajehzadeh and Kauppinen, 2015; El Haddad et al., 2019; Rossi et al., 2014; McMillan et al., 2007; Pease and Tcha- kerian, 2014), gems (McManus et al., 2017; Farnsworth-Pinkerton et al., 2018; Defnet et al., 2021; McManus et al., 2008; Dubey et al., 2021; Syvilay et al., 2019), and rock samples (Senesi et al., 2023; Müller and Meima, 2022; Gottfried et al., 2009; Chen et al., 2022; El-Saeid et al., 2019; Han et al., 2018; Zhu et al., 2014; Roux et al., 2015; Panya et al., 2018). Also, as a rapid and non-destructive method, LIBS offers a faster alternative for chemical mapping by providing spatially-resolved geochemical data to visualize the distribution of trace and major elements in rock and mineral samples (Kuhn et al., 2016; Ribeiro et al.,

* Corresponding author.
E-mail address: naila.mezoued@univ-lorraine.fr (N. Mezoued).
https://doi.org/10.1016/j.gexplo.2025.107689
Received 13 June 2024; Received in revised form 18 December 2024; Accepted 26 January 2025
Available online 29 January 2025
0375-6742/© 2025 Elsevier B.V. All rights are reserved, including those for text and data mining, AI training, and similar technologies.

2021; Capela et al., 2023; Jain et al., 2018; Mohamed et al., 2021; Xu et al., 2016). While achieving reliable and reproducible quantitative analyses on geological materials using LIBS can be challenging (El Haddad et al., 2014), this application is spreading swiftly (Foucaud et al., 2019; Tucker et al., 2010; Fontana et al., 2023; Fagundes Fontana et al., 2022), especially, considering the LIBS ability to detect strategic light elements (Fabre et al., 2022; Xing et al., 2021), in particular Li which is not identified by other field analyzers, within a context of what is described as the "white gold rush" (Lafitte, 2023; EBSCOhost, 2024; Eisler, 2019).

Yet, LIBS application to raw and unprocessed rock remains limited (Fontana et al., 2023). Analysis of powders is by far the most favored method, as it facilitates the homogenization of element distribution in a sample at the laser beam scale (>50 μm), particularly, in geological materials, which typically are characterized by a multi-mineral composition coupled with intricate textures. Additionally, LIBS use aligns with established protocols acquired over decades of onsite analyses dominated by quantitative (XRF) (Da Silva et al., 2023; Fisher et al., 2014). Indeed, crushing heterogeneous material to smaller particles allows for more precise predictions (El Haddad et al., 2014), but does significantly extend acquisition times and takes little consideration of the challenges and the technological constraints associated with mineral exploration. Preparing and analyzing powders takes time, especially during a drilling campaign, in which the volumes of extracted rock are substantial. The possibility of analyzing entire drill core sections, with no prior processing, as will be demonstrated by the results described here, confirms handheld LIBS as an effective and reliable multi-element quantitative technique, suitable for large-scale operations, such as ore prospecting. Ultimately, handheld LIBS analyses could be included in the first stages of ore exploration, focusing on exploitable or pathfinder elements on untreated compact targets, to more advanced stages of exploitation, on extracted rocks in powder form (Foucaud et al., 2019).

The focus of this study was to develop a practical and time-efficient solution for on-site geochemical analyses. During drilling campaigns for ore exploration, the volume of rock samples extracted is often substantial. In the case of the Beauvoir granite, eighty boreholes were drilled over three stages to refine geological models and develop an effective exploitation strategy. This results in hundreds of meters of core samples being transported for crushing and chemical analysis. The timeframe from drilling to the availability of element concentrations can range from several weeks to months.

Integrating handheld LIBS during prospecting aims to enhance on-site decision-making by providing near real-time chemical data on the targeted element. Access to immediate response can guide the operating team in making strategic decisions about whether to continue or cease drilling, or whether to reposition or add additional drilling sites, choices that can impact both costs and delays. While LIBS cannot replace conventional laboratory geochemical analyses, which are essential for precise economic evaluations, it serves as a valuable supplementary tool for optimizing financial and human resources in the quest for mineral resources.

In this study, an analytical protocol was followed to build and compare different quantitative models to determine the optimal approach for each of the targeted elements, Li and Rb. The consistency of the results obtained on successive measurements on the same sample was investigated to ensure prediction reliability. Finally, alternative acquisition parameters were tested from the perspective of reducing the acquisition time, considering the size (4 m) of the analyzed rock samples.

2. Background

Quantitative data are crucial at every stage of mining operations. During prospecting, large-scale surveys are designed to collect geochemical data within defined geographical limits (Li et al., 2014; Salminen and Tarvainen, 1995). The concentrations of major and trace elements, as well as isotopes, are measured in various materials, such as soils, outcrops, stream sediments, and regoliths. The spatial distribution of specific elements can reveal geochemical anomalies or hidden patterns at a regional scale, providing valuable clues for geologists to prioritize and delineate high-potential zones for detailed investigation (Grunsky, 2010). Advanced exploration campaigns involve more localized analyses, typically conducted on core segments from systematic drilling campaigns (i.e., EMILI21 project (EMILI, n.d.)). Elemental analysis, focused on the targeted elements, contributes to refining the geological knowledge of the deposit and build 3-D models of the ore body, providing insight into the project economic viability. Continuous monitoring using quantitative geochemical data is crucial during ore extraction. Regular analyses of processed ore and tailings are conducted to ensure optimal ore recovery. In this context, the idea of identifying and quantifying chemical elements in geological samples, beyond the limits of laboratory techniques, represents a significant improvement in the mining industry (Senesi et al., 2020).

The growing interest in handheld LIBS applications for mineral resources is largely driven by the expanding lithium industry. Lithium has emerged as a strategic element in recent years due to its unique physicochemical properties, becoming quickly essential in numerous industrial supply chains (e.g., batteries, ceramics, pharmaceuticals, and technological devices) (Talens Peiro´ et al., 2013; Oruch et al., 2014; USGS, n.d.). Therefore, the ability of LIBS to detect light elements, including lithium, has positioned handheld LIBS as a game-changer in lithium exploration, especially considering the limitation of handheld XRF in detecting elements with low atomic numbers (atomic number < 11). Handheld LIBS can both identify lithium in samples, even at very low concentrations (LOD around 10 ppm) (Fabre et al., 2022), and quantify its levels across various sample types (i.e., pegmatites, brines, ect) using customized quantification models (Xing et al., 2021; Ferreira et al., 2022). As a result, the application of LIBS to lithium exploration and analysis has become one of the leading areas of research and publication in recent years, further fueling the mining sector's curiosity for LIBS technique (Laser-Induced Breakdown Spectroscopy, 2024).

In hard rock deposits, lithium is disseminated in specific minerals such as spodumene, petalite, and Li-rich micas. Determining the type, composition, and proportion of the Li-bearing phase in a rock is essential for evaluating the potential of a deposit, which can be a challenging task on-site. Fabre et al., (Fabre et al., 2021a) used a handheld LIBS analyzer to identify the spectral signatures of Li-bearing minerals, including spodumene, petalite, lepidolite, zinnwaldite, amblygonite, and montebrasite. The study, conducted on macroscopic mineral samples, thin sections, and powder pellets of pulverized minerals, characterized the signals from major elements (Li, Al, Si, K, Fe, Na) and trace elements (Rb, Cs, Be, Ba, Mn, Mg) specific to each mineral phase. The spectra gathered (> 4000 spectra) can be used for quantitative analysis or as training data for classification or clustering algorithms. Following this study, in Fabre et al., (Fabre et al., 2022), the relative intensities of Si, Al, and K were measured to differentiate the spectra from petalite, spodumene, and lepidolite samples, which can be difficult to distinguish visually on outcrops due to their similar physical characteristics. Additionally, a calibration curve was built to predict lithium content in the same mineral samples. The results were consistent with conventional methods, providing rapid analysis with a RMSE (Root Mean Squared Error) of 0.19 wt% Li. In a similar approach, the work of Dias et al., (Calibrating a Handheld LIBS for Li Exploration, 2024) on the Barroso-Alva˜o aplite-pegmatite field led to the development of two calibration curves for determining the concentrations of Li, Al, and Si in spodumene and petalite samples. The results exhibited errors of <20 % when compared to reference data obtained through ICP-MS. Since spodumene, petalite, and K-fedspar can display similar physical characteristics, a qualitative calibration curve was first developed to differentiate between the three minerals.

Wise et al., (Wise et al., 2022) and Harmon et al., (Harmon et al.,

2023) investigated the potential of handheld LIBS analyzer to differentiate between barren and fertile pegmatites using the K/Rb signal ratio and Li concentration in muscovite. Muscovite can serve as a mineralization vector (Steiner, 2019) when spodumene is absent from outcrops for chemical analysis. Additionally, Harmon et al. (Harmon et al., 2023) developed calibration curves using the handheld LIBS analyzer to determine Li, K, and Rb concentrations in muscovite samples containing Li (0–3 wt%), K (0–12 wt%), and Rb (0–1 wt%). Quantitative analyses were performed both in the laboratory and on-site, including on mica from drill cores, pegmatite outcrops, and muscovite in soil samples.

For estimating lithium concentrations in rock samples, the study of Wise et al., [64]focuses on pegmatite deposits, which are the primary source of hard rock Li production. A set of calibration curves covering low- and high-range Li concentrations were constructed using pressed pellets from 1-m core intervals of ground pegmatite segments (Li = 0.015–1.12 wt%). The quantification models were then tested on pegmatite samples from the Kleiber Oy lithium deposit in western Finland (Li = 0.01–1.12 wt%), yielding reliable results (Li LIBS = 0.941 × Li assay, R^2 = 0.97). However, when soil samples were analyzed using the pegmatite powder calibration, the results were less accurate (Li LIBS = 0.828 × Li assay, R^2 = 0.18). The results confirm the effectiveness of handheld LIBS for on-site quantitative analysis of rock samples, while emphasizing the importance of using matrix-matched samples during the development and application of calibration models.

Lithium quantification is also critical during mineral processing. The study of Korbel et al., (Korbel et al., 2024) evaluated the capacity of handheld LIBS and XRF in assessing lithium concentrations, both directly and indirectly, in powder pellets of granite that have undergone multiple processing steps. Multiple LIBS measurement points were averaged to simulate bulk composition for each sample. A multivariate linear regression model was developed using signals from Li and matrix elements, including Rb, Cs, and K. Although LIBS produced accurate lithium predictions, achieving optimal performance required more analytical steps (i.e., pulverization, pellet formation, grid analysis) than Energy Dispersion-XRF technique. The LIBS method was deemed the most suitable for detecting low-moderate lithium concentrations (below 1 wt%).

Lithium quantification in geological samples using handheld LIBS analyzer has been extensively studied, but the models developed focusing on Li-rich minerals (Fabre et al., 2021a; Fabre et al., 2022; Harmon et al., 2023) or pulverized rocks (Wise et al., 2022; Korbel et al., 2024), address only part of the challenges faced during mining operations. The volume of rock extracted during exploration and exploitation operations is substantial, while on-site resources remain limited. Consequently, the use of models that require pressed pellets is impractical under field conditions. Furthermore, detailed analyses using mineral-based models are not appropriate, as for estimating grades across the deposit, the spatial distribution of lithium proportion is determined using rock segments that may extend several meters in length.

This study aims to address the question of on-site lithium quantification while accounting for the operational conditions of a mining project. The methodological approach developed focuses on raw rock samples without prior treatment (i.e., grinding, homogenization) to facilitate the seamless integration of the technique into routine core processing procedures. Additionally, this study marks the first application of handheld LIBS quantification on rare-metal granite. The Beauvoir deposit is considered as an unconventional lithium source since lithium is traditionally extracted from two primary sources: pegmatites and brine (Kesler et al., 2012). The growing global demand has pushed the industry to explore alternative options to diversify supply chains (Demeusy et al., 2023; Zhao et al., 2023). Although exploiting this kind of deposits requires more resources than conventional sources, where well-established extraction techniques offer more cost-effective production.

Furthermore, developing this work during an ongoing exploration project has provided practical feedback and raised several key questions such as: Are the predicted values consistent and reliable over different measurements? To what extent can the acquisition time be minimized given the size of the studied segments? What are the limits of the models developed?

3. Case study

The Beauvoir rare-metal granite was thoroughly studied in the 1980s during the first GPF (G´eologie Profonde de la France) project (Cuney and Autran, 1987). Yet, the increasing need for Li renewed the scientific and economic interest in this geological prospect. Currently, an extensive drilling campaign (EMILI21), supervised by Imerys S.A., (Paris, France), the operating company, aims to refine the geological model of the deposit and plan the beginning of Li extraction by 2028 (EMILI, n.d.). The selection of the Beauvoir granite was motivated by several factors: i) the exceptional concentrations of lithium and rubidium: ii) the availability of fresh and diverse granite samples and the associated geochemical data; and iii) the opportunity to engage in an ongoing exploration campaign, to get a better understanding of the expectations and constraints of a mining company during on-site operations.

3.1. Geological setting

The Beauvoir granite is located in the northern part of the French Massif Central within the internal domain of the Variscan chain (Feybesse and Tegyey, 1987). It represents only a fraction of the Echassie`res magmatic massif extending over 65 $km^3$ (Vigneresse, 1987). The Echassie`res magmatic complex, a dome-shaped structure intruding the Sioule metamorphic sequence (Grolier, 1971; Ledru et al., 1989), is composed of two outcropping granite units, the biotite-muscovite-cordierite Colettes granite and the topaze-albite-lepidolite Beauvoir granite. A hypothetic third unit, less evolved, the La Bosse granite, is thought to be buried at greater depth and linked to the ferberite stockwork (Aubert, 1969; Cuney et al., 1992; Harlaux et al., 2017). The crystallization of the Beauvoir granite was dated at 308 ± 2 Ma and 317 ± 8 Ma (Monnier, 2018; Alexandre et al., 2002; Cheilletz et al., 1992) is described to be the latest episode of successive magmatic intrusions during a compressive episode at the end of the Carboniferous. While the specific process leading to this type of enriched granites is still debated, several hypotheses have been proposed ranging from fluid transfer of the rare-metal at the top of a silicic magma chamber (Kovalenko and Kovalenko, 1984) to a direct melting of an anomalous source (Cuney et al., 1992). In the case of the Beauvoir granite, the model widely accepted implies that the rare-metal enrichment is linked to purely magmatic processes (e.g., partial melting and fractional crystallization) (Cuney et al., 1992; Pichavant, 2022), although meteoric fluids played a secondary role in remobilizing some of the elements (Rossi et al., 1987; Charoy et al., 2003).

3.2. Geochemistry

The superficial part of the Beauvoir granite was altered by hydrothermal circulation resulting in greisenization and kaolinization. The unaltered rock, present at depths (> 100 m), is organized from top to bottom in three separate petrographic facies, B1, B2, and B3 (Rossi et al., 1987). The three units are delimited by geochemical discontinuities (Raimbault and Azencott, 1987) and are described as the results of successive magmatic pulses (Jacquot, 1990). The Beauvoir leucogranite deposit is characterized by high concentrations in Li (>8000 ppm), Rb (>5000 ppm), Cs (>1000 ppm), Nb (>300 ppm), Ta (>500 ppm) and Sn (>7000 ppm) (Imerys, unpublished data).

In terms of mineralogy, the pluton maintains a relatively uniform composition, although variations in major and trace elements from top to bottom affect the chemical composition of specific phases, as well as, the occurrence or disappearance of certain accessory minerals within

each facies. The matrix is predominantly composed of quartz, feldspars, and micas. The feldspars transition from Na-rich albite in the upper sections of the granite to K-rich orthoclase in the B3 unit. Li mineralization is primarily contained in Li-rich micas (Demeusy et al., 2023), lepidolite ($K(Li,Al)_3(Si,Al)4O_{10}(F,OH)_2$) and zinnwaldite (KLi-Fe)Al2$Si_3O_{10}(F,OH)_2$). Although Li-rich phosphate minerals such as amblygonite ($(Li,Na)AlPO_4(F,OH)$) and montebrasite $LiAl(PO_4)(OH,F)$ have also been observed, they are not targeted for Li extraction due to processing challenges (Demeusy et al., 2023). Accessory mineral phases present are cassiterite, niobium-tantalite, topaz, zircon, fluorite, and apatite (Rossi et al., 1987). Of the three units composing the Beauvoir granite, the B1, which extends from 100 to 420 m (Rossi et al., 1987; Raimbault and Azencott, 1987), is the most enriched and the main target for critical elements exploitation, and therefore the focus of our study.

4. Methodology

4.1. Sample description

Eleven hand samples (12x5x0.5 cm) and four drill core segments (400x5x3 cm) from the Beauvoir granite were analyzed using handheld LIBS. Considering the impact of matrix effects on LIBS signal (Tognoni and Cristoforetti, 2016; Wang et al., 2021), choosing reference samples from the deposit is necessary to build quantification models that are accurate and adapted to the characteristics of the samples to be analyzed. No prior preparation was conducted, but a flat and smooth surface was required to limit signal fluctuation (Mao et al., 2004; Lednev et al., 2023). The samples were specifically selected to cover the broad range of concentrations observed for Li [min = 120 ppm, max = 9360 ppm, mean = 3411 ppm] and Rb [min = 0.5 ppm, max = 6180 ppm, mean = 2759 ppm] in the Beauvoir granite. The drill core sections used were either unaltered or presented low alteration percentages. The highly greisenized or kaolinized facies, not targeted for Li extraction, were excluded as they represents a significant textural variation. Three additional granite samples from the FMC region (i.e., Fabras granite, Quatre-Vios granite, and Laulagn´e granite) were used to extend the calibration curves to low values (Li > 400 ppm). Additionally, a set of twenty test samples were analyzed to evaluate and compare the different calibration models built for each element.

Reference geochemical data were obtained using ICP-AES for major elements, ICP-MS for trace elements, and ICP-OES for Li. Elemental concentrations of the drill core segments were obtained from the analysis of 2–4 m intervals of drill core that were reduced to powder and homogenized.

4.2. Handheld LIBS analysis

Similar to a laboratory instrument, the handheld LIBS analyzer focuses a rapidly pulsed high-energy laser onto the surface of a sample to vaporize a fraction of the material and create a micro-plasma plume. As the surplus of energy is expelled from the plasma in the form of photons, when the excited atoms, ions, and molecules within the plasma return to low energy levels. The plasma light is collected through detectors and then processed by spectrometers. The spectra obtained record the signal intensity at each wavelength. The elemental composition of the sample is revealed by the presence of emission lines or molecular bands at distinct wavelengths.

The specific instrument used is a Z300 handheld LIBS analyzer manufactured by SciAps Inc. (Woburn, MA, USA). It is equipped with a high energy 1064 nm pulsed Nd-YAG laser that delivers 5–6 mJ per pulse at a repetition rate up to 50 Hz. Three compact CCD spectrometers cover a spectral range from 190 to 950 nm allowing the detection of both major and trace elements present in a geological sample above their intrinsic limit of detection. The acquisition process is performed at atmospheric pressure and ambient temperature but under constant argon flush to enhance signal intensity. The compact dimensions of the analyzer (size = 20x28x10 cm, weight = 1.8 kg) and a total of 4 h of autonomy per battery charge, make it convenient for field uses.

4.3. Signal acquisition

When analyzing heterogeneous materials, a key factor is the strategy employed to achieve a representative LIBS signal of the bulk sample composition (Fabre, 2020; El Haddad et al., 2014). This is particularly significant for rock samples because despite creating a crater during laser ablation, only a very small amount of the material is analyzed. In contrast to the surface analysis using LIBS, the geochemical values used as reference are typically obtained from crushed and homogenized volumes of rocks. A common LIBS (and XRF) practice is the use of powder pellets to ensure compositional uniformity of heterogeneous samples (Foucaud et al., 2019; Wise et al., 2022; Rosenwasser et al., 2001). However, for on-site applications, such an approach extends considerably the analytical procedure and imposes additional technical constraints and costs. Several studies have demonstrated that the average signal obtained by increasing the number of analyzed spots on a sample surface is an effective way to represent the composition of heterogeneous materials, as well as minimizing the effects of local irregularities (e.g., surface texture, chemical gradient, etc.…), not only in powdered samples but also on raw geological samples (Fontana et al., 2023; Fabre et al., 2022; Salle´ et al., 2006; Agresti et al., 2022).

In the case of the Beauvoir granite, the LIBS crater at each spot has an average size of 250 μm. This implies that at the scale of the textures observed in the B1 unit, grain size varying between 50 and 600 μm for major minerals, the signal obtained per spot would more likely represent a single mineral of the matrix (e.g., quartz, Li-micas, or feldspar) or a mixture of two minerals, rather than the composition of a whole rock. Thus, to obtain the average LIBS bulk signal per sample, a systematic approach was implemented. One analysis point was placed every centimeter to create a vertical profile covering the total length of the granite samples. The smaller hand samples (3x2x1 cm) were analyzed using a rectangular grid covering both the top and bottom surfaces. An analysis point corresponds to 36 spots organized in a 6 × 6 square pattern to cover the maximum surface allowed by the analysis window of the LIBS analyzer. The LIBS spectrum recorded at each spot is an average of four laser shots to limit shot-to-shot variations. An initial cleaning shot was fired to remove any possible surface contamination. One analysis point takes <30 s at a frequency of 10 Hz. The samples must be completely dry during acquisition. High moisture content impacts the LIBS spectra, causing the widening of the hydrogen peak at 656 nm and reducing the total emission intensities, due to significant effects on plasma formation (i.e., plasma temperature, electron density, plasma size, and ablated mass) (Chen et al., 2015; Rauschenbach et al., 2008). The processing of LIBS spectra, including baseline correction, normalization (e.g., SNV, normalization to the total spectrum area), and the extraction of the spectral parameters of interest, were executed using Spectragryph software (Menges, n.d.).

4.4. Quantitative models

Determining the optimal model for a given element is not a straightforward process using the LIBS technique. It is common to adopt a trial-and-test strategy by building multiple models while varying the spectral parameters, preprocessing techniques, and statistical approaches. Fig. 1 illustrates the reasoning behind the different calibration models tested for the Beauvoir granite. The spectral parameters computed from both raw and normalized spectra to build univariate linear regression models include: i) the individual signal from a major emission line (i.e., selected based on maximum intensity), ii) the total signal from the element across specific emission lines, iii) the signal ratio obtained by dividing the signal from the elements by the signal from other elements related to the matrix composition or the analyte distribution. In the case of the multivariate method, partial least square

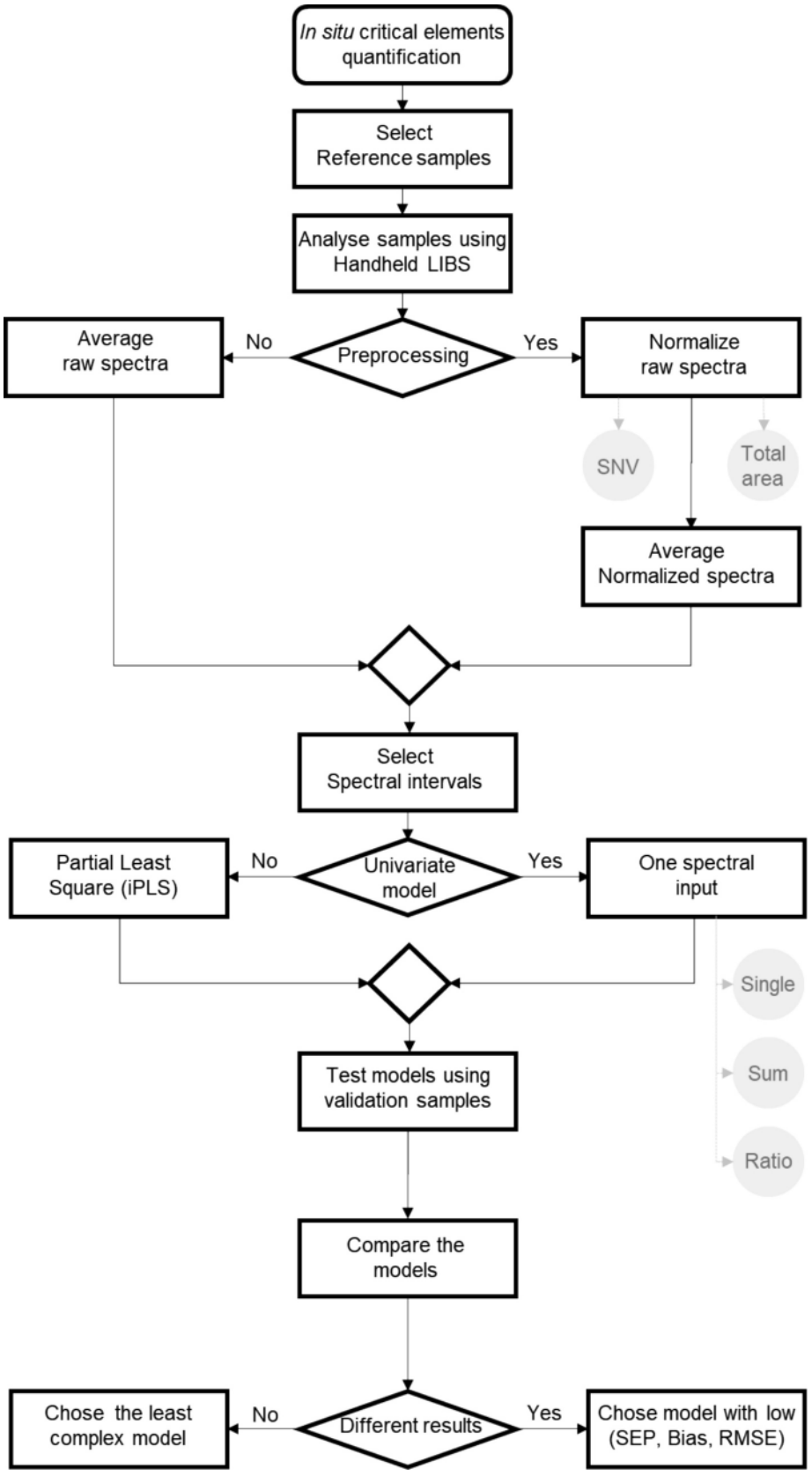

/ig. 1. The analytical protocol followed to build and test the LIBS quantification models for Li and Rb on the Beauvoir granite samples.

regression was applied using specific spectral intervals (iPLS), that encompassed the signal of the targeted element, lithium or rubidium, as well as major and trace elements present in the Beauvoir granite. The ultimate number of factors and variables used for the final iPLS model was determined by combining iterative training and testing steps (i.e., k-fold cross-validation, loadings plot).

The coefficient of determination (R^2), the Root Mean Squared Error (RMSE), and the Mean Absolute Error (MAE) were calculated to assess the performance of the various models developed for each element.

These metrics, as detailed in eqs. (1), (2), and (3), offer an understanding of the goodness of fit (R^2), the accuracy of predictions (RMSE), and the magnitude of errors (MAE).

$$R^2 = \frac{SS_{residual}}{SS_{total}} \quad (1)$$

- SSresidual is the sum of squared differences between the reference element concentration and the predicted element concentration, and SStotal is the total sum of squared differences between the reference element concentration and the mean of the element concentration.

$$RMSE = \sqrt{\frac{1}{n}\sum_{i=1}^{n}(y_i - y_i)^2} \quad (2)$$

$$MAE = \frac{1}{n}\sum_{i=1}^{n}|y_i - y_i| \quad (3)$$

- n is the number of data points, y_i is the reference element concentration for the i observation, and y_i is the predicted element concentration for the i observation.

The selection process of the optimal models involved a two-step statistical procedure. The concept of it, originally proposed by Pitman in 1939 (Pitman, 1939) and comprehensively described in the recent work of Duponchel et al., (2023) (Duponchel et al., 2023), aims to determine if the results of two populations of data present a significant statistical difference. The calculation steps, including Bias (Eq. 4) and the Standard Error of Prediction (SEP) (Eq. 5), along with the corresponding MATLAB code used, are available in L.Duponchel et al., 2023 (Duponchel et al., 2023).

$$Bias = \frac{1}{n}\sum_{i=1}^{n}(y_i - y_i) \quad (4)$$

$$SEP = \sqrt{\frac{\sum_{i=1}^{n}((y_i - y_i) - bias)^2}{n-1}} \quad (5)$$

- n is the number of data points, y_i is the reference element concentration for the i observation, and y_i is the predicted element concentration for the i observation.

5. Results

5.1. Element detection

Fig. 2 displays an example of the average LIBS signal obtained for granite samples presenting high and low Li concentrations. An essential step when developing quantitative models using LIBS data is selecting appropriate spectral intervals devoid of any interferences from matrix elements. In particular, given the broad spectral range (190–950 nm) of the handheld LIBS analyzer which includes, potentially, all the chemical elements composing the Beauvoir granite, increasing the risk of emission lines overlapping. The LIBS spectra revealed that Li is primarily observed at 610.33 nm and 670.75 nm, aligning with prior studies (Fabre et al., 2021b). Additionally, two emission lines in the Near Infrared Region at 812.66 nm and 922.40 nm, along with a triplet in the visible spectrum at 460 nm, were recorded. However, referenced emission lines at 274, 367, 391, 413 and 427 nm (NIST, 2016) were either undetected or disregarded due to interference with other elements (e.g. Al, Si, etc.). Spectral intervals were defined for the emission line selected to extract the integral of signal intensity, as this commonly yielded superior results compared to alternative spectral parameters (e.g. signal intensity). The Pearson correlation coefficient (R) was calculated (Table 1) to confirm the strength of the linear relationship between the targeted element signal and its abundance in the analyzed samples. The Li emission lines selected have R values ranging from 0.96 to 0.82 indicating strong positive correlations between the signal extracted and the element abundance. As for Rb signal, the two characteristic emission lines at 794.2 nm and 779.95 nm display values of the Pearson coefficients equal to 0.86 and 0.70, respectively. No additional emission

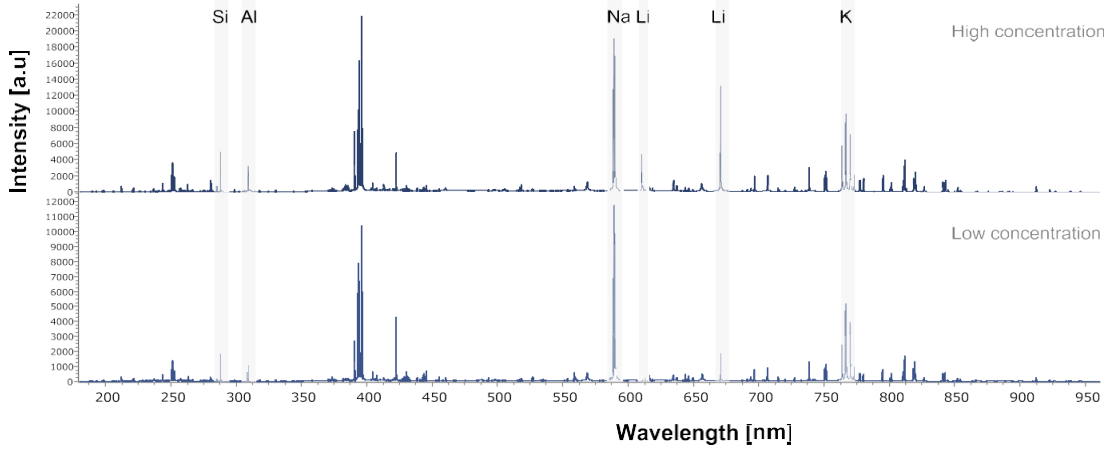

/ig. 2. An example of handheld LIBS spectra (190-950 nm) for low and high-concentration samples from the Beauvoir granite deposit.

Table 1
The Li and Rb emission lines observed in the LIBS spectra, including their specific locations, the spectral ranges determined for signal extraction and the Pearson coefficient calculated using the reference geochemical data.

Emission line	Wavelength (nm)	Spectral range (nm)	Pearson coefficient
Li I	670.75	670.45–671.10	0.96
Li I	610.33	610.05–610.65	0.96
Li I	460.74	460.55–460.90	0.82
Li I	812.66	812.35–812.90	0.93
Li I	922.40	922.15–922.60	0.58
Rb I	779.95	779.60–780.30	0.93
Rb I	794.80	794.40–795.40	0.84

lines were identified for Rb. The signal of matrix elements, Si (288.05 nm), Al (309.15 nm), K (766.33 nm), Na (589.14 nm), Cs (852.20 nm), Mn (259.25 nm), and Be (312.98 nm), were extracted to be tested in the multivariate and signal ratio models.

5.2. Quantification models

The device software, Profile Builder, can be used to build internal calibration curves (Wise et al., 2022; Fabre et al., 2021b). Once developed, a calibration is instantly operational, minimizing the need for additional processing time. However, the substantial size of the drill core portions (2-4 m), necessitates a considerable number of analyses, between 200 and 400 points, exceeding the maximum permissible number of spectra using the Z-300 analyzer interface. Therefore, developing the models externally was preferred. Each reference sample is represented by an average spectrum calculated from the total number of spectra acquired per sample (400–14,500). This strategy was designed to accurately portray the multi-mineral composition of granite. The LIBS being a surface analysis technique, only a fraction of the material is extracted (µg) during plasma formation. Meanwhile, conventional geochemical analyses that provide the reference concentrations are typically conducted on a volume of rock powder. The gap between the amount of material analyzed and the heterogeneous nature of geological materials emphasizes the challenge of quantitative analysis of rock samples using the LIBS device.

The quantitative values obtained can be found in Table S1 and Table S2. The coefficients of determination R2 in Table 2 describe the proportion of variance explained between the average LIBS signal and the proportion of the targeted element in the analyzed rock. The high values ($R^2 > 0.80$) of the Li models imply that the sampling strategy used effectively represents the composition of the granite samples. The results of Rb quantification models show less uniformity, with two discernible groups: models with limited representativeness ($R^2 < 0.62$) and more efficient models demonstrating R^2 values higher than 0.80. Consequently, these less representative models were preliminarily excluded, while the different Li quantification models were all retained for the statistical comparative analysis using the test samples. The statistical metrics, RMSE and MAE (Table 2) were calculated to evaluate the predictive performance of the different models. Low values of RMSE and MAE suggest the ability of a model to generate predictions close to the actual concentrations. In the same way, it allows us to observe if a specific statistical approach or spectral parameter systematically improves prediction. RMSE varies from a minimum of 0.04 wt% to 0.10 wt % for Li, while it ranges between 0.03 wt% and 0.15 wt% for Rb models. The MAE is generally higher for Li models compared to the RMSE, whereas it tends to be lower for Rb models. The absolute error ranges from 0.044 wt% to 0.14 wt% for Li, and from 0.02 wt% to 0.09 wt% for Rb. Normalizing the LIBS spectra improves the performance of the multivariate models (iPLS), but has an inverse effect on univariate models using a major emission line signal or the signal sum of multiple emission lines.

To understand the errors within the scale of concentrations studied, normalized values of RMSE and MAE (i.e., NRMSE and NMAE). Dividing the error metrics by the range of the observed values provides a standardized way to evaluate and compare models, in addition to offering a more intuitive understanding of the magnitude of errors relative to the scale of the predicted values. Low percentage values indicate predictions that are close to the reference values, reflecting good accuracy while high percentage values suggest poor model performance. The results presented in Table 2 show NMRSE values ranging from 10.0 % to 28.8 % for Li models, with a median value of 17.7 %, while, Rb models error percentages range from 10.2 % to 43.2 %, with a median value of 21.5 %. The models predictions, on average, deviate about 23.8 % from the observed values for Li and 20.2 % for the Rb models.

5.3. Statistical comparison

When developing multiple models to quantify a specific element, it implies comparing their respective performances to determine the optimal solution. A preliminary assessment can be performed using

Table 2
The calculated values of Mean Absolute Error (MAE), Root Mean Squared Error (RMSE), and R-squared (R^2) to assess the predictive power of the different LIBS quantification models developed for Li and Rb.

Element	Model	Preprocessing	R^2	RMSE (wt%)	MAE (wt%)	NRMSE (%)	NMAE (%)
Li	Li *670 nm*	Raw spectra	0.93	0.07	0.08	19	21.8
		SNV	0.83	0.11	0.10	28.8	28.3
		Total spectrum	0.93	0.07	0.08	18.2	20.8
	Sum signal	Raw spectra	0.93	0.07	0.08	18.6	21.3
	Li	SNV	0.89	0.09	0.10	23.8	26.5
		Total spectrum	0.94	0.06	0.08	17.3	21.1
	Ratio	Raw spectra	0.94	0.06	0.04	16.7	11.8
		SNV	0.95	0.06	0.14	16.5	38.2
		Total spectrum	0.95	0.06	0.14	16.5	38.1
	iPLS	Raw spectra	0.93	0.07	0.08	18.5	21.9
		SNV	0.98	0.04	0.06	10.1	17.2
		Total spectrum	0.96	0.05	0.07	13.5	18.5
Rb	Rb *779 nm*	Raw spectra	0.86	0.05	0.06	20.9	23.9
		SNV	0.41	0.11	0.09	43.9	37.3
		Total spectrum	0.61	0.09	0.08	35.1	33.5
	Sum signal	Raw spectra	0.85	0.06	0.04	22.1	15.3
	Rb	SNV	0.22	0.12	0.08	49.9	30.2
		Total spectrum	0.55	0.10	0.06	38.2	24.1
	iPLS	Raw spectra	0.92	0.04	0.02	16.1	9.5
		SNV	0.93	0.04	0.07	15.5	27.4
		Total spectrum	0.96	0.03	0.06	10.6	25.3

metrics such as R^2, RMSE, and MAE, allowing a comprehensive understanding of both the predictive capacity and how well a model fits the evolution of the element in the reference samples. However, these parameters only define a model individually and do not examine the differences between the results obtained while considering the variability of the input data or the uncertainties linked with the model fitting process (Duponchel et al., 2023).

To address this limitation, the statistical comparison of Li and Rb quantification models was based on a two-step mathematical protocol (Pitman, 1939). This approach was applied to a test dataset not included in the model construction to ascertain the dissimilarity between two distinct populations of data. For this purpose, the values of Bias and SEP calculated on the test analyses are assessed for each pair of models. If two models exhibit significant differences through the results obtained, choosing the best-performing model is justifiable. Conversely, in cases where results demonstrate similarity, the best choice tends to be the simpler model because it is considered statistically more robust (Duponchel et al., 2023).

A detailed description of the successive mathematical steps, as well as the MATLAB code employed, can be found in (Duponchel et al., 2023). The 20 test samples are exclusively from the Beauvoir granite and exhibit Li concentrations ranging from 0.01 wt% to 0.66 wt% and Rb concentrations from 0.14 wt% to 0.39 wt%. Physical characteristics, acquisition parameters, and LIBS spectra processing remained consistent with the initial conditions used to build the models. Considering the substantial number of calibration curves developed,twelve for Li and six for Rb, the outcomes have been graphically synthesized in Fig. 3 and Fig. 4 to simplify the reading. The color-coded tables focus on highlighting the presence or absence of statistically significant differences between a pair of models. The predicted values of Li and Rb for the test sample can be found in Table S3 and Table S4.

An examination of Fig. 3 reveals that the outcomes of the statistical comparisons of LIBS quantification models for Li can be categorized into four discernible groups:

- Group 1: Significant differences in terms of Bias only.
- Group 2: Bias values show no significant difference, contrary to SEP values, which are statistically different.
- Group 3: Both Bias and SEP values are statistically different.
- Group 4: Bias and SEP values show no significant differences.

The results obtained fail to pinpoint a model in particular but lead to the conclusion that the predicted values from the different models are indeed dissimilar. This, in turn, justifies the selection of the best performing model, based on statistical metrics computed for the test samples (i.e., MAE, Bias, SEP), despite an increased complexity. Fig. 5 is a

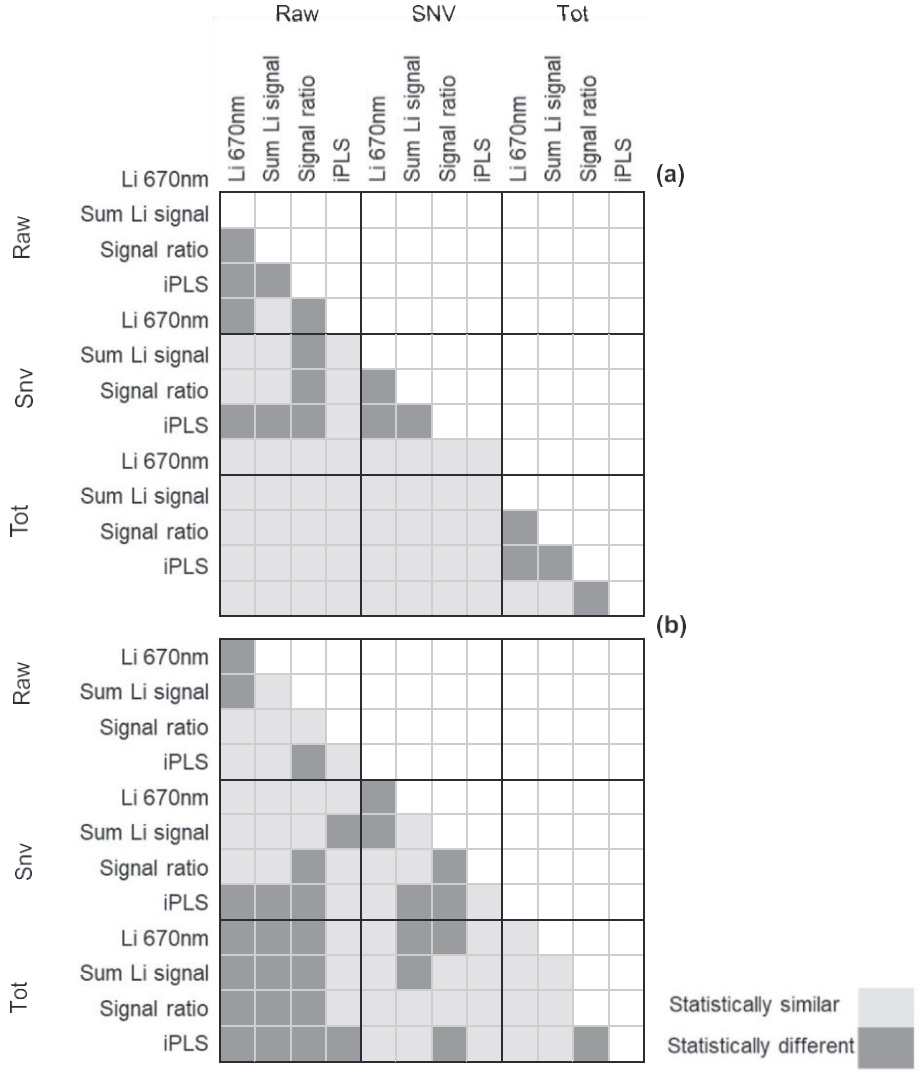

/ig. 3. comparing the different LIBS quantification models built for Li using a statistical procedure based on (a) Bias and (b) Standard Error of Prediction (SEP).

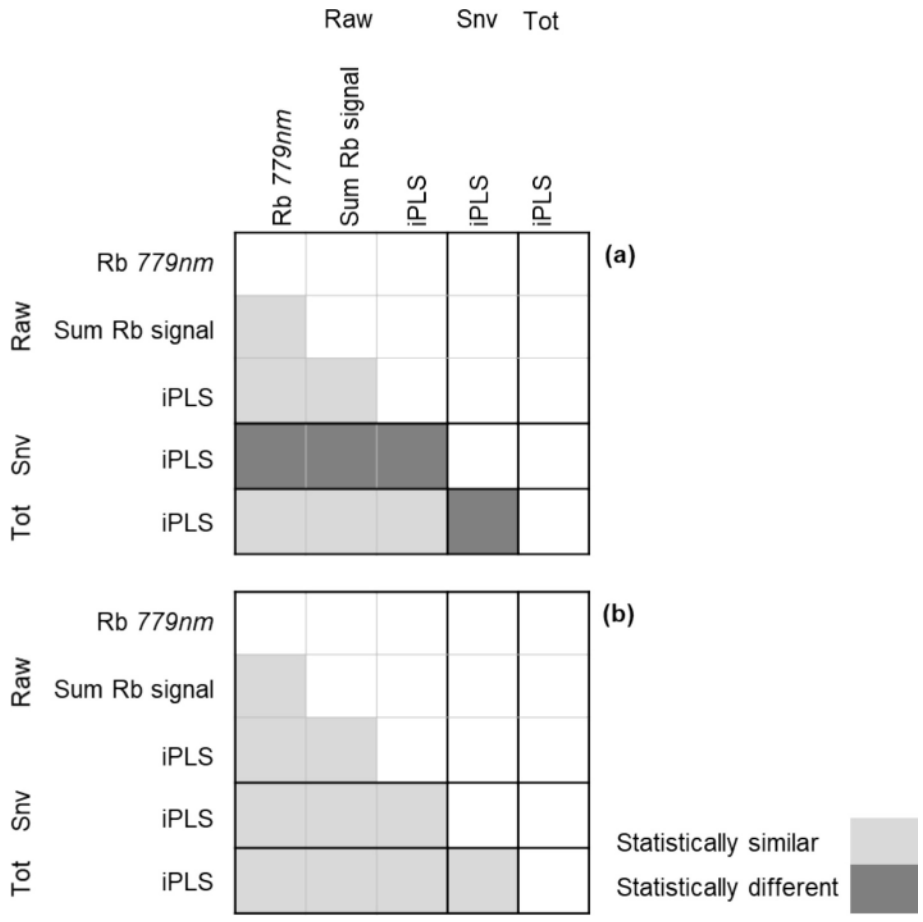

/ig. 4. Visual representation illustrating the results obtained while comparing the different LIBS quantification models built for Rb using a two-step statistical procedure based on (a) Bias and (b) Standard Error of Prediction (SEP).

radar diagram that represents the MAE, Bias, and SEP for the Li models in a 2-D space. The distance from the center to a data point indicates the values (wt%) of the corresponding model in the respective metric. The objective is to identify the model that minimizes those values to obtain predicted concentrations as close as possible to the actual geochemical values obtained in a laboratory setting. At its center, the graph highlights two models in particular: one using the ratio of Li signal to the matrix elements on raw LIBS spectra, while the second is the model using the ratio of Li signal to the matrix elements on normalized LIBS spectra (SNV). As the two models exhibit similar performances and are based on the same methodology (a ratio of the Li signal and matrix element), choosing the model using raw data rather than normalized data to reduce the degree of complexity was preferred.

The outcomes of the Rb models comparative analysis (Fig. 6), offer a more straightforward interpretation. The Bias values demonstrate dissimilarity specifically between the univariate approach (e.g., Sum of Signal, Signal Ratio) and the multivariate approach (iPLS). But, no statistically significant difference in SEP values is observed among any of the model pairs. Once examined in a 2-D triangle chart (Fig. 4), the Bias, SEP, and MAE values indicate that the optimal model for quantifying Rb in Beauvoir granite samples is the multivariate iPLS model using normalized LIBS data (SNV preprocessing).

5.4. *Reproducibility*

Considering the heterogeneous nature of rocks and the inherent variability associated with the LIBS method, evaluating the reproducibility of LIBS predictions was important. Ensuring the precision and consistency of measurements provides crucial evidence that the method is valid and well-suited for supporting practical decision-making during mining operations. To address this, several reference samples were systematically analyzed multiple times. The idea was to compare the MAE obtained from the set of predictions during successive analyses to determine whether it is consistent or reflects a significant difference.

The MAE was computed for three sets of measurements. The first and second measurement sets were positioned centrally, aligning with the initial organization used to build the models. In contrast, the third set of measurements was acquired at the edge of the reference granite samples. The predicted concentrations of Li remained consistent, exhibiting minimal variation from one measurement to another (ΔMAE = 0.003 wt %). However, the values for Rb predictions increased noticeably in the second and third measurement sets (ΔMAE = 0.081 wt%). The question arose as to whether the observed variations were statistically significant. The results of each pair of measurements were compared using Student test (*t*-test) via JMP software (Table 3).

Given the related nature of the observations and measurements taken on the same group of samples, a pairwise comparison approach was chosen. Table 3 illustrates the calculated *p*-values obtained for the different pairs. These values are juxtaposed against a chosen significance level, set at 95 % (0.05). If a calculated p-value is lower than 0.05, the null hypothesis can be rejected, indicating a significant difference in the MAE between the compared pairs of measurements. The paired t-test results indicate that there is no statistically significant difference between the MAE obtained on different sets of LIBS analyses (p-values >0.05) for both Li and Rb predictions. However, the Rb quantification model's response appears to be more sensitive to the spatial variability of the analyzed granite samples.

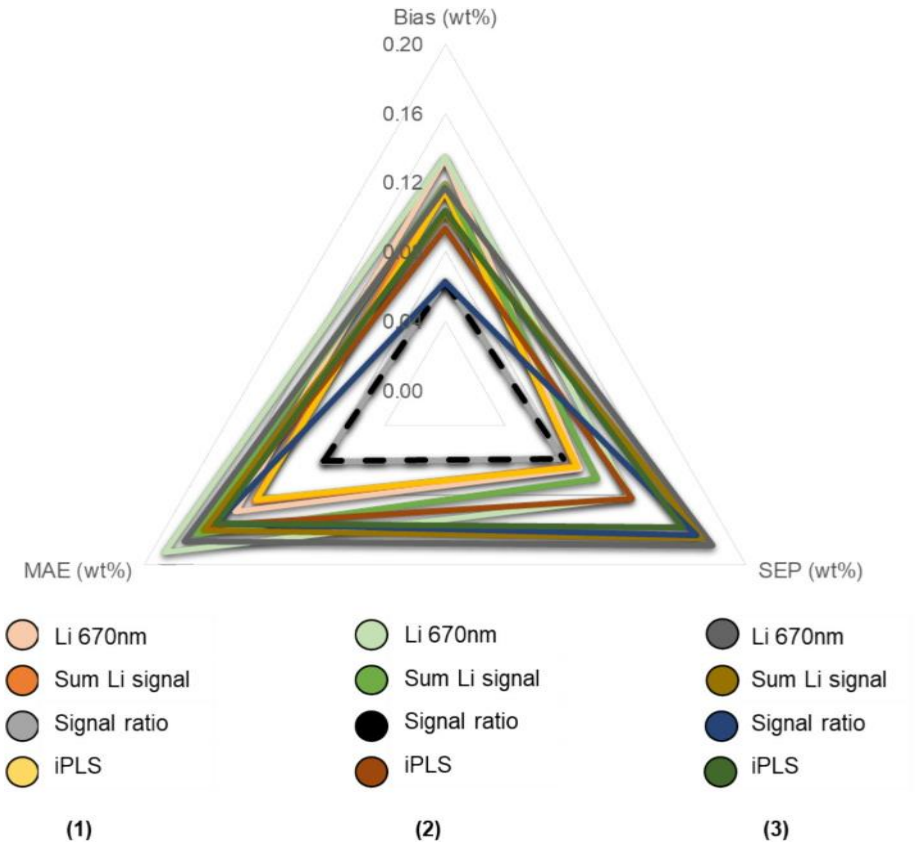

/ig. 5. A radar chart displaying the results of Bias, SEP, and MAE obtained on the test dataset to compare the different Li quantification models built and select the optimal solution for the Beauvoir granite deposit. (1) Raw spectra, (2) SNV normalized spectra, (3) Total spectrum normalized spectra.

5.5. Acquisition time

Another question arose during the development of this study: would it be possible to minimize the acquisition time? Analyzing a specific point using a handheld LIBS required a few seconds (< 30 s per analysis point), but covering the entire length of a 2 to 4 m sized drill core section with a point sampled every centimeter significantly increased the amount of time required. To optimize this step, we evaluated the variation of the MAE for the predicted values of Li and Rb (Table S5 and Table S6) by: i) gradually reducing the number of considered LIBS points for the average signal of a sample (10 %, 20 %, 30 %, ect), ii) reducing the total number of spectra obtained per point (< 144 shots).

For both scenarios, the MAE of the new set of predictions was compared to the initial ones using a *t*-test to determine if the values were different, thus indicating an effect on the quality of predictions. The calculations were performed using the statistical software JMP, and the associated mathematical concepts can be found in detail at (Livingston, 2004). The statistical test (Student, 1908) relies on two initial hypotheses: i) Null Hypothesis (H0): There is no significant difference between the means of the two groups, ii) Alternative Hypothesis (H1): There is a significant difference between the means of the two groups. The critical value (*P*-value) is computed based on the means, standard deviations, dataset sizes, and degree of freedom. This value is compared to the significance level set at 0.05. In Fig. 7a, the MAE obtained while predicting LIBS concentrations remains relatively consistent even as the overall percentage of analyzed data decreases. When considering Li results, the MAE increases by 7 % when going from 90 % to 50 % of the data, reaching 17 % when using less than half of the collected spectra. With a value of 0.0368 wt% for 10 % of the data compared to 0.0314 wt % for the entire analysis, the comparative analysis of MAE using a *t*-test confirms no statistically significant difference between the absolute errors obtained by the sub-datasets. For Rb, the gap in MAE varies from 0.6 to 3 %. The ability to use a fraction of the initial LIBS data (10 %) depends on the physical properties of the analyzed samples. The equigranular structure of the Beauvoir granite and the absence of textural anomalies in the samples treated (e.g., veins, massive alteration) in the considered samples guarantee a relatively homogeneous distribution of the targeted element distribution and therefore necessitates fewer analysis points.

The predictions obtained by adjusting the acquisition parameters either by reducing the number of shots (2 shots instead of 4) per analysis zone or by shrinking the analysis area per point (9 zones instead of 36) show contrasting results (Fig. 7b). For Li, the MAE value triples when we decrease the number of spectra averaged per analysis zone, while it doubles when we reduce the analyzed surface per point. As for Rb, the increase in prediction error is consistent across both tested protocols. These differences are likely due to ablating less material when reducing the number of shots per zone, thereby decreasing the total LIBS signal obtained. Decreasing the analysis area would have a more pronounced impact on Rb because of its occurrence in two different mineral phases (Li-micas and feldspars), making it more sensitive to the spatial arrangement of LIBS analyses.

6. Discussion

The predicted values, consistent with laboratory data (MAE_{Li} = 0.043 wt%, MAE_{Rb} = 0.068 wt%), confirm the possibility of capturing a representative signal of the entire rock volume with no preparation while covering a fraction of the drill core (1.8 %) of the total surface.

The good performance of the LIBS models is tightly linked to the isotropic nature of the material analyzed. In the case of the Beauvoir granite, the facies studied (B1) is described as an equigranular textured leucogranite with no significant structure and therefore meets these criteria. The standard samples were purposefully selected to represent

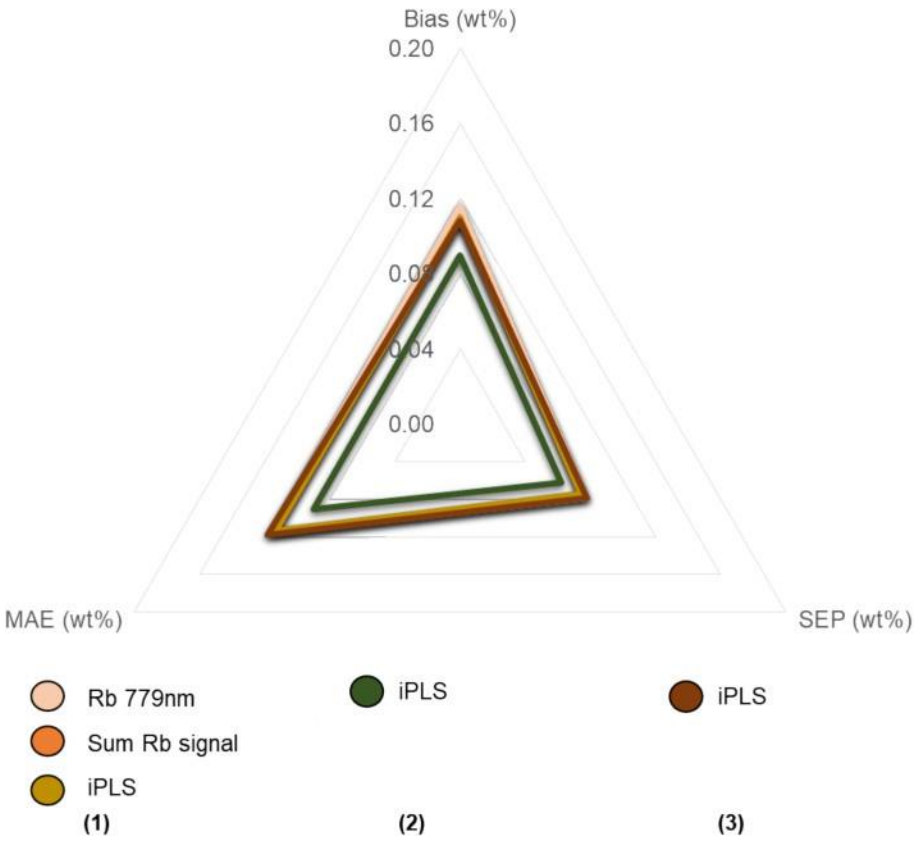

/ig. 6. A radar chart displaying the results of Bias, SEP, and MAE obtained on the test dataset to compare the different Rb quantification models built and select the optimal solution for the Beauvoir granite deposit. (1) Raw spectra, (2) SNV normalized spectra, (3) Total spectrum normalized spectra.

Table 3
The results of the Student test comparing the Mean Absolute Errors (MAE) of prediction for successive LIBS measurements on reference granite samples to assess reproducibility.

Paired comparison		Critical t-value	P-value (Li)	P-value (Rb)
Measurement 1	Measurement 2	0.05	0.78	0.09
Measurement 1	Measurement 3		0.82	0.10
Measurement 2	Measurement 3		0.95	0.98

the best typical unaltered granite targeted for exploitation. But, as the study progresses, completing the database by analyzing segments showcasing textural anomalies observed in the field (e.g., massive quartz zone, albitic cumulat, veins), would enable a more realistic representation of the deposit. Although the B1 facies of the Beauvoir granite was initially described as a homogeneous leucogranite, logging data from the extensive drilling campaign (EMILI21 project) has revealed a more complex structure, characterized by alteration zones at depth, along with localized textural and mineralogical variations. The overall structure of a magmatic rock is the result of multiple parameters such as pressure and temperature conditions, cooling depth and geochemical composition, and hydrothermal phenomena. The fluids, expelled from the magma during cooling or deriving from external meteoric sources, circulate along zones of weakness and pore spaces in the rocks (Pirajno, 2008). Within the context of the Beauvoir granite, an in-depth study of various fluid inclusion types confirms circulation patterns of several generations of magmatic-hydrothermal fluids (Monnier et al., 2018). Some were exsolved from the magma during its emplacement, while others exhibit combined characteristics attributed to mixing dynamics with meteoric components, leading to greisenized and kaolinized zones, massive quartz zones, and the development of quartz veins. It is important to understand the impact of textural variations on the models results, as bias in the analysis should therefore be expected for any area that is not similar to the samples used as references while building the LIBS quantitative models.

The impact of a structural anomaly on the calibration curve developed for Li can be observed in Fig. 8. The sample MC_B39 deviates from the expected or typical pattern observed for the remaining data points. This is explained by a quartz vein that diagonally intersects this sample (Fig. 9). The final quantification model for Li selected through the validation protocol normalizes the total Li signal by summing the signals of Si, Al, Rb, and Cs. Thus, depending on the number of LIBS analysis points coinciding with the vein, the average signal of Si changes, leading to fluctuation in the signal ratio used, which in turn affects the predicted value of Li. Hence, in the next steps of the work, it is imperative to organize strategies that account for the textural characteristics of samples in the presence of anomalies to limit their impact on the quantification model results. This could be achieved by considering: 1) adapting the sampling strategy to accurately represent the existing structures via testing 2) visually preselecting samples to exclude anomalous types, and 3) utilizing alternative quantification models that disregard the signal of other elements in the presence of significant textural variations even if considerate less performant.

The final quantification models for Li and Rb were selected based on performance metrics (RMSE, SEP, Bias) calculated using test samples that closely resemble the reference samples used to construct these models. Put simply, these models perform optimally when the characteristics of the targeted samples match those of the typical samples from the Beauvoir granite, the unaltered B1 facies rock type. However, in the field, beyond the influence of textural anomalies, previously mentioned, on the average LIBS signal obtained, any compositional variations can also impact prediction quality, potentially restricting the applicability of these calibration curves within the Beauvoir granite itself. The spectral

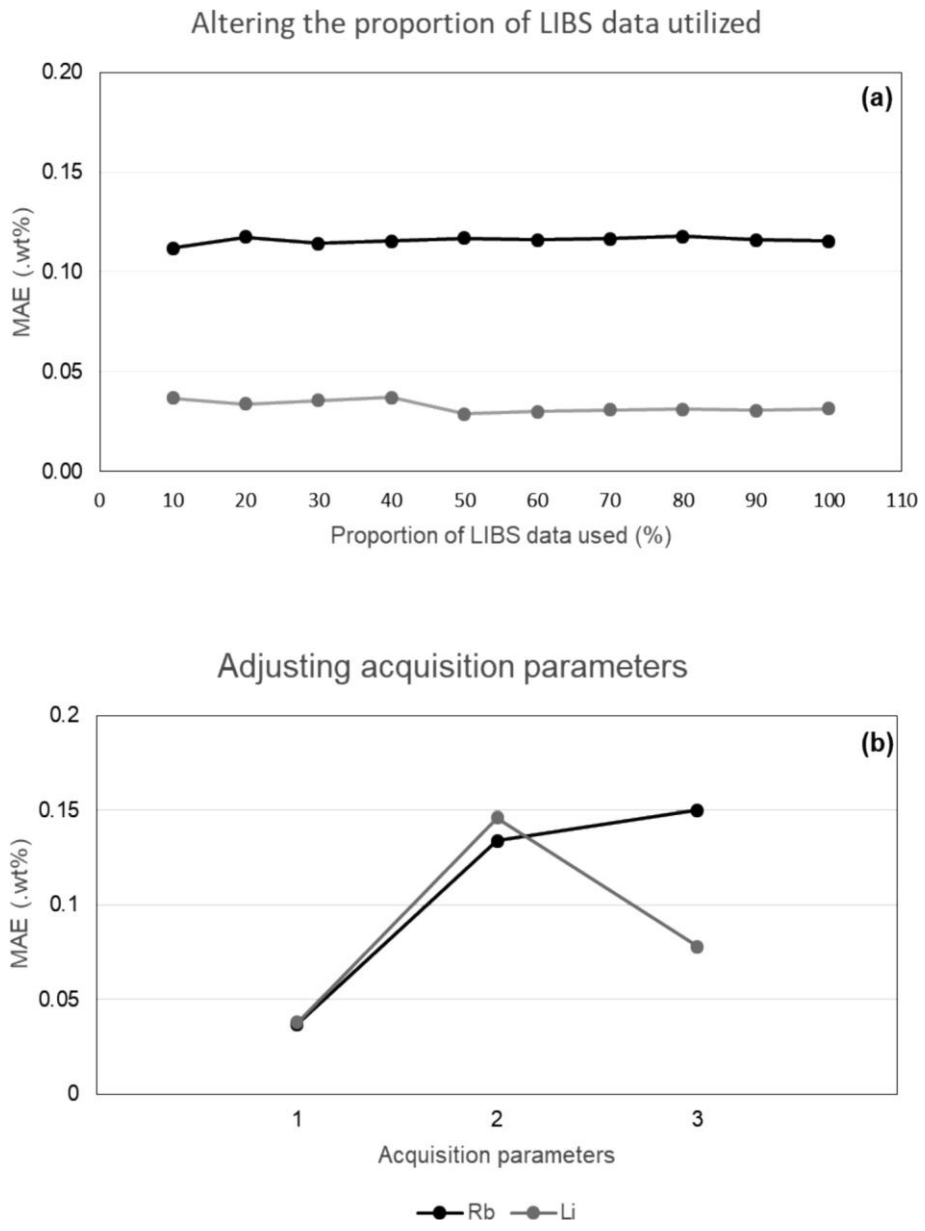

/ig. 7. The mean absolute error (MAE) of predictions calculated under different conditions. (a) varying the proportion of LIBS data used to obtain the average signal per sample. (b) modifying acquisition parameters: 1- Initial parameters, 2- Reducing the number of shots per point, 3- Reducing the total surface area of analysis point. Lithium (Grey), and rubidium (Black).

parameters included in the calibration curves of Li and Rb are derived from the signal of interconnected elements, which evolve in a specific manner within the B1 unit. This implies that any disturbance in the system, such as changes in the modal proportion, and the appearance or disappearance of a mineral phase, can cause fluctuations in the signals of various chemical elements (e.g., Si, Al, Rb, Cs, Li, Na), affecting the established signal ratios used for Li quantification. Using such biased signals to predict Li values could result in either underestimation or overestimation of the predicted concentrations.

The geochemical analyses conducted along the GPF borehole, which traverses the Beauvoir granite for 850 m, show that chemical elements generally exhibit a continuous evolution from top to bottom (Rossi and Autran, 1987). However, the behavior of elements used to develop the LIBS models is not uniform (Fig. S1). For instance, elements such as Rb, Cs, and Al show correlations with Li content, decreasing from the top to the base of the granite. While the total rock content of Si (71–66 wt% SiO_2) and Mn (0.1–0.02 wt% MnO) increases from top to bottom (Raimbault and Azencott, 1987). These variations could alter the signal ratios by decreasing significantly its value, leading to potential inaccuracies in Li estimations. Conversely, the increase in some of the components of the PLS model for Rb could result in an overestimation of the predicted values.

Additionally, the transition from lepidolite to zinnwaldite as the primary Li-bearing mineral, throughout the granite depth could introduce further complexity due to higher iron content, potentially affecting the models predictions. This shift in the predominant form of Li-rich micas, transitioning from lepidolite to a more Fe-rich type, zinnwaldite, from the B1 facies to the B3 facies (Monnier et al., 1987), led by an overall increase in iron content, a chemical element characterized by numerous emission lines due to its complex electronic structure, may introduce spectral interferences affecting neighboring elements, particularly Si and Al. thus, impacting the spectral ranges selected for the models developed.

Considering the possible effects of chemical and textural variations

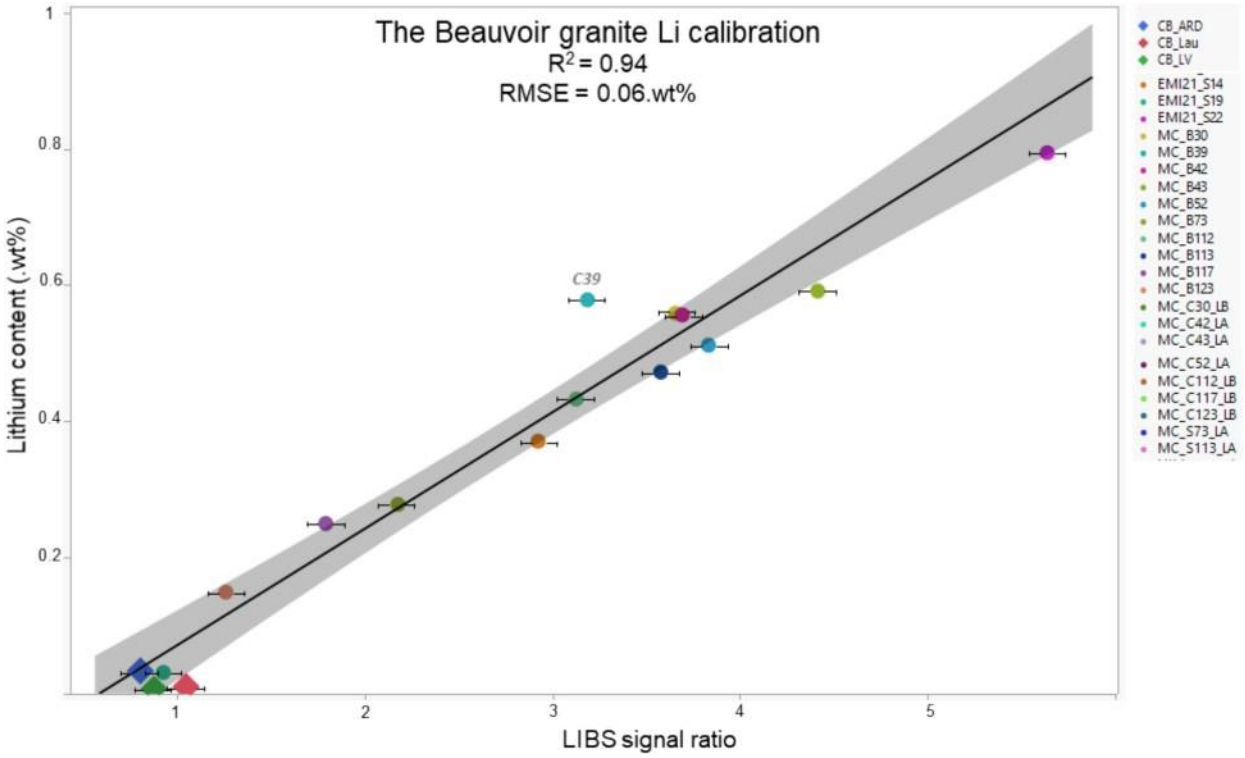

/ig. 8. Handheld LIBS quantification model selected to quantify Li in the Beauvoir granite drill core sections.

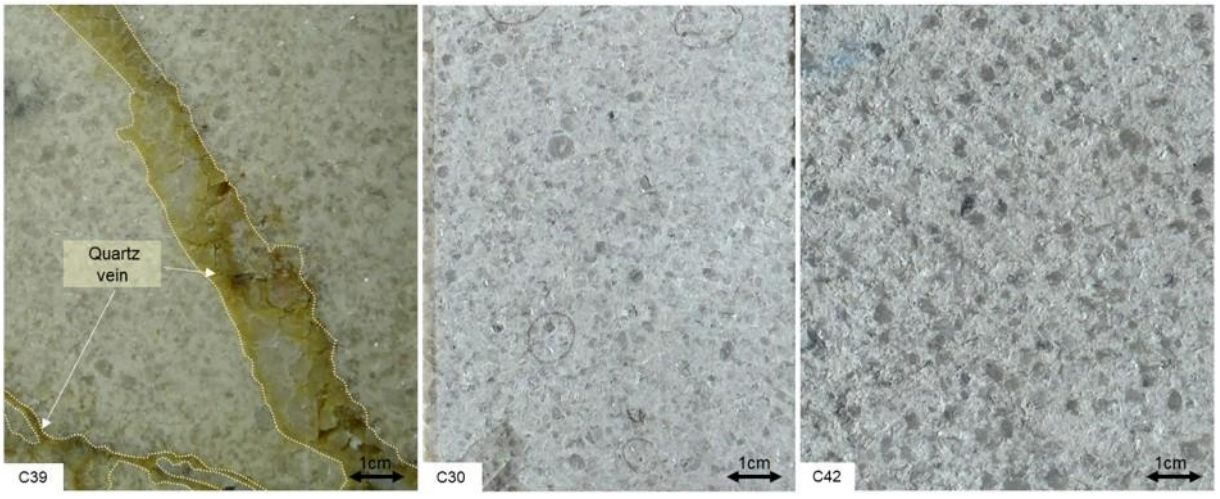

/ig. 9. Photographs of reference samples used for LIBS quantification models: typical unaltered B1 facies (C30, C42), and presenting textural anomalies (C39).

observed in the Beauvoir granite on the LIBS calibrations, a generalized use of these models, across the entirety of the deposit, would entail reiterating the validation protocol for each geochemical unit (B2 and B3). Alternatively, models based solely on the signal of the target element could be used, despite their generally lower performance, to account for the chemical and textural diversity.

To broaden the concentration range covered, samples depleted in Li and Rb sourced from deposits within the French Massif Central region were analyzed (CB_Lau, CB_ARD, and CB_LV). The results (Fig. 8) indicate an alignment of these samples with the rest of the reference samples sourced from the Beauvoir granite. These observations offer new directions on the possibility to enhance LIBS calibration curves with analogous rock samples, outside the selected perimeter.

7. Conclusion

Handheld LIBS is a valuable analytical tool for ore exploration. This study outlines the methodology developed to generate reliable quantitative data on the critical elements, Li and Rb, on the Beauvoir granite. A particular focus was to minimize sample preparation by analyzing unprepared drillcores to reduce technical constraints and guarantee practical application during exploration campaigns. Reference samples sourced from the deposit were used to replicate the chemical and physical characteristics of the targeted samples, limiting matrix effects. To obtain a representative signal of the entire rock volume, LIBS analyses were organized along a vertical profile covering the sample length while maximizing the analyzed surface per point (1 point = 36 areas - 4 laser pulses per area). In total, 12 quantitative models for Li and 9 for Rb

were constructed, covering concentration intervals of (0.007–0.795 wt %) for Li and (0.033–0.453 wt%) for Rb. A two-step statistical procedure, based on Bias and SEP values, was performed to determine the optimal solution for each element. The results led to the selection of the signal ratio model using raw spectra (RMSE = 0.062 wt%; MAE = 0.081 wt%; Bias = 0.064 wt%; SEP = 0.078 wt%) for Li and the iPLS model using normalized SNV data (RMSE = 0.039 wt%; MAE = 0.090 wt%; Bias = 0.090 wt%; SEP = 0.062 wt%) for Rb. Considering the spatial scale of the target samples, various acquisition parameters were tested to reduce acquisition time. Reducing the percentage of utilized raw data did not significantly impact the MAE of the predicted values, but minimizing the analyzed surface or decreasing the number of shots per point increased the MAE. Successive measurements at different locations revealed no significant difference in MAE for both Li and Rb values, confirming the consistency of LIBS predictions for this particular type of sample, an isotropic equigranular, non-oriented granite rock. Additionally, the ability to calibrate the LIBS signal across samples from different geographic locations, provided that the rock texture, lithological type, and the nature of the constituent elements are preserved, hints at the potential to construct generalized models that could be applied to specific rock types (ie, leucogranite, LCT pegmatites, etc.…) across diverse geographical locations rather than individual sites. It would be interesting for the next stages of this work to apply the models developed for the Beauvoir granite to a deposit presenting similar features (i.e., Cinovec) to validate or refute this hypothesis. Promising results could be a significant advancement especially when considering that one of the main challenges for a wider implementation of LIBS methodology within the mining sector is the need to develop customized quantification models for every individual deposit, while this constraint is not present in alternative techniques like X-ray Fluorescence.This study demonstrates the potential of the handheld LIBS analyzer to provide valuable geochemical data to support efficient and rapid decision-making to optimize resource management during exploration operations.

CRediT authorship contribution statement

Naila Mezoued: Visualization, Methodology, Formal analysis, Data curation, Conceptualization. **Ce´cile /abre:** Visualization, Validation, Supervision, Project administration, Methodology, Funding acquisition, Conceptualization, Writing – review & editing. **Jean Cauzid:** Visualization, Validation, Supervision, Project administration, Methodology, Funding acquisition, Conceptualization, Writing – review & editing. **Zia Steven Kahou:** Resources, Writing – review & editing. **NAILA MEZOUED:** Writing – review & editing, Writing – original draft. **Oceane Rocher:** Writing – review & editing.

/unding

This study was supported by the French National Research Agency via the Labex Ressources 21 project [reference ANR–10–LABX–21-01] and partially financed by Imerys, the operating company of the Beauvoir Granite.

Declaration of competing interest

The authors declare the following financial interests/personal relationships which may be considered as potential competing interests: Naila Mezoued reports financial support was provided by Imerys SA. Naila Mezoued reports a relationship with Imerys SA that includes: funding grants and non-financial support. If there are other authors, they declare that they have no known competing financial interests or personal relationships that could have appeared to influence the work reported in this paper.

Acknowledgments

We would like to acknowledge the support of Michel Cathelineau, Steven Kahou, and Christophe Ballouard for providing some of the reference granite samples used to build and compare the quantification models. A special appreciation to the Imerys team for their valuable help, granting us convenient access to the Beauvoir granite mining site and providing essential geochemical data. We would like to express our sincere gratitude to Russel Harmon and the anonymous reviewer for their valuable time, insightful comments, and thoughtful suggestions, which have significantly contributed to improving the quality and clarity of this work.

AI disclosure

During the preparation of this work, the author used ChatGPT and Deeple to translate some parts of the text from French to English. After using these AI interfaces, the author reviewed and edited the content as needed and take full responsibility for the content of the publication.

Appendix A. Supplementary data

Supplementary data to this article can be found online at https://doi.org/10.1016/j.gexplo.2025.107689.

Data availability

Data will be made available on request.

References

Agresti, J., Indelicato, C., Perotti, M., et al., 2022. Quantitative Compositional analyses of Calcareous Rocks for Lime Industry using LIBS. Molecules 27, 1813. https://doi.org/10.3390/molecules27061813.

Alexandre, P., Carlier, Le, de Veslud, C., Cuney, M., et al., 2002. Datation 40Ar/39Ar des leucogranites sous couverture du complexe plutonique de Charroux–Civray (Vienne). Compt. Rendus Geosci. 334, 1141–1148. https://doi.org/10.1016/S1631-0713(02)01859-X.

Aubert, G., 1969. Les coupoles granitiques de Montebras et d'´echassi`eres et la gene`se de leurs mine´ralisations.

Calibrating a Handheld LIBS for Li Exploration, 2024. in the Barroso–Alvão Aplite-Pegmatite Field, Northern Portugal: Textural Precautions and Procedures When Analyzing Spodumene and Petalite. https://www.mdpi.com/2075-163X/13/4/470. Accessed 23 Sep.

Capela, D., Ferreira, M.F.S., Lima, A., et al., 2023. Robust and interpretable mineral identification using laser-induced breakdown spectroscopy mapping. Spectrochim. Acta B At. Spectrosc. 206, 106733. https://doi.org/10.1016/j.sab.2023.106733.

Charoy, B., Chaussidon, M., Le Carlier De Veslud, C., Duthou, J.L., 2003. Evidence of Sr mobility in and around the albite–lepidolite–topaz granite of Beauvoir (France): an in-situ ion and electron probe study of secondary Sr-rich phosphates. Contrib. Mineral. Petrol. 145, 673–690. https://doi.org/10.1007/s00410-003-0458-x.

Cheilletz, A., Cuney, M., Charoy, B., Archibald, D.A., 1992. 40 Ar/39 Ar ages of the Beauvoir topaze-lepidolite leucogranite and the Chedeville sodolithic pegmatite (North French Massif Central) Petrologic and geodynamic signification. Comp. Rendus Acad. Sci. Serie 2 (315), 329–336.

Chen, M., Yuan, T., Hou, Z., et al., 2015. Effects of moisture content on coal analysis using laser-induced breakdown spectroscopy. Spectrochim. Acta B At. Spectrosc. 112, 23–33. https://doi.org/10.1016/j.sab.2015.08.003.

Chen, T., Sun, L., Yu, H., et al., 2022. Deep learning with laser-induced breakdown spectroscopy (LIBS) for the classification of rocks based on elemental imaging. Appl. Geochem. 136, 105135. https://doi.org/10.1016/j.apgeochem.2021.105135.

Cuney, M., Autran, A., 1987. Objectifs g´ene´raux du projet GPF Echassie`res n◦1 et r´esultats essentiels aquis par le forage de 900 m du granite albitique a` topaze-le´pidolite micas.

Cuney, M., Marignac, C., Weisbrod, A., 1992. The Beauvoir topaz-lepidolite albite granite (Massif Central, France); the disseminated magmatic Sn-Li-Ta-Nb-be mineralization. Econ. Geol. 87, 1766–1794. https://doi.org/10.2113/gsecongeo.87.7.1766.

Da Silva, A.C., Triantafyllou, A., Delmelle, N., 2023. Portable x-ray fluorescence calibrations: Workflow and guidelines for optimizing the analysis of geological samples. Chem. Geol. 623, 121395. https://doi.org/10.1016/j.chemgeo.2023.121395.

Defnet, P.A., Wise, M.A., Harmon, R.S., et al., 2021. Analysis of Garnet by Laser-Induced Breakdown Spectroscopy—two Practical applications. Minerals 11, 705. https://doi.org/10.3390/min11070705.

Demeusy, B., Arias-Quintero, C.A., Butin, G., et al., 2023. Characterization and Liberation Study of the Beauvoir Granite for Lithium Mica Recovery. Minerals 13, 950. https://doi.org/10.3390/min13070950.

Dubey, S., Kumar, R., Rai, A.K., et al., 2021. Rapid Analysis of Chemical Composition and Physical Properties of Gemstones using LIBS and Chemometric Technique. Appl. Sci. 11, 6156. https://doi.org/10.3390/app11136156.
Duponchel, L., Fabre, C., Bousquet, B., Motto-Ros, V., 2023. Statistical comparison of predictive models for quantitative analysis and classification in the framework of LIBS spectroscopy: a tutorial. Spectrochim. Acta B At. Spectrosc. 208, 106776. https://doi.org/10.1016/j.sab.2023.106776.
EBSCOhost, 2024. Of Life and Lithium: Why the "White Gold" Rush Won't Save The Planet. | CounterPunch. https://openurl.ebsco.com/EPDB%3Agcd%3A16%3A9413408/detailv2?sid=ebsco%3Aplink%3Ascholar&id=ebsco%3Agcd%3A176480118&crl=c.
Eisler, M., 2019. Bolivian lithium: Why you Should Not Expect any 'White Gold Rush' in the Wake of Morales Overthrow. The Conversation, In. http://theconversation.com/bolivian-lithium-why-you-should-not-expect-any-white-gold-rush-in-the-wake-of-morales-overthrow-127139. Accessed 16 Sep 2024.
El Haddad, J., Canioni, L., Bousquet, B., 2014. Good practices in LIBS analysis: Review and advices. Spectrochim. Acta B At. Spectrosc. 101, 171–182. https://doi.org/10.1016/j.sab.2014.08.039.
El Haddad, J., de Lima Filho, E.S., Vanier, F., et al., 2019. Multiphase mineral identification and quantification by laser-induced breakdown spectroscopy. Miner. Eng. 134, 281–290. https://doi.org/10.1016/j.mineng.2019.02.025.
El-Saeid, R.H., Abdel-Salam, Z., Pagnotta, S., et al., 2019. Classification of sedimentary and igneous rocks by laser induced breakdown spectroscopy and nanoparticle-enhanced laser induced breakdown spectroscopy combined with principal component analysis and graph theory. Spectrochim. Acta B At. Spectrosc. 158, 105622. https://doi.org/10.1016/j.sab.2019.05.011.
EMILI. Beauvoir Lithium Mining Project. https://emili.imerys.com/en. Accessed 10 Jan 2024.
Fabre, C., 2020. Advances in Laser-Induced Breakdown Spectroscopy analysis for geology: a critical review. Spectrochim. Acta B At. Spectrosc. 166, 105799. https://doi.org/10.1016/j.sab.2020.105799.
Fabre, C., Boiron, M.-C., Dubessy, J., et al., 2002. Advances in lithium analysis in solids by means of laser-induced breakdown spectroscopy: an exploratory study. Geochim. Cosmochim. Acta 66, 1401–1407. https://doi.org/10.1016/S0016-7037(01)00858-4.
Fabre, C., Ourti, N.E., Mercadier, J., et al., 2021a. Analyses of Li-Rich Minerals using Handheld LIBS Tool. Data 6, 68. https://doi.org/10.3390/data6060068.
Fabre, C., Ourti, N.E., Mercadier, J., et al., 2021b. Analyses of Li-Rich Minerals using Handheld LIBS Tool. Data 6, 68. https://doi.org/10.3390/data6060068.
Fabre, C., Ourti, N.E., Ballouard, C., et al., 2022. Handheld LIBS analysis for in situ quantification of Li and detection of the trace elements (be, Rb and Cs). J. Geochem. Explor. 236, 106979. https://doi.org/10.1016/j.gexplo.2022.106979.
Fagundes Fontana, F., van der Hoek, B., Tassios, S., et al., 2022. Laser Induced Breakdown Spectroscopy (Libs) for Whole Rock Geochemistry.
Farnsworth-Pinkerton, S., McMillan, N.J., Dutrow, B.L., Henry, D.J., 2018. Provenance of detrital tourmalines from Proterozoic metasedimentary rocks in the Picuris Mountains, New Mexico, using Laser-Induced Breakdown Spectroscopy. Austrian J. Geosci. 193–198. https://doi.org/10.3190/jgeosci.261.
Ferreira, M.F.S., Capela, D., Silva, N.A., et al., 2022. Comprehensive comparison of linear and non-linear methodologies for lithium quantification in geological samples using LIBS. Spectrochim. Acta B At. Spectrosc. 195, 106504. https://doi.org/10.1016/j.sab.2022.106504.
Feybesse, J.L., Tegyey, M., 1987. Evolution tectonome´tamorphique d´evonienne et carbonife`re de la s´erie de la Sioule.
Fisher, L., Gazley, M.F., Baensch, A., et al., 2014. Resolution of geochemical and lithostratigraphic complexity: a workflow for application of portable X-ray fluorescence to mineral exploration. GEEA 14, 149–159. https://doi.org/10.1144/geochem2012-158.
Fontana, F.F., van der Hoek, B., Tassios, S., et al., 2023. Laser Induced Breakdown Spectroscopy (LIBS) for whole rock geochemistry. J. Geochem. Explor. 246, 107160. https://doi.org/10.1016/j.gexplo.2023.107160.
Foucaud, Y., Fabre, C., Demeusy, B., et al., 2019. Optimisation of fast quantification of fluorine content using handheld laser induced breakdown spectroscopy. Spectrochim. Acta B At. Spectrosc. 158, 105628. https://doi.org/10.1016/j.sab.2019.05.017.
Gottfried, J.L., Harmon, R.S., De Lucia, F.C., Miziolek, A.W., 2009. Multivariate analysis of laser-induced breakdown spectroscopy chemical signatures for geomaterial classification. Spectrochim. Acta B At. Spectrosc. 64, 1009–1019. https://doi.org/10.1016/j.sab.2009.07.005.
Grolier, J., 1971. La tectonique du Massif hercynien dans le Massif central français. pp 215–248.
Grunsky, E.C., 2010. The interpretation of geochemical survey data. Geochemistry: Exploration. Environment, Analysis 10, 27–74. https://doi.org/10.1144/1467-7873/09-210.
Han, D., Joe, Y.J., Ryu, J.-S., et al., 2018. Application of laser-induced breakdown spectroscopy to Arctic sediments in the Chukchi Sea. Spectrochim. Acta B At. Spectrosc. 146, 84–92. https://doi.org/10.1016/j.sab.2018.05.002.
Harlaux, M., Mercadier, J., Bonzi, W.M.-E., et al., 2017. Geochemical Signature of Magmatic-Hydrothermal Fluids Exsolved from the Beauvoir Rare-Metal Granite (Massif Central, France): Insights from LA-ICPMS Analysis of primary Fluid Inclusions. Geofluids 2017, 1–25. https://doi.org/10.1155/2017/1925817.
Harmon, R.S., Senesi, G.S., 2021. Laser-Induced Breakdown Spectroscopy – a geochemical tool for the 21st century. Appl. Geochem. 128, 104929. https://doi.org/10.1016/j.apgeochem.2021.104929.
Harmon, R.S., Lawley, C.J.M., Watts, J., et al., 2019. Laser-Induced Breakdown Spectroscopy—an Emerging Analytical Tool for Mineral Exploration. Minerals 9, 718. https://doi.org/10.3390/min9120718.
Harmon, R.S., Wise, M.A., Curry, A.C., et al., 2023. Rapid Analysis of Muscovites on a Lithium Pegmatite Prospect by Handheld LIBS. Minerals 13, 697. https://doi.org/10.3390/min13050697.
Jacquot, T., 1990. Dynamique de mise en place d'un appareil leucogranitique dans la chaîne hercynienne : le Massif d'E´chassie`res, Allier. Phdthesis, Universite´ Henri Poincar´e - Nancy, Massif Central Français, p. 1.
Jain, J., Quarles, C.D., Moore, J., et al., 2018. Elemental mapping and geochemical characterization of gas producing shales by laser induced breakdown spectroscopy. Spectrochim. Acta B At. Spectrosc. 150, 1–8. https://doi.org/10.1016/j.sab.2018.09.010.
Jehlič̆cka, J., Culka, A., 2022. Critical evaluation of portable Raman spectrometers: from rock outcrops and planetary analogs to cultural heritage – a review. Anal. Chim. Acta 1209, 339027. https://doi.org/10.1016/j.aca.2021.339027.
Jolivet, L., Leprince, M., Moncayo, S., et al., 2019. Review of the recent advances and applications of LIBS-based imaging. Spectrochim. Acta B At. Spectrosc. 151, 41–53. https://doi.org/10.1016/j.sab.2018.11.008.
Kesler, S.E., Gruber, P.W., Medina, P.A., et al., 2012. Global lithium resources: Relative importance of pegmatite, brine and other deposits. Ore Geol. Rev. 48, 55–69. https://doi.org/10.1016/j.oregeorev.2012.05.006.
Khajehzadeh, N., Kauppinen, T.K., 2015. Fast mineral identification using elemental LIBS technique. IFAC-PapersOnLine 48, 119–124. https://doi.org/10.1016/j.ifacol.2015.10.089.
Korbel, C., Mezoued, N., Demeusy, B., et al., 2024. Quantification of lithium using handheld instruments: application of LIBS and XRF spectroscopy to assay the lithium content of mineral processing products. J. Anal. At. Spectrom. 39, 1838–1853. https://doi.org/10.1039/D3JA00423F.
Kovalenko, V.I., Kovalenko, N.I., 1984. Problems of the origin, ore-bearing and evolution of rare-metal granitoids. Phys. Earth Planet. Inter. 35, 51–62. https://doi.org/10.1016/0031-9201(84)90033-5.
Kuhn, K., Meima, J.A., Rammlmair, D., Ohlendorf, C., 2016. Chemical mapping of mine waste drill cores with laser-induced breakdown spectroscopy (LIBS) and energy dispersive X-ray fluorescence (EDXRF) for mineral resource exploration. J. Geochem. Explor. 161, 72–84. https://doi.org/10.1016/j.gexplo.2015.11.005.
Lafitte, G., 2023. The 'White Gold Rush': Tibet as a New Frontline in the Global race for Renewable Energy. Asian Affairs 54, 717–735. https://doi.org/10.1080/03068374.2023.2288762.
Laser-Induced Breakdown Spectroscopy, 2024. in Mineral Exploration and Ore Processing. https://www.mdpi.com/2075-163X/14/7/731. Accessed 23 Sep.
Lednev, V.N., Sdvizhenskii, P.A., Dorohov, A.S., et al., 2023. Improving LIBS analysis of non-flat heterogeneous samples by signals mapping. Appl. Opt, AO 62, 2030–2038. https://doi.org/10.1364/AO.473111.
Ledru, P., Lardeaux, J.M., Santallier, D., et al., 1989. Ou sont les nappes dans le massif central francais? Bull. Soc. G´eol. France V:605–618. https://doi.org/10.2113/gssgfbull.V.3.605.
Lemi`ere, B., Harmon, R.S., 2021. XRF and LIBS for Field Geology. In: Portable Spectroscopy and Spectrometry. John Wiley & Sons, Ltd, pp. 455–497.
Lemi`ere, B., Uvarova, Y.A., 2019. New developments in field-portable geochemical techniques and on-site technologies and their place in mineral exploration. Geochemistry: Exploration. Environment, Analysis 20, 205–216. https://doi.org/10.1144/geochem2019-044.
Li, M., Xi, X., Xiao, G., et al., 2014. National multi-purpose regional geochemical survey in China. J. Geochem. Explor. 139, 21–30. https://doi.org/10.1016/j.gexplo.2013.06.002.
Livingston, E.H., 2004. Who was student and why do we care so much about his *t*-test?1. J. Surg. Res. 118, 58–65. https://doi.org/10.1016/j.jss.2004.02.003.
Lusty, P.A.J., Gunn, A.G., 2015. Challenges to global mineral resource security and options for future supply. Geol. Soc. Lond. Spec. Publ. 393, 265–276. https://doi.org/10.1144/SP393.13.
Mao, S.S., Zeng, X., Mao, X., Russo, R.E., 2004. Laser-induced breakdown spectroscopy: flat surface vs. cavity structures. J. Anal. At. Spectrom. 19, 495–498. https://doi.org/10.1039/B315725C.
McManus, C., Dowe, J., Mcmillan, N., 2017. Use of C-C and C-N Molecular Emissions in Laser-Induced Breakdown Spectroscopy Data to Determine Diamond Provenance. Microsc. Microanal. 23, 2282–2283. https://doi.org/10.1017/S1431927617012077.
McManus, C.E., McMillan, N.J., Harmon, R.S., et al., 2008. Use of laser induced breakdown spectroscopy in the determination of gem provenance: beryls. Appl. Opt. 47, G72–G79. https://doi.org/10.1364/ao.47.000g72.
McMillan, N.J., Harmon, R.S., De Lucia, F.C., Miziolek, A.M., 2007. Laser-induced breakdown spectroscopy analysis of minerals: Carbonates and silicates. Spectrochim. Acta B At. Spectrosc. 62, 1528–1536. https://doi.org/10.1016/j.sab.2007.10.037.
McMillan, N.J., Rees, S., Kochelek, K., McManus, C., 2014. Geological applications of Laser-Induced Breakdown Spectroscopy. Geostand. Geoanal. Res. 38, 329–343. https://doi.org/10.1111/j.1751-908X.2014.00308.x.
F. Menges Spectragryph - optical spectroscopy software (n.d.).
Mohamed, N., Rifai, K., Selmani, S., et al., 2021. Chemical and Mineralogical Mapping of Platinum-Group Element Ore Samples using Laser-Induced Breakdown Spectroscopy and Micro-X-Ray Fluorescence. Geostand. Geoanal. Res. 45, 539–550. https://doi.org/10.1111/ggr.12385.
Monnier, G., Charoy, B., Cuney, M., Ohnenstetter, D., Robert, J.L., 1987. Evolution spatiale et temporelle de la composition des micas du granite albitique `a topaze-le´pidolite de Beauvoir. G´eol. Fr. 179–188.
Monnier, L., 2018. Utilisation de la signature LA-ICPMS des quartz et des micas pour la reconstitution du fonctionnement d'un syste`me magmatique et hydrothermal

polyphas´e. In: Application au complexe Sn-W d'Echassi`eres (Massif central, France) (These de doctorat, Toulouse 3).
Monnier, L., Lach, P., Salvi, S., et al., 2018. Quartz trace-element composition by LA-ICP-MS as proxy for granite differentiation, hydrothermal episodes, and related mineralization: the Beauvoir Granite (Echassie`res district), France. Lithos 320–321, 355–377. https://doi.org/10.1016/j.lithos.2018.09.024.
Müller, S., Meima, J.A., 2022. Mineral classification of lithium-bearing pegmatites based on laser-induced breakdown spectroscopy: Application of semi-supervised learning to detect known minerals and unknown material. Spectrochim. Acta B At. Spectrosc. 189, 106370. https://doi.org/10.1016/j.sab.2022.106370.
Oruch, R., Elderbi, M.A., Khattab, H.A., et al., 2014. Lithium: a review of pharmacology, clinical uses, and toxicity. Eur. J. Pharmacol. 740, 464–473. https://doi.org/10.1016/j.ejphar.2014.06.042.
Panya, S.N.P., Galmed, A.H., Maaza, M., et al., 2018. Laser-Induced Breakdown Spectroscopy (LIBS) on Geological Samples: Compositional Differentiation. MRS Adv. 3, 1969–1983. https://doi.org/10.1557/adv.2018.401.
Pease, P., Tchakerian, V., 2014. Source provenance of carbonate grains in the Wahiba Sand Sea, Oman, using a new LIBS method. Aeolian Res. 15, 203–216. https://doi.org/10.1016/j.aeolia.2014.06.001.
Pichavant, M., 2022. Experimental Crystallization of the Beauvoir Granite as a Model for the Evolution of Variscan rare Metal Magmas. J. Petrol. 63, egac120. https://doi.org/10.1093/petrology/egac120.
Pirajno, F., 2008. Hydrothermal Processes and Mineral Systems. Springer Science & Business Media.
Pitman, E.J.G., 1939. A Note on Normal Correlation. Biometrika 31, 9–12. https://doi.org/10.2307/2334971.
Raimbault, L., Azencott, C., 1987. Ge´ochimie des ´ele´ments majeurs et traces du granite a` m´etaux rares de Beauvoir (sondage GPF, Echassie`res). G´eol. Fr. 189–198.
Rauschenbach, I., Lazic, V., Pavlov, S.G., et al., 2008. Laser induced breakdown spectroscopy on soils and rocks: Influence of the sample temperature, moisture and roughness. Spectrochim. Acta B At. Spectrosc. 63, 1205–1215. https://doi.org/10.1016/j.sab.2008.08.006.
Ribeiro, R., Capela, D., Ferreira, M., et al., 2021. X-ray Fluorescence and Laser-Induced Breakdown Spectroscopy Analysis of Li-Rich Minerals in Veins from Argemela Tin Mine. Central Portugal. Minerals 11, 1169. https://doi.org/10.3390/min11111169.
Romppanen, S., Po¨lo¨nen, I., H¨akka¨nen, H., Kaski, S., 2023. Optimization of spodumene identification by statistical approach for laser-induced breakdown spectroscopy data of lithium pegmatite ores. Appl. Spectrosc. Rev. 58, 297–317. https://doi.org/10.1080/05704928.2021.1963977.
Rosenwasser, S., Asimellis, G., Bromley, B., et al., 2001. Development of a method for automated quantitative analysis of ores using LIBS. Spectrochim. Acta B At. Spectrosc. 56, 707–714. https://doi.org/10.1016/S0584-8547(01)00191-4.
Rossi, M., Dell'Aglio, M., De Giacomo, A., et al., 2014. Multi-methodological investigation of kunzite, hiddenite, alexandrite, elbaite and topaz, based on laser-induced breakdown spectroscopy and conventional analytical techniques for supporting mineralogical characterization. Phys. Chem. Miner. 41, 127–140. https://doi.org/10.1007/s00269-013-0631-3.
Rossi, P., Autran, A., Burnol, L., et al., 1987. Logs pe´trographiques et ge´ochimiques du granite de Beauvoir dans le sondage Echassi`eres I. Min´eralogie et ge´ochimie compar´ees. G´eol. Fr. 111–135.
Rossi, Ph., Autran, A., 1987. Log pe´trographique et ge´ochimique du granite de Beauvoir dans le sondage "Echassie`re I" Min´eralogie ete g´eochimie compar´ees. G´eol. Fr. 111–135.
Roux, C.P.M., Rakovský, J., Musset, O., et al., 2015. In situ Laser Induced Breakdown Spectroscopy as a tool to discriminate volcanic rocks and magmatic series, Iceland. Spectrochim. Acta B At. Spectrosc. 103–104, 63–69. https://doi.org/10.1016/j.sab.2014.11.013.
Sall´e, B., Lacour, J.-L., Mauchien, P., et al., 2006. Comparative study of different methodologies for quantitative rock analysis by Laser-Induced Breakdown Spectroscopy in a simulated Martian atmosphere. Spectrochim. Acta B At. Spectrosc. 61, 301–313. https://doi.org/10.1016/j.sab.2006.02.003.
Salminen, R., Tarvainen, T., 1995. Geochemical mapping and databases in Finland. J. Geochem. Explor. 55, 321–327. https://doi.org/10.1016/0375-6742(94)00062-X.
Senesi, G.S., Harmon, R.S., 2023. Application of LIBS to Terrestrial Geological Research. In: Laser Induced Breakdown Spectroscopy (LIBS). John Wiley & Sons, Ltd, pp. 593–614.
Senesi, G.S., Harmon, R.S., Hark, R.R., 2020. Chapter 23 - Field-portable and handheld LIBS. In: Singh, J.P., Thakur, S.N. (Eds.), Laser-Induced Breakdown Spectroscopy, Second edition. Elsevier, Amsterdam, pp. 537–560.
Senesi, G.S., Allegretta, I., Marangoni, B.S., et al., 2023. Geochemical identification and classification of cherts using handheld laser induced breakdown spectroscopy (LIBS) supported by supervised machine learning algorithms. Appl. Geochem. 151, 105625. https://doi.org/10.1016/j.apgeochem.2023.105625.
Steiner, B.M., 2019. Tools and Workflows for Grassroots Li–Cs–Ta (LCT) Pegmatite Exploration. Minerals 9, 499. https://doi.org/10.3390/min9080499.
Student, 1908. The Probable Error of a mean. Biometrika 6, 1–25. https://doi.org/10.2307/2331554.
Syvilay, D., Bousquet, B., Chapoulie, R., et al., 2019. Advanced statistical analysis of LIBS spectra for the sourcing of obsidian samples. J. Anal. At. Spectrom. 34, 867–873. https://doi.org/10.1039/C8JA00340H.
Talens Peiro´, L., Villalba M´endez, G., Ayres, R.U., 2013. Lithium: sources, production, Uses, and Recovery Outlook. JOM 65, 986–996. https://doi.org/10.1007/s11837-013-0666-4.
Tognoni, E., Cristoforetti, G., 2016. [INVITED] Signal and noise in Laser Induced Breakdown Spectroscopy: an introductory review. Opt. Laser Technol. 79, 164–172. https://doi.org/10.1016/j.optlastec.2015.12.010.
Tucker, J.M., Dyar, M.D., Schaefer, M.W., et al., 2010. Optimization of laser-induced breakdown spectroscopy for rapid geochemical analysis. Chem. Geol. 277, 137–148. https://doi.org/10.1016/j.chemgeo.2010.07.016.
USGS. Circular 1371: Lithium Use in Batteries. https://pubs.usgs.gov/circ/1371/. Accessed 13 Sep 2023.
Vigneresse, J.L., 1987. Organisation tridimensionnelle du massif d'Echassie`res et bilan des mesures g´eophysiques de surface. Ge´ologie profonde de la France 27–32.
Wang, W., Sun, L., Zhang, P., et al., 2021. Study of matrix effects in laser-induced breakdown spectroscopy by laser defocus and temporal resolution. J. Anal. At. Spectrom. 36, 1977–1985. https://doi.org/10.1039/D1JA00179E.
Wise, M.A., Harmon, R.S., Curry, A., et al., 2022. Handheld LIBS for Li Exploration: an example from the Carolina Tin-Spodumene Belt, USA. Minerals 12, 77. https://doi.org/10.3390/min12010077.
Xing, P., Dong, J., Yu, P., et al., 2021. Quantitative analysis of lithium in brine by laser-induced breakdown spectroscopy based on convolutional neural network. Anal. Chim. Acta 1178, 338799. https://doi.org/10.1016/j.aca.2021.338799.
Xu, T., Liu, J., Shi, Q., et al., 2016. Multi-elemental surface mapping and analysis of carbonaceous shale by laser-induced breakdown spectroscopy. Spectrochim. Acta B At. Spectrosc. 115, 31–39. https://doi.org/10.1016/j.sab.2015.10.008.
Young, K.E., Evans, C.A., Hodges, K.V., et al., 2016. A review of the handheld X-ray fluorescence spectrometer as a tool for field geologic investigations on Earth and in planetary surface exploration. Appl. Geochem. 72, 77–87. https://doi.org/10.1016/j.apgeochem.2016.07.003.
Zhao, H., Wang, Y., Cheng, H., 2023. Recent advances in lithium extraction from lithium-bearing clay minerals. Hydrometallurgy 217, 106025. https://doi.org/10.1016/j.hydromet.2023.106025.
Zhu, X., Xu, T., Lin, Q., et al., 2014. Advanced statistical analysis of laser-induced breakdown spectroscopy data to discriminate sedimentary rocks based on Czerny–Turner and Echelle spectrometers. Spectrochim. Acta B At. Spectrosc. 93, 8–13. https://doi.org/10.1016/j.sab.2014.01.001.

Table S1 : Lithium predicted values of the reference samples using the LIBS quantification models built.

Samples	Raw				SNV				Total Spectrum Area				Refrence Li (.wt%)
	Li *670nm*	Sum Li signal	Signal ratio	iPLS	Li *670nm*	Sum Li signal	Signal ratio	iPLS	Li *670nm*	Sum Li signal	Signal ratio	iPLS	
S19_108_112	0.116	0.111	0.058	0.058	0.227	0.183	0.057	0.032	0.177	0.158	0.057	0.044	0.031
S22_110_114	0.737	0.753	0.865	0.808	0.801	0.838	0.866	0.748	0.828	0.840	0.866	0.814	0.795
C112	0.437	0.448	0.435	0.445	0.427	0.447	0.546	0.443	0.429	0.444	0.546	0.447	0.433
C113	0.506	0.475	0.512	0.471	0.455	0.433	0.400	0.471	0.472	0.443	0.400	0.461	0.473
C117	0.265	0.240	0.207	0.229	0.391	0.340	0.434	0.246	0.270	0.242	0.434	0.241	0.250
C123	0.152	0.156	0.115	0.178	0.035	0.046	0.512	0.127	0.072	0.088	0.512	0.157	0.149
S13_131_135	0.766	0.773	0.547	0.741	0.529	0.554	0.220	0.604	0.665	0.675	0.221	0.692	0.665
S14_211_215	0.457	0.433	0.400	0.433	0.499	0.474	0.114	0.424	0.475	0.448	0.114	0.436	0.371
C30	0.505	0.489	0.526	0.476	0.455	0.450	0.525	0.529	0.494	0.479	0.525	0.498	0.559
C39	0.420	0.430	0.445	0.414	0.462	0.478	0.445	0.567	0.453	0.464	0.445	0.474	0.579
C42	0.447	0.448	0.532	0.451	0.541	0.547	0.532	0.576	0.511	0.510	0.532	0.475	0.557
C43	0.643	0.677	0.656	0.687	0.599	0.650	0.656	0.678	0.638	0.674	0.656	0.676	0.592
C52	0.501	0.501	0.556	0.477	0.397	0.409	0.556	0.517	0.459	0.463	0.556	0.491	0.512
C73	0.307	0.277	0.272	0.286	0.435	0.383	0.271	0.269	0.300	0.269	0.271	0.304	0.278
ARD_13_92	0.011	0.029	0.037	0.042	0.005	0.019	0.036	0.010	0.012	0.033	0.036	0.016	0.033
Lau_CB	0.011	0.025	0.079	0.047	0.036	0.035	0.077	0.036	0.033	0.041	0.077	0.036	0.010
LV_14_01	0.013	0.028	0.050	0.050	0.000	0.009	0.048	0.000	0.006	0.024	0.048	0.032	0.007

Table S2 : Rubidium predicted values of the reference samples using the LIBS quantification models built.

Samples	Raw			SNV			Total Spectrum Area			Reference Rb (.wt%)
	Rb 779*nm*	Sum Rb signal	iPLS	Rb 779*nm*	Sum Rb signal	iPLS	Rb 779*nm*	Sum Rb signal	iPLS	
S19_108_112	0.214	0.246	0.172	0.342	0.388	0.185	0.317	0.404	0.158	0.147
S22_110_114	0.460	0.386	0.448	0.399	0.309	0.493	0.459	0.386	0.447	0.453
C112	0.281	0.307	0.283	0.242	0.254	0.270	0.257	0.276	0.256	0.289
C113	0.221	0.239	0.243	0.186	0.203	0.254	0.187	0.191	0.288	0.307
C117	0.249	0.262	0.238	0.313	0.321	0.305	0.250	0.264	0.231	0.259
C123	0.082	0.169	0.110	0.088	0.149	0.073	0.053	0.098	0.092	0.088
S13_131_135	0.450	0.481	0.515	0.267	0.256	0.389	0.354	0.366	0.477	0.484
S14_211_215	0.357	0.351	0.337	0.330	0.302	0.318	0.344	0.337	0.361	0.306
C30	0.246	0.252	0.266	0.203	0.209	0.286	0.219	0.216	0.313	0.314
C39	0.295	0.285	0.295	0.276	0.260	0.332	0.294	0.284	0.325	0.325
C42	0.306	0.291	0.279	0.306	0.282	0.312	0.319	0.307	0.296	0.337
C43	0.434	0.403	0.397	0.335	0.285	0.342	0.391	0.357	0.361	0.328
C52	0.164	0.221	0.228	0.128	0.175	0.234	0.134	0.171	0.224	0.188
C73	0.261	0.254	0.263	0.317	0.305	0.339	0.248	0.237	0.297	0.308
ARD_13_92	0.088	0.055	0.065	0.188	0.207	0.052	0.158	0.152	0.031	0.055
Lau_CB	0.062	0.014	0.040	0.166	0.178	0.043	0.130	0.103	0.057	0.034
LV_14_01	0.088	0.042	0.077	0.172	0.176	0.032	0.144	0.110	0.047	0.036

Table S3 : Lithium predicted values of the test samples used to statistically compare the different LIBS quantification models built for the Beauvoir granite deposit.

Sample	Raw				SNV				Total Spectrum Area				Reference Li (.wt%)
	Li *670nm*	Sum Li signal	Signal ratio	iPLS	Li *670nm*	Sum Li signal	Signal ratio	iPLS	Li *670nm*	Sum Li signal	Signal ratio	iPLS	
C117	0.440	0.408	0.375	0.306	0.496	0.457	0.344	0.305	0.412	0.381	0.359	0.305	0.250
C30	0.575	0.574	0.571	0.516	0.480	0.493	0.492	0.516	0.529	0.530	0.547	0.516	0.559
C42	0.501	0.507	0.502	0.542	0.543	0.559	0.608	0.542	0.532	0.539	0.517	0.542	0.557
C43	0.629	0.655	0.652	0.571	0.513	0.553	0.575	0.571	0.577	0.606	0.632	0.571	0.592
C52	0.709	0.735	0.741	0.730	0.583	0.626	0.628	0.730	0.676	0.703	0.719	0.730	0.512
0008_242_246	0.217	0.207	0.200	0.157	0.318	0.289	0.108	0.155	0.000	0.000	0.000	0.155	0.100
C68_245_248	0.727	0.719	0.687	0.547	0.506	0.516	0.652	0.547	0.665	0.659	0.662	0.547	0.482
C59_S13	0.903	0.894	0.935	0.677	0.697	0.711	0.590	0.677	0.819	0.810	0.847	0.677	0.665
S17_146_151	0.294	0.267	0.246	0.206	0.389	0.340	0.310	0.205	0.296	0.266	0.265	0.205	0.097
S22_153_156	0.516	0.491	0.495	0.499	0.551	0.530	0.545	0.499	0.550	0.521	0.495	0.499	0.355
SK_S06_196	0.368	0.339	0.337	0.244	0.390	0.354	0.286	0.243	0.445	0.434	0.437	0.366	0.185
SK_S06_198	0.325	0.284	0.274	0.285	0.443	0.373	0.357	0.284	0.130	0.109	0.165	0.075	0.203
SK_S10_177	0.375	0.342	0.309	0.254	0.470	0.420	0.357	0.253	0.254	0.218	0.203	0.171	0.165
SK_S10_182	0.196	0.189	0.208	0.075	0.087	0.086	-0.042	0.073	0.330	0.284	0.266	0.284	0.107
SK_S10_208	0.502	0.494	0.514	0.503	0.659	0.651	0.559	0.502	0.336	0.309	0.323	0.243	0.465
SK_S10_211	0.447	0.422	0.421	0.463	0.595	0.559	0.579	0.463	0.395	0.357	0.318	0.253	0.365
SK_S16_214	0.496	0.469	0.462	0.436	0.424	0.407	0.436	0.435	0.117	0.122	0.194	0.073	0.273
SK_S18_74	0.411	0.402	0.390	0.367	0.426	0.417	0.556	0.366	0.589	0.546	0.512	0.463	0.174
SK_S19_111	0.160	0.138	0.148	0.076	0.165	0.127	0.016	0.075	0.483	0.456	0.445	0.435	0.010
SK_S23_100	0.243	0.213	0.185	0.172	0.320	0.264	0.274	0.171	0.565	0.552	0.531	0.502	0.241

Table S4: Rubidium predicted values of the test samples used to statistically compare the different LIBS quantification models built for the Beauvoir granite deposit.

Sample	Raw			SNV	Total Spectrum Area	Reference Rb (.wt%)
	Rb 779nm	Sum Rb signal	iPLS	iPLS	iPLS	
C117	0.316	0.365	0.349	0.155	0.273	0.259
C30	0.344	0.358	0.362	0.140	0.336	0.314
C42	0.339	0.333	0.322	0.163	0.305	0.337
C43	0.386	0.391	0.394	0.155	0.334	0.328
C52	0.278	0.323	0.361	0.140	0.296	0.188
0008_242_246	0.299	0.306	0.270	0.159	0.000	0.172
C68_245_248	0.485	0.473	0.513	0.152	0.495	0.338
C59_S13	0.495	0.490	0.563	0.252	0.497	0.341
S17_146_151	0.339	0.333	0.294	0.164	0.328	0.237
S22_153_156	0.383	0.352	0.368	0.183	0.416	0.390
SK_S06_196	0.451	0.424	0.428	0.176	0.381	0.221
SK_S06_198	0.267	0.272	0.278	0.142	0.285	0.201
SK_S10_177	0.364	0.377	0.354	0.172	0.336	0.185
SK_S10_182	0.471	0.460	0.429	0.112	0.343	0.186
SK_S10_208	0.422	0.382	0.401	0.223	0.436	0.332
SK_S10_211	0.356	0.313	0.320	0.189	0.483	0.281
SK_S16_214	0.327	0.329	0.325	0.127	0.354	0.206
SK_S18_74	0.415	0.366	0.344	0.163	0.466	0.190
SK_S19_111	0.346	0.308	0.286	0.133	0.339	0.148
SK_S23_100	0.255	0.262	0.251	0.124	0.272	0.169

Table S5 : The concentrations of lithium and rubidium predicted using different percentages of LIBS data acquired on 4m drill core portions. The total data (100%) corresponds to the entire set of LIBS points analyzed along a vertical profile across the entire length of the sample.

Sample	Percentage of LIBS data used	Predicted Li (.wt%)	Reference Li (.wt%)	Predicted Rb (.wt%)	Reference Rb (.wt%)
S22_110_114	10%	0.859	0.795	0.279	0.453
	20%	0.843		0.269	
	30%	0.839		0.273	
	40%	0.842		0.272	
	50%	0.823		0.269	
	60%	0.835		0.275	
	70%	0.841		0.275	
	80%	0.840		0.273	
	90%	0.839		0.278	
	100%	0.841		0.277	
S19_108_112	10%	0.067	0.031	0.127	0.147
	20%	0.055		0.116	
	30%	0.059		0.117	
	40%	0.063		0.115	
	50%	0.060		0.115	
	60%	0.058		0.116	
	70%	0.057		0.116	
	80%	0.055		0.113	
	90%	0.056		0.114	
	100%	0.056		0.115	

Table S5: The concentrations of lithium and rubidium predicted using different percentages of LIBS data acquired on 4m drill core portions. The total data (100%) corresponds to the entire set of LIBS points analyzed along a vertical profile across the entire length of the sample

Sample	Percentage of LIBS data used	Predicted Li (.wt%)	Reference Li (.wt%)	Predicted Rb (.wt%)	Reference Rb (.wt%)
S14_211_215	10%	0.381	0.371	0.164	0.306
	20%	0.399		0.169	
	30%	0.405		0.174	
	40%	0.403		0.172	
	50%	0.401		0.170	
	60%	0.395		0.167	
	70%	0.392		0.166	
	80%	0.395		0.167	
	90%	0.394		0.166	
	100%	0.395		0.167	

Table S6: the predicted concentrations of lithium and rubidium obtained using various LIBS acquisition parameters, including reducing the number of areas analyzed and the number of laser shots per analysis point, to optimize acquisition time.

Sample	Acquisition parameters	Predicted Li (.wt%)	Reference Li (.wt%)	Predicted Rb (.wt%)	Reference Rb (.wt%)
C117	Initial parameters 1 analysis point	0.207		0.305	
C30	= 36 areas - 4 laser shots per area	0.526		0.286	
C117	1 analysis point =	0.371	C117 = 0.250 C30=0.559	0.145	C117 = 0.259 C30=0.314
C30	36 areas - 2 laser shots per area	0.730		0.16	
C117	1 analysis point =	0.388		0.152	
C30	9 areas - 4 laser shots per area	0.577		0.121	

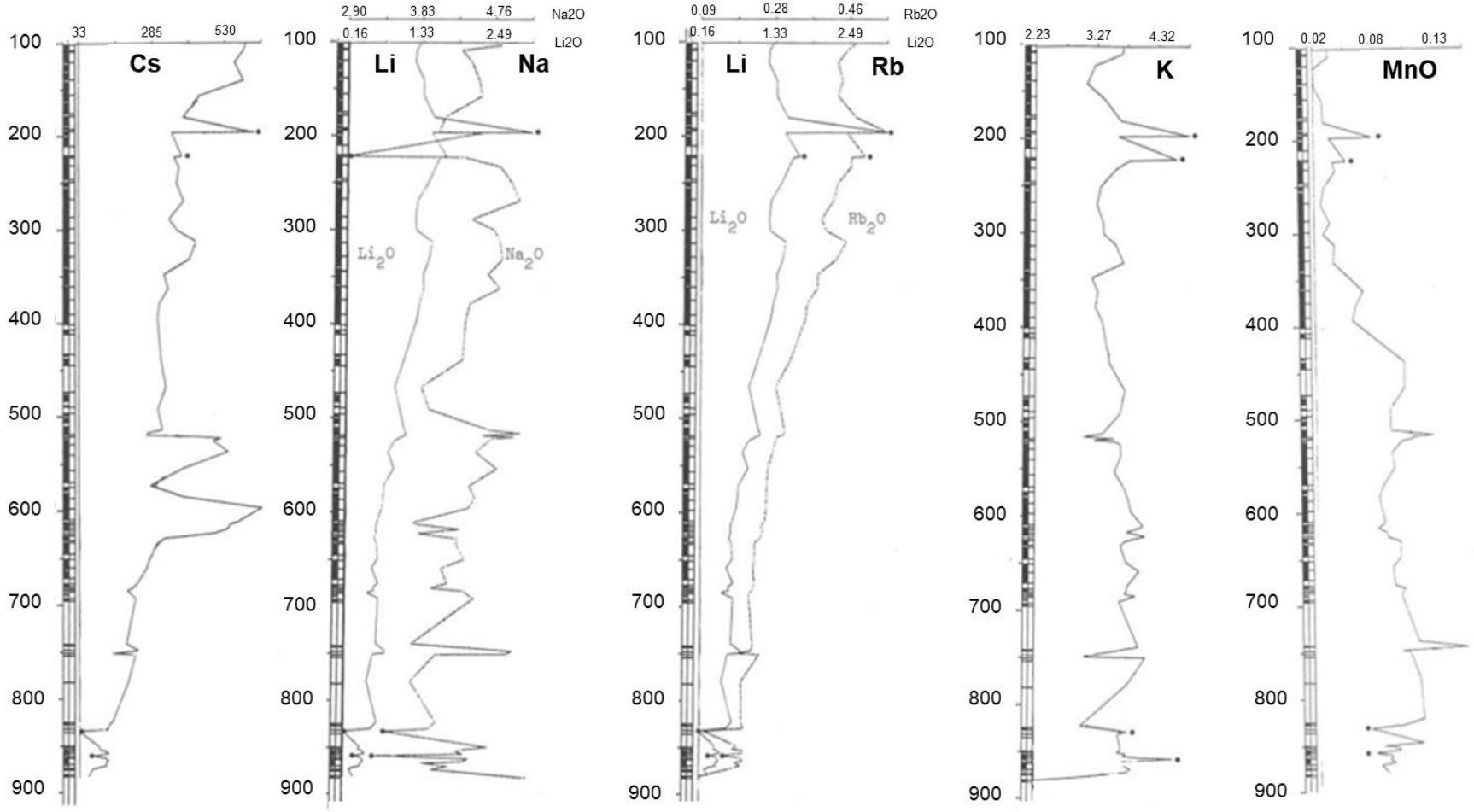

Fig. S 1: Geochemical log of the Beauvoir granite: distribution of critical elements (li, rb, cs) and matrix-associated elements (na, k, mn). Adapted from rossi et al. (1987).

Chapitre IV.
Transferability of LIBS quantitative models

Quantitative Analysis Using Handheld LIBS: Assessing Model Transferability Across Similar Deposits.

Naila Mezoued[1,], Cécile Fabre[1], Jean Cauzid[1], Christophe Ballouard[1]*

[1]CNRS, GeoRessources Laboratory, Université de Lorraine, Nancy F54000, France

Corresponding author*. E-mail: naila.mezoued@univ-lorraine.fr

Abstract

Quantitative analysis using handheld LIBS requires calibrating the spectral signal through reference samples with known concentrations that closely match the chemical and physical characteristics of the target samples, to minimize matrix effects. However, developing unique calibration models for each geological site is time-consuming, as it requires extensive sampling and detailed geochemical characterization, challenging the broader implementation of handheld LIBS for quantitative analysis, especially in the mining sector. This study evaluates to what extent a LIBS quantification model developed for a specific deposit can be generalized to rock samples of similar composition sourced from a different geographic location. For this purpose, rock samples from the Blond Massif were analyzed using quantitative models built during the Beauvoir granite exploration project to predict lithium concentrations in unprocessed rock samples. The model showed good overall performance (R^2 = 0.92) but systematically overestimated Li values. The error distribution highlighted sample texture as a key factor influencing prediction accuracy. The mean absolute error (MAE) of prediction varied substantially depending on the textural facies (rhyolite and microgranular), with the lowest error for the microgranular facies ($MAE_{Microgranular}$ = 870 ppm) and higher error values for the volcanic rhyolite facies ($MAE_{Rhyolite}$= 2697 ppm). Adjusting the analysis protocol for the rhyolite facies by reducing the number of laser shots from 4 to 1, to account for the higher ablated matter in volcanic texture, significantly reduced the prediction error in rhyolite samples ($MAE_{Rhyolite}$= 1264 ppm). This study confirms the potential to transfer LIBS quantification models across similar deposits, provided physical characteristics are consistent with reference samples, supporting the perspective of standardized quantitative approaches using handheld LIBS.

Keywords: Handheld LIBS, quantitative analysis, Beauvoir granite, The Blond massif, lithium.

1 Introduction

The potential of handheld LIBS for geoscience applications, particularly in the mining industry, is increasingly recognized (1,2). The versatility of handheld LIBS provides the ability to acquire multi-elemental data at varying scales, from individual mineral grains to whole-rock compositions, effectively addressing the challenges associated with analyzing heterogeneous and complex geological objects. Handheld LIBS has been successfully used to trace and quantify element distribution in minerals and rocks, as well as discriminating between lithological facies and different mineral phases. However, it is the capacity to generate quantitative values, especially for light elements, that has driven significant interest for handheld LIBS in the mining industry. Access to quantitative analysis through conventional laboratory methods typically takes several weeks to months, notably delaying decision-making during field operations. In contrast, by calibrating the LIBS signal with reference samples of known concentrations, the elemental composition of unknown samples can be predicted within minutes. However, the composition and texture of geological samples influence the intensity and consistency of the LIBS signal due to matrix effects, requiring the development of individual calibration curves for each specific location considered. While this approach guarantees more precise results, it is both resource-intensive and time-consuming, challenging the core advantage of field analytical devices, designed to be rapid and practical.

This study investigates the ability to transfer a LIBS calibration model developed in a specific geological context to a deposit exhibiting similar compositional characteristics. LIBS quantitative model, initially implemented to predict lithium concentrations in unprepared rock samples during the Beauvoir granite exploration project (3,4), was applied to highly differentiated rock samples sourced from the Blond Massif. No preprocessing techniques (e.g., pulverization, homogenization) were applied to either sample group, ensuring that the analysis accurately reflects field conditions and the operational constraints of mining operations. Understanding the limitations and conditions under which LIBS quantitative models can be generalized to similar deposits could enhance the applicability of LIBS for quantitative analysis. The challenge of developing new calibration curves for each project limits a broader adoption of the technique, especially in the mining sector, given the availability of more established methods, such as portable XRF.

2 Methodology

2.1 Handheld LIBS

Handheld LIBS is a compact optical system designed for field-based elemental analysis (5,6). The instrument operates by generating a micro-plasma at the surface of a sample using a pulsed laser. The light emitted by the plasma, produced as excited atoms and ions return to

lower energy states, is collected and analyzed using multiple detectors and spectrometers to produce a spectrum illustrating signal intensity (a.u.) as a function of wavelength (nm). Emission lines observed at specific wavelengths correspond to the chemical elements present in the sample, while an emission line intensity is influenced by several factors, including the element concentration, ionization potential, sample type, etc. In this study, the handheld LIBS analyzer used was the Z300 model manufactured by SciAps Inc. (Woburn, MA, USA). The same instrument was employed to develop the Beauvoir quantitative model. This analyzer is equipped with a 1064 nm pulsed laser, delivering 5–6 mJ per pulse at a repetition rate up to 50 Hz. This model was designed specifically for geochemical applications (7–9), offering an extended spectral range from 190 nm (UV) to 950 nm (IR), to detect both light (10,11) and heavy elements (12,13). All analyses were conducted in an open-air environment under ambient temperature and atmospheric pressure. An argon purge was automatically activated during measurements to enhance the signal-to-noise ratio and improve detection sensitivity in the UV range (14).

2.2 Data acquisition

To ensure a representative signal in heterogeneous materials such as rocks, each sample was analyzed multiple times at different locations. The rectangular chip samples (**Fig.1**) with an average size of 2x3 cm were analyzed using a grid of three horizontal lines and three vertical lines. Each line consisted of three analysis points, nine points in total. Each analysis point represents 36 spot analyses, with 4 laser shots averaged per spot. For the irregularly shaped CB95 and BLO120 samples (**Fig.1**), the analyses focused on the available flat surfaces (CB95 = 10 points, and BLO120 = 15 points). The acquisition parameters were kept consistent with those used during model development (cleaning shot = 1, integration delay = 19, step size = 50). LIBS spectra were processed using Spectragryph software (15). The processing steps included: (i) averaging all data points per sample to generate a mean spectrum representative of the overall rock composition; (ii) baseline correction; and (iii) extraction of selected emission line signals (Li, Rb, Si, Al, Cs, Mn) based on the spectral intervals previously used to construct the calibration models for the Beauvoir granite.

2.3 Quantitative model

The quantitative model applied in this study was initially developed as part of a research initiative related to the Beauvoir granite exploration project for lithium mining (3,4).The handheld LIBS technique was used to develop field-based analytical protocols for predicting lithium concentrations in unprocessed core sections. This approach was designed to: (i) provide a practical solution for the rapid identification of lithium-enriched zones with minimal sample preparation, and (ii) support strategic, cost-effective decisions, such as optimizing



Figure.1. Photographies illustrating the textural features of the granite samples used in this study. Upper panels: Blond granite samples, including microgranular facies (indicated by a star) and predominant very fine-grained rhyolitic textures. Lower panels: Beauvoir granite samples used to develop the lithium calibration model.

borehole positioning during drilling campaigns. Multiple models were evaluated, including various normalization methods, univariate and multivariate regressions, and spectral parameters. A two-step statistical protocol was applied to identify the optimal model for lithium prediction (16). The best-performing model **consists** of signal **ratio**, normalizing the sum of **Li** signal by the matrix elements (Si, Al, Rb, Cs, and Mn) using raw LIBS spectra (4). The performance obtained on the Beauvoir granite samples are MAE = 815 ppm, RMSE = 620 ppm. The model was developed using reference samples from the Beauvoir deposit, including 4m core segments, which were selected to represent the chemical and textural properties of the target materials. The unaltered Beauvoir granite (Facies B1)(17), targeted for lithium extraction, exhibits a non-oriented equigranular texture, with grain sizes ranging from 20–50 µm for minor phases and 300–1000 µm for major phases (18). The matrix is predominantly composed of quartz, albite, and lithium-bearing micas, particularly lepidolite, which serves as the primary lithium ore phase (19).

2.4 Samples

To assess whether the models developed for the Beauvoir granite can be applied to similar magmatic deposits, two conditions were established. First, the selected deposit must have a chemical and mineralogical composition that aligns with the Beauvoir granite. The second condition relates to the targeted element concentrations: the samples should have lithium levels within the range represented in the Beauvoir models to ensure optimal performance. In the Beauvoir model, only a small fraction of the reference dataset (7%) includes low concentrations below 500 ppm, as the average lithium concentration in the B1 facies targeted for exploitation is above 3000 ppm. Consequently, the model efficiency is likely to decrease for samples with very low concentrations (below 500 ppm). In contrast, most of the reference samples have concentrations ranging from 1000 to 3500 ppm, thereby better performance is expected for moderate lithium concentrations. Samples within the concentration range most represented in the reference data were prioritized to ensure that prediction errors are more likely resulting from the limitations of the LIBS technique or sample characteristics, rather than insufficient representation in the model training data.

Based on these criteria, ten samples from the Blond Massif were selected for LIBS analysis. The Blond Massif is located approximately 30 km northwest of Limoges and extends over an area of 60 km² (**Fig.2**). Dated at 319 ± 7 Ma (20), it represents the final magmatic stage associated with the Hercynian orogeny in the Limousin region of the French Massif Central. The magmatic pluton is composed of a series of granite intrusions, including leucogranites containing protholithionite, andalusite, and Li-muscovite in the western part of the massif, as well as a large outcropping leucogranites with Li-muscovite. It also hosts genetically related aplite and apatite veins, in addition to porphyritic microgranite dykes, such as Richemont and

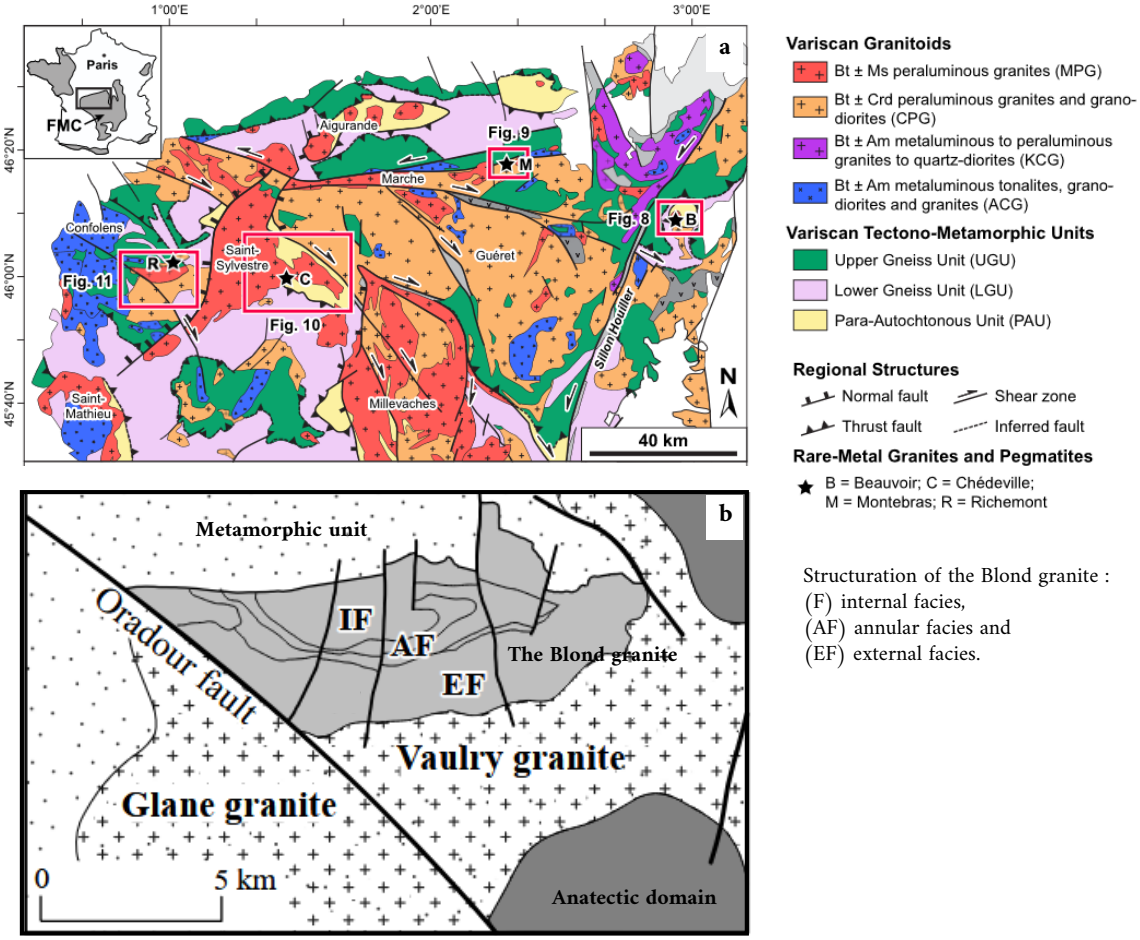

Figure.2.a) Schematic geological map of the northern French Massif Central (FMC), highlighting the locations of major rare-metal granites, including the Beauvoir granite (Modified from Harlaux et al.2017) (B) in the east and the Blond granite (R) in the west. b) Simplified geological map of the Blond granite (Modified from Alexandrov et al. 2000).

La Puelle. Although mineralogical variation occurs across different facies, the dominant lithologies are primarily composed of quartz, lithium-bearing micas (muscovite, protolithionite, and biotite), and feldspars (albite, K-feldspar, and plagioclase). Accessory minerals such as zircon, andalusite, apatite, and tourmaline were also observed. The selected samples, illustrated in **Fig.2** and summarized in **Table.1**, display a leucocratic character and exhibit textures ranging from very fine-grained microgranular (aplitic) to coarser-grained varieties. In addition, a series of granite processing samples (flotation concentrates)(21) and unaltered Beauvoir granite slabs were analyzed for comparative assessment of signal intensities. The powdered materials were compacted into 10 mm diameter pellets using a 10-ton hydraulic press.

3 Results and discussion

3.1 Lithium signal

Fig.3 compares the average LIBS signal between the Beauvoir granite sample S73 (Li=2781 ppm) and the Blond sample M13 (Li=2775 ppm). Although the lithium content is comparable, the signal intensities at 610 nm and 670 nm, the primary emission lines for lithium, are significantly higher in the Blond sample than in the Beauvoir granite. This pattern is further observed in **Fig.4**, which compares the lithium signals of six samples, three from the Beauvoir granite and three from the Blond massif, which are closely matched in lithium content. The results confirm higher signal intensities in the Blond massif samples, 1.17 and 1.10 times greater than in the Beauvoir granite. For sample CB95, however, the difference is smaller. The LIBS signal intensity of an element is influenced by several factors, including ionization potential, concentration, acquisition parameters (i.e., number of shots, laser energy, frequency), and the textural characteristics of the analyzed material. In this instance, the observed variation in signal intensity cannot be attributed to differences in analyte composition or handheld LIBS parameters. The same element was targeted, and the lithium concentrations in the selected samples from both deposits are nearly identical. Furthermore, the acquisition and spectral processing parameters were maintained consistent with those used for the Beauvoir granite deposit.

Therefore, the variation in physical properties is the most likely explanation for the observed gap in signal intensity. To assess the impact of sample physical properties on LIBS signal in samples with similar chemical compositions, LIBS analyses were performed on two sample types, powder, and solid rock, of comparable lithium concentrations (**Fig.5**). The powder pellets were obtained by the processing and homogenization of Beauvoir granite samples, ensuring consistent chemical and mineralogical characteristics across all samples considered. The hard rock sample set consisted of six specimens in total: three sourced from the Beauvoir

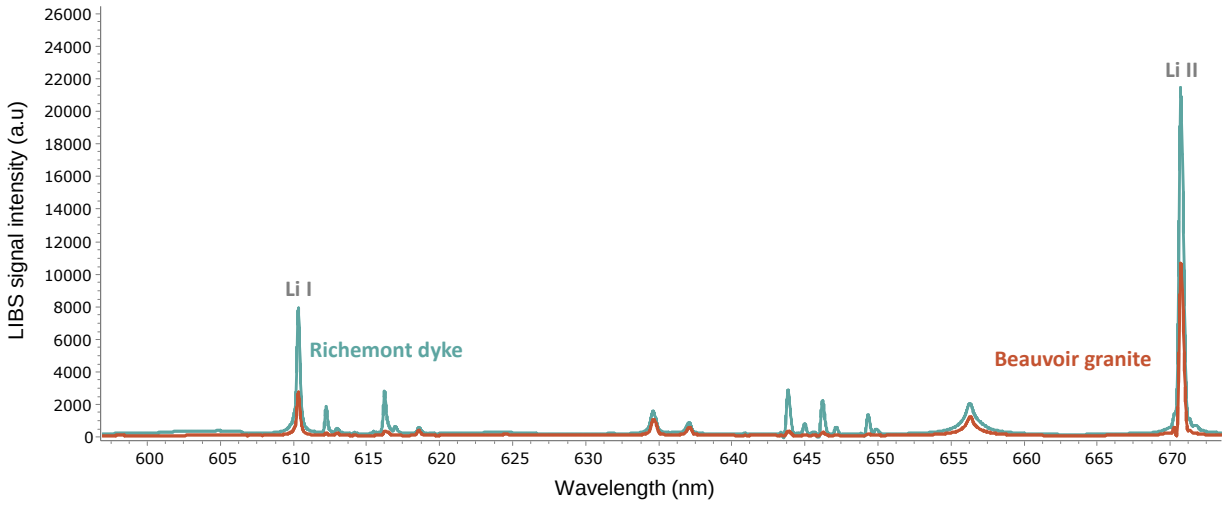

Figure.3. Average LIBS signal for two primary lithium emission lines at 610 and 670 nm for the Richemont dyke sample (green) and Beauvoir granite sample (red), both with comparable lithium concentrations (2781 ppm - 2775 ppm)

granite and three from the Blond massif. As illustrated in **Fig.5**, the signal intensity for powder pellets is higher than for unprocessed rock samples. Among the hard rock group, a distinct difference in signal intensity was observed between the Beauvoir granite and the Blond massif, with the latter exhibiting higher signal intensities. Despite identical acquisition parameters, and analyte proportions, variations in LIBS results can arise due to differences in the structural properties of the analyzed samples (21–23). Powder pellets, with a less consolidated structure than unaltered granite, absorb laser energy more efficiently. The ease of particle fragmentation in powders enhances vaporization when exposed to laser pulses.

Table 1 : The geographic location and textural, petrographic, and geochemical characteristics of the analyzed samples from the Richemont dyke.

ID	General location	Detailed location	Texture	Petrography	Li (ppm)
BLO120	The Blond massif	Monsac	Microgranite		1445
CB95		Pouzinière	Microgranite		1688
PU-93-1		La Puelle	Microgranite	Q-Ab-Or-Ms- Lep-Tpz- Cst	1205
PU-93-3		La Puelle	Microgranite	Q- Ab-Or-Ms-Lep-Tpz- Cst	1260
M-13		Richemont	Rhyolite	Q- Ab-Lep-Or-OxNb/Ta-Amb-	2775
M-12		Richemont	Rhyolite	Q-Ab- Lep-Or- OxNb-Ta-Amb-	2940
M-11		Richemont	Rhyolite	Q-Ab- Lep-Or- OxNb-Ta-Amb-	2905
BLO-23-10-V1		Richemont	Rhyolite		3 201
BLO-23-10-V2		Richemont	Rhyolite		3 870
BLO-23-10-V3		Richemont	Rhyolite		3 065

In contrast, solid rock samples require higher energy input or more laser shots to achieve similar ablation efficiency. Within the hard rock sample group, the structural characteristics of the Beauvoir granite and the Blond massif differ notably. Petrographic analysis of the Blond rhyolite facies reveals that the original volcanic glass has undergone devitrification, forming microcrystalline phases approximately 10 µm in size (25). The volcanic textures, resulting from the rapid cooling of surface lava, are less thermodynamically stable than microcrystalline texture and gradually reorganize into more stable structures, during which amorphous glass is replaced by crystalline mineral aggregates under environmental influences. The fine microcrystalline aggregates of the rhyolite facies are less consolidated, which leads to greater material ablation and, consequently, higher LIBS signal intensities at comparable lithium concentrations. This is further supported by the smaller signal discrepancy observed in texturally similar samples to the Beauvoir granite. For instance, sample CB95, which exhibits microgranitic facies, shows signal intensities comparable with those of the Beauvoir granite, highlighting the significant influence of sample texture on LIBS signal response and its implications for applying models across similar deposit types.

3.2 Lithium predictions

Fig.6a presents the predicted lithium concentrations for the Blond granite samples, obtained using the Beauvoir calibration model, compared to the reference laboratory values. The high Pearson correlation coefficient (0.92) indicates a strong linear relationship between the LIBS predictions and the reference values, suggesting a good performance of the Beauvoir model on the Blond samples. However, the MAE of the prediction is 1966 ppm, which is higher than the 815 ppm MAE observed for the Beauvoir granite validation samples. The distribution of absolute errors for the Blond Massif samples, as shown in **Fig.6b**, reveals a systematic bias correlated with sample textural properties. The rhyolitic facies samples from the Richemont dyke (northern Blond Massif) exhibit larger prediction errors (MAE = 2697 ppm) compared to the microgranular facies (MAE = 870 ppm) sourced from other locations within the massif and align more closely with the error values observed in the Beauvoir granite samples. The physical properties of the microgranular textures closely match those of the Beauvoir pluton, suggesting a higher degree of compatibility with the calibration model, while the devitrified texture is likely less consolidated and more altered compared to the reference samples used to build the model.

To address this limitation, future work should focus on incorporating textural indicators (e.g., grain size, alteration state, etc.) as input data to account for the non-chemical variability present in natural rock samples, which can contribute to signal fluctuations and affect model accuracy. Additionally, expanding the training dataset to include a wider range of rock textures, from fine-grained volcanic rocks to coarse-grained plutonic rocks, is crucial for improving the robustness

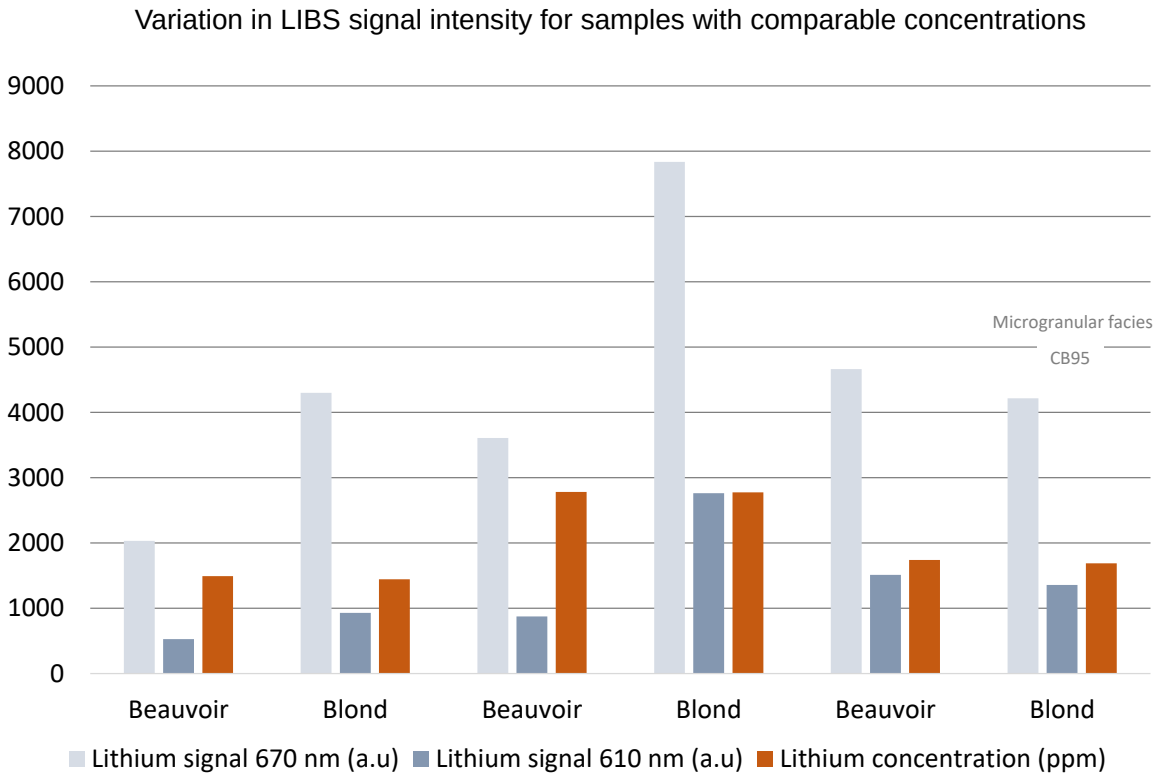

Figure.4. Comparative analysis of lithium LIBS signal intensities at 610 nm and 670 nm for samples from the Richemont Dyke (a. CB120, c. CB95, e. M13) and Beauvoir Granite Deposit (b. C73 d. C123, f. SK_S18_74)

Variation in LIBS signal intensity forpowder and hard rock samples

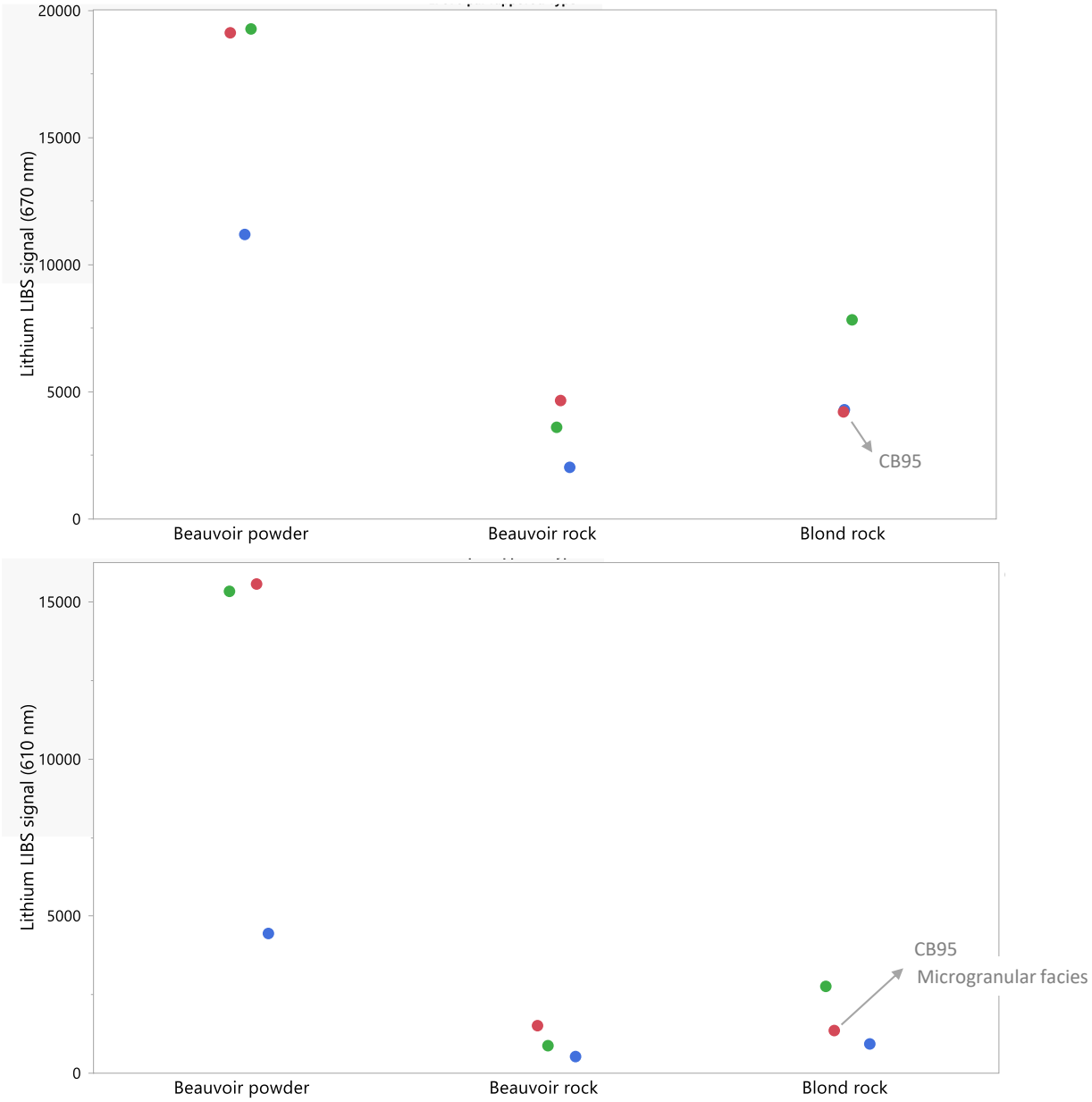

Figure.5. Comparative LIBS analysis of lithium signals at 610 nm and 670 nm for samples with comparable lithium concentrations (ppm). Groups with similar lithium content are marked by a similar color.

and the generalization potential of the calibration model across similar deposits, specifically when targeting magmatic rocks. Variations in texture observed both within an individual magmatic body and across different deposits result from the complex crystallization history of magmatic systems, which often consist of multiple intrusions that crystallize at varying rates and depths. This is reflected in the Blond Massif samples, which consist of different units (i.e., pegmatite, rhyolite, aplite, microgranite). The rhyolitic facies, characterized by a devitrified volcanic texture observed in the Richemont dyke (north of the massif), indicate rapid cooling near the surface. In contrast, microgranular facies found at other locations within the massif illustrate slower cooling at greater depths, allowing for more stable crystal growth. The coexistence of these contrasting textural zones highlights the importance of incorporating textural heterogeneity into LIBS calibration models to more accurately represent the structural heterogeneity observed in geological objects. In parallel, machine learning algorithms could provide an effective solution for improving the adaptability of LIBS models to heterogeneous data by integrating both spectral and physical features, and modeling nonlinear relationships. This approach would increase the robustness and transferability of LIBS quantitative models across multiple deposits. Additionally, machine learning algorithms could provide an effective solution for improving the adaptability of LIBS models to heterogeneous rock samples by integrating both spectral and physical features, better suited for modeling nonlinear relationships, thus enhancing the robustness and transferability of LIBS quantitative models across multiple deposits.

3.3 Data acquisition optimization

To minimize the impact of increased ablation in the devitrified texture of rhyolite samples, the acquisition parameters of the portable LIBS instrument were adjusted to reduce the material vaporized by the laser on rhyolitic facies. Since the laser energy on the SciAps handheld LIBS analyzer is fixed at 6 mJ per analysis, the approach was to assess whether reducing the number of laser shots per analysis zone, initially set to four (1 analysis point = 36 zones, 4 laser shots per zone), could rescale the LIBS signal obtained from volcanic samples to match the magnitudes observed in unaltered granite samples used in the Beauvoir calibration model.

LIBS analyses were conducted on six rhyolite samples, with the number of shots per analysis zone reduced to one, in addition to a preliminary cleaning shot on each zone to eliminate surface contamination. The adjusted acquisition parameters resulted in an average 21% reduction in signal compared to the original four-shot configuration. The absolute error for the Blond rhyolite samples decreased by 52%, reaching MAE of 1264 ppm (**Fig.7**). Although the MAE remains higher than that of the Beauvoir granite and microgranular samples from the

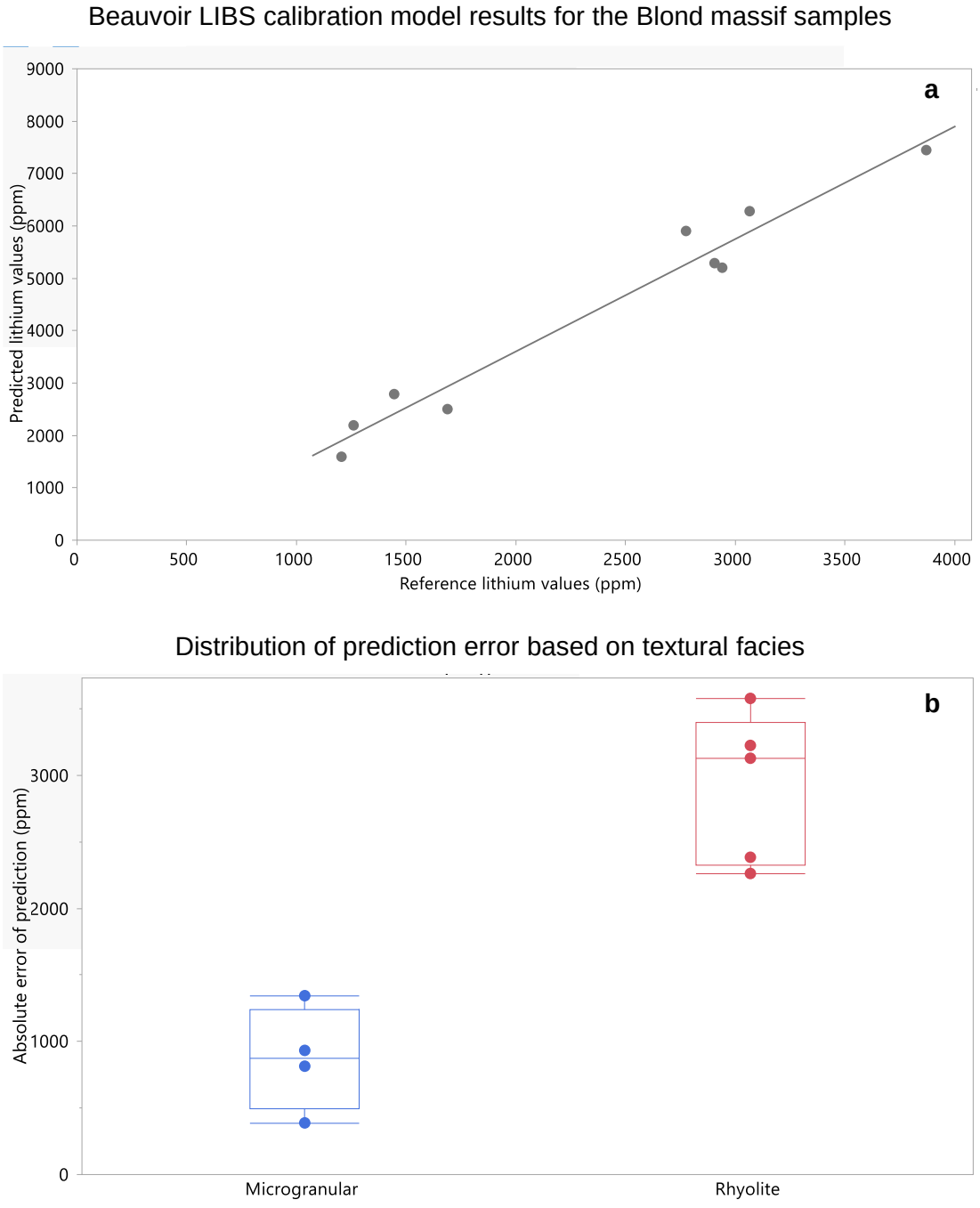

Figure.6. Lithium predictions in Richemont dyke samples using the Beauvoir granite quantitative model: a) Linear regression of the reference geochemical values and the predicted values, and b) Distribution of the absolute error based on the textural characteristics of the analyzed samples.

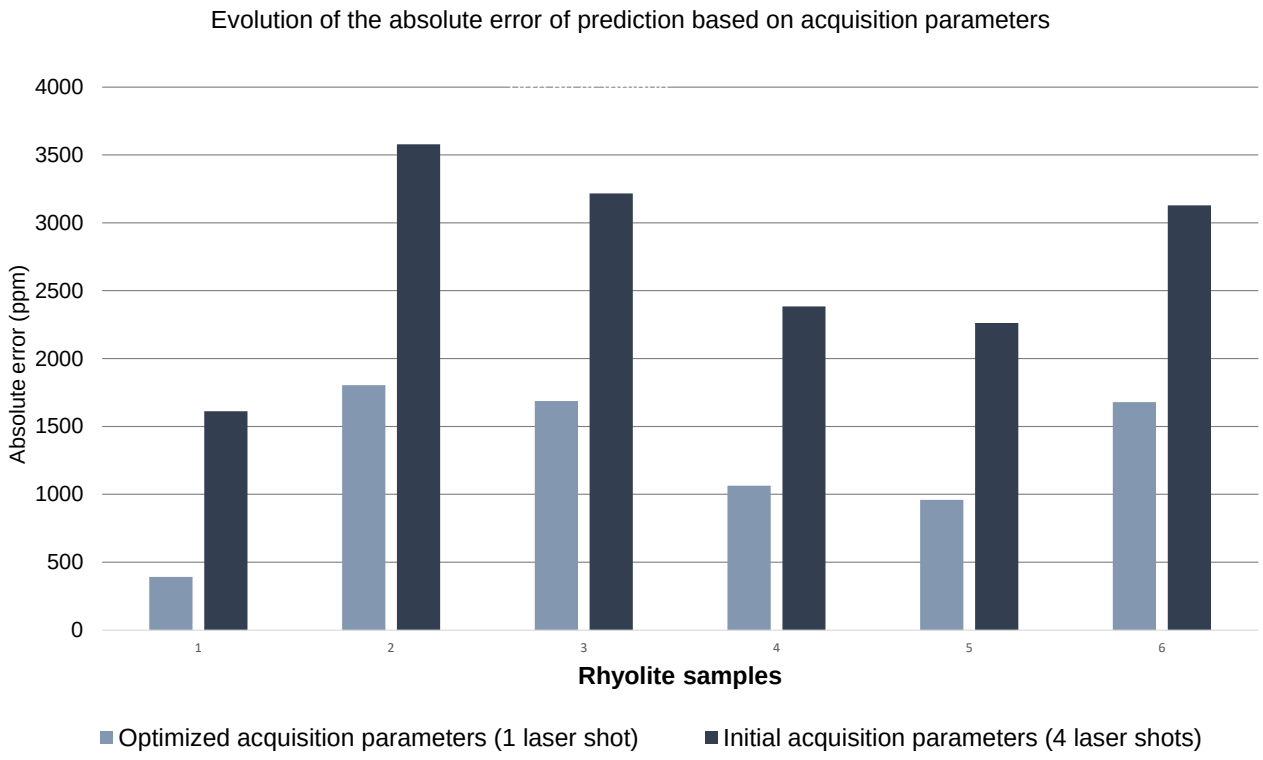

Figure.7. Evolution of the absolute prediction error for rhyolite samples from the Blond Massif using LIBS analysis. Results are shown for both the initial acquisition parameters (4 laser shots per zone) and the optimized parameters (1 laser shot per zone).

Blond massif, the optimization of acquisition parameters significantly improved the performance of the LIBS calibration model.

Although adjusting acquisition parameters to align the LIBS signal of rhyolite texture with that of microgranular texture improved lithium predictions, this approach can introduce other methodological biases. Determining the appropriate acquisition parameters for a sample often relies on preliminary visual characterization, which can be misleading during field operations. Additionally, adjusting the data acquisition to meet expected outcomes may suppress anomalies or mask the true heterogeneity of the sample. To address this, a broader range of volcanic samples with diverse textures should be analyzed to assess whether varying textures necessitate different analysis protocols, the conditions under which these protocols should be applied, and the specific criteria for their implementation. This will help determine whether such adjustments lead to meaningful improvements or if alternative approaches should be considered for more accurate predictions.

4 Conclusion

In this study, the potential to generalize a LIBS quantification model developed in a specific geological context to geochemically similar deposits was evaluated. the calibration model developed using reference samples from the Beauvoir granite deposit to predict lithium values in unprocessed rocks was applied to rock samples from the Blond massif, a highly differentiated magmatic intrusion exhibiting comparable compositional characteristics. The results obtained (R^2 = 0.92, MAE = 1966 ppm) indicate good predictive performance. However, lithium values are systematically overestimated and the absolute prediction errors are higher compared to those recorded for the validation samples from the Beauvoir granite (R^2 = 0.94, MAE = 815 ppm). In addition, the distribution of the prediction error was not homogeneous across all samples. The MAE was significantly lower for the microgranitic facies (870 ppm), whereas the fine-grained rhyolitic facies exhibited substantially higher errors (2697 ppm). The difference in prediction error is likely due to inconsistencies in the physical properties between the samples from the Blond Massif and the reference materials used to develop the model. The microgranitic samples have a texture similar to the equigranular B1 facies from the Beauvoir granite used to calibrate the model. In contrast, the fine-grained rhyolitic facies characterized by a recrystallized texture formed through devitrification represents a less consolidated texture that facilitates increased material ablation, resulting in much stronger emission lines. The results emphasize that, beyond chemical compatibility, the textural uniformity of the geological samples is a crucial factor to consider when applying LIBS quantification models across varying deposit sites. This suggests that incorporating structural factors, such as grain size and degree of alteration, into calibration models could help account for the textural variability observed in rock samples, improving the robustness and

generalizability of LIBS quantification across different geological contexts. As an alternative, the LIBS acquisition parameters were adjusted to compensate for the increased ablation intensity in the rhyolite samples. The number of laser shots per analysis zone was reduced from four to one, excluding the initial cleaning shots to remove surface contamination. Adapting the acquisition protocol resulted in 52% reduction in MAE for rhyolite samples, from 2697 ppm to 1264 ppm, effectively rescaling the LIBS signal intensity to align with the range observed for the unaltered granite samples from the Beauvoir deposit. Reiterating this experiment on similar magmatic rocks from different deposits would provide valuable insights into the influence of various volcanic and plutonic textures on the LIBS signal for comparable compositions, which would facilitate the development of more efficient LIBS data acquisition strategies to balance the influence of texture and degree of alteration on LIBS signal.

Acknowledgments

We would like to thank Christophe Ballouard for providing the rock samples from the Blond massif as well as the geochemical data associated.

Funding

This study was supported by the French National Research Agency via the Labex Ressources 21 project [reference ANR–10–LABX–21-01] and partially financed by Imerys, the operating company of the Beauvoir Granite.

AI disclosure

The author applied ChatGPT and Deeple to translate some parts of the text from French to English. After using these AI interfaces, the author reviewed and edited the content as needed and take full responsibility for the content of the publication.

Reference

1. Fabre C. Advances in Laser-Induced Breakdown Spectroscopy analysis for geology: A critical review. Spectrochimica Acta Part B: Atomic Spectroscopy. 2020 Apr;166:105799.

2. Harmon RS. Laser-Induced Breakdown Spectroscopy in Mineral Exploration and Ore Processing. Minerals. 2024 Jul 1;14:731.

3. The EMILI project | EMILI [Internet]. 2025 [cited 2025 Apr 18]. Available from: https://emili.imerys.com/en/emili-project

4. Mezoued N, Fabre C, Cauzid J, Kahou ZS, Rocher O. Handheld LIBS contribution to quantify critical elements during mining operations: The Beauvoir granite case study. Journal of Geochemical Exploration. 2025 Apr 1;271:107689.

5. Senesi GS, Harmon RS, Hark RR. Field-portable and handheld laser-induced breakdown spectroscopy: Historical review, current status and future prospects. Spectrochimica Acta Part B: Atomic Spectroscopy. 2021 Jan 1;175:106013.

6. Senesi GS, De Pascale O. Laser-Induced Breakdown Spectroscopy (LIBS) In-Situ: From Portable to Handheld Instrumentation. In: D'Amico S, Venuti V, editors. Handbook of Cultural Heritage Analysis [Internet]. Cham: Springer International Publishing; 2022 [cited 2025 Apr 25]. p. 465–503. Available from: https://doi.org/10.1007/978-3-030-60016-7_17

7. Defnet PA, Wise MA, Harmon RS, Hark RR, Hilferding K. Analysis of Garnet by Laser-Induced Breakdown Spectroscopy—Two Practical Applications. Minerals. 2021 Jul;11(7):705.

8. Lawley CJM, Somers AM, Kjarsgaard BA. Rapid geochemical imaging of rocks and minerals with handheld laser induced breakdown spectroscopy (LIBS). Journal of Geochemical Exploration. 2021 Mar 1;222:106694.

9. Hark RR, Remus JJ, East LJ, Harmon RS, Wise MA, Tansi BM, et al. Geographical analysis of "conflict minerals" utilizing laser-induced breakdown spectroscopy. Spectrochimica Acta Part B: Atomic Spectroscopy. 2012 Aug 1;74–75:131–6.

10. Fabre C, Ourti NE, Ballouard C, Mercadier J, Cauzid J. Handheld LIBS analysis for in situ quantification of Li and detection of the trace elements (Be, Rb and Cs). Journal of Geochemical Exploration. 2022 May 1;236:106979.

11. Wise MA, Harmon RS, Curry A, Jennings M, Grimac Z, Khashchevskaya D. Handheld LIBS for Li Exploration: An Example from the Carolina Tin-Spodumene Belt, USA. Minerals. 2022 Jan;12(1):77.

12. Pochon A, Desaulty AM, Bailly L. Handheld laser-induced breakdown spectroscopy (LIBS) as a fast and easy method to trace gold. J Anal At Spectrom. 2020 Feb 12;35(2):254–64.

13. Pochon A, Desaulty AM, Bailly L, Lach P. Challenging the traceability of natural gold by combining geochemical methods: French Guiana example. Applied Geochemistry. 2021 Jun 1;129:104952.

14. Kim CK, In JH, Lee SH, Jeong S. Influence of Ar buffer gas on the LIBS signal of thin CIGS films. J Anal At Spectrom. 2013 Mar 13;28(4):460–7.

15. F. Menges. Spectragryph - optical spectroscopy software [Internet]. [cited 2024 Jan 11]. Available from: http://spectragryph.com/

16. Duponchel L, Fabre C, Bousquet B, Motto-Ros V. Statistical comparison of predictive models for quantitative analysis and classification in the framework of LIBS spectroscopy: A tutorial. Spectrochimica Acta Part B: Atomic Spectroscopy. 2023 Oct 1;208:106776.

17. G.Monnier, B.Charoy, M.Cuney, D.Ohnenstetter, J.L.Robert. Evolution spatiale et temporelle de la composition des micas du granite albitique à topaze-lépidolite de Beauvoir. Géologie de la france. n°2-3. 1987;179–88.

18. Ph.Rossi, A.Autran. Log pétrographique et géochimique du granite de Beauvoir dans le sondage "Echassière I" Minéralogie ete géochimie comparées. Géologie de la France. n°2-3. 1987;111–35.

19. Cuney M, Marignac C, Weisbrod A. The Beauvoir topaz-lepidolite albite granite (Massif Central, France); the disseminated magmatic Sn-Li-Ta-Nb-Be mineralization. Economic Geology. 1992 Nov 1;87(7):1766–94.

20. Alexandrov P, Cheilletz A, Deloule É, Cuney M. 319 ± 7 Ma crystallization age for the Blond granite (northwest Limousin, French Massif Central) obtained by U/Pb ion-probe dating of zircons. Comptes Rendus de l'Académie des Sciences - Series IIA - Earth and Planetary Science. 2000 May 30;330(9):617–22.

21. Korbel C, Mezoued N, Demeusy B, Fabre C, Cauzid J, Filippova IV, et al. Quantification of lithium using handheld instruments: application of LIBS and XRF spectroscopy to assay the lithium content of mineral processing products. J Anal At Spectrom. 2024 Jul 3;39(7):1838–53.

22. Pandey SJ, Locke R, Gaume RM, Baudelet M. Effect of powder compact density on the LIBS analysis of Ni impurities in alumina powders. Spectrochimica Acta Part B: Atomic Spectroscopy. 2018 Oct 1;148:99–104.

23. Foucaud Y, Fabre C, Demeusy B, Filippova IV, Filippov LO. Optimisation of fast quantification of fluorine content using handheld laser induced breakdown spectroscopy. Spectrochimica Acta Part B: Atomic Spectroscopy. 2019 Aug 1;158:105628.

24. Xu W, Sun C, Tan Y, Gao L, Zhang Y, Yue Z, et al. Total alkali silica classification of rocks with LIBS: influences of the chemical and physical matrix effects. J Anal At Spectrom. 2020;35(8):1641–53.

25. Raimbault L, Burnol L. The Richemont rhyolite dyke, Massif Central, France; a subvolcanic equivalent of rare-metal granites. Canadian Mineralogist [Internet]. 1998 Apr 1 [cited 2024 Nov 19]; Available from: https://www.semanticscholar.org/paper/The-Richemont-rhyolite-dyke%2C-Massif-Central%2C-a-of-Raimbault-Burnol/44b27d7e01c07626db0b48cccdf38913e89a5eee

Table S1 : Lithium concentration predictions for Blond Massif samples using the Beauvoir granite calibration model. Results are shown for both initial (4 shots) and optimized (1 shot) LIBS acquisition parameters, along with corresponding absolute prediction errors compared to reference laboratory values.

ID	Texture	Li (ppm)	Lithium prediction	Error of prediction	Lithium prediction (1 shot)	Error of prediction
BLO120	Microgranite	1445	2789.20	1344.2	-	-
CB95	Microgranite	1688	2502.4	814.4	-	-
PU-93-1	Microgranite	1205	1593.1	388.1	-	-
PU-93-3	Microgranite	1260	2193.0	933.0	-	-
M-13	Rhyolite	2775	5903.5	3128.5	4452.7	1678.7
M-12	Rhyolite	2940	5202.4	2262.4	3899.9	959.9
M-11	Rhyolite	2905	5289.4	2384.4	3968.6	1063.6
BLO-23-10-V1	Rhyolite	3 201	4813.3	1612.3	3592.9	391.5
BLO-23-10-V2	Rhyolite	3 870	7448.1	3578.1	5674.0	1804.0
BLO-23-10-V3	Rhyolite	3 065	6281.4	3216.4	4752.3	1687.36

Chapitre V.

Analysis of Minerals Using Handheld LIBS Technology

data

MDPI

Data Descriptor

Analysis of Minerals Using Handheld Laser-Induced Breakdown Spectroscopy Technology

Naila Mezoued *, Cécile Fabre, Jean Cauzid, YongHwi Kim and Marjolène Jatteau

GeoRessources, Faculté des Sciences et Technologies, Université de Lorraine, CNRS, F-54506 Vandœuvre-lès-Nancy, France; cecile.fabre@univ-lorraine.fr (C.F.); jean.cauzid@univ-lorraine.fr (J.C.); yonnykim1112@gmail.fr (Y.K.); marjolene.jatteau@univ-lorraine.fr (M.J.)

* Correspondence: naila.mezoued@univ-lorraine.fr

Abstract: Laser-induced breakdown spectroscopy (LIBS), a rapid and versatile analytical technique, is becoming increasingly widespread within the geoscience community. Suitable for fieldwork analyses using handheld analyzers, the elemental composition of a sample is revealed by generating plasma using a high-energy laser, providing a practical solution to numerous geological challenges, including identifying and discriminating between different mineral phases. This data paper presents over 12,000 reference mineral spectra acquired using a handheld LIBS analyzer (© SciAps), including those of silicates (e.g., beryl, quartz, micas, spodumene, vesuvianite, etc.), carbonates (e.g., dolomite, magnesite, aragonite), phosphates (e.g., amblygonite, apatite, topaz), oxides (e.g., hematite, magnetite, rutile, chromite, wolframite), sulfates (e.g., baryte, gypsum), sulfides (e.g., chalcopyrite, pyrite, pyrrhotite), halides (e.g., fluorite), and native elements (e.g., sulfur and copper). The datasets were collected from 170 pure mineral samples in the form of crystals, powders, and rock specimens, during three research projects: NEXT, Labex Ressources 21, and ARTeMIS. The extensive spectral range covered by the analyzer spectrometers (190–950 nm) allowed for the detection of both major (>1 wt.%) and trace (<1 wt.%) elements, recording a unique spectral signature for each mineral. Mineral spectra can serve as reference data to (i) identify relevant emission lines and spectral ranges for specific minerals, (ii) be compared to unknown LIBS spectra for mineral identification, or (iii) constitute input data for machine learning algorithms.

Dataset: https://doi.org/10.24396/ORDAR-165.

Dataset License: CC-BY-NC-SA

Keywords: laser-induced breakdown spectroscopy; handheld LIBS; minerals; spectra; database

check for updates

Academic Editors: Yu Tao, Siting Xiong and Rui Song

Received: 24 January 2025
Revised: 20 February 2025
Accepted: 21 February 2025
Published: 20 March 2025

Citation: Mezoued, N.; Fabre, C.; Cauzid, J.; Kim, Y.; Jatteau, M. Analysis of Minerals Using Handheld Laser-Induced Breakdown Spectroscopy Technology. *Data* **2025**, *10*, 40. https://doi.org/10.3390/data10030040

Copyright: © 2025 by the authors. Licensee MDPI, Basel, Switzerland. This article is an open access article distributed under the terms and conditions of the Creative Commons Attribution (CC BY) license (https://creativecommons.org/

1. Summary

The laser-induced breakdown spectroscopy (LIBS) technique is a rapid and versatile analytical solution for analyzing various geological materials: rocks [1–3], powders [4–6], and minerals [7,8]. Additionally, by overcoming the limitations of laboratory-based systems through the development of handheld analyzers [9–12], the LIBS technique has significantly increased its potential and attractiveness to the geoscience community. The ability to access geochemical information onsite during field investigations is particularly valuable in geology as the spatial scale of the studied objects ranges from microns (min- erals) to hundreds of kilometers (geological structures). Handheld LIBS has successfully

been used to address several challenges in geology, including determining the proportion of targeted elements in mining operations [6,13–15] and the spatial distribution of chemical elements [16,17], identifying geological samples [1,18], and exploring extraterrestrial rocks and soils during space missions [19–21]. Furthermore, by processing LIBS analysis using chemometric algorithms [22], the spectra of known samples can be used as references to identify rock species [18,23], highlight chemical variation within a specific mineral phase [24–27], and discriminate between minerals presenting similar physical characteristics that might complicate onsite identification [28,29].

The presence or absence of minerals, as well as the chemical variations observed in different minerals or within a specific mineral phase, can reveal the genesis conditions and the geological processes leading to the deposit formation. Mineral phase identification can be performed in the field based on physical characteristics (i.e., color, crystal form) but might be challenging, especially with small-sized textures (e.g., phaneritic and microgranular matrices) or if different minerals are visually similar (e.g., spodumene, petalite, Li micas). The idea is to apply LIBS to automate mineral identification in rock samples based on the fact that an LIBS spectrum obtained from a mineral sample reflects the nature, structure, and proportions of the elements it contains, generating a unique spectral fingerprint for each mineral. While these types of approaches are powerful tools [3,28–30], their implementation depends on the availability of comprehensive and high-quality reference data. Accurate recognition, classification, and clustering depend on reliable and representative input variables, highlighting the critical importance of LIBS spectral libraries.

This study provides access to more than 12,000 reference LIBS spectra for several mineral species, including silicates, carbonates, sulfides, sulfates, oxides, and native elements (Table 1). Multiple samples of the same mineral species were analyzed to portray the geochemical diversity observed in a mineral phase across different deposits. The number of analyses per sample was maximized to generate large datasets compatible with advanced chemometric techniques. Ultimately, this spectral library is a foundational step meant to be expanded and enriched by future research contributions, such as those focused on lithium-rich minerals [8] and other relevant studies, to support the future application of the LIBS technique in mineral discrimination and automatic mineral identification.

Table 1. Summary of the mineral samples analyzed: the mineral species, chemical formulas, number of samples analyzed, and total spectra acquired. Detailed metadata are available in the database.

Mineral	Formula	Sample	Spectra
Albite	$Na(AlSi_3O_8)$	5	356
Amblygonite	$(Li,Na)Al(PO_4)(F,OH)$	1	96
Apatite	$Ca_5(PO_4)_3(Cl/F/OH)$	5	368
Apophyllite	$KCa_4(Si_4O_{10})2F_8(H_2O)$	1	46
Aragonite	$CaCO_3$	1	49
Arsenopyrite	FeAsS	4	304
Baryte	$BaSO_4$	1	60
Beryl	$Be_3Al_2(Si_6O_{18})$	2	192
Biotite	$K(Fe^{2+}/Mg)_2(Al/Fe^{3+}/Mg/Ti)([Si/Al/Fe]_2Si_2O_{10})(OH/F)_2$	4	207
Calcite	$CaCO_3$	2	97
Cassiterite	SnO_2	6	486
Chalcopyrite	$CuFeS_2$	5	363
Chlorite	$A_{5-6}T_4Z_{18}$/A = Al, Fe, Li, Mg, Mn, Ni/T = Al, Fe, S /Z = O, OH	3	223
Chromite	$FeCr_2O_4$	1	40
Columbite	$(Fe,Mn)Nb_2O_6$	1	96
Copper	Cu	1	30
Dolomite	$CaMg(CO_3)_2$	1	40
Fluorite	CaF_2	11	731
Galena	PbS	1	29
Garnet	$X_3Z_2(SiO_4)_3$/X = Mg, Ca, Fe, Mn/Z = Al, Fe, Cr, V	4	160
Gypsum	$Ca(SO_4)2(H_2O)$	1	50
Hematite	Fe_2O_3	5	317

s

Table 1. *Cont.*

Mineral	Formula	Sample	Spectra
Illite	$(K,H_3O)Al_2Si_4O_{10}(OH)_2$	1	80
Ilmenite	$FeTiO_3$	1	109
Kaolinite	$Al_2Si_2O_5(OH)_4$	1	40
K-feldspars	$KAlSi_3O_8$	7	592
Kyanite	Al_2SiO_5	1	40
Li micas	$KLi_2Al(Si_4O_{10})(F,OH)_2$ to $K(Li_{1.5}Al_{1.5})(AlSi_3O_{10})(F,OH)_2$	22	2550
Magnesite	$MgCO_3$	1	40
Magnetite	$Fe^{2+}Fe^{3+}{}_2O_4$	1	10
Malachite	$Cu_2(CO_3)(OH)_2$	1	20
Molybdenite	MoS_2	3	145
Muscovite	$KAl_2(AlSi_3O_{10})(OH)_2$	5	272
Pyrite	FeS_2	4	248
Pyrrholite	**Fe_7S_8**	**1**	**50**
Quartz	SiO_2	8	349
Rhodochrosite	$MnCO_3$	1	40
Rutile	TiO_2	4	266
Serpentinite	$(Mg,Fe)_3Si_2O_5(OH)_4$	1	40
Sphalerite	(Zn,Fe)S	8	534
Spodumene	$LiAlSi_2O_6$	1	125
Stannite	$(Mn,Fe)(Ta,Nb)_2O_6$	1	96
Sulfur	S	1	10
Talc	$Mg_3Si_4O_{10}(OH)_2$	1	40
Tantalite	$(Fe, Mg, Mn)Ta^2O^6$	1	96
Topaz	$Al_2SiO_4(F,OH)_2$	1	44
Tourmaline	AD_3G_6 $(T_6O_{18})(BO_3)_3X_3Z$ A = Ca, Na, K, Pb D = Al, Fe, Li, Mg, Mn, Ti/G = Al, Cr, Fe, V T = Si, Al/X = O, OH/Z = F, O, OH	11	709
Vermiculite	$(Mg,Fe,Al)_3(Al,Si)_4O_{10}(OH)_24H_2O$	1	40
Vesuvianite	$Ca_{10}Al_4(SiO_4)_5(OH)_4$	1	40
Wolframite	$(Mn, Fe)WO_4$	6	429
Wollastonite	$CaSiO_3$	1	40
Zinnwaldite	$KFe_2Al(Al_2Si_2O_{10})(OH)_2$ to $KLi_2Al(Si_4O_{10})(F,OH)_2$	4	128
Zircon	$ZrSiO_4$	1	96

2. Data Description

The spectral database is available open access (license CC-BY-NC-SA) on the ORDaR platform (OTELo Research Data Repository), managed by the Observatory Earth Environment of Lorraine (OTELo), via the following doi: https://doi.org/10.24396/ORDAR-165. The database, titled "Mineral spectra acquired using handheld LIBS", includes a metadata file summarizing essential information: the sample ID, mineral type, chemical formula, sample type, matrix type, number of data points, spectra per sample, and spectra per mineral. To simplify data manipulation, the spectra are organized into individual zip files corresponding to the 55 mineral species analyzed, including albite, amblygonite, apophyllite, aragonite, apatite, arsenopyrite, baryte, beryl, cassiterite, calcite, chalcopyrite, chlorite, chromite, columbite, copper, kyanite, dolomite, fluorite, galena, garnet, gypsum, hematite, illite, ilmenite, kaolinite, k-feldspars, magnetite, magnesite, malachite, muscovite, pyrite, pyrrhotite, quartz, rhodochrosite, rutile, serpentinite, sulfur, sphalerite, spodumene, stannite, talc, tantalite, topaz, tourmaline, vermiculite, vesuvianite, wolframite, wollastonite, and zircon.

2.1. Spectra Files

The spectra files are organized as follows: Individual spectra (e.g., spectrum1, spectrum2, spectrum3) represent the average signal obtained by multiple laser shots in each zone, with two to four laser pulses. The labeled "Average" spectra are the mean spectra for each analysis grid. As detailed in the "Data acquisition" Section, one analysis point represents a grid of multiple analyzed zones, with each zone analyzed using successive laser shots. Further details on data acquisition are available in the Methodology Section.

LIBS data were exported from the LIBS analyzer in CSV format. A spectrum corre- sponds to a file containing 23,432 rows recording the signal intensity as a function of the wavelength. The downloaded files were wavelength-normalized by resampling the spectral data to a consistent wavelength scale, correcting for variations in the pixel-to-wavelength mapping due to detector inconsistencies or calibration shifts. The high spectral resolu- tion (0.033 nm) is particularly valuable for accurately analyzing complex matrices such as geological materials. In minerals composed of various elements, this degree of precision minimizes emission line overlap and enhances the ability to detect weak signals from trace elements even next to the stronger emission lines of major components. However, the large number of variables per spectrum can increase processing times, especially for large-scale datasets. To optimize the computational time, targeted strategies can be implemented:
(i) focusing on relevant spectral regions based on emission line selection, (ii) reducing the data dimensionality using PCA, SOM, etc., and (iii) spectral binning.

2.2. LIBS Signal

The baseline of LIBS spectra varies significantly depending on the elemental composition of the mineral analyzed (Figure 1a). A flat baseline is observed in minerals such as quartz, Li micas, albite, calcite, etc. Meanwhile, minerals rich in metallic elements (e.g., Fe, Cu, Cr, Zn, etc.), including pyrite, chromite, and arsenopyrite, exhibit an elevated back- ground signal across the visible and ultra-violet wavelength range due to the high thermal conductivity of these elements affecting the plasma density and temperature [30,31]. In minerals containing higher-atomic-mass elements (e.g., Nb, Ta, Zr), such as columbite, tantalite, and zircon, a higher signal results from increased Bremsstrahlung radiation. These differences emphasize the need for custom spectral processing when involving multimin- eral LIBS data. Baseline correction and normalization should be specifically adapted to the mineral species targeted. Additionally, the physical nature of the analyzed samples is reflected in the signal intensity. As shown in Figure 1b, the LIBS signal intensity of quartz differs between powdered and crystalline samples. The signal intensities recorded from powdered samples are substantially higher than those obtained in crystals. Intensity gaps caused by textural variations are attributed to higher ablation rates in unconsoli- dated powders and reduced scattering, which enhances the laser interaction with powder particles [14,32,33].

2.3. Element Detection

For each mineral, characteristic emission lines at specific wavelengths and varying intensities define a unique and distinctive spectral signature. In this sense, the distribution of emission lines across the entire spectral range of an LIBS spectrum differs significantly from one mineral to another (Figure 1a). For instance, minerals rich in transition metals (e.g., Fe), characterized by complex atomic structures and numerous energy level transitions, lead to a higher density of emission lines, generating spectra with densely packed lines. A higher emission density increases the potential for spectral interference, and the signal of less abundant trace elements may be concealed (Figures 1a and 2c).

Even if the presence of known emission lines reveals the chemical composition of the mineral, the signal intensities recorded of these lines do not correlate directly with the absolute abundance of the elements in the mineral. The signal intensity of an element is the result of various factors besides its concentration. Elements with lower ionization energies (e.g., Li ~ 5.39 eV, Na ~ 5.14 eV) produce stronger emission signals (Figure 2a), while elements with moderate ionization energies (e.g., Si ~ 8.15 eV) yield comparatively weaker signals even at higher concentrations (Figure 2b).

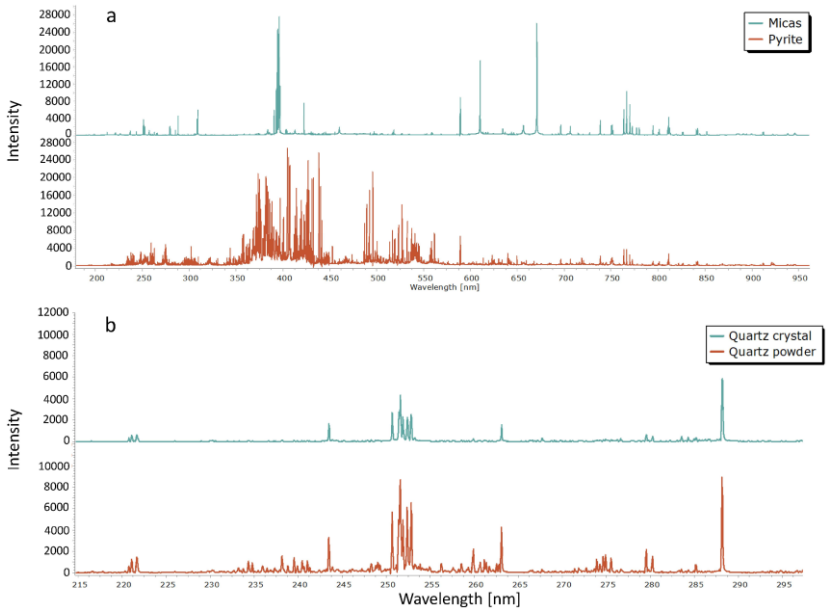

Figure 1. Mineral LIBS spectra: (**a**) the baseline variation based on the mineral composition, showing higher density plasma for pyrite due to metallic elements' presence, compared to a flat baseline for Li-rich micas; (**b**) the signal intensity variation for quartz analyzed as powder samples, exhibiting stronger signals compared to those of crystal phases.

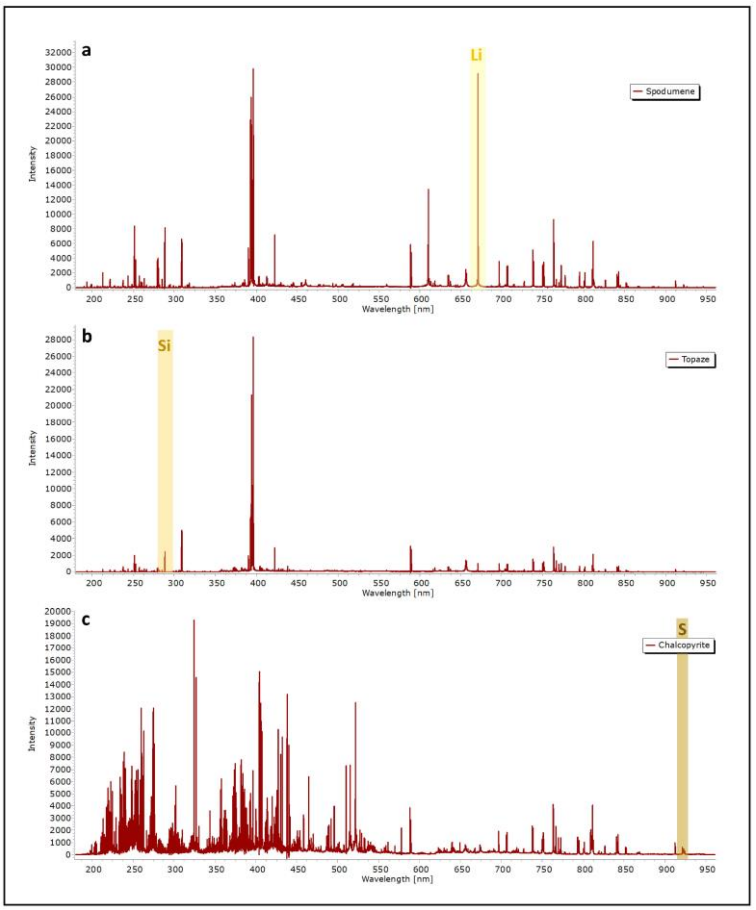

Figure 2. Variation in the LIBS signal intensity for different elements: (**a**) Li, an element with low ionization energy, is a major component of spodumene; (**b**) Si, an element with moderate ionization energy, is a primary constituent of topaz; and (**c**) S, an element with high ionization energy, is a key component of chalcopyrite.

3. Methods

3.1. Samples

Table 1 summarizes the samples analyzed to obtain the mineral spectra contained in the database. In total, 171 mineral samples were analyzed using a handheld LIBS analyzer: 127 were crystal hand specimens, 25 were phenocrysts included in rock matrices, and 19 were compressed powder pellets (<50 µm) shaped using a 13 mm diameter, 2 mm thick cylindrical mold and a 10-ton hydraulic press [34]. The pellets were formed using a pressure of 7 tons for approximately 2 minutes to ensure the cohesion of the mineral powders. The solid samples were unprocessed and selected for their flat surface to ensure proper adhesion to the analysis window, ensuring good plasma quality.

Most samples were sourced from the teaching and research collections of the École Nationale Supérieure de Géologie (ENSG, University of Lorraine, Nancy, France) and the GeoRessources laboratory (University of Lorraine, Nancy, France). Additional contributions came from the San Finx mine (Spain) and the University of Thessaloniki (Greece).

3.2. LIBS Techniques

The fundamental principles of LIBS have been detailed in numerous publications [35–37]. In summary, plasma is generated on the surface of a sample using a high-power pulsed laser. The excited chemical components of the plasma (atoms, ions, and molecules) emit light to release excess energy and return to stable energy states. The spectral signal is collected and analyzed using optical collectors and spectrometers to produce a spectrum, illustrating the signal intensity (a.u.) as a function of the wavelength (nm). Emission lines at specific positions reveal the elemental composition, while the signal intensity depends on several factors (i.e., the element concentration, ionization potential, acquisition parameters, etc.).

3.3. Handheld LIBS Analyzer

The handheld LIBS analyzer used in this study was the SciAps Z300 model (MA, USA), composed of a Nd:YAG laser with an output energy of 5-6 mJ per pulse, operating at a wavelength of 1064 nm, a pulse duration of 1 nanosecond, and a pulse repetition rate of up to 50 Hz. Characterized by 4 hours of autonomy per battery and a compact design (weight: 2 kg), the device is user-friendly and convenient for field missions. An integrated camera allows for the precise visualization of the sample surface before an analysis, facilitating the accurate targeting of specific minerals in rock samples. A constant argon flush is used during measurements to enhance the signal-to-noise ratio and improve signal intensity, particularly in the UV range [36,37]. The combination of spectrometers enables the coverage of a large spectral band (190–950 nm), detecting elements from light (H) to heavy (U) with a spectral resolution of 0.03 nm. The detection limits vary from a few ppm (Li = 5 ppm) to hundreds of ppm (C = 400 ppm). The instrument includes automated drift correction, performed when starting the device and approximately every hour using an onboard reference material, ensuring result consistency over time. Two data acquisition modes are available. In the “standalone mode”, the analyzer operates independently of external devices, providing flexibility during field operations. The “connected mode”, accessed via ProfileBuilder software, allows for more control over the acquisition parameters for detailed spectra visualization and emission line identification using an integrated spectral database. The first mode is ideal for onsite analysis, while the connected mode is better suited for comprehensive data inspection during data acquisition.

3.4. Data Acquisition

Four averaged analysis points were measured for each sample. An analysis point consisted of multiple zones arranged in a grid (e.g., 3 × 3, 5 × 5, 6 × 6). At least two laser shots were averaged per zone, following an initial cleaning shot to remove any surface contaminants. Increasing the number of laser shots per location, minimizing variations caused by plasma instability and maximizing the number of analysis points across the sample surface, ensured a representative signal, accounting for chemical variations and inhomogeneous element distribution within the crystal (e.g., zoning, inclusions). The distance between two zones ranged from 100 to 200 µm, ensuring independent plasma formation and no interference from prior shots. A flat surface was a key point when selecting samples, as topographic irregularities can affect the signal by altering the laser absorption, ablation efficiency, and plasma formation [38]. An onboard sensor prevented the laser from firing when the sample was not correctly aligned with the analysis window, guaranteeing safe operation under laser class 1M conditions. However, this mechanism complicated the analysis of clear crystals (e.g., quartz, fluorite), potentially not detected due to their transparency or high reflectivity, hindering laser interaction. The analysis was aborted in such cases, and no spectra were recorded.

3.5. Spectra Visualization

The CSV files can be imported into a similar handheld LIBS analyzer via the analyzer software (ProfileBuilder) for detailed visualization and emission peak identification using the integrated spectral database. External software, like SpectraGryph [39], offer a user- friendly interface for visualizing and processing LIBS spectra. Multiple spectra can be pro- cessed simultaneously, including baseline correction, normalization, and feature extraction.

3.6. Applications

LIBS spectra obtained from mineral samples can be used to build custom spectral datasets, providing input data for training mathematical models to generate qualitative, quantitative, and mineralogical information for unknown rock and mineral samples. In this sense, numerous studies have demonstrated the potential of the LIBS technique, when combined with chemometric methods, as a tool for automatic mineral identification [29,40,41]. Machine learning algorithms have been designed to identify patterns to make predictions based on the data features.

The performance of these models highly depends on the quality of input data points and their ability to emphasize relevant characteristics, as the equations and rules imple- mented are calibrated using these attributes. The ability to determine the mineralogical composition of rocks by associating LIBS spectra with specific minerals based on spectral features represents a rapid and practical solution for resource optimization during field op- erations. This highlights the importance of generating extensive and high-quality mineral spectral libraries to support advanced mathematical approaches for LIBS applications in geology. In order to enable use by any type of processing method already available or to be developed, the database is provided without any postprocessing of the spectra.

4. User Note

The samples, as well as the methodology followed during this study, are described in the metafile and the present article, respectively. Various Li-rich mica samples, grouped under the keyword “calibration”, are associated with additional geochemical quantita- tive data, which are not included in the paper or metafile but can be made accessible upon request.

Author Contributions: Conceptualization, N.M., C.F. and J.C.; methodology, N.M., C.F., J.C. and Y.K.; validation, N.M., C.F. and J.C.; investigation, N.M. and Y.K.; resources, N.M., C.F. and J.C.; data curation, N.M.; writing—original draft preparation, N.M., C.F. and J.C.; writing—review and editing, N.M., C.F., J.C. and M.J.; visualization, N.M., C.F. and J.C.; supervision, C.F. and J.C.; project administration, C.F. and J.C.; funding acquisition, C.F. and J.C. All authors have read and agreed to the published version of the manuscript.

Funding: The data acquisition was supported by funding from the European Union's Horizon 2020 research and innovation program (NEXT project) under Grant Agreement No. 776804–H2020- SC5-2017, the French National Research Agency via the Labex Ressources 21 project [reference ANR–10–LABX–21-01], and the ARTeMIS ERASMUS+ project (Action for Research and Teaching Mineral Exploration Inclusive School), Grant Agreement No. 2021-1-FR01-KA220-HED-000029934.

Institutional Review Board Statement: Not applicable.

Informed Consent Statement: Not applicable.

Data Availability Statement: All of the files mentioned in this study can be found open access (ORDaR platform) at the following address: https://doi.org/10.24396/ORDAR-165.

Acknowledgments: We would like to thank P. Marion, R. Mosser-Ruck, A.S. André-Mayer, M.C. Caumon, C. Ballouard, and P. Carr for providing some of the mineral and rock samples analyzed. We acknowledge V. Melfos from the Aristotle University of Thessaloniki for providing mineral samples sourced in Greece. We acknowledge R. Harmon for providing Li-rich mica samples. Thank you, Pierre-Yves Arnould, for the technical support in uploading the spectral database to the ORDaR (OTELo Research Data Repository) platform.

Conflicts of Interest: The authors declare no conflicts of interest. The funders had no role in the design of the study; in the collection, analyses, or interpretation of data; in the writing of the manuscript; or in the decision to publish the results.

References

1. El-Saeid, R.H.; Abdel-Salam, Z.; Pagnotta, S.; Palleschi, V.; Harith, M.A. Classification of sedimentary and igneous rocks by laser induced breakdown spectroscopy and nanoparticle-enhanced laser induced breakdown spectroscopy combined with principal component analysis and graph theory. *Spectrochim. Acta Part B At. Spectrosc.* **2019**, *158*, 105622. [CrossRef]
2. Syvilay, D.; Bousquet, B.; Chapoulie, R.; Orange, M.; Bourdonnec, F.X.L. Advanced statistical analysis of LIBS spectra for the sourcing of obsidian samples. *J. Anal. At. Spectrom.* **2019**, *34*, 867–873. [CrossRef]
3. Alvarez-Llamas, C.; Tercier, A.; Ballouard, C.; Fabre, C.; Hermelin, S.; Margueritat, J.; Duponchel, L.; Dujardin, C.; Motto-Ros, V. Ultrafast μLIBS imaging for the multiscale mineralogical characterization of pegmatite rocks. *J. Anal. At. Spectrom.* **2024**, *39*, 1077–1086. [CrossRef]
4. Fabre, C.; Ourti, N.E.; Ballouard, C.; Mercadier, J.; Cauzid, J. Handheld LIBS analysis for in situ quantification of Li and detection of the trace elements (Be, Rb and Cs). *J. Geochem. Explor.* **2022**, *236*, 106979. [CrossRef]
5. Foucaud, Y.; Fabre, C.; Demeusy, B.; Filippova, I.V.; Filippov, L.O. Optimisation of fast quantification of fluorine content using handheld laser induced breakdown spectroscopy. *Spectrochim. Acta Part B At. Spectrosc.* **2019**, *158*, 105628. [CrossRef]
6. Korbel, C.; Mezoued, N.; Demeusy, B.; Fabre, C.; Cauzid, J.; Filippova, I.V.; Filippov, L.O. Quantification of lithium using handheld instruments: Application of LIBS and XRF spectroscopy to assay the lithium content of mineral processing products. *J. Anal. At. Spectrom.* **2024**, *39*, 1838–1853. [CrossRef]
7. Fabre, C.; Marulier, L.; Monfaredi, B.; Motto-Ros, V.; Bousquet, B.; Eglinger, A.; Tarantola, A. Exploring rare earth elements in complex microscopic mineral phases: Inputs from μLIBS imaging. *Spectrochim. Acta Part B At. Spectrosc.* **2024**, *216*, 106954. [CrossRef]
8. Fabre, C.; Ourti, N.E.; Mercadier, J.; Cardoso-Fernandes, J.; Dias, F.; Perrotta, M.; Koerting, F.; Lima, A.; Kaestner, F.; Koellner, N.; et al. Analyses of Li-Rich Minerals Using Handheld LIBS Tool. *Data* **2021**, *6*, 68. [CrossRef]
9. Harmon, R.S.; De Lucia, F.C.; Miziolek, A.W.; McNesby, K.L.; Walters, R.A.; French, P.D. Laser-induced breakdown spectroscopy (LIBS)—an emerging field-portable sensor technology for real-time, in-situ geochemical and environmental analysis. *Geochem. Explor. Environ. Anal.* **2005**, *5*, 21–28. [CrossRef]
10. Lemiere, R.; Harmon, R.H. XRF and LIBS for Field Geology. In *In Portable Spectroscopy and Spectrometry*, 1st ed.; Crocombe, R., Leary, P., Kammrath, B., Eds.; Wiley: Hoboken, NJ, USA, 2021; pp. 455–497. [CrossRef]

11. Lemière, B.; Uvarova, Y.A. New developments in field-portable geochemical techniques and on-site technologies and their place in mineral exploration. *Geochem. Explor. Environ. Anal.* **2019**, *20*, 205–216. [CrossRef]
12. Harmon, R.S. Laser-Induced Breakdown Spectroscopy in Mineral Exploration and Ore Processing. *Minerals* **2024**, *14*, 731. [CrossRef]
13. Fontana, F.F.; van der Hoek, B.; Tassios, S.; Tiddy, C.; Stromberg, J.; Francis, N.; Uvarova, Y.A.; Lancaster, D.G. Laser Induced Breakdown Spectroscopy (LIBS) for whole rock geochemistry. *J. Geochem. Explor.* **2023**, *246*, 107160. [CrossRef]
14. Wise, M.A.; Harmon, R.S.; Curry, A.; Jennings, M.; Grimac, Z.; Khashchevskaya, D. Handheld LIBS for Li Exploration: An Example from the Carolina Tin-Spodumene Belt, USA. *Minerals* **2022**, *12*, 77. [CrossRef]
15. Harmon, R.S.; Wise, M.A.; Curry, A.C.; Mistele, J.S.; Mason, M.S.; Grimac, Z. Rapid Analysis of Muscovites on a Lithium Pegmatite Prospect by Handheld LIBS. *Minerals* **2023**, *13*, 697. [CrossRef]
16. Sweetapple, M.T.; Tassios, S. Laser-induced breakdown spectroscopy (LIBS) as a tool for in situ mapping and textural interpre- tation of lithium in pegmatite minerals. *Am. Mineral.* **2015**, *100*, 2141–2151. [CrossRef]
17. Pochon, A.; Desaulty, A.M.; Bailly, L. Handheld laser-induced breakdown spectroscopy (LIBS) as a fast and easy method to trace gold. *J. Anal. At. Spectrom.* **2020**, *35*, 254–264. [CrossRef]
18. Jin, X.; Yang, G.; Sun, X.; Qu, D.; Li, S.; Chen, G.; Li, C.; Tian, D.; Yao, L. Discrimination of rocks by laser-induced breakdown spectroscopy combined with Random Forest (RF). *J. Anal. At. Spectrom.* **2022**, *38*, 243–252. [CrossRef]
19. Maurice, S.; Wiens, R.C.; Saccoccio, M.; Barraclough, B.; Gasnault, O.; Forni, O.; Mangold, N.; Baratoux, D.; Bender, S.; Berger, G.; et al. The ChemCam Instrument Suite on the Mars Science Laboratory (MSL) Rover: Science Objectives and Mast Unit Description. *Space Sci Rev.* **2012**, *170*, 95–166. [CrossRef]
20. Maurice, S.; Wiens, R.C.; Bernardi, P.; Caïs, P.; Robinson, S.; Nelson, T.; Gasnault, O.; Reess, J.-M.; Deleuze, M.; Rull, F.; et al. The SuperCam Instrument Suite on the Mars 2020 Rover: Science Objectives and Mast-Unit Description. *Space Sci. Rev.* **2021**, *217*, 47. [CrossRef]
21. Xu, W.; Liu, X.; Yan, Z.; Li, L.; Zhang, Z.; Kuang, Y.; Jiang, H.; Yu, H.; Yang, F.; Liu, C.; et al. The MarSCoDe Instrument Suite on the Mars Rover of China's Tianwen-1 Mission. *Space Sci. Rev.* **2021**, *217*, 64. [CrossRef]
22. Brunnbauer, L.; Gajarska, Z.; Lohninger, H.; Limbeck, A. A critical review of recent trends in sample classification using La-ser-Induced Breakdown Spectroscopy (LIBS). *TrAC Trends Anal. Chem.* **2023**, *159*, 116859. [CrossRef]
23. Senesi, G.S.; Allegretta, I.; Marangoni, B.S.; Ribeiro, M.C.; Porfido, C.; Terzano, R.; De Pascale, O.; Eramo, G. Geochemical identification and classification of cherts using handheld laser induced breakdown spectroscopy (LIBS) supported by supervised machine learning algorithms. *Appl. Geochem.* **2023**, *151*, 105625. [CrossRef]
24. Dutrow, B.L.; McMillan, N.J.; Henry, D.J. A multivariate statistical approach for mineral geographic provenance determination using laser-induced breakdown spectroscopy and electron microprobe chemical data: A case study of copper-bearing tour-malines. *Am. Mineral.* **2024**, *109*, 1085–1095. [CrossRef]
25. Shih, M.; Yuan, Y.; Shi, G.-H. Comparative analysis of LDA, PLS-DA, SVM, RF, and voting ensemble for discrimination origin in greenish-white to white nephrites using LIBS. *J. Anal. At. Spectrom.* **2024**, *39*, 1560–1570. [CrossRef]
26. Defnet, P.A.; Wise, M.A.; Harmon, R.S.; Hark, R.R.; Hilferding, K. Analysis of Garnet by Laser-Induced Breakdown Spectrosco- py—Two Practical Applications. *Minerals* **2021**, *11*, 705. [CrossRef]
27. Ali, A.; Khan, M.Z.; Rehan, I.; Rehan, K.; Muhammad, R. Quantitative Classification of Quartz by Laser Induced Breakdown Spectroscopy in Conjunction with Discriminant Function Analysis. *J. Spectrosc.* **2016**, *2016*, 1835027. [CrossRef]
28. Capela, D.; Lopes, T.; Dias, F.; Ferreira, M.F.S.; Teixeira, J.; Lima, A.; Jorge, P.A.; Silva, N.A.; Guimarães, D. Advancing automated mineral identification through LIBS imaging for lithium-bearing mineral species. *Spectrochim. Acta Part B At. Spectrosc.* **2025**, *223*, 107085. [CrossRef]
29. Capela, D.; Ferreira, M.F.S.; Lima, A.; Dias, F.; Lopes, T.; Guimarães, D.; Jorge, P.A.; Silva, N.A. Robust and interpretable mineral identification using laser-induced breakdown spectroscopy mapping. *Spectrochim. Acta Part B At. Spectrosc.* **2023**, *206*, 106733. [CrossRef]
30. El Haddad, J.; de Lima Filho, E.S.; Vanier, F.; Harhira, A.; Padioleau, C.; Sabsabi, M.; Wilkie, G.; Blouin, A. Multiphase mineral identification and quantification by laser-induced breakdown spectroscopy. *Miner. Eng.* **2019**, *134*, 281–290. [CrossRef]
31. Ismail, A.M.; Imam, H.; Elhassan, A.; Youniss, T.W.; Harith, A.M. LIBS limit of detection and plasma parameters of some elements in two different metallic matrices. *J. Anal. At. Spectrom.* **2004**, *19*, 489–494. [CrossRef]
32. Cousin, A.; Sautter, V.; Fabre, C.; Dromart, G.; Montagnac, G.; Drouet, C.; Meslin, P.-Y.; Gasnault, O.; Beyssac, O.; Bernard, S.; et al. SuperCam calibration targets on board the Perseverance rover: Fabrication and quantitative characterization. *Spectrochim. Acta Part B At. Spectrosc.* **2022**, *188*, 106341. [CrossRef]
33. Kim, Y.; Fabre, C.; Cauzid, J. Access to quantitative analysis of carbonates using a portable LIBS instrument: First applications to single minerals and mineral mixtures. *Spectrochim. Acta Part B At. Spectrosc.* **2022**, *191*, 106397. [CrossRef]
34. Harmon, R.H.; Senesi, G.S. Laser-Induced Breakdown Spectroscopy—A geochemical tool for the 21st century. *Appl. Geochem.* **2021**, *128*, 104929. [CrossRef]

35. Radziemski, L.; Cremers, D. A brief history of laser-induced breakdown spectroscopy: From the concept of atoms to LIBS 2012. *Spectrochim. Acta Part B At. Spectrosc.* **2013**, *87*, 3–10. [CrossRef]
36. Aguilera, J.A.; Bengoechea, J.; Aragón, C. Spatial characterization of laser induced plasmas obtained in air and argon with different laser focusing distances. *Spectrochim. Acta Part B At. Spectrosc.* **2004**, *59*, 461–469. [CrossRef]
37. Ya-xiong, H.; Wen-qi, Z.; Bin, Z.; Yong-sheng, Z.; Chuan, K.; Tao, X.; Yong, Z. Study on Time-Resolved Characteristics of Laser-Induced Argon Plasma. *Spectrosc Spectr Anal.* **2022**, *42*, 1049–1057.
38. Xu, W.; Sun, C.; Tan, Y.; Gao, L.; Zhang, Y.; Yue, Z.; Shabbir, S.; Wu, M.; Zou, L.; Chen, F.; et al. Total alkali silica classification of rocks with LIBS: Influences of the chemical and physical matrix effects. *J. Anal. At. Spectrom.* **2020**, *35*, 1641–1653. [CrossRef]
39. Menges, F. Spectroscopy. Spectroscopy Ninja—Optical Spectroscopy Software and Services. Available online: http://spectroscopy.ninja/ (accessed on 15 January 2025).
40. Rifai, K.; Michaud Paradis, M.C.; Swierczek, Z.; Doucet, F.; Özcan, L.; Fayad, A.; Li, J.; Vidal, F. Emergences of New Technology for Ultrafast Automated Mineral Phase Identification and Quantitative Analysis Using the CORIOSITY Laser-Induced Breakdown Spec-troscopy (LIBS) System. *Minerals* **2020**, *10*, 918. [CrossRef]
41. Janovszky, P.; Jancsek, K.; Palásti, J.D.; Kopniczky, J.; Hopp, B.; Tóth, T.M.; Galbács, G. Classification of minerals and the assessment of lithium and beryllium content in granitoid rocks by laser-induced breakdown spectroscopy. *J. Anal. At. Spectrom.* **2021**, *36*, 813–823. [CrossRef]

Disclaimer/Publisher's Note: The statements, opinions and data contained in all publications are solely those of the individual author(s) and contributor(s) and not of MDPI and/or the editor(s). MDPI and/or the editor(s) disclaim responsibility for any injury to people or property resulting from any ideas, methods, instructions or products referred to in the content.

Chapitre VI.

Automated mineral identification using machine learning methods part I

Automated mineral recognition combining handheld LIBS spectra and machine learning: assessing ore mineral abundance in the Beauvoir granite

Naila Mezoued[*,1]*, Cécile Fabre*[1]*, Jean Cauzid*[1]

[1]CNRS, GeoRessources Laboratory, Université de Lorraine, Nancy F54000, France

Corresponding author[*]. E-mail: naila.mezoued@univ-lorraine.fr

Abstract

Preliminary insights into mineral composition and distribution during ore exploration are essential and mainly obtained through visual characterization. However, mineral identification based on physical characteristics can be challenging, particularly when multiple minerals exhibit similar properties. In the Beauvoir granite, a rare-metal deposit targeted for lithium extraction, lepidolite, the ore mineral, is difficult to distinguish from matrix components. In this context, handheld LIBS is presented as a rapid, on-site solution for automated mineral recognition by combining handheld LIBS spectra with machine learning models to translate elemental data into mineralogical information. The performance of four classification models, LDA, SVM, Random Forest, and PLS-DA, was evaluated using reference datasets derived from pure mineral spectra, mimicking a simplified mineralogical composition of the Beauvoir granite (albite, lepidolite, muscovite, topaz, quartz, and phosphates). To reduce the dimensionality of handheld LIBS spectra (24,000 variables per spectrum), emission lines corresponding to major, minor, and trace elements of the target minerals were extracted from both raw and SNV-normalized spectra. Principal Component Analysis (PCA) and Partial Least Squares (PLS) were also tested to further refine spectral information. When applied to the Beauvoir granite samples to estimate mineral abundance, the PLS-DA classification model demonstrated the highest accuracy for multi-class classification (MAEP = 11.74%). In contrast, SVM model provided more precise predictions for lepidolite (MAEP = 9.27%). The results highlighted the impact of deposit-specific chemical variations and sample physical features, such as alteration and grain size, on prediction accuracy. While further refinements are necessary, these findings demonstrate the potential of handheld LIBS as a powerful tool for improving geological material characterization during mining operations, ultimately contributing to more precise preliminary resource assessments and informed decision-making.

Keywords: Handheld LIBS, classification, machine learning, lepidolite, ore exploration.

Introduction

Collecting structural, textural, and mineralogical data to provide preliminary insights into ore distribution is a critical step during prospecting campaigns. At early stages, mineral identification and estimation in rock samples typically rely on the physical properties of individual minerals. Yet, when the minerals lack sufficient visual contrast for macroscopic identification, this approach becomes challenging and necessitates complementary analytical methods (1–3). However, obtaining comprehensive mineralogical data through conventional procedures often necessitates laboratory-based analytical techniques, a time-consuming process extending from weeks to months, potentially delaying critical decision-making during this timeframe.

The potential of handheld LIBS as an innovative analytical technique has been increasingly recognized by the geosciences community (4–6). Its ability to provide rapid, multi-elemental data across various sample types (i.e., powder pellets, outcrops, drill core sections) makes it particularly valuable during field work where samples are often voluminous, chemically heterogeneous, and logistically challenging to transport. Numerous studies have demonstrated the potential of handheld LIBS for qualitative (7) and quantitative (8–11) analyses, as well as mineral characterization (1,12,13). While automated mineral recognition using LIBS is primarily associated with LIBS imaging due to its high spatial resolution (14), which allows for detailed representation of mineralogical features like grain boundaries, inclusions, and compositional variations, handheld LIBS has also been explored for this purpose. Different approaches were tested, ranging from using the relative intensities of major elements for pegmatite exploration (8,12) and Li-rich mineral discrimination (e.g., lepidolite, spodumene, petalite) (1) to geochemical imaging of mantle xenoliths on drill core surfaces, employing semi-automated spectral processing (PCA and KNN) and image stitching (15).

The following work was designed specifically to address ore mineral automated recognition in the Beauvoir granite deposit, with the potential for broader applicability to other exploration sites. The Beauvoir granite, located in the northern part of the Massif Central, is a highly differentiated pluton characterized by significant concentrations of critical elements, including lithium, niobium, tantalum, and tin, which are incorporated into the crystal structures of specific ore minerals such as lepidolite, cassiterite, and niobium-tantalite. Extensively studied for scientific purposes (16), the deposit is now recognized as an important regional lithium resource for France, playing a key role in securing local mineral supplies for various industries, reducing the dependence on external sources. An extensive exploration campaign of the Beauvoir granite [EMILI21] was launched in 2021 (17), aiming to refine the geological model of the deposit and identify high-interest areas for the exploitation strategy planned for early 2028. The petrographic characteristics of the leucogranite B1 facies, targeted for lithium

extraction, constitute a challenge for macroscopic mineral identification. This facies appears predominantly white to grayish, making the distinction of Li-micas difficult. Although lepidolite typically exhibits a pinkish hue, in this context, it is predominantly white and translucent, further complicating its differentiation from matrix elements such as albite and quartz (18,19). As a result, visual assessments remain approximate, necessitating advanced analytical techniques to refine the characterization of mineralized zones and accurately quantify the distribution of lepidolite, the primary lithium-bearing mineral targeted for extraction.

This study introduces handheld LIBS as an efficient and rapid field technique for automated mineral recognition during drilling campaigns for mineral resources exploration, particularly when visual characterization is complex. Four machine learning algorithms, Linear Discriminant Analysis (LDA), Support Vector Machine (SVM), Random Forest, and Partial Least Squares Discriminant Analysis (PLS-DA), were tested and evaluated to classify LIBS spectra into distinct mineral classes, converting spectral data into mineralogical information. Training datasets were created using reference spectra of pure minerals (Albite, Lepidolite, Muscovite, Quartz, Topaz, and Phosphates) to simulate the mineralogical composition of the Beauvoir granite. The second validation step involved processing data obtained from Beauvoir granite samples. The classification results were then converted into relative mineral abundances and compared to reference values to assess the models' ability to predict mineral distribution in granite samples.

1 Methodlogy

1.1 Samples

The rock samples analyzed consist of four rectangular granite slabs (12x5x0.5cm) obtained from drill core portions of the Beauvoir granite. The rare metal-bearing granite samples belong to the B1 facies (19), the uppermost part of the magmatic formation, consisting of three successive units (B1, B2, and B3) (20). The petrographic studies of the Beauvoir granite (B1) revealed a mineral composition consisting predominantly of three mineral phases: albite, lepidolite, and quartz, composing the granite matrix, and accessory phases such as muscovite, topaz, apatite, fluorite, amblygonite, and cassiterite (21). Additionally, zircon, microlite, montebrasite, and niobium-tantalite crystals have also been observed (19,22). Lepidolite, as the main host of lithium (18), is the focus of this study. The textural characteristics observed in the three selected samples are consistent across all samples (**Fig.1**). The texture is equigranular and unaligned, with grain sizes ranging from 200 to 600 µm for the matrix minerals. No preprocessing was performed aside from ensuring a flat surface to guarantee optimal signal acquisition.

1.2 Handheld LIBS

Spectral data were acquired using a handheld LIBS analyzer. Initially developed as a stationary, laboratory-based technique (23,24), LIBS has progressively evolved for field applications with the emergence of portable devices (4,25). This evolution has been driven by advancements in high-quality miniaturized physical components (26), facilitating the design of stable, robust, and cost-effective compact optical systems. The fundamental physical principles of LIBS, extensively documented in the literature (27,28), can be summarized as follows: A laser generates the energy required to excite the surface of a sample, leading to melting, ablation, and the expansion of a microplasma. The excited chemical components within the plasma return to stable energy states by emitting photons. A combination of detectors and multiple spectrometers collects, records, and processes the optical signal to generate LIBS spectra, illustrating signal intensity (a.u.) as a function of wavelength (UV-Vis-IR). The presence of specific emission lines at defined positions reveals the elemental composition of the analyzed samples, while the signal intensity recorded results from various parameters, including element concentration, sample texture, and acquisition settings. Several commercial models are currently available (26,29), including the Z300 model from SciAps (MA, USA), used in this study. SciAps analyzers are equipped with a solid-state Nd:YAG pulsed laser operating at a wavelength of 1064 nm, delivering energy (5–6 mJ) in pulsed mode, with pulse durations lasting a few nanoseconds and frequencies reaching up to 50 Hz. This model is specifically designed for geoscientific applications, offering a large spectral range (190–950 nm), including emission lines from all chemical elements (H-U), effectively addressing the multi-elemental and heterogeneous nature of geological materials. The use of handheld LIBS in this study was motivated by multiple factors: i) its ability to detect light elements, such as lithium in lepidolite, as well as sodium, a key component of albite, a dominant mineral phase in the matrix, ii) its rapid data acquisition within seconds, which enhances time and resource efficiency during large-scale exploration campaigns, iii) its analytical spot size of 50-200 µm, judged to be suited for the textural characteristics observed in the Beauvoir granite.

1.3 Data acquisition

Each granite slab was analyzed at 10 different locations, arranged along a vertical profile, from the top to the bottom of the sample (**Fig.1**). Each area consisted of 90 analysis points, spaced 30 µm apart, organized into a square grid that covered the full analysis window of the device. At each point, two laser shots were fired: the first one was a cleaning shot for potential surface contamination, and the second one was recorded. In total, 900 spectra were collected per granite sample. The number of laser shots per area was reduced to a single shot on the Beauvoir granite samples, compared to the multiple shots performed on the pure mineral

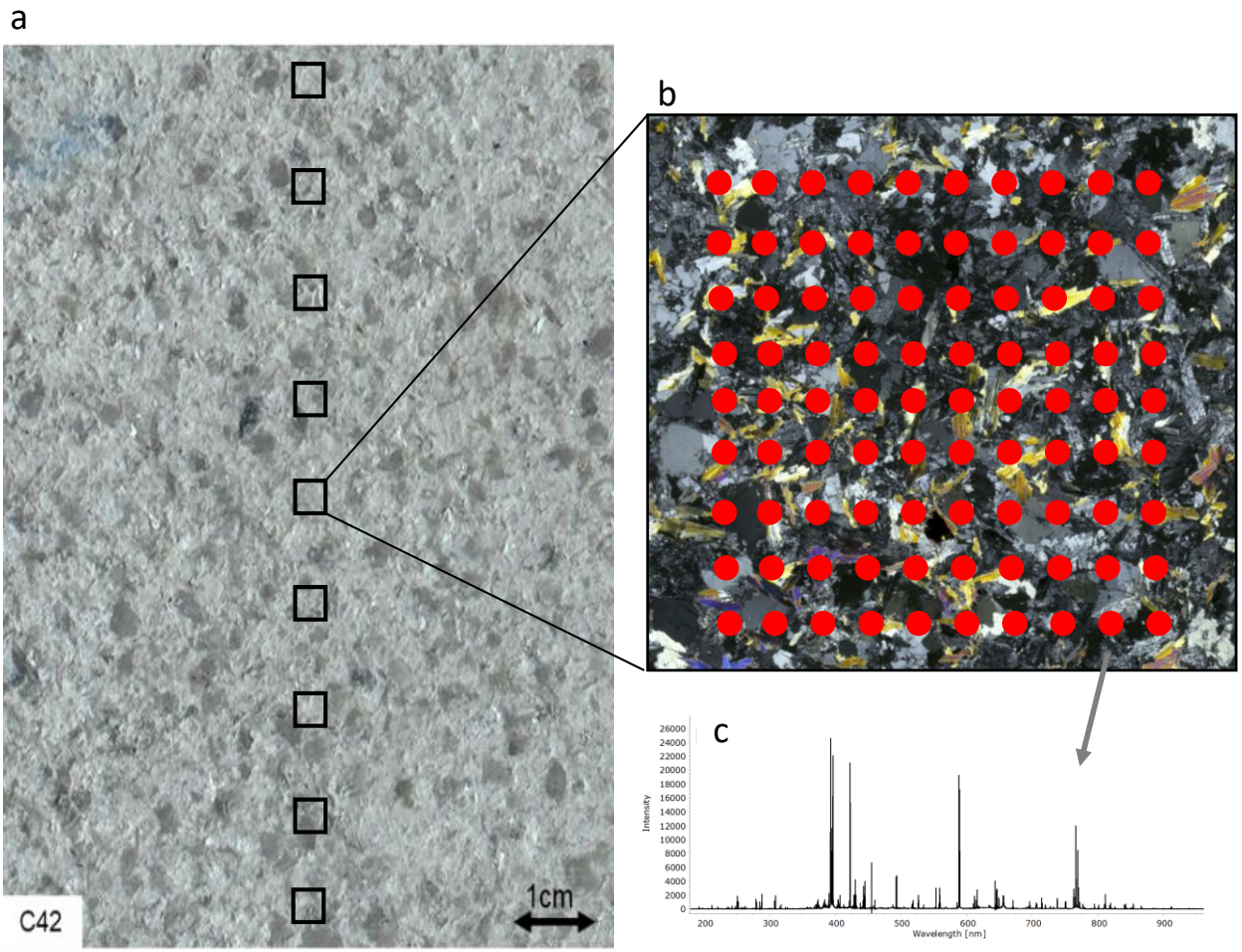

Figure.1. Schematic representation of handheld LIBS data acquisition on Beauvoir granite samples: a) Granite slab with 10 organized LIBS analysis zones arranged vertically from top to bottom of the sample; b) Zoomed-in view of a single analysis zone, representing 90 analysis points organized in a grid; c) Illustration of the LIBS spectrum obtained at each analysis point (900 spectra per sample).

samples (30), to ensure that the resulting craters had minimal horizontal and vertical amplitude, aiming to capture only one mineral per spectrum. The analysis frequency (10 Hz), focal length, and integration gate were kept consistent across both mineral and rock data acquisition sessions. The analysis time per grid was 1 minute, including both the analysis time and the time required to register the spectra in the device's software, ProfileBuilder. An additional minute was needed to transfer the spectra generated (900) in CSV format. In total, 20 minutes were necessary to cover a granite sample of that size.

1.4 Training data

The training dataset consisted of two sub-datasets: training (75%) and validation (25%). The reference data, were generated from LIBS spectra acquired on pure mineral samples. These spectra were selected to represent a simplified version of the mineralogical composition of the Beauvoir granite, focusing on major mineral phases (> 1%) (**Table.1**). The mineral spectra were sourced from the spectral database « Spectral Analysis of Minerals with Handheld LIBS Technology », available in open access on the ORDaR platform, and detailed in Mezoued et al. (30). These spectra were acquired from macroscopic mineral samples sourced from collections of the Georesources Laboratory (Nancy, France), ENSG (Nancy, France), and the University of Thessaloniki (Thessaloniki, Greece) (30). Given that minerals in nature exhibit significant compositional variation due to geological formation processes and environmental conditions, collecting analyses from samples sourced in different locations ensures a more realistic representation of the chemical variability in mineral species.

Table.1. Summary of the reference mineral LIBS spectra selected to mimic the Beauvoir granite mineral composition for training machine learning models: mineral species, chemical formulas, number of samples analyzed, and total spectra acquired (30).

Mineral	Chemical composition	Samples	LIBS spectra
Albite	$Na(AlSi_3O_8)$	5	300
Orthose	$KAlSi_3O_8$	3	300
Quartz	SiO_2	4	300
Topaze	$Al_2SiO_4(F,OH)_2$	1	44
Muscovite	$KAl_2(AlSi_3O_{10})(OH)_2$	4	272
Lepdiolite	$K(Li_{1.5}Al_{1.5})(AlSi_3O_{10})(F,OH)_2$	6	300
Phosphates	$(Li,Na)Al(PO_4)(F,OH)$[a] $Ca_5(PO_4)_3(Cl/F/OH)$[b]	5	300

[a] Amblygonite formula

[b] Phosphates formula

The training data, summarized in **Table.1**, includes LIBS spectra of albite, quartz, and lepidolite, as well as secondary phases, muscovite, topaz, orthoclase, and phosphates. The

selected lepidolite spectra were from samples with Li concentrations greater than 5000 ppm, while muscovite samples had Li concentrations below 1000 ppm. The phosphate class includes spectra from both apatite and amblygonite, Li-rich phosphates, though not targeted for Li extraction. To ensure accurate and unbiased predictions, the number of spectra in the dataset was carefully determined to produce a balanced distribution across classes. An imbalanced dataset, where some classes are overrepresented while others are underrepresented, could introduce bias in the model's predictions (31).

Using a simplified system to train and evaluate the machine learning models provides a clearer understanding of each model's performance in a controlled environment by minimizing the complexity and variability typically encountered in rock data (e.g., mixed phases, signal variation, etc.) while understanding the parameters contributing to each mineral classification and optimizing models settings. A second validation phase involved applying the models to the Beauvoir granite data to assess how the models perform in more complex systems, such as natural rocks.

1.4.1 **Training data processing**

To address the complexity of LIBS spectra, a two-step processing workflow was applied to the mineral reference spectra constituing the training data: first, signals corresponding to selected spectral intervals were extracted from both raw and SNV-normalized spectra; second, additional dimensionality reduction techniques were employed to generate supplementary datasets for evaluating the most effective approach for classification purposes

The handheld LIBS analyzer generates high-dimensional data, with each spectrum containing 24,000 variables and a spectral resolution of 0.03 nm. Processing such high-dimensional data using machine learning presents challenges (47,48), as an increased number of variables demands more memory and longer training times, reducing computational efficiency. Additionally, relevant signals may be obscured by irrelevant, redundant, or noisy data, potentially affecting classification accuracy. Therefore, dimensionality reduction can significantly influence model performances and improve result interpretability (49). A key advantage of LIBS analysis on mineral/rock samples is that dimensionality reduction can be guided by mineral chemistry rather than arbitrary statistical selection (50). Since each mineral has a specific chemical composition (**Table.1**), variable selection can be focused on the emission lines of major, minor, and trace elements. This ensures that the most relevant spectral features are retained while drastically reducing data complexity. **Table.2** lists the selected emission lines and spectral intervals used for feature extraction. These were chosen based on the NIST LIBS database, prioritizing the strongest emission lines. Each peak was verified to ensure sufficient signal intensity and no spectral interference. The area under the

curve for each emission line was extracted using Spectragryph software (51). Fluorine (F), though present in the mineral composition, was not detected in the spectra and was therefore excluded from the variables selected.

Table.2. Emission line positions and spectral ranges for libs signal extraction of major, minor, and trace elements in targeted minerals (albite, orthose, quartz, topaz, phosphates, lepidolite, and muscovite)

Element	Emission line position *(nm)*	Spectral range *(nm)*
Na	588.99 589.54	[588.2 – 590.2]
Al	309.26	[309 – 309.6]
Si	251.43 288.16 285.8	[251-2 – 251.75] [287.9 – 288.4] [285.2 – 286.2]
Ca	422.63	[422.33-423.23]
K	766.46 769.89	[765.76 – 767.30] [769.42 – 770.60]
Mg	279.7	[279.36 – 279.7]
Fe	238.20	[238 – 238.35]
Li	670 610.36 812.63	[670-671.5] [609.2 – 611.2] [812.3 – 813]
Be	313	[312.4 – 313.8]
Ba	455.5	[455.15 – 455.6]
Sr	407.8	[407.4- 407.97]
Rb	780.05 794.71	[779.8 – 780.2] [794.4 – 795.4]
O	777.19	[776.8 – 777.9]
Ti	375.79	[375.5 – 376]
H	656.27	[655 – 657.2]
Cs	852.10	[851.7-852.6]
Mn	257.6	[257.4-257.75]
P	213.62 214.93	[213.35-213.93] [214.68-215.11]
Cl	472 474	[471.94-472.44] [473.93-474.41]

Principal Component Analysis (PCA) and Partial Least Squares (PLS) regression were applied as a second processing step for additional datasets, using both raw and SNV-normalized data to further refine input features. PCA was used to transform the extracted LIBS data into a lower-dimensional space by generating independent principal components (PCs) that capture most of the variance in the datasets, in order to: (i) eliminate redundant data and multicollinearity by grouping variables with similar trends, as some elements are represented by multiple emission lines (e.g., Li, K, Si), and (ii) optimize computational efficiency by shortening training and prediction times. This is particularly important for scaling the workflow to larger datasets, such as those generated during exploration campaigns, where volumes of 10 to 20 meters of rock are processed daily. In parallel, PLS regression was employed to calculate latent components, which were subsequently used as independent variables in discriminant analysis (PLS-DA). Mineral class labels were encoded as numerical values ranging from 0 to 6, as PLS requires quantitative input. For both approaches, the optimal number of components was determined based on the cumulative variance explained (**Fig.S2**). As a result, six distinct training datasets were generated from the LIBS reference spectra:

I. Emission line extraction from raw spectra
   i. PCA
   ii. PLS
II. Emission line extraction from SNV spectra
   i. PCA
   ii. PLS

1.5 Workflow

Applications of machine learning solutions have become increasingly widespread within the field of geosciences (32–35). The ability of these models to simplify the interpretation of high-dimensional data, identify patterns and anomalies, and uncover new perspectives in large and complex datasets addresses the current challenges faced by the sector in analyzing extensive and intricate databases. In this study, machine learning algorithms were employed to translate LIBS elemental data into mineralogical information. The idea is to automate the task of mineral identification by training models for classifying LIBS elemental analysis into distinct mineral classes, thereby determining the mineralogical composition and relative abundance of targeted mineral phases in rock samples. Four classification approaches, LDA (36,37), SVM (38–40), PLS-DA (41–43), and Random Forest (35), were trained, optimized, and evaluated to classify unknown data. The models, described in **Table.3**, were selected for their ability to handle high-dimensional data (44,45) from low to high computational complexity and account for both linear and non-linear relationships in decision-making. All models, as well as the organization of training and testing datasets and the Beauvoir granite analysis, were implemented using the statistical software JMP ® Pro 18 (46). **Fig.2** illustrates the successive steps involved in implementing, evaluating, and selecting the optimal approach for multi-class classification and

lepidolite discrimination. The workflow is composed of two primary stages: i) training and evaluation inwhich the classification models are trained using reference LIBS data of pure minerals, and ii) case study application in which the models from phase 1 were applied to the Beauvoir granite samples to assess the performance of the models in complex systems that represent rock samples.

Table.3. Comparative Analysis of Machine Learning Models for LIBS data classification: SVM, Random Forest, LDA, and PLS-DA through Mathematical features, Computational Complexity, Hyperparameters, and Limitations

Model	Mathematical features	Computational Complexity	Hyperparameters	Limits
LDA (Linear Discriminant Analysis)	- Based on eigenvalue decomposition of covariance matrices - Maximizes class separation in a lower-dimensional space	Low	- Variables selection	-Assumes linear class boundaries. -Sensitive to outliers and non-normal data.
SVM (Support Vector Machine)	- Finds optimal hyperplane to maximize class margin - Uses kernel functions (linear, polynomial, RBF) to handle non-linearity	Moderate	- Kernel type (linear, RBF, polynomial). - C (regularization). - Gamma (kernel coefficient).	-Computationally expensive for large datasets. -Requires careful hyperparameters tuning.
Random Forest	- Generate multiple decision trees - Aggregates tree predictions using majority voting	High	- Number of trees. - Max depth of trees. - Minimum samples per split.	Computationally expensive, especially with many trees. biased toward dominant classes.
PLS-DA (Partial Least Squares Discriminant Analysis)	- Projects high-dimensional data onto latent variables - Maximizes covariance between predictors	Moderate	- Number of components	Assumes a linear relationship between predictors and response. Requires careful selection of the number of latent variables.

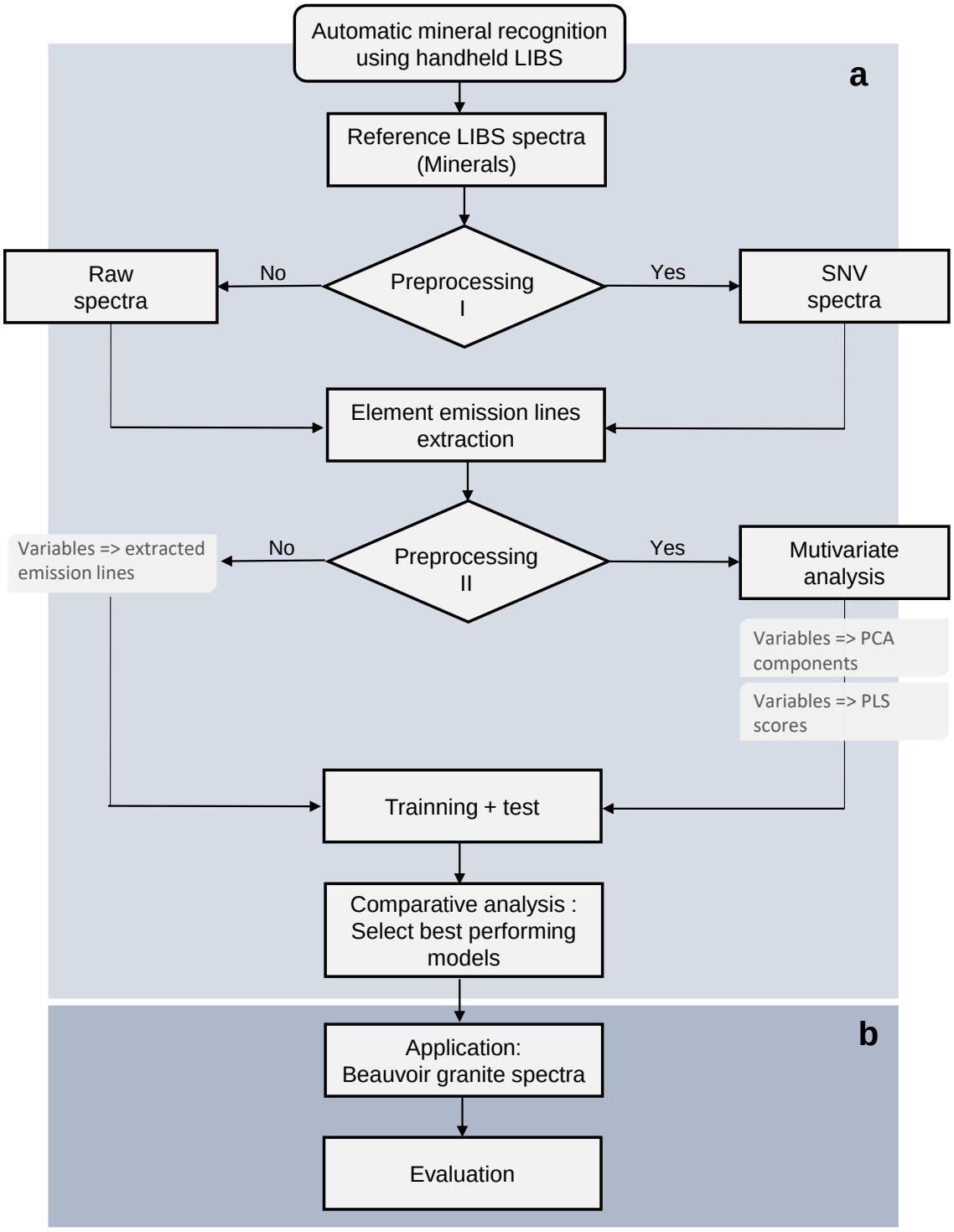

Figure.2. Workflow for implementing machine learning models for automated mineral recognition using libs data: (a) phase 1: model training and testing, (b) phase 2: application to the case study. In this study, the datasets used correspond to emission line signals extracted from LIBS spectra, with some datasets further processed through a second stage of multivariate analysis (PCA and PLS).

2 Results

2.1 Principal Component Analysis (PCA)

The first 10 principal components were selected for classification, as they explained 87% of the cumulative variance in both raw and SNV datasets. Additional components beyond the 10th showed only marginal increases in explained variance, suggesting that the first 10 components capture the most important patterns in the data (**Fig.S1**). **Fig.3** presents score and loading plots showing the distribution of data points in a 2-D space defined by Principal Components 1 and 2 for both raw and normalized datasets. Within this mineral group, the presence of outliers is likely due to sample heterogeneity. For the SNV dataset (**Fig.3b**), lepidolite clusters tightly around key elements such as Li and Rb. However, some data points are linked to quartz, likely due to heterogeneous Li distribution within the lepidolite sample. Quartz is well-separated but has some outliers, primarily driven by variables like Sr, Ti, and Si. Albite, muscovite, feldspars, and topaz form a compact cluster in the center, similar to the raw data. Phosphate data points form two distinct clusters: one for Li-rich phosphates (amblygonite) and one for Li-poor phosphates (apatite). These observations underscore the need for more advanced processing to distinguish between similar mineral classes. Challenges include heterogeneity within the same mineral phase and difficulty in differentiating closely related compositions. While SNV-normalized data provides better clustering, these issues persist.

2.2 Partial Least Square (PLS)

Eleven latent components were retained for both raw and SNV-normalized data. These components collectively explained 85% of the variance in the predictor variables (X) and 80% of the variance in the response variables (Y) for the raw dataset, while 83% of the variance in X and 70% in Y were explained for the SNV-normalized dataset. Increasing the number of components further resulted in a minimal increase in the cumulative variance explained for the predictor variables and no substantial improvement in the response variance. Of the retained variables, 17 emission lines corresponding to major elements (Li, Na, Al, etc.) exhibited a Variable Importance in Projection (VIP) value greater than 0.8, indicating their significant contribution to modeling both X and Y. The remaining variables (VIP < 0.8) were primarily emission lines of trace elements (Mg, Fe, Ca, Be, Sr, Cl). The PLS score plot of the first two components (PLS1 vs. PLS2) for the raw data (**Fig.3c**) allows clear discrimination between the albite, lepidolite, and K-feldspar classes, while the rest of minerals form a compact cluster. In contrast, the SNV-normalized data reveals a distinct cluster for apatite and amblygonite (phosphates), with albite and lepidolite overlapping. Muscovite is separated into three distinct groups, likely reflecting chemical variation across different samples. The remaining data points

form a compact cluster. Despite variations between data types (Raw vs. SNV) and multivariate methods (PCA-PLS), lepidolite data points generally form a distinguishable cluster from the rest of mineral classes

2.3 Machine learning models

The models were evaluated with a test dataset representing 25% of the initial data (469 spectra). Before that, cross-validation was performed to optimize hyperparameters for SVM and Random Forest models, including tuning the regularization parameter (C) and the gamma coefficient for SVM (**Fig.S3** and **Fig.S4**). For Random Forest, adjustments were made to the number of trees (**Fig.S5**), maximum tree depth, minimum samples required to split a node, and minimum samples required at a leaf node. The optimal model across all iterations was selected by minimizing the prediction error. Predicted mineral classes were compared to reference labels and organized into a confusion matrix, generating a 7×7 table that provided essential classification metrics: i) True Positives (TP): Correctly classified positive instances, ii) True Negatives (TN): Correctly classified negative instances, iii) False Positives (FP) (Type I Error): Incorrectly classified positive instances, iv) False Negatives (FN) (Type II Error): Incorrectly classified negative instances. Based on these values, five evaluation metrics were computed for each mineral class and averaged across all classes to assess overall model performance:

i. Accuracy: measures the overall correctness of predictions.

$$\text{Formula} = (TP + TN) / (TP + TN + FP + FN)$$

ii. Precision: the proportion of true positive predictions among all predicted positives.

$$\text{Formula} = TP / (TP + FP)$$

iii. Recall: the ability to correctly identify all actual positives.

$$\text{Formula} = TP / (TP + FN)$$

iv. F1-Score: the harmonic mean of precision and recall, balancing both metrics.

$$\text{Formula} = 2 \times (\text{Precision} \times \text{Recall}) / (\text{Precision} + \text{Recall})$$

v. Misclassification Index: adjusted score that takes into account both types of misclassifications FN and FP.

$$\text{Formula} = 1 - ((FP + FN)/ (FP + FN + TP + TN))$$

Fig.4 presents the calculated metrics in spider diagrams, comparing dataset performances for multi-class predictions. **Fig.5** follows the same approach but focuses specifically on the lepidolite class results, as accurately identifying ore minerals is a key objective of this study. Since all values range between 0 and 1, one major axis was projected; values close to 1 indicate good performance. The comparative analysis of multi-class classification demonstrates that all tested models achieved evaluation metric values above 0.8, indicating

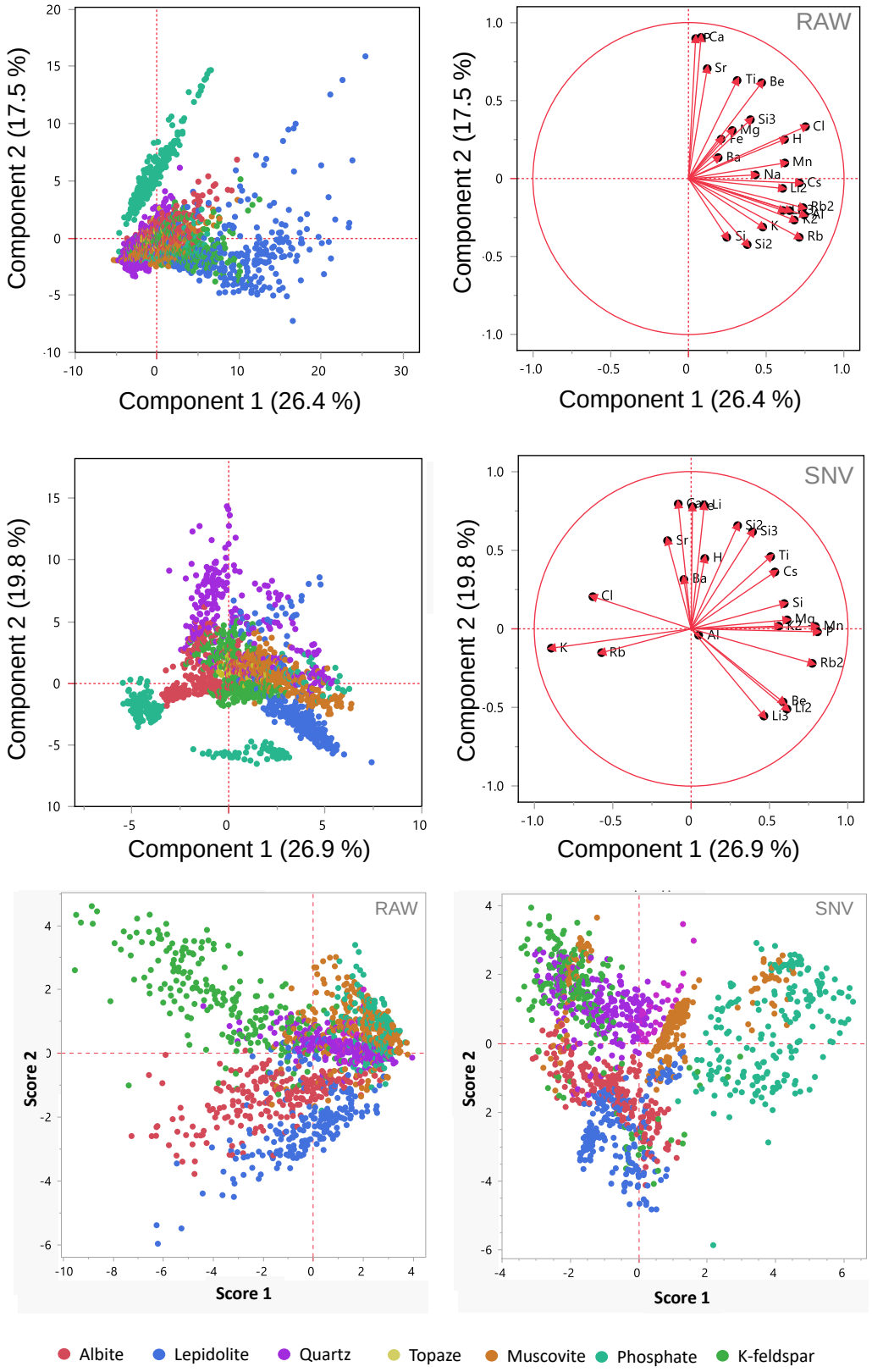

Figure.2. Multivariate Analysis of Reference Mineral Data—(a, b) PCA Score and Loading Plots for Raw (Top) and SNV-Normalized (Bottom) Data; (c) PLS Score Plots for Raw (Left) and SNV-Normalized (Right) Data.

strong performance in classifying LIBS spectral data into mineral classes. SVM models showed the highest accuracy (0.99), while Random Forest variants exhibited the lowest performance (0.81). Normalized datasets performed slightly better than raw datasets for LDA, SVM, and PLS-DA, whereas Random Forest performed best with raw data. The trends observed in multi-class classification were consistent with those seen in lepidolite classification, except for a slight performance improvement when using SNV-normalized data with Random Forest. The optimal model selection was primarily influenced by lepidolite classification performance; however, the final choices also aligned with multi-class classification results. The four selected machine learning models for Beauvoir application are: LDA using raw data, SVM using SNV normalized data, Random forest using raw data, and PLS-DA using SNV normalized data.

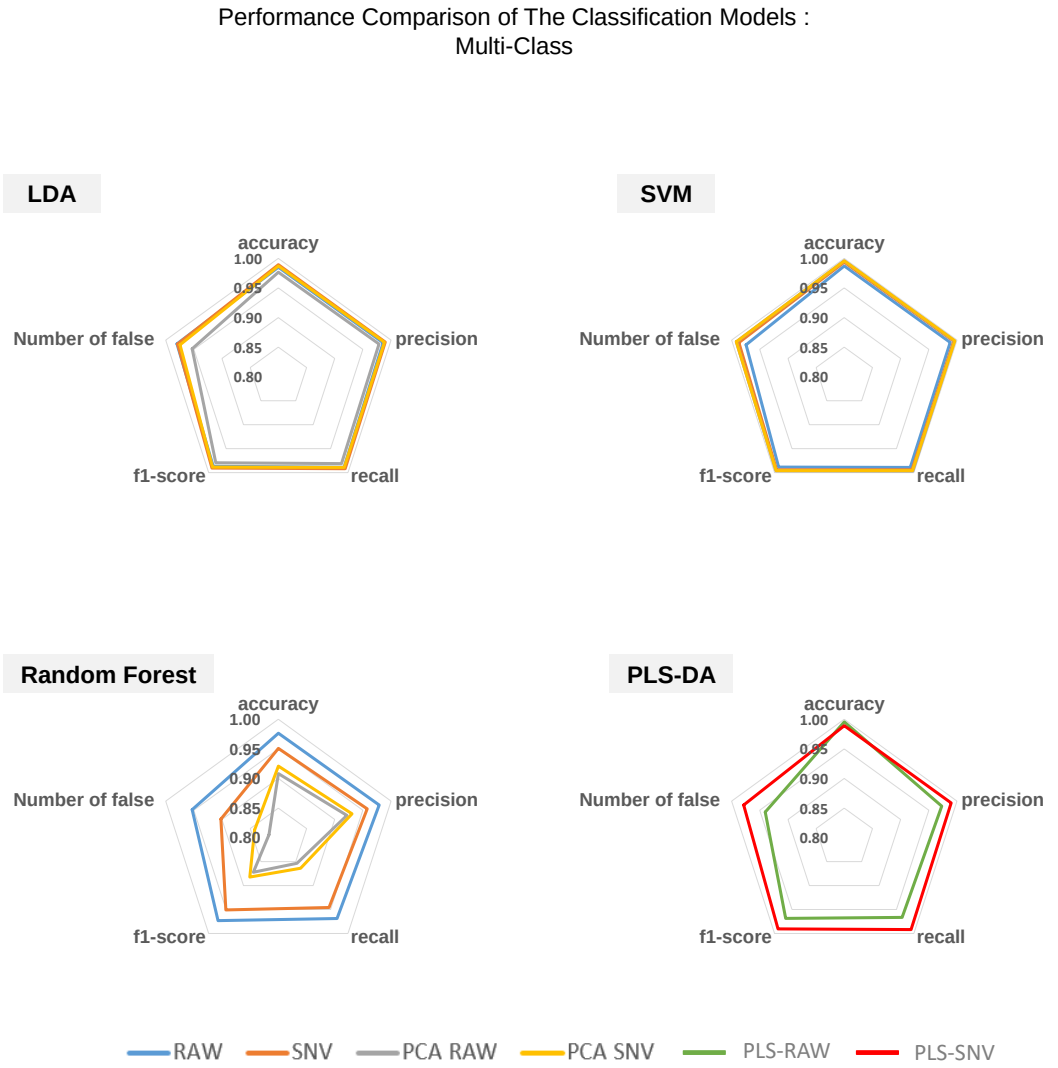

Figure.4. Comparison of LDA, SVM, Random Forest, and PLS-DA Model Performance for multi-class classification.



Figure.5. Comparison of LDA, SVM, Random Forest, and PLS-DA Model Performance for lepidolite classification.

2.4 Beauvoir granite application

To test the models' abilities to generalize predictions to rock analyses, the second phase evaluates the retained classification models on four Beauvoir granite samples. Granite data introduces additional complexities arising from the physical and chemical specificities of the deposit (i.e., grain size, alteration, etc.), possibly leading to spectral variations that were not accounted for in the first phase of testing using pure mineral data.

For each granite data point, a mineral class was assigned. The predicted mineral proportions were then calculated by dividing the number of classified points per mineral by the total number

of measurement points per sample and multiplying by 100. These predictions were compared to reference values obtained through detailed petrographic analysis and µXRF geochemical mapping (S. Z. Kahou, unpublished data) (**Table.4**). Prediction errors were computed for each class and each sample to determine the best-performing model for both multi-class classification and lepidolite identification. The results, illustrated in **Fig.6**, **Fig.7**, and **Fig.8**, illustrate models performances when applied to granite samples. **Fig.6** compares the predicted and reference proportions of lepidolite (**Fig.6a**), and the absolute prediction error for each model across the four samples (**Fig.6b**). The Random Forest model achieved the best accuracy for samples C42 and C117, while the SVM model performed best for lepidolite classification in samples C52 and C112 (**Fig.6a**). Lepidolite is mainly overestimated, though SVM provides more balanced results.

Table 4: Reference values of mineral abundances in Beauvoir granite samples.

	Albite	Lepidolite	Quartz	Topaze	Orthose	Phosphates	Muscovite
C42	39.3	25.2	24	1.6	5.5	4.3	0
C52	54.1	16.7	24.5	1	0	3.8	0
C112	44	9.6	28.3	2.5	11.8	1.2	0
C117	0	15.7	51.1	0	12.9	0	17.4

Fig.7 compares predicted and reference mineral abundances across all classes, highlighting systematic trends in model performance. Albite is consistently underestimated, except in the PLS-DA model, while quartz is underrepresented in all cases. Predictions for accessory minerals, including muscovite, K-feldspar, phosphates, and topaz, vary significantly, with LDA and SVM tending to overestimate these phases, whereas topaz is consistently underestimated across all models. **Fig.8** further illustrates prediction errors, showing that quartz classification remains poor across all approaches, while K-feldspar is particularly misclassified by the Random Forest model. Lepidolite is generally overestimated in LDA and PLS-DA, whereas Random Forest and SVM provide more balanced but variable results. Among the samples, C117 exhibits the highest error, up to 60% in each model, suggesting that sample-specific characteristics influence classification accuracy despite consistent acquisition parameters and instrumentation. In **Fig.8**, the mean absolute error (MAE) for each mineral class reveals that no single model outperforms all others across all classes. While SVM provides the best results for albite, lepidolite, and phosphates, PLS-DA performs better for muscovite and K-feldspar. Although LDA achieves the most accurate quartz classification, its error remains significant (>25%). The absolute classification error for topaz (0.5–2.4%) appears low compared to other

minerals, it remains critical when considered relative to its true abundance (typically between 0% and 2.5%), where even small errors can lead to major overestimation.

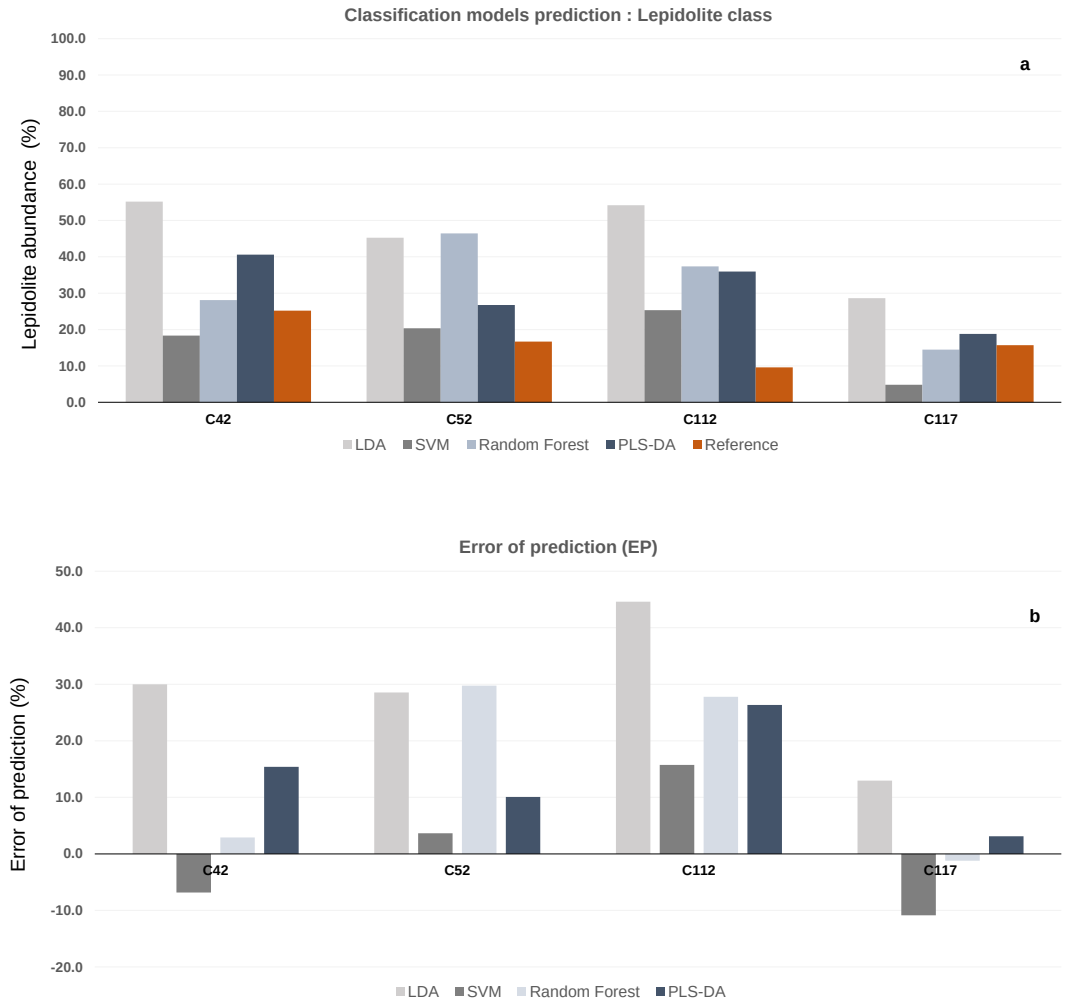

Figure.6. Distribution of Prediction Errors for lepidolite Class**:** a) Comparative analysis of the absolute prediction errors obtained by each model for each Beauvoir granite sample. b) Comparison of the mean absolute prediction error averaged across Beauvoir granite samples.

Overall, SVM is the most effective model for lepidolite classification, with an error of 11.7%, followed by PLS-DA and Random Forest, which show errors of 14.7 and 15.4%, respectively. LDA performs the worst, with an error of 28.6%. For multi-class classification, PLS-DA using SNV-normalized data achieves the highest accuracy, with a mean absolute error (MAE) of 9.2%, outperforming LDA (18.8%), SVM (12.2%), and Random Forest (17.0%). These results underscore the importance of selecting an appropriate classification model based on the mineralogical characteristics of the samples, with SVM and PLS-DA emerging as the most reliable approaches for Beauvoir samples.

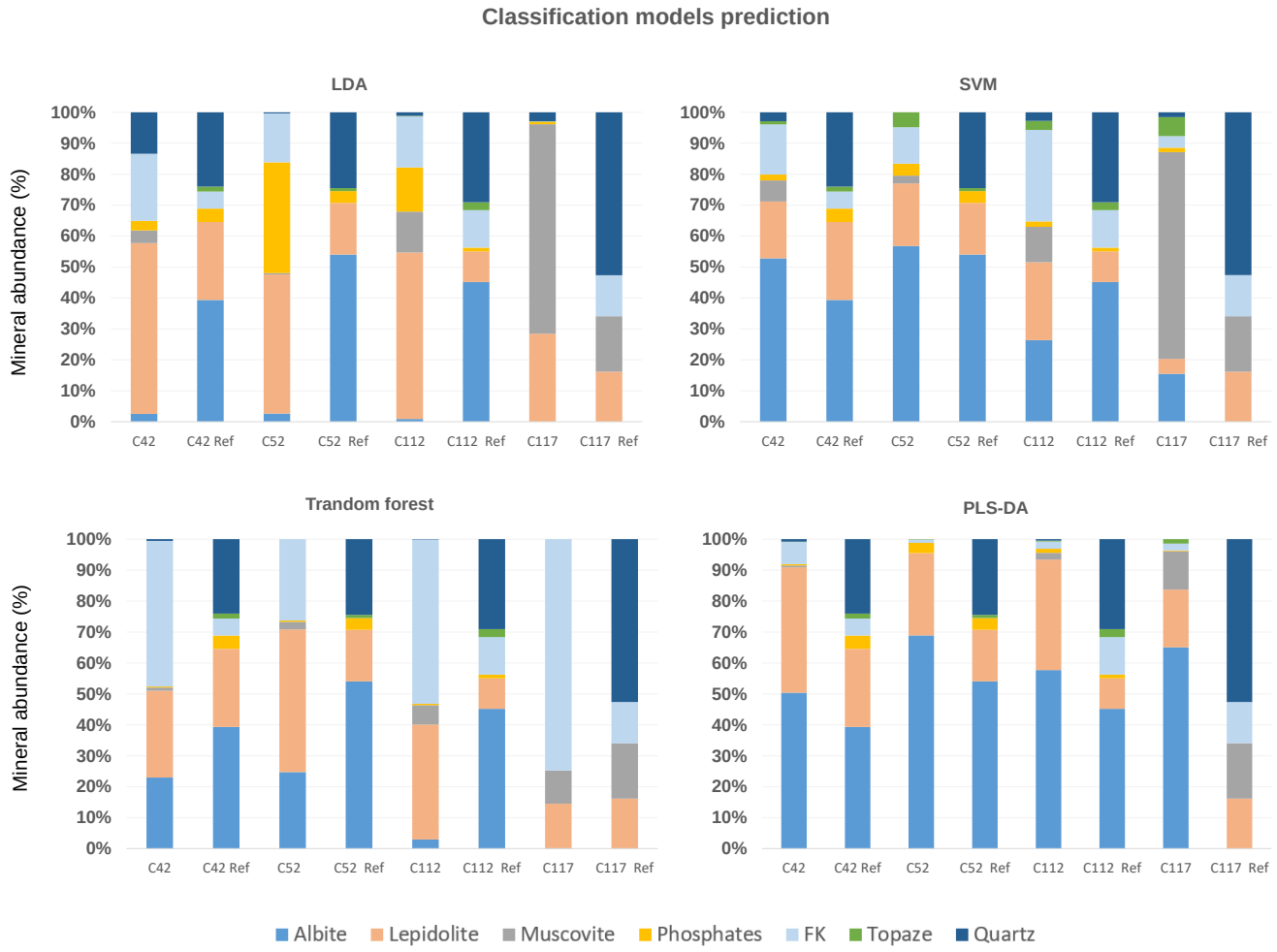

Figure.7. Comparative analysis of mineral abundance predictions and reference values for the Beauvoir granite samples.

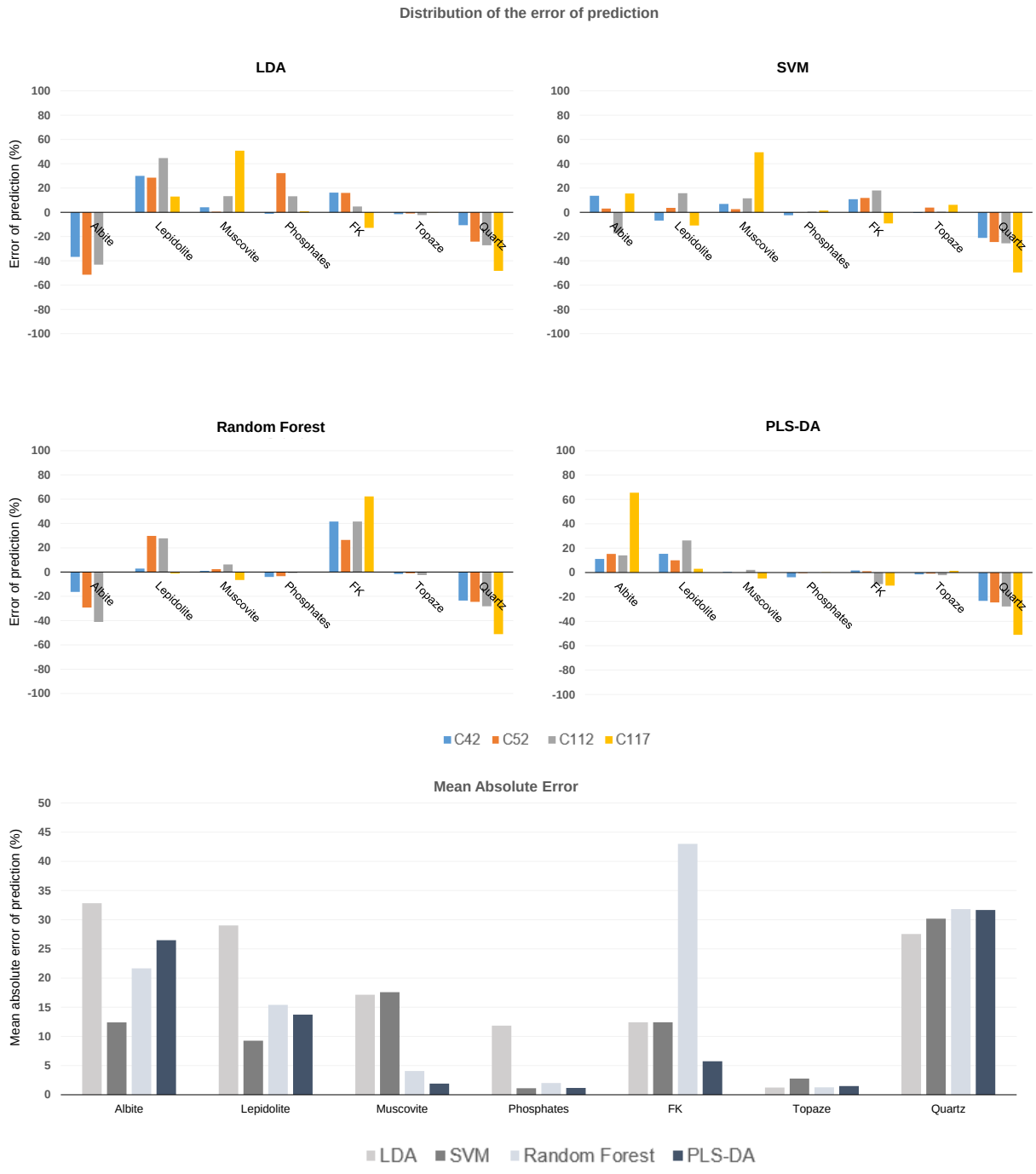

Figure.8. Prediction error distribution across mineral classes and machine learning models: (a-d) error distribution per mineral class, (e) mean absolute error averaged across Beauvoir granite samples.

3 Discussion

The distribution of LIBS data, based on Li and Si signals, as illustrated in the **Fig.9,** shows that mineral data primarily cluster into two groups: a Li-rich cluster representing lepidolite and Li-phosphates, and a Li-poor cluster corresponding to the other mineral phases. The Beauvoir granite data form a compact cluster, with Li LIBS signal ranging from 2000 to 6000 a.u., in addition to a subset of Li-rich data points (>6000 a.u.) aligning with the lepidolite cluster. The proportion of data points exhibiting relatively higher Li signal intensity in the Beauvoir granite samples raises some questions. Indeed, LIBS analyses performed on a 10×9 grid covering a 5×5 mm surface are expected to capture a distribution of both Li-rich points (>5000 a.u.), corresponding to Li-bearing phases, and Li-depleted points (<1000 a.u.), representing matrix minerals such as albite and quartz. However, this expected distribution is not reflected in **Fig.9**, as a significant portion of the data is concentrated around moderate Li values, exceeding those typically observed for quartz or albite, which should statistically be more represented. Two key points emerge from this observation:

I. Geochemical Variability in Mineral Composition

Mineral compositions can vary depending on the geochemical conditions during deposit genesis. During the crystallization of the Beauvoir granite, in a Li-rich environment, lithium is primarily incorporated into ore minerals such as lepidolite and amblygonite, but it can also be incorporated into other crystal structures through substitution mechanisms. ICP-MS analyses of quartz reveal elevated Li concentrations (90–199 ppm) (52), exceeding values reported in other geological contexts (53). This enrichment reflects the effects of fractional crystallization, where incompatible elements like Li preferentially remain in the melt, progressively concentrating as differentiation advances. In highly evolved magmatic systems, such as pegmatites and rare-metal granites, Li can reach exceptionally high levels, persisting in the melt until the final stages of crystallization (54). Such variations influence the spectral signals, causing deviations from reference mineral spectra. As a result, some data points fall outside the expected feature space of quartz and albite, leading to systematic misclassification, often favoring Li-rich minerals like lepidolite. This highlights the need to incorporate deposit-specific reference spectra to improve classification accuracy.

I. Spectral Mixing Due to Mineral Size and LIBS Spot Size

Unlike mineral data points, in which each point corresponds to a single mineral, LIBS analyses of the Beauvoir granite may include mixed-phase spectra due to the mineral grain size (200–600 µm). Since the LIBS crater size is between 100 and 200 µm, depending on the spatial position of the data points, a single measurement can capture multiple mineral phases, producing an averaged spectrum rather than a pure mineral signal.

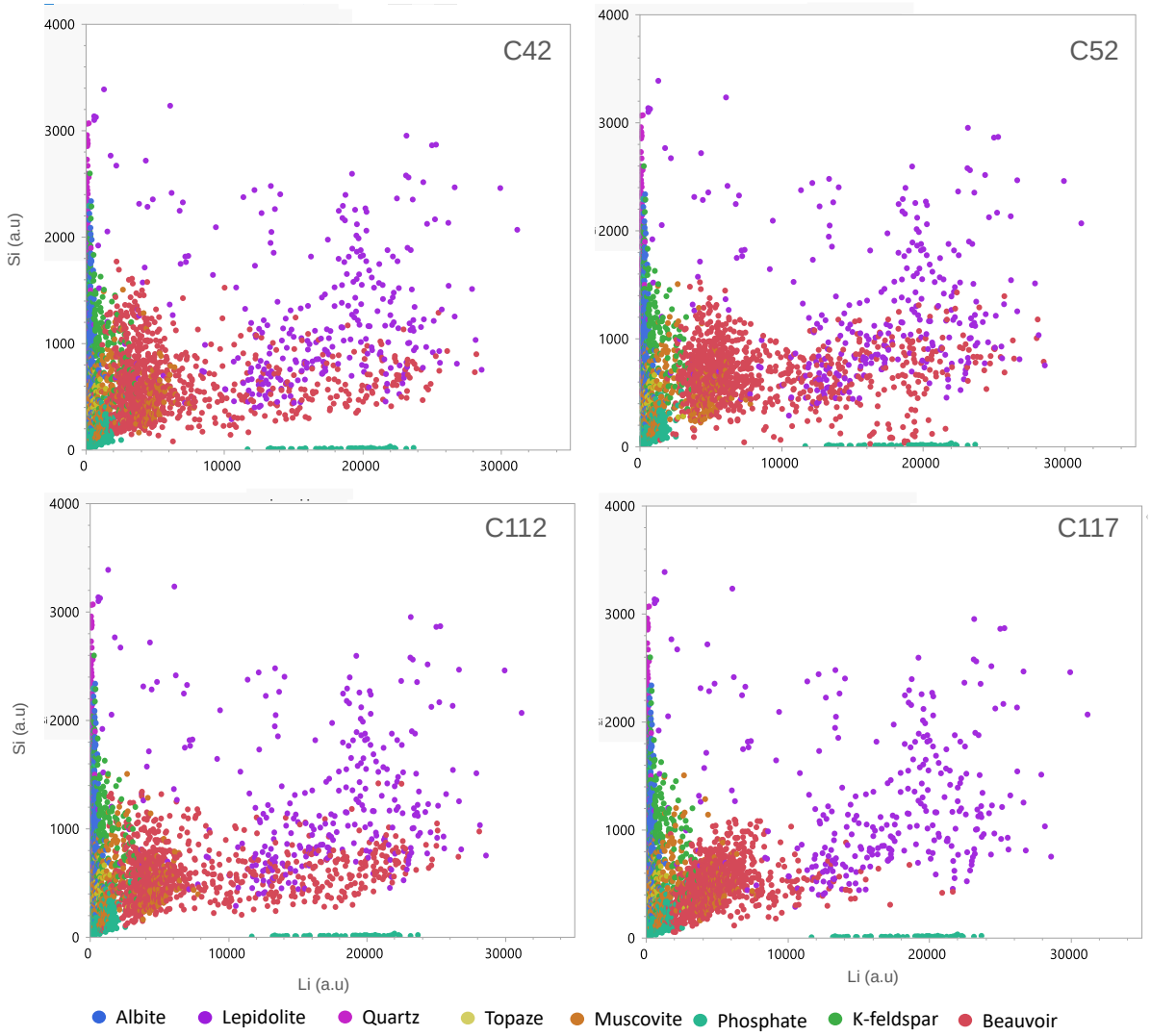

Figure.9.LIBS data distribution for pure minerals and beauvoir granite samples: color-coded signal intensity diagram for Si and Li.

Additionally, lithium's high emissivity and low detection limit emphasize this phenomenon as a measurement point primarily located on quartz and partially on lepidolite crystal will still display a high Li signal. To minimize classification errors caused by mixed points, it is crucial to study and optimize the spatial distribution of LIBS analysis, including both spot and step sizes, to align with the textural characteristics of the targeted samples. This approach will help reduce misclassification due to signal biases resulting from mixed spectra. **Fig.10** shows the absolute error of prediction for the lepidolite class (**Fig.10a**) and multi-class classification (**Fig.10b**), color-coded according to the alteration of the granite samples. The results suggest that the error scale is correlated with the alteration state of the sample. The alteration index was determined through petrographic analysis and the F' (K-Na)) index (55,56), commonly used to assess the mineralogical evolution of rocks resulting from the alteration in felsic rocks (55). Fresh granite samples are characterized by negative F' values, while altered samples exhibit positive F' values. Sample C52 (F' = -150.5), the fresh granite sample, shows the lowest prediction errors and performs best for both lepidolite and multi-class classification. In contrast, sample C117 (F' = 121.5), which is highly greisenized, exhibits the highest prediction error for lepidolite classification, and poor performance for multi-class prediction.

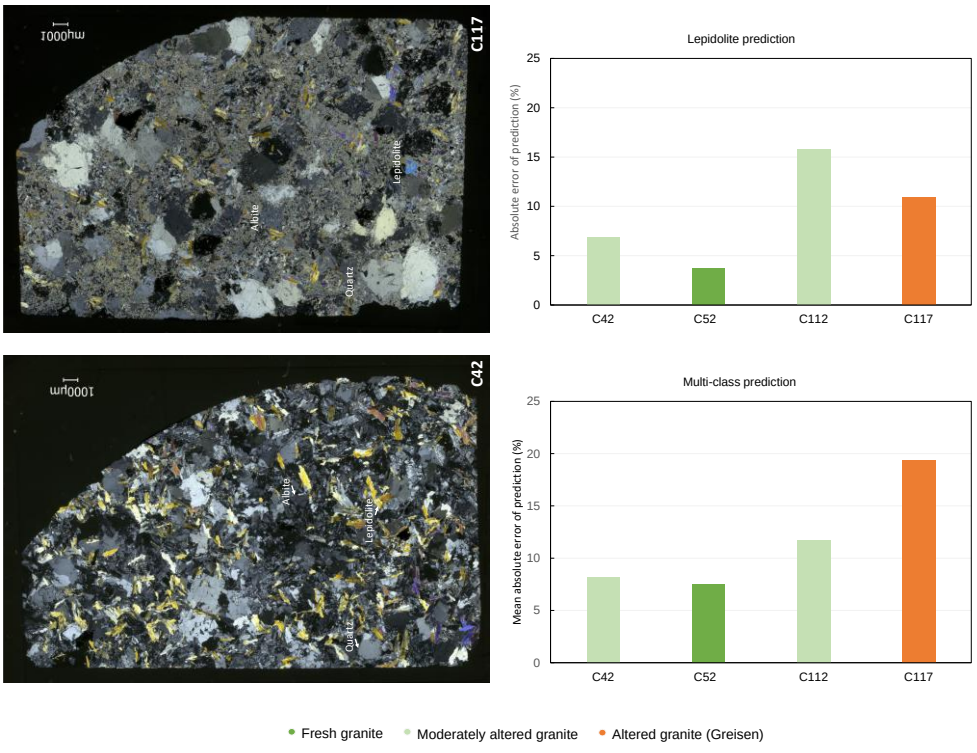

Figure.10. Petrographical images of an altered granite sample (top, C117) and a relatively fresh granite sample (bottom, C42), a) the distribution of absolute prediction error for the lepidolite class, and b) the mean absolute prediction error for multi-class classification across granite samples, both color-coded according to the degree of alteration.

For moderately altered samples, C42 and C112, the results are mixed. Sample C112 (F' = -81) performs worse than C42 (F' = 19) despite showing an increasing F' value. These results, however, should be interpreted with caution and require validation through a larger sample size to confirm the observed trend. Alternative hypotheses may explain these patterns, such as the influence of sample composition on the mean absolute error. For instance, a sample with a higher quartz content would likely exhibit a greater mean absolute error compared to a sample dominated by better-predicted mineral classes. This is exemplified by sample C117, which demonstrates the highest quartz content (51.1 %) and correspondingly elevated error values. Although further analyses are required to fully understand how varying degrees of alteration affect LIBS-based classification, these preliminary findings imply that, in addition to chemical matrix effects, physical properties such as alteration states should also be considered for automatic mineral recognition using LIBS data. Models trained on non-altered, macro-scale mineral spectra might face difficulties in classifying data from altered rocks. This is consistent with broader studies highlighting the impact of physical characteristics on LIBS studies (57,58).

Conclusion

Mineral identification during logging operations relies mainly on visual interpretation, which can become increasingly difficult when mineral exhibit similar physical properties. To address this limitation, we investigated the possibility to process handheld LIBS analysis using machine learning algorithms to automate rapid and field-based mineral identification, specifically in the case of the Beauvoir rare-metal deposit exploration, as discriminating the ore-phase, lepidolite, from matrix phases is particularly challenging.

Pure mineral spectra, representing the mineralogical composition of the Beauvoir granite were used as reference data to train and evaluate four classification approaches: LDA, SNV, Random Forest, and PLS-DA. To reduce the high dimensionality of LIBS spectra (>24,000 variables), key emission lines of major and minor elements were extracted. PCA and PLS scores were also tested as input variables. Both raw and SNV-normalized LIBS data were considered. A total of four datasets were used for each model, excluding PLS-DA, resulting in 14 model iterations. The classification models were evaluated using the statistical metrics: Accuracy, Precision, Recall, F1 Score, and Misclassification Index. The best-performing models were then tested on the Beauvoir granite data. The results enabled both identifying the mineralogical composition of the analyzed rock sample and calculating the relative abundance of each phase based on the total number of LIBS data points classified per class. Prediction errors, calculated using reference values obtained through laboratory methods, highlighted PLS-DA as the most effective model for multi-class classification (MAE = 9.27%), while SVM performed best for lepidolite discrimination (MAE = 11.74%). A systematic underestimation of

quartz and an overestimation of lepidolite were observed, while other classes showed mixed performances.

While the results are promising, certain issues remain to be addressed. In terms of data acquisition, the potential impact of mixed spectra on misclassification resulting in the overestimation of one phase over another, emphasizes the need for customized LIBS analysis strategies. Optimizing point spacing and positioning, based on the sample texture, particularly grain size and distribution, is essential to ensure the accurate placement of LIBS shots within individual mineral grains. Additionally, the increasing prediction error percentage, dependent on the samples alteration states, confirms the critical importance of carefully considering physical matrix effects that can affect the ablation process during data acquisition. Furthermore, the variability in error distribution across mineral classes highlights the importance of incorporating deposit-specific reference data into the model training to better account for chemical variations within the deposit and improve prediction accuracy. Combining multiple models in successive classification steps or further tuning the model features could improve performance; however, increasing the complexity of the classification models necessitates careful evaluation when generalized to larger scales, particularly in the context of drilling campaigns, where the volume of rock analyzed far exceeds the dataset used in this study. Applying these models to larger datasets will provide valuable insights into the balance to achieve between computational complexity, resource requirements, and predictive accuracy. In conclusion, integrating handheld LIBS data with supervised machine learning algorithms provides reliable mineralogical information confirming the value of handheld LIBS as a rapid, field-based analytical technique for advanced applications in sample characterization, enabling faster and more reliable assessments of ore distribution to support informed and strategic decision-making during mining operations.

Acknowledgments

We would like to thank Michel Cathelineau and Steven Zia Kahou for providing the Beauvoir granite samples and the geochemical data used to validate and evaluate the machine-learning models. A special appreciation to the Imerys team for their valuable help, granting us convenient access to the Beauvoir granite mining site and providing essential data on the deposit.

Funding

This study was financed by the French National Research Agency via the Labex Ressources 21 project [reference ANR–10–LABX–21-01] and a collaboration with Imerys, the operating company of the Beauvoir Granite.

AI disclosure

ChatGPT and DeepL were used to translate some parts of the text from French to English. After using these AI interfaces, the text was reviewed and edited as needed. The author takes full responsibility for the content of the publication.

References

1. Fabre C, Ourti NE, Mercadier J, Cardoso-Fernandes J, Dias F, Perrotta M, et al. Analyses of Li-Rich Minerals Using Handheld LIBS Tool. Data. 2021 Jun;6(6):68.

2. Balaram V, Sawant SS. Indicator Minerals, Pathfinder Elements, and Portable Analytical Instruments in Mineral Exploration Studies. Minerals. 2022 Apr;12(4):394.

3. Kim Y, Caumon MC, Barres O, Sall A, Cauzid J. Identification and composition of carbonate minerals of the calcite structure by Raman and infrared spectroscopies using portable devices. Spectrochimica Acta Part A: Molecular and Biomolecular Spectroscopy. 2021 Nov 15;261:119980.

4. Lemière B, Harmon RS. XRF and LIBS for Field Geology. In: Portable Spectroscopy and Spectrometry [Internet]. John Wiley & Sons, Ltd; 2021 [cited 2022 Aug 24]. p. 455–97. Available from: https://onlinelibrary.wiley.com/doi/abs/10.1002/9781119636489.ch42

5. Harmon RS. Laser-Induced Breakdown Spectroscopy in Mineral Exploration and Ore Processing. Minerals. 2024 Jul 1;14:731.

6. Fabre C. Advances in Laser-Induced Breakdown Spectroscopy analysis for geology: A critical review. Spectroc Acta Pt B-Atom Spectr. 2020 Apr;166:105799.

7. Fontana FF, Tassios S, Stromberg J, Tiddy C, van der Hoek B, Uvarova YA. Integrated Laser-Induced Breakdown Spectroscopy (LIBS) and Multivariate Wavelet Tessellation: A New, Rapid Approach for Lithogeochemical Analysis and Interpretation. Minerals. 2021 Mar;11(3):312.

8. Wise MA, Harmon RS, Curry A, Jennings M, Grimac Z, Khashchevskaya D. Handheld LIBS for Li Exploration: An Example from the Carolina Tin-Spodumene Belt, USA. Minerals. 2022 Jan;12(1):77.

9. Fabre C, Ourti NE, Ballouard C, Mercadier J, Cauzid J. Handheld LIBS analysis for in situ quantification of Li and detection of the trace elements (Be, Rb and Cs). Journal of Geochemical Exploration. 2022 May 1;236:106979.

10. Kim Y, Fabre C, Cauzid J. Access to quantitative analysis of carbonates using a portable LIBS instrument: First applications to single minerals and mineral mixtures. Spectrochimica Acta Part B: Atomic Spectroscopy. 2022 May 1;191:106397.

11. Fontana FF, van der Hoek B, Tassios S, Tiddy C, Stromberg J, Francis N, et al. Laser Induced Breakdown Spectroscopy (LIBS) for whole rock geochemistry. Journal of Geochemical Exploration. 2023 Mar;246:107160.

12. Harmon RS, Wise MA, Curry AC, Mistele JS, Mason MS, Grimac Z. Rapid Analysis of Muscovites on a Lithium Pegmatite Prospect by Handheld LIBS. Minerals. 2023 May;13(5):697.

13. Defnet PA, Wise MA, Harmon RS, Hark RR, Hilferding K. Analysis of Garnet by Laser-Induced Breakdown Spectroscopy—Two Practical Applications. Minerals. 2021 Jul;11(7):705.

14. Capela D, Ferreira MFS, Lima A, Dias F, Lopes T, Guimarães D, et al. Robust and interpretable mineral identification using laser-induced breakdown spectroscopy mapping. Spectrochimica Acta Part B: Atomic Spectroscopy. 2023 Aug 1;206:106733.

15. Lawley CJM, Somers AM, Kjarsgaard BA. Rapid geochemical imaging of rocks and minerals with handheld laser induced breakdown spectroscopy (LIBS). Journal of Geochemical Exploration. 2021 Mar 1;222:106694.

16. M Cuney, A Autran. Objectifs généraux du projet GPF Echassières n°1 et résultats essentiels aquis par le forage de 900 m du granite albitique à topaze-lépidolite micas. 1987.

17. Le projet de mine de lithium EMILI reconnu en Projet d'Intérêt National Majeur | Imerys [Internet]. [cited 2024 Sep 26]. Available from: https://www.imerys.com/fr/media-room/communiques-de-presse/le-projet-de-mine-de-lithium-emili-reconnu-en-projet-dinteret

18. G.Monnier, B.Charoy, M.Cuney, D.Ohnenstetter, J.L.Robert. Evolution spatiale et temporelle de la composition des micas du granite albitique à topaze-lépidolite de Beauvoir. Géologie de la france. n°2-3. 1987;179–88.

19. Ph.Rossi, A.Autran. Log pétrographique et géochimique du granite de Beauvoir dans le sondage "Echassière I" Minéralogie ete géochimie comparées. Géologie de la France. n°2-3. 1987;111–35.

20. Pichavant M. Experimental Crystallization of the Beauvoir Granite as a Model for the Evolution of Variscan Rare Metal Magmas. Journal of Petrology. 2022 Dec 1;63(12):egac120.

21. Cuney M, Marignac C, Weisbrod A. The Beauvoir topaz-lepidolite albite granite (Massif Central, France); the disseminated magmatic Sn-Li-Ta-Nb-Be mineralization. Economic Geology. 1992 Nov 1;87(7):1766–94.

22. R.C. Wang, F. Fontan, P. Monchoux. Interrelations et évolution comparée de la cassitérite et des niobotantalates dans les différents faciès du granite de Beauvoir (Massif d'échassières). 1987.

23. Sabsabi M. LIBS Fundamentals. In: Chemometrics and Numerical Methods in LIBS [Internet]. John Wiley & Sons, Ltd; 2022 [cited 2024 Dec 25]. p. 5–18. Available from: https://onlinelibrary.wiley.com/doi/abs/10.1002/9781119759614.ch1

24. Costa VC, Augusto AS, Castro JP, Machado RC, Andrade DF, Babos D, et al. Laser Induced-Breakdown Spectroscopy (libs): History, Fundamentals. Applications and Potentialities. Quim Nova. 2019 May;42(5):527–45.

25. Senesi GS, Harmon RS, Hark RR. Chapter 23 - Field-portable and handheld LIBS. In: Singh JP, Thakur SN, editors. Laser-Induced Breakdown Spectroscopy (Second Edition) [Internet]. Amsterdam: Elsevier; 2020 [cited 2024 Sep 23]. p. 537–60. Available from: https://www.sciencedirect.com/science/article/pii/B978012818829300023X

26. Lemière B, Uvarova YA. New developments in field-portable geochemical techniques and on-site technologies and their place in mineral exploration. Geochemistry: Exploration, Environment, Analysis. 2019 Oct 31;20(2):205–16.

27. Asquini CP. 19 - Laser induced breakdown spectroscopy (LIBS). In: Denker B, Shklovsky E, editors. Handbook of Solid-State Lasers [Internet]. Woodhead Publishing; 2013 [cited 2025 Jan 4]. p. 551–71. (Woodhead Publishing Series in Electronic and Optical Materials). Available from: https://www.sciencedirect.com/science/article/pii/B9780857092724500191

28. Radziemski L, Cremers D. A brief history of laser-induced breakdown spectroscopy: From the concept of atoms to LIBS 2012. Spectrochimica Acta Part B: Atomic Spectroscopy. 2013 Sep 1;87:3–10.

29. Senesi GS, Harmon RS, Hark RR. Field-portable and handheld laser-induced breakdown spectroscopy: Historical review, current status and future prospects. Spectrochimica Acta Part B: Atomic Spectroscopy. 2021 Jan 1;175:106013.

30. Mezoued N, Fabre C, Cauzid J, Kim Y, Jatteau M. Analysis of Minerals Using Handheld Laser-Induced Breakdown Spectroscopy Technology. Data. 2025 Mar;10(3):40.

31. Menardi G, Torelli N. Training and assessing classification rules with imbalanced data. Data Min Knowl Disc. 2014 Jan 1;28(1):92–122.

32. Bergen KJ, Johnson PA, de Hoop MV, Beroza GC. Machine learning for data-driven discovery in solid Earth geoscience. Science. 2019 Mar 22;363(6433):eaau0323.

33. Dramsch JS. Chapter One - 70 years of machine learning in geoscience in review. In: Moseley B, Krischer L, editors. Advances in Geophysics [Internet]. Elsevier; 2020 [cited 2022 Aug 24]. p. 1–55. (Machine Learning in Geosciences; vol. 61). Available from: https://www.sciencedirect.com/science/article/pii/S0065268720300054

34. Lary DJ, Alavi AH, Gandomi AH, Walker AL. Machine learning in geosciences and remote sensing. Geoscience Frontiers. 2016 Jan 1;7(1):3–10.

35. Rodriguez-Galiano V, Sanchez-Castillo M, Chica-Olmo M, Chica-Rivas M. Machine learning predictive models for mineral prospectivity: An evaluation of neural networks, random forest, regression trees and support vector machines. Ore Geology Reviews. 2015 Dec 1;71:804–18.

36. Izenman AJ. Linear Discriminant Analysis. In: Izenman AJ, editor. Modern Multivariate Statistical Techniques: Regression, Classification, and Manifold Learning [Internet]. New York, NY: Springer; 2008 [cited 2025 Mar 23]. p. 237–80. Available from: https://doi.org/10.1007/978-0-387-78189-1_8

37. Kuhn M, Johnson K. Discriminant Analysis and Other Linear Classification Models. In: Kuhn M, Johnson K, editors. Applied Predictive Modeling [Internet]. New York, NY: Springer; 2013 [cited 2025 Mar 23]. p. 275–328. Available from: https://doi.org/10.1007/978-1-4614-6849-3_12

38. Awad M, Khanna R. Support Vector Machines for Classification. In: Awad M, Khanna R, editors. Efficient Learning Machines: Theories, Concepts, and Applications for Engineers and System Designers [Internet]. Berkeley, CA: Apress; 2015 [cited 2025 Mar 23]. p. 39–66. Available from: https://doi.org/10.1007/978-1-4302-5990-9_3

39. Brereton RG, Lloyd GR. Support Vector Machines for classification and regression. Analyst. 2010 Jan 25;135(2):230–67.

40. Cervantes J, Garcia-Lamont F, Rodríguez-Mazahua L, Lopez A. A comprehensive survey on support vector machine classification: Applications, challenges and trends. Neurocomputing. 2020 Sep 30;408:189–215.

41. Ballabio D, Consonni V. Classification tools in chemistry. Part 1: linear models. PLS-DA. Anal Methods. 2013 Jul 26;5(16):3790–8.

42. Liu Y, Rayens W. PLS and dimension reduction for classification. Computational Statistics. 2007 Jul 1;22(2):189–208.

43. Stocchero M, De Nardi M, Scarpa B. PLS for classification. Chemometrics and Intelligent Laboratory Systems. 2021 Sep 15;216:104374.

44. Ghaddar B, Naoum-Sawaya J. High dimensional data classification and feature selection using support vector machines. European Journal of Operational Research. 2018 Mar 16;265(3):993–1004.

45. Lee LC, Liong CY, Jemain AA. Partial least squares-discriminant analysis (PLS-DA) for classification of high-dimensional (HD) data: a review of contemporary practice strategies and knowledge gaps. Analyst. 2018 Jul 23;143(15):3526–39.

46. JMP® , Version . SAS Institute Inc., Cary, Caroline du Nord, 1989–2023. 1989.

47. Johnstone IM, Titterington DM. Statistical challenges of high-dimensional data. Philosophical Transactions of the Royal Society A: Mathematical, Physical and Engineering Sciences. 2009 Nov 13;367(1906):4237–53.

48. Steinbach M, Ertöz L, Kumar V. The Challenges of Clustering High Dimensional Data. In: Wille LT, editor. New Directions in Statistical Physics: Econophysics, Bioinformatics, and Pattern Recognition [Internet]. Berlin, Heidelberg: Springer; 2004 [cited 2025 Mar 23]. p. 273–309. Available from: https://doi.org/10.1007/978-3-662-08968-2_16

49. Howley T, Madden MG, O'Connell ML, Ryder AG. The Effect of Principal Component Analysis on Machine Learning Accuracy with High Dimensional Spectral Data. In: Macintosh A, Ellis R, Allen T, editors. Applications and Innovations in Intelligent Systems XIII. London: Springer; 2006. p. 209–22.

50. Ray P, Reddy SS, Banerjee T. Various dimension reduction techniques for high dimensional data analysis: a review. Artif Intell Rev. 2021 Jun 1;54(5):3473–515.

51. F. Menges. Spectragryph - optical spectroscopy software [Internet]. [cited 2024 Jan 11]. Available from: http://spectragryph.com/

52. Monnier L, Lach P, Salvi S, Melleton J, Bailly L, Béziat D, et al. Quartz trace-element composition by LA-ICP-MS as proxy for granite differentiation, hydrothermal episodes, and related mineralization: The Beauvoir Granite (Echassières district), France. Lithos. 2018 Nov;320–321:355–77.

53. Götze J, Pan Y, Müller A. Mineralogy and mineral chemistry of quartz: A review. MinMag. 2021 Oct;85(5):639–64.

54. Michaud J. Les granites à métaux rares: origine, mise en place et mécanismes de la transition magmatique-hydrothermale. 2019;366.

55. Cathelineau M, Kahou ZS. Discrimination of Muscovitisation Processes Using a Modified Quartz–Feldspar Diagram: Application to Beauvoir Greisens. Minerals. 2024 Aug;14(8):746.

56. CATHELINEAU M. The Hydrothermal Alkali Metasomatism Effects on Granitic Rocks: Quartz Dissolution and Related Subsolidus Changes. Journal of Petrology. 1986 Aug 1;27(4):945–65.

57. Lednev VN, Sdvizhenskii PA, Dorohov AS, Gudkov SV, Pershin SM. Improving LIBS analysis of non-flat heterogeneous samples by signals mapping. Appl Opt, AO. 2023 Mar 10;62(8):2030–8.

58. Mao SS, Zeng X, Mao X, Russo RE. Laser-induced breakdown spectroscopy: flat surface vs. cavity structures. J Anal At Spectrom. 2004 Apr 8;19(4):495–8.

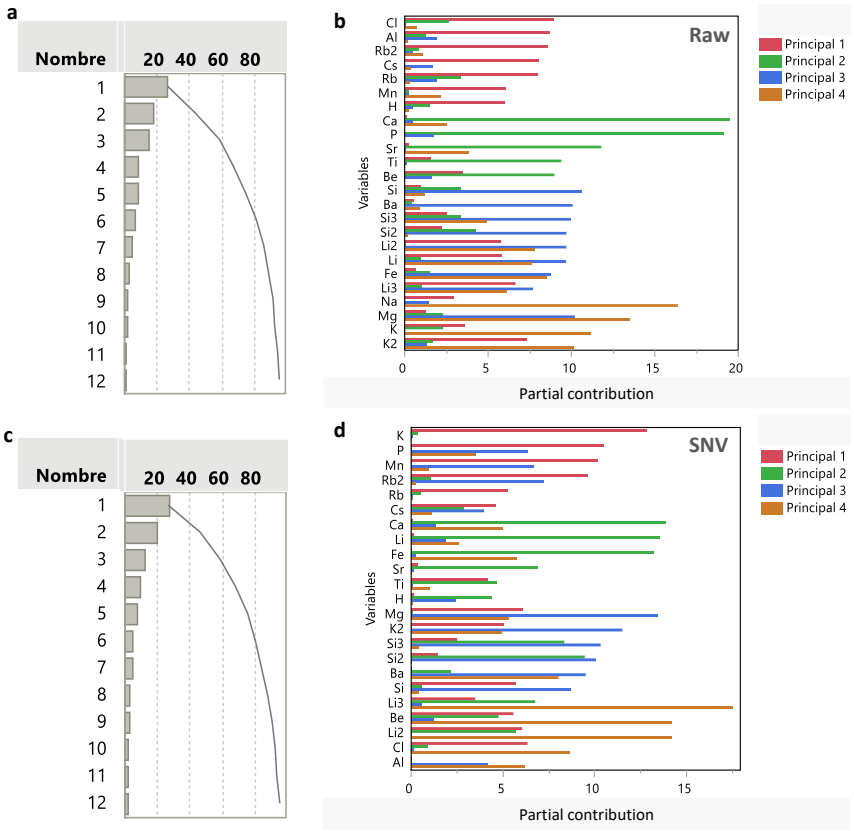

Figure S1: Cumulative Variance Explained and Variable Contributions in Principal Component Analysis (PCA) for Raw and SNV-Normalized Data : (a)Cumulative variance explained for principal components using raw data; (b)Contribution of each initial variable to the principal components for raw data; (c)Cumulative variance explained for principal components using SNV-normalized data; (d) Contribution of each initial variable to the principal components for SNV-normalized data.

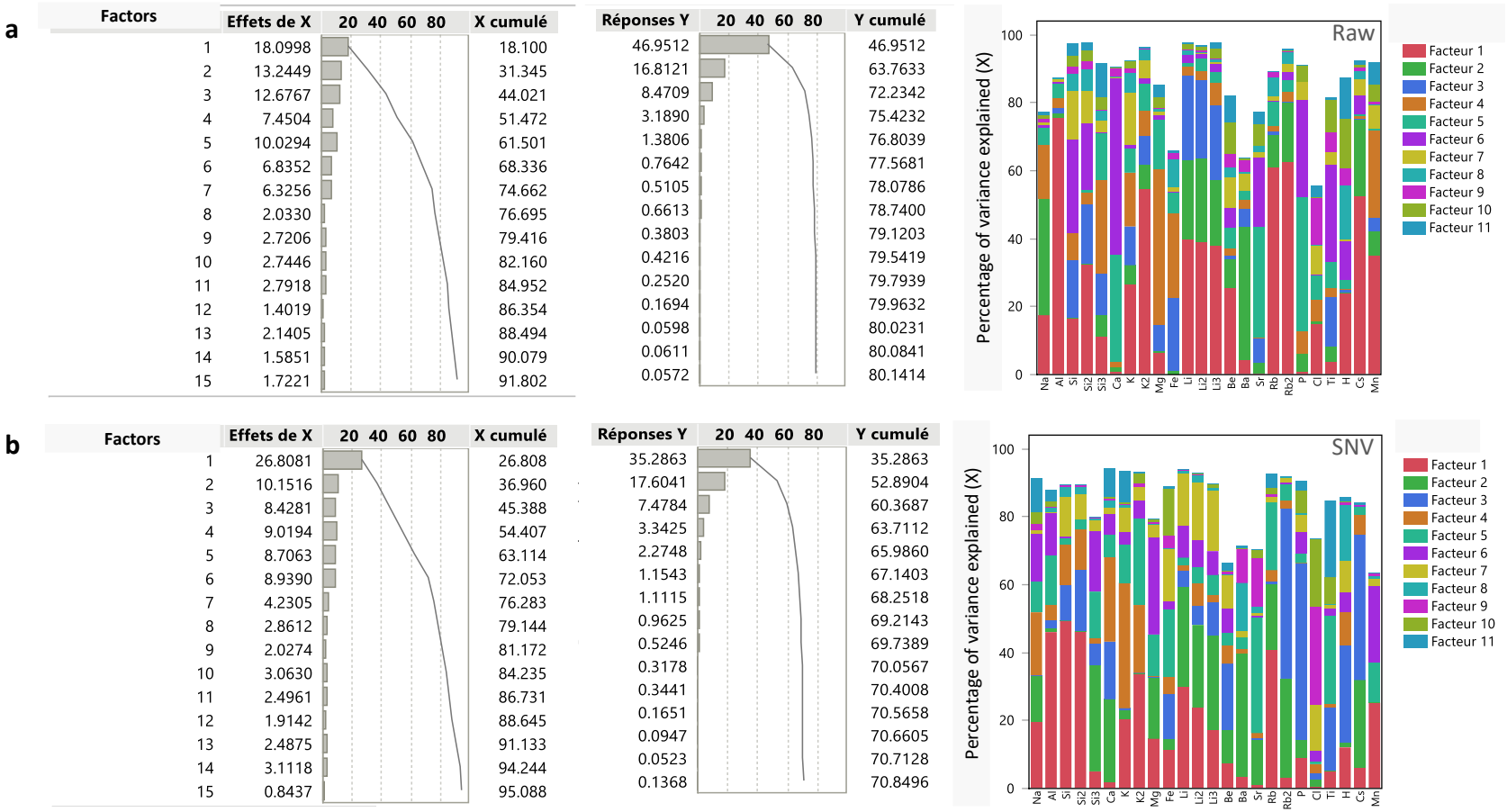

Figure S2: The cumulative variance explained in x (predictor variables) and y (response variables) captured by the pls components, and the contributions by factor for a) raw data, and b) normalized SNV data.

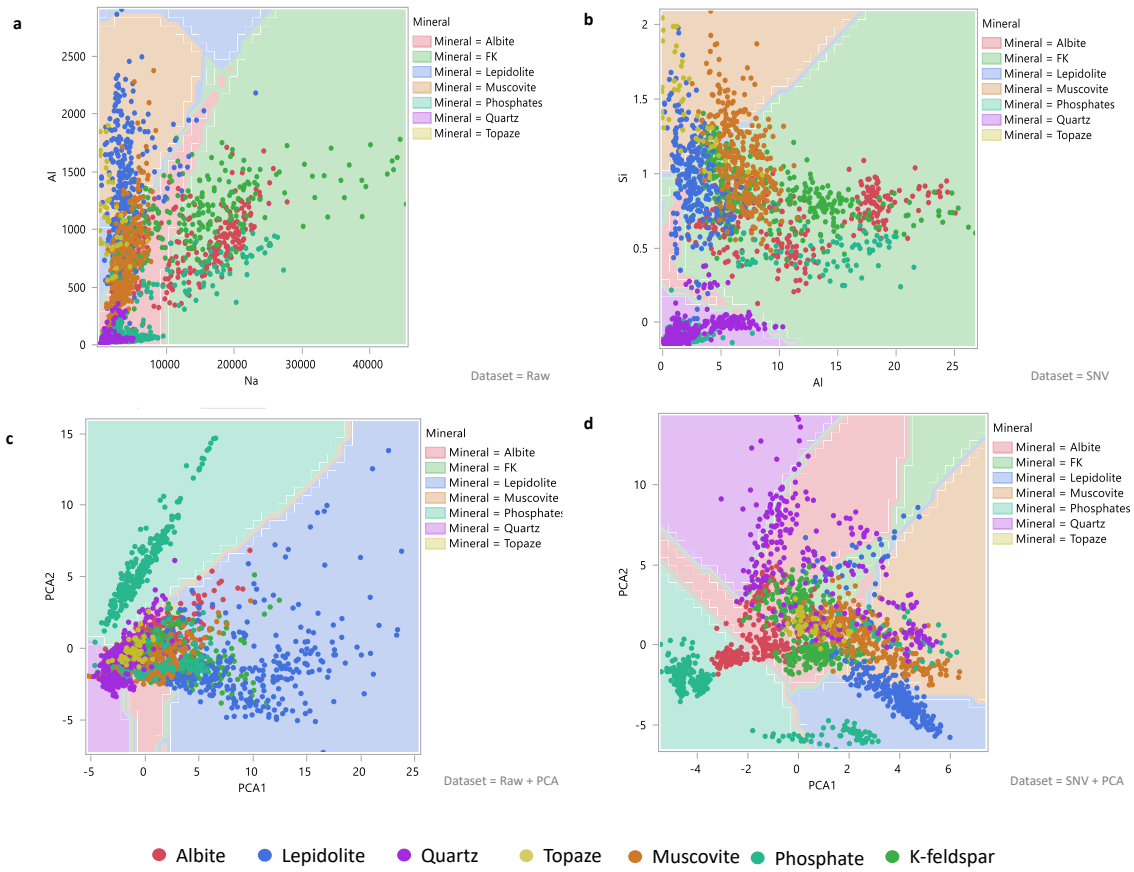

Figure S3 : Results of SVM Classification for : a) Raw data, b) SNV normalized data, c) Principal component on Raw data, and d) Principal component on SNV normalized data. The data points are Color-Coded by Mineral Classes.

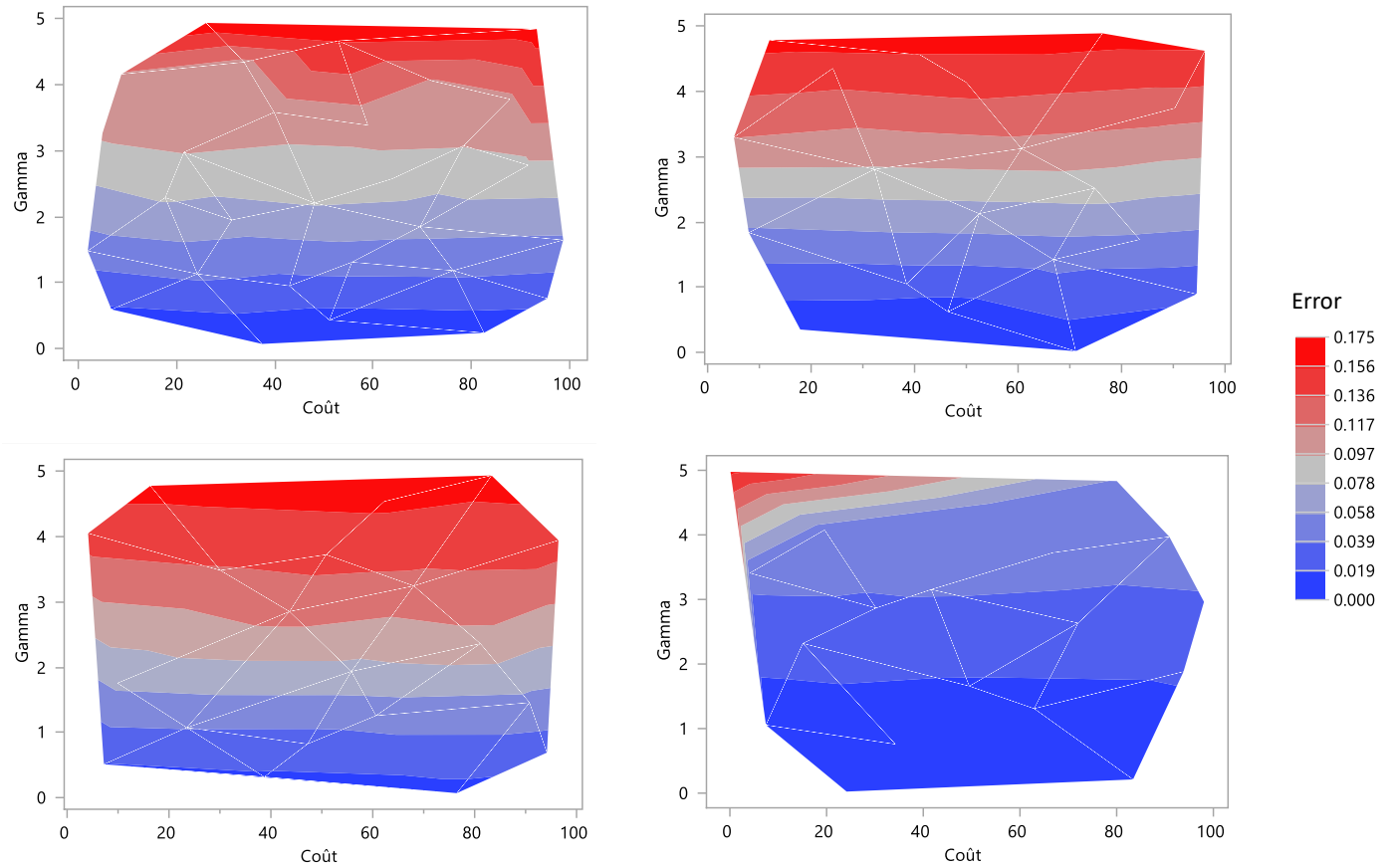

Figure S4 : optimization of SVM model parameters (gamma and c) for: a) Raw data, b) SNV normalized data, c) Principal components from raw data, and d) Principal components from SNV normalized data.

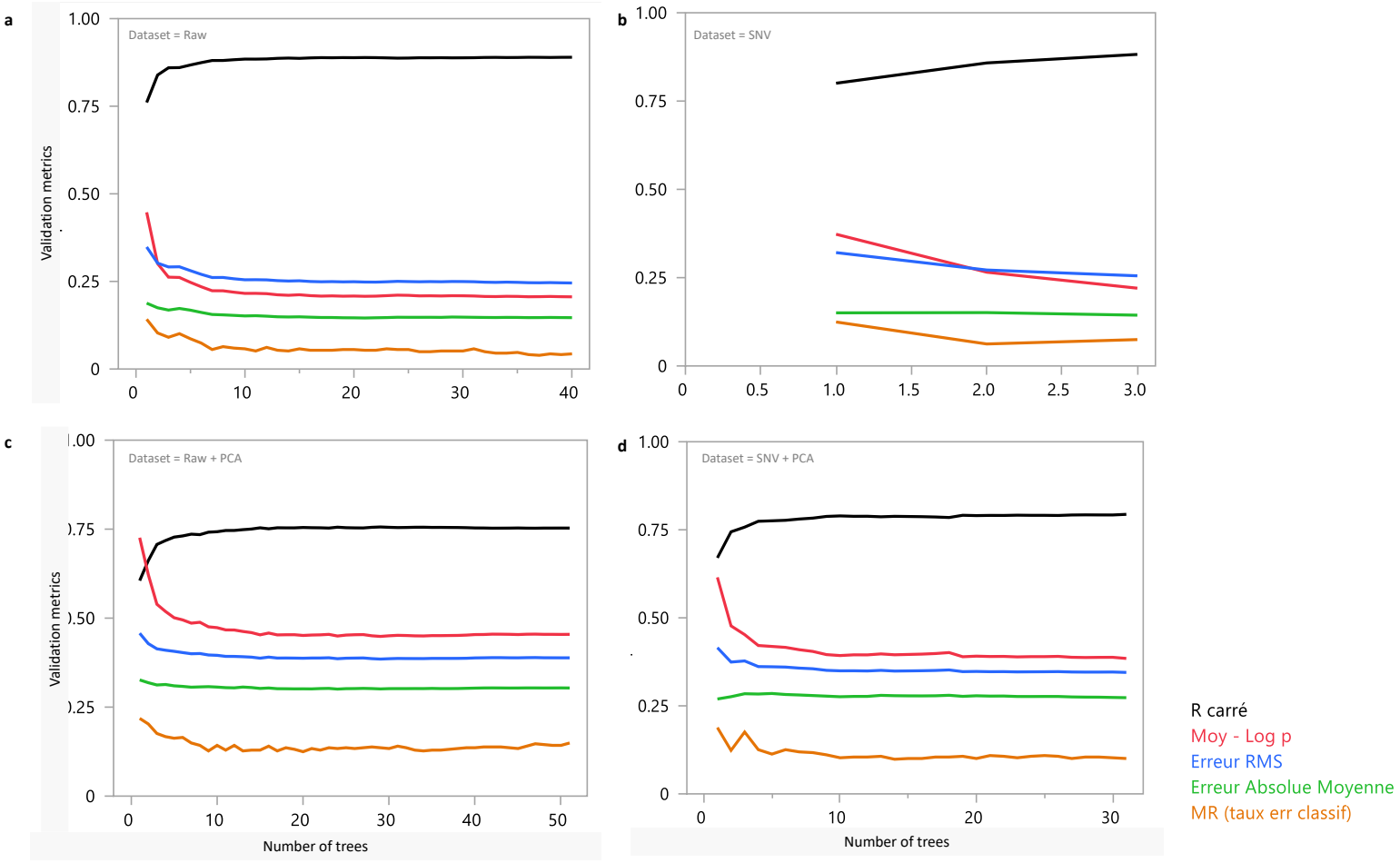

Figure S5 : Evaluation of Random Forest Models Using Validation Metrics: R^2, Log P, MAE, and Misclassification Rate a) Raw data, b) SNV normalized data, c) Principal component on Raw data, and d) Principal component on SNV normalized data.

Chapitre VII.

Automated mineral identification using machine learning methods part II

Artificial neural network for handheld LIBS data processing: application to automated mineral identification in granite samples

Naila Mezoued[*,1]*, Cécile Fabre*[1]*, Jean Cauzid*[1]

[1]CNRS, GeoRessources Laboratory, Université de Lorraine, Nancy F54000, France

Corresponding author[*]. E-mail: naila.mezoued@univ-lorraine.fr

Abstract

Handheld LIBS technology, especially analyzers developed for geoscience applications, enables the rapid, on-site acquisition of high-resolution (> 24,000 variables) and multi-element (H–U) geochemical data, opening new perspectives for mineral and rock characterization beyond standard qualitative and quantitative analysis. This study explores using artificial neural networks (ANN) for automated mineral identification in granite samples sourced from the Beauvoir deposit. The ANN was trained using LIBS spectral data acquired from pure mineral samples representative of the Beauvoir granite composition, to classify unlabelled LIBS data points into specific mineral classes based on major and trace elements spectral features. The classification results were used to (i) identify the mineralogical composition of the granite samples and (ii) estimate the relative abundance of each mineral class, with particular attention to lepidolite, the primary lithium-bearing phase. Data processing workflow and model parameters were enhanced to improve the generalization potential of the model to rock samples. Results showed variable accuracy depending on the mineral type and sample properties, highlighting the influence of texture and chemical variations on model predictions when applied to rock samples. Additionally, the LIBS acquisition process was adapted to maintain results consistency while reducing acquisition time to align with field operations requirements. Overall, the results confirm the input of handheld LIBS combined with supervised machine learning as a fast and practical solution to facilitate mineral identification during field operations supporting resource management and sampling strategy efficiency.

Keywords: Handheld LIBS, Artificial Neural Network, Beauvoir granite, ore exploration.

Introduction

In recent years, the use of handheld LIBS technology in geoscience applications has increased and diversified significantly (1–3). Its ability to perform rapid, multi-elemental analysis on a wide range of sample types, from outcrops (4,5) to powder pellets(6,7), is well-suited to address key challenges in geological material analysis, including complex and heterogeneous chemical compositions and varying spatial resolution requirements.

Handheld LIBS has proven effective in analyzing element distribution in volcanic deposits (8), weathered terrestrial analogs of meteorites (9), and rock varnish (10), as well as mapping element distribution in rocks and minerals (11,12). Additionally, spectral intensities can be calibrated to quantify elemental content in rocks and minerals (13,14). While qualitative and quantitative applications have established its potential in geosciences, the ability of LIBS data to support advanced geological sample characterization further enhances its value (15). When combined with spectral preprocessing or machine learning algorithms, handheld LIBS data has been successfully employed to identify lithological facies (16), classify gemstones (17), determine host lithologies of tourmaline and obsidian (18,19), and distinguish volcanic rock types and magmatic series (20). It also facilitates geochemical fingerprinting of ore phases, including coltan, gold, copper minerals, and Li-rich phases (21–26).

This study explores the application of handheld LIBS as a rapid and practical solution for automated mineral recognition on rock samples during field operations. Typically, mineral identification during field campaigns relies on visual cues based on macroscopic features (i.e., color, shape, etc) however, this can become challenging in outcrops or specific lithological facies where minerals exhibit similar characteristics. In the Beauvoir granite, a rare-metal deposit currently under investigation for lithium extraction (27), the targeted zone for mining consists of a leucogranite (28), matrix minerals, and the lithium-bearing phase lepidolite, are visually indistinct, increasing the uncertainty of ore evaluation during core logging, potentially leading to higher error rates in assessing lithium-bearing intervals. To support mineralogical characterization of granite samples collected during the exploration campaign, an artificial neural network (ANN) was trained to classify LIBS spectral data into predefined mineral classes. The main objectives were (1) to determine the mineralogical composition of the samples and (2) to estimate the relative proportion of lithium-bearing micas. This approach aims to improve ore-phase estimation in rock samples during mining operations using analytical data to reduce the uncertainty and potential misidentification associated with traditional visual inspection methods.

1 Methodology

1.1 Artificial Neural Network (ANN)

Neural networks are mathematical models consisting of multiple layers of interconnected nodes or functions, each processing data and passing it to the next layers. The typical architecture includes an input layer, one or more hidden layers depending on a model complexity, and an output layer. The input layer introduces vector data to the system, reference data during the training phase, and unlabeled data during practical applications. The output layer generates the predicted classes in classification (29). During the training phase, reference data with known outputs are used to recognize patterns and adjust model parameters. The mathematical functions associated with each neuron are iteratively adjusted to minimize the error between the predicted and actual results, refining parameters such as the activation function, bias, and weight, improving its ability to make accurate predictions for unlabeled data (30).

In this study, an artificial neural network (ANN) was implemented with LIBS spectral data as input and predefined mineral classes as output (Figure). The model was trained using reference spectra from pure mineral samples representative of the target geological system. Once trained, the ANN was capable of classifying new, unlabeled LIBS spectra into specific mineral classes, effectively translating elemental data into mineralogical information to support enhanced characterization of geological samples. Different ANN architectures were tested by varying the number of hidden layers, neurons per layer, and input datasets to assess their effect on classification performance. The models were trained using LIBS spectra from mineral reference samples with known class labels. The best-performing model was selected based on its prediction accuracy on a validation dataset. This model was then applied to LIBS data from Beauvoir granite samples to identify the mineral composition and estimate the proportion of lepidolite. Finally, data acquisition settings were optimized to ensure results consistency while minimizing acquisition time.

1.2 Handheld LIBS

A handheld LIBS analyzer was used to collect spectral data from both mineral and rock samples. The technique involves focusing a pulsed laser onto the sample surface, inducing localized melting and vaporization (31,32). This process generates a microplasma, which emits light as excited atoms relax to lower energy states. The plasma emission is collected by detectors and spectrometers, generating spectra that display signal intensity (a.u.) as a function of wavelength (nm). Elemental identification is based on the characteristic positions of emission lines, while the corresponding signal intensities reflect various influencing factors, including elemental concentration, acquisition parameters, and ionization potential(33). The

resulting data can then be processed for qualitative analysis, quantitative evaluation, or advanced applications. The SciAps Z300 handheld LIBS analyzer used in this study is equipped with a solid-state Nd:YAG laser operating at 1064 nm, delivering 5–6 mJ per pulse with nanosecond durations and a repetition rate of 1–50 Hz. It features a broad spectral range (190–950 nm), enabling the detection of a wide range of elements, including light elements common in granite compositions. The device enables rapid data acquisition, with spectra available in under 30 seconds, and provides fine spatial resolution (>50 µm), making it well-suited for the geochemical characterization of complex geological samples such as the Beauvoir granite case.

1.3 Beauvoir granite data

The rock samples from the Beauvoir deposit consist of four rectangular granite slabs (12 x 5 x 0.5 cm), sourced from the B1 facies (28), the uppermost unit of the multi-stage pluton comprising B1, B2, and B3 (34). The mineral composition of Beauvoir granite (B1) is primarily composed of albite, quartz, and lepidolite, the latter of which is the primary focus of this study due to its role as the main lithium-bearing mineral (35). Accessory minerals such as muscovite, topaz, apatite, fluorite, amblygonite, and cassiterite were also identified, as well as crystals of zircon, microlite, montebrasite, and niobium-tantalite (28,36). The textural characteristics of the three selected samples are consistent, exhibiting an equigranular and unaligned texture, with matrix mineral grain sizes ranging from 200 to 600 µm, while accessory phases are generally smaller (< 100 µm). No preprocessing was performed, other than ensuring a flat surface to facilitate a consistent signal acquisition, to align with the technological constraints encountered during field operations.

A total of 900 spectra were acquired per granite sample. Granite slabs were analyzed at 10 locations, organized in a vertical profile from the top to the bottom of each sample. At each location, 90 measurement points, spaced 30 µm apart in a square grid, were analyzed to cover the full device window. For each point, two laser pulses were fired: the first to clean the surface, and the second for spectral analysis, minimizing crater size and ensuring that only one mineral was analyzed per spectrum. Each grid analysis required approximately 1 minute, including data acquisition and spectra loading in ProfileBuilder software. An additional minute was needed to transfer the 900 spectra in CSV format, resulting in a total analysis time of 20 minutes per granite sample. Consistent analysis settings, including a laser frequency of 10 Hz, focal length, and integration gate, were applied across both mineral training data and Beauvoir granite rock samples.

1.4 Training Data

The reference data used to train the ANN were obtained from LIBS spectra acquired on pure mineral samples. The mineral spectra were sourced from the open-access "Spectral Analysis of Minerals with Handheld LIBS Technology" database on the ORDaR platform, as described by Mezoued et al. 2025 (37). The samples were collected from macroscopic mineral specimens from the collections of the Georesources Laboratory (Nancy, France), ENSG (Nancy, France), and the University of Thessaloniki (Greece) (37). The training dataset was designed as a simplified representation of the mineralogical composition of the Beauvoir granite, focusing on major mineral phases present in proportions greater than 1%. It includes LIBS spectra of albite, quartz, and lepidolite, as well as secondary phases such as muscovite, topaz, orthoclase, and phosphates. Due to varying lithium concentrations observed in micas, the lepidolite spectra refer to samples with lithium concentrations greater than 5000 ppm, while muscovite spectra imply samples with lithium concentrations below 1000 ppm. The phosphate group includes spectra from apatite and lithium-rich amblygonite. To ensure balanced class distribution and limit bias towards a specific class during the model training stage, the dataset was carefully curated to prevent overrepresentation of specific classes, which could affect model performance. Each mineral phase was represented by 300 spectra, except for muscovite (272 spectra) and topaz (44 spectra), due to limited data availability.

1.5 Preprocessing

Each spectrum acquired with the SciAps Z300 handheld LIBS analyzer with a spectral resolution of 0.03 nm contains over 24,000 variables. Although this high-dimensional dataset illustrates the detailed geochemical composition of each phase, it introduces computational challenges for machine learning, including increased memory requirements, longer training times, and the potential for decreased model accuracy due to the presence of irrelevant, redundant, or noisy variables (38,39). To address these limitations, the dimensionality reduction of LIBS spectral data was performed using a mineral chemistry–guided approach, rather than relying solely on statistical criteria. Elemental emission lines were selected based on their relevance to the chemical composition of the target mineral phases, including major (Si, Al, Li, K, Na), minor (Ca, Rb, Cs, P, and Cl), and trace (Ti, Mg, Fe, Sr, Ba, and Be) elements. Line selection was guided by the NIST LIBS database, prioritizing primary emission lines while avoiding spectral interference. Peak integration was conducted using Spectragryph software on both raw and SNV-normalized spectra.

In both PCA and PLS analyses, the number of components selected was determined based on the cumulative variance explained (> 80%). For PCA, the first ten principal components were selected for subsequent classification tasks. These components captured approximately

87% of the total variance in both raw and SNV-normalized datasets. Additional components beyond this threshold contributed negligibly to the cumulative variance. For PLS regression, eleven latent variables were retained for both spectral datasets. In the raw dataset, these components accounted for 85% of the variance in the predictor variables (X = Spectral signal) and 80% of the variance in the response variable (Y = Mineral class). In the SNV-normalized dataset, the corresponding variance explained was 83% for X and 70% for Y. Beyond this point, further inclusion of components resulted in marginal gains in predictor variance and no notable improvement in response variance.

Therefore, to identify the most effective input data for automated mineral classification using artificial neural networks (ANN), six training datasets were derived from LIBS spectra of both pure minerals and rock samples: 1) Emission lines extracted from raw spectra (24 variables), 2) Emission lines from SNV-normalized spectra (24 variables), 3) PCA applied to raw spectra (10 variables, 4) PCA applied to SNV-normalized spectra (10 variables), 5) PLS components derived from raw data (11 variables), and 6) PLS components derived from SNV-normalized data (11 variables).

2 Results and discussion

2.1 ANN models

The twelve artificial neural network (ANN) models developed for mineral classification using handheld LIBS spectra (**Fig.1**) demonstrated consistently high performance on the test set, with mean squared error (RMSE) values ranging from 0.08 to 0.9, limiting the ability to distinguish optimal performance based solely on these metrics. To evaluate generalization capability under more application-relevant conditions, the models were applied to an independent LIBS dataset acquired from the unaltered granite slab (C52) of the Beauvoir granite. This allowed for assessment of model robustness and predictive accuracy on real geological material, facilitating identification of the most appropriate ANN architecture for field-based mineral classification. From the ANN classification results relative mineral phase proportions were estimated from the classification results by calculating the ratio of datapoints assigned to each mineral class to the total number of analysis points per sample. Prediction errors were subsequently quantified by comparing these proportions to reference values obtained through laboratory-based (µXRF) mapping, supported by petrographic analysis.

The ANN models were built using varying configurations to investigate the influence of model architecture on classification accuracy (**Fig.1**), including learning rate, activation function (i.e., hyperbolic tangent (TanH) or linear (Lin)), the number of hidden layers (either one or two), and number of neurons per layer (from 30, 60, to 100). This design allowed systematic evaluation of the effects of non-linearity and network depth on model performance. The results presented

in **Fig.2** indicate that no clear trend emerges regarding the distribution of prediction errors. Neither the choice of activation function (TanH or Lin) nor the number of hidden layers (one or two) distinguished themselves in terms of overall performance. The comparative analysis of prediction errors indicates that Model 1 demonstrates the best overall performance for both lepidolite (AEP = 3.08%) and multi-class classfication (AEP = 7.72%). However, Models 2, 4, 8, and 9 exhibit improved accuracy in lepidolite classification, achieving an AEP of 0.42%. Despite this, these models display higher prediction errors for multi-class classification, with respective errors of 18.63%, 20.48%, 17.12% and 19.41%.

ANN	Activation Function	Number of Layers	Number of Neurons
Model 1: 0.1_Tan_Layer1_30	TanH	1	30
Model 2: 0.1_Tan_Layer1_60	TanH	1	60
Model 3: 0.1_Tan_Layer1_100	TanH	1	100
Model 4: 0.1_Lin_Layer1_30	Lin	1	30
Model 5: 0.1_Lin_Layer1_60	Lin	1	60
Model 6: 0.1_Tan_Layer1_100	TanH	1	100
Model 7: 0.1_Tan_Layer2_30;15	TanH	2	30, 15
Model 8: 0.1_Tan_Layer2_60;30	TanH	2	60, 30
Model 9: 0.1_Tan_Layer2_100;50	TanH	2	100, 50
Model 10: 0.1_Lin_Layer2_30;15	Lin	2	30, 15
Model 11: 0.1_Lin_Layer2_60;30	Lin	2	60, 30
Model 12: 0.1_Lin_Layer2_100;50	Lin	2	100, 50

Figure.1. Summary of the 12 ANN models developed for handheld libs data classification.

The influence of learning rate and input data preprocessing on model performance was evaluated in model 1 confirguration. As shown in **Fig.3**, variations in learning rate (00.1, 0.01, and 0.1) had no significant effect on classification accuracy. In contrast, the choice of preprocessing method impacted predictive performance. Models trained on raw spectral data and raw spectra processed with PCA (RAW PCA) demonstrated superior results for both lepidolite and multi-class classification tasks. PCA combined on SNV-normalized data also

yielded satisfactory performance for lepidolite, whereas SNV-normalized data consistently underperforms compared to raw datasets. Based on these results, the raw spectral dataset consisting of 24 selected variables, major and trace elements emission lines, was retained as the optimal input format, providing low absolute prediction errors for both lepidolite (3.08%) and multi-class estimation (7.72%). Model 1 was applied to the remaining Beauvoir granite dataset to evaluate its performance in both lepidolite and multi-class classification tasks (**Fig.4**). In parallel, Model 2 was specifically implemented for lepidolite proportion estimation to assess its potential for improved accuracy in ore-phase targeting (**Fig.5a**). The findings suggest that distinct models may be required depending on the intended use case whether maximizing overall classification performance or enhancing the precision of ore-phase identification in mineral exploration contexts.

2.2 Beauvoir granite application

The prediction errors for the Beauvoir granite samples (C42, C52, C112, and C117) are summarized in **Fig.4**. The results demonstrate that classification accuracy is mineral-dependent, with no consistent error pattern across all phases. Quartz consistently exhibits the highest prediction errors, exceeding 50% for the sample C117. In contrast, phases such as lepidolite, albite, muscovite, potassium feldspar, and topaz generally present lower prediction errors, typically remaining below 15%, except for sample C117. The comparative analysis of lepidolite classification performance (**Fig.4a**) shows that sample C52 exhibits the lowest absolute error, followed by C42, whereas sample C112 records the highest error at 13.12%. Across all samples, the MAE for lepidolite prediction using Model 1 is 9.14%. When considering all mineral classes (**Fig.4b**), altered samples (C117) tend to yield higher prediction errors, yet, confirming this conclusion requires further analysis on a larger and more representative dataset. Overall, the MAE for multi-class classification ranges from 6.83% to 18.96%, with an average of 11.20%.

Concerning ANN Model 2, the results for lepidolite classification shown in **Fig. 5a** demonstrate an improvement in predictions, with an average decrease of 50% for C42, C52, and C117 compared to the results from Model 1, while C112 exhibits a similar error scale. Therefore, for lepidolite-specific targeting, Model 2 would be a better option for automated classification, with an average prediction error of 6.28%, representing a 30% reduction in absolute prediction error. To assess the relevance of our results in terms of primary evaluation for the mineralogical composition of rocks during mining exploration operations, we compared the errors obtained for lepidolite estimation (the ore phase) for both Model 1 and Model 2 to the logging errors obtained through visual identification.

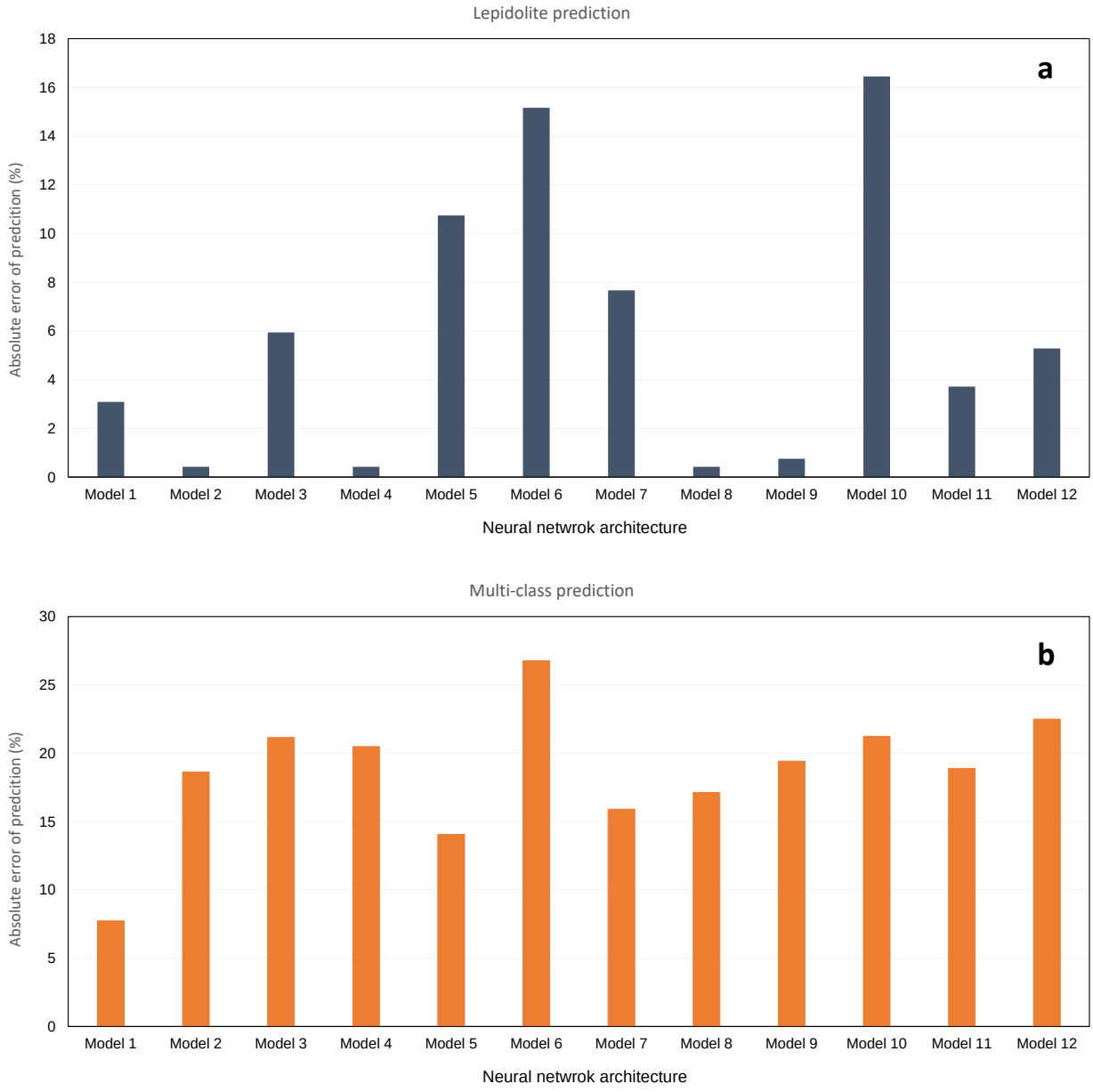

Figure.2. Distribution of the absolute prediction errors obtained from the classification results of lepidolite (a) and multi-class proportion predictions (b) using ann models. The models parameters and configurations are detailed in Figure 1.

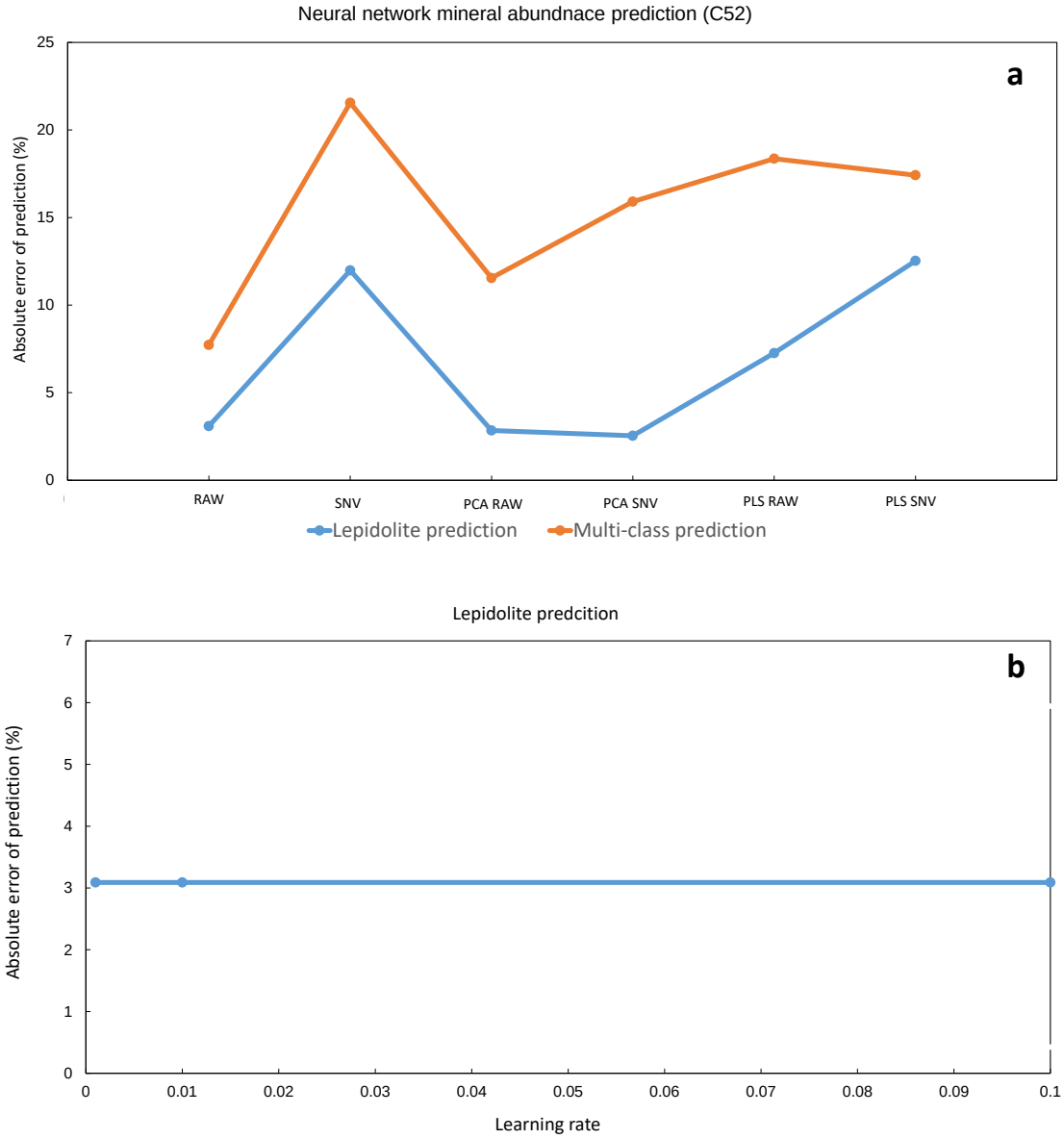

Figure.3. a) Distribution of the absolute prediction error across different input datasets tested. b) Distribution of the absolute prediction error for different learning rates (0.001, 0.01, and 0.1).

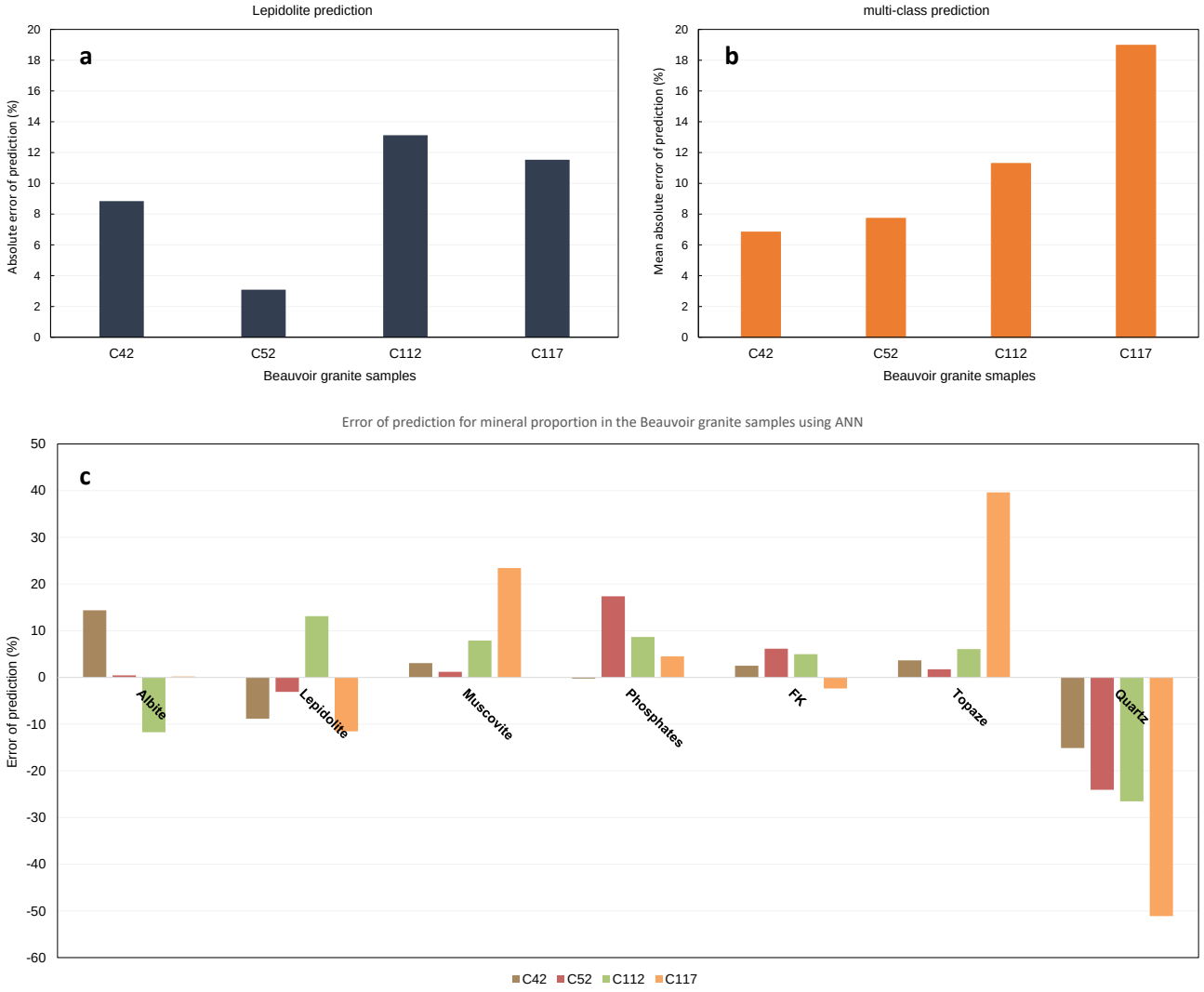

Figure.4. Results of ANN Model 1 for the Beauvoir samples. a) AEP for lepidolite classification. (b) AEP for multi-class classification. c) Error distribution for each mineral class, categorized by sample, demonstrating the variation in prediction accuracy for different mineral classes.

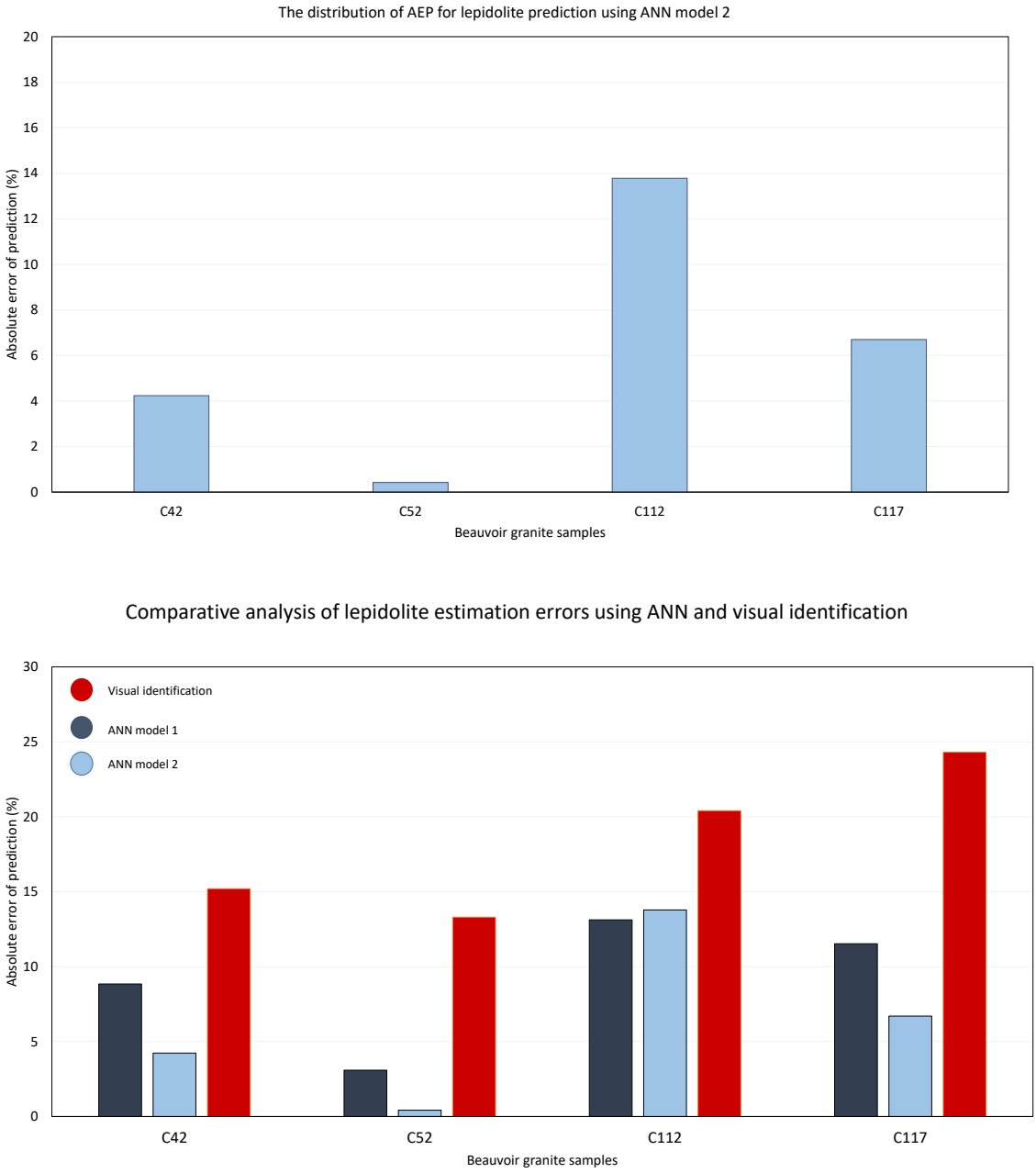

Figure.5. a) Prediction error for lepidolite classification using ANN Model 2. b) Comparative analysis of the absolute error of prediction (AEP) between visual identification and the LIBS-ANN-based approach for automated mineral recognition.

Conclusion

This study investigates the potential of handheld LIBS for automated mineral identification in rock samples using an artificial neural network (ANN). The results demonstrate that LIBS spectra effectively capture the chemical complexity of different mineral phases, even when using a subset of the spectral signal selected representing the major and trace elements emission lines. Evaluation of multiple ANN architectures for mineral data classification demonstrated that even models composed of a single hidden layer (three layers in total) achieved robust classification performance. This indicates that relatively simple ANN designs are sufficient to extract meaningful patterns from LIBS spectral data and accurately classify mineral phases. When applied to samples from the Beauvoir granite, ANN performance varied depending on the mineral class and the considered sample. Quartz was consistently underestimated and showed the highest prediction errors. The overall absolute prediction error remained below 20% for all mineral phases except quartz, with a mean absolute error (MAE) of 11%. Textural characteristics appear to influence classification accuracy, as unaltered samples (C52) generally yielded more accurate predictions than altered ones (C117). However, since this trend is not consistent across all models, further investigation is needed using a larger and more representative sample set. For lepidolite, the best-performing model achieved prediction errors ranging from 3% to 13%, with a mean absolute error of below 10%, outperforming traditional visual estimation methods, which typically yield errors between 10% and 24%. These findings confirm that handheld LIBS combined with ANN offers a rapid and reliable approach for enhancing mineralogical characterization during field operations.

Acknowledgments

We gratefully acknowledge all those who contributed to acquiring reference data essential for training the neural network model. We sincerely thank Ahmed Aboutaj for his valuable input and insightful discussions regarding the implementation of this approach for the processing of LIBS spectra. We also thank Michel Cathelineau and Steven Zia Kahou for providing the Beauvoir granite samples, along with the associated geochemical and mineralogical data. We extend our appreciation to the Imerys team for their collaboration and support, particularly in facilitating access to the Beauvoir granite mining site and providing critical information about the deposit. Finally, we thank the reviewers for their time and constructive feedback, which contributed to the improvement and enrichment of this work.

Funding

This research was possible through the funding of the French National Research Agency via the Labex Ressources 21 project [reference ANR–10–LABX–21-01] and a collaboration with Imerys, the operating company of the Beauvoir Granite.

AI disclosure

We acknowledge the use of AI platforms (ChatGPT and DeepL) for the translation from French to English and for assisting with grammatical consistency throughout the manuscript. All content was subsequently reviewed and edited as necessary. The author assumes full responsibility for the final version of the publication.

References

1. Harmon RS. Laser-Induced Breakdown Spectroscopy in Mineral Exploration and Ore Processing. Minerals. 2024 Jul 1;14:731.

2. Fabre C. Advances in Laser-Induced Breakdown Spectroscopy analysis for geology: A critical review. Spectroc Acta Pt B-Atom Spectr. 2020 Apr;166:105799.

3. Senesi GS. Laser-Induced Breakdown Spectroscopy (LIBS) applied to terrestrial and extraterrestrial analogue geomaterials with emphasis to minerals and rocks. Earth-Science Reviews. 2014 Dec 1;139:231–67.

4. Dias F, Ribeiro R, Gonçalves F, Lima A, Roda-Robles E, Martins T. Calibrating a Handheld LIBS for Li Exploration in the Barroso–Alvão Aplite-Pegmatite Field, Northern Portugal: Textural Precautions and Procedures When Analyzing Spodumene and Petalite. Minerals. 2023 Apr;13(4):470.

5. Wise MA, Harmon RS, Curry A, Jennings M, Grimac Z, Khashchevskaya D. Handheld LIBS for Li Exploration: An Example from the Carolina Tin-Spodumene Belt, USA. Minerals. 2022 Jan;12(1):77.

6. Foucaud Y, Fabre C, Demeusy B, Filippova IV, Filippov LO. Optimisation of fast quantification of fluorine content using handheld laser induced breakdown spectroscopy. Spectrochimica Acta Part B: Atomic Spectroscopy. 2019 Aug 1;158:105628.

7. Korbel C, Mezoued N, Demeusy B, Fabre C, Cauzid J, Filippova IV, et al. Quantification of lithium using handheld instruments: application of LIBS and XRF spectroscopy to assay the lithium content of mineral processing products. J Anal At Spectrom. 2024 Jul 3;39(7):1838–53.

8. Roux CPM, Rakovský J, Musset O, Monna F, Buoncristiani JF, Pellenard P, et al. In situ Laser Induced Breakdown Spectroscopy as a tool to discriminate volcanic rocks and magmatic series, Iceland. Spectrochimica Acta Part B: Atomic Spectroscopy. 2015 Jan 1;103–104:63–9.

9. Gómez-Nubla L, Aramendia J, Fdez-Ortiz de Vallejuelo S, Madariaga JM. Analytical methodology to elemental quantification of weathered terrestrial analogues to meteorites using a portable Laser-Induced Breakdown Spectroscopy (LIBS) instrument and Partial Least Squares (PLS) as multivariate calibration technique. Microchemical Journal. 2018 Mar 1;137:392–401.

10. Harmon RS, Khashchevskaya D, Morency M, Owen LA, Jennings M, Knott JR, et al. Analysis of Rock Varnish from the Mojave Desert by Handheld Laser-Induced Breakdown Spectroscopy. Molecules. 2021 Aug 27;26(17):5200.

11. Meyer JM, Swayze GA, Kokaly RF, Benzel WM, Orkild-Norton ARA, Stillings LL, et al. Mapping Lithium Bearing Hectorite in the Western United States using EMIT Data. In 2023 [cited 2025 May 12]. p. SY33C-1028. Available from: https://ui.adsabs.harvard.edu/abs/2023AGUFMSY33C1028M

12. Sweetapple MT, Tassios S. Laser-induced breakdown spectroscopy (LIBS) as a tool for in situ mapping and textural interpretation of lithium in pegmatite minerals. American Mineralogist. 2015 Oct 1;100(10):2141–51.

13. Fabre C, Ourti NE, Ballouard C, Mercadier J, Cauzid J. Handheld LIBS analysis for in situ quantification of Li and detection of the trace elements (Be, Rb and Cs). Journal of Geochemical Exploration. 2022 May 1;236:106979.

14. Fontana FF, van der Hoek B, Tassios S, Tiddy C, Stromberg J, Francis N, et al. Laser Induced Breakdown Spectroscopy (LIBS) for whole rock geochemistry. Journal of Geochemical Exploration. 2023 Mar;246:107160.

15. Brunnbauer L, Gajarska Z, Lohninger H, Limbeck A. A critical review of recent trends in sample classification using Laser-Induced Breakdown Spectroscopy (LIBS). TrAC Trends in Analytical Chemistry. 2023 Feb 1;159:116859.

16. Fontana FF, Tassios S, Stromberg J, Tiddy C, van der Hoek B, Uvarova YA. Integrated Laser-Induced Breakdown Spectroscopy (LIBS) and Multivariate Wavelet Tessellation: A New, Rapid Approach for Lithogeochemical Analysis and Interpretation. Minerals. 2021 Mar;11(3):312.

17. Dubey S, Kumar R, Rai AK, Pati JK, Kiefer J, Rai AK. Rapid Analysis of Chemical Composition and Physical Properties of Gemstones Using LIBS and Chemometric Technique. Applied Sciences. 2021 Jan;11(13):6156.

18. Farnsworth-Pinkerton S, McMillan NJ, Dutrow BL, Henry DJ. Provenance of detrital tourmalines from Proterozoic metasedimentary rocks in the Picuris Mountains, New Mexico, using Laser-Induced Breakdown Spectroscopy. Jour Geosci. 2018 Jul 18;193–8.

19. Syvilay D, Bousquet B, Chapoulie R, Orange M, Bourdonnec FXL. Advanced statistical analysis of LIBS spectra for the sourcing of obsidian samples. J Anal At Spectrom. 2019 May 8;34(5):867–73.

20. Roux CPM, Rakovský J, Musset O, Monna F, Buoncristiani JF, Pellenard P, et al. In situ Laser Induced Breakdown Spectroscopy as a tool to discriminate volcanic rocks and magmatic series, Iceland. Spectrochimica Acta Part B: Atomic Spectroscopy. 2015 Jan 1;103–104:63–9.

21. Senesi GS, Allegretta I, Marangoni BS, Ribeiro MCS, Porfido C, Terzano R, et al. Geochemical identification and classification of cherts using handheld laser induced breakdown spectroscopy (LIBS) supported by supervised machine learning algorithms. Applied Geochemistry. 2023 Apr 1;151:105625.

22. Pochon A, Desaulty AM, Bailly L. Handheld laser-induced breakdown spectroscopy (LIBS) as a fast and easy method to trace gold. J Anal At Spectrom. 2020 Feb 12;35(2):254–64.

23. Pochon A, Desaulty AM, Bailly L, Lach P. Challenging the traceability of natural gold by combining geochemical methods: French Guiana example. Applied Geochemistry. 2021 Jun 1;129:104952.

24. Wójcik M, Brinkmann P, Zdunek R, Riebe D, Beitz T, Merk S, et al. Classification of Copper Minerals by Handheld Laser-Induced Breakdown Spectroscopy and Nonnegative Tensor Factorisation. Sensors. 2020 Jan;20(18):5152.

25. Fabre C, Ourti NE, Mercadier J, Cardoso-Fernandes J, Dias F, Perrotta M, et al. Analyses of Li-Rich Minerals Using Handheld LIBS Tool. Data. 2021 Jun;6(6):68.

26. Harmon RS, Wise MA, Curry AC, Mistele JS, Mason MS, Grimac Z. Rapid Analysis of Muscovites on a Lithium Pegmatite Prospect by Handheld LIBS. Minerals. 2023 May;13(5):697.

27. The EMILI project | EMILI [Internet]. 2025 [cited 2025 Apr 18]. Available from: https://emili.imerys.com/en/emili-project

28. Ph.Rossi, A.Autran. Log pétrographique et géochimique du granite de Beauvoir dans le sondage “Echassière I” Minéralogie ete géochimie comparées. Géologie de la France. n°2-3. 1987;111–35.

29. Féraud R, Clérot F. A methodology to explain neural network classification. Neural Networks. 2002 Mar 1;15(2):237–46.

30. Artificial Neural Network Architectures and Training Processes | SpringerLink [Internet]. [cited 2025 May 12]. Available from: https://link.springer.com/chapter/10.1007/978-3-319-43162-8_2

31. Asquini CP. 19 - Laser induced breakdown spectroscopy (LIBS). In: Denker B, Shklovsky E, editors. Handbook of Solid-State Lasers [Internet]. Woodhead Publishing; 2013 [cited 2024 Aug 4]. p. 551–71. (Woodhead Publishing Series in Electronic and Optical Materials). Available from: https://www.sciencedirect.com/science/article/pii/B9780857092724500191

32. Harmon RussellS, De Lucia FC, Miziolek AW, McNesby KL, Walters RA, French PD. Laser-induced breakdown spectroscopy (LIBS) – an emerging field-portable sensor technology for real-time, ***in-situ*** geochemical and environmental analysis. GEEA. 2005 Feb;5(1):21–8.

33. Bousquet B, Sirven JB, Canioni L. Towards quantitative laser-induced breakdown spectroscopy analysis of soil samples. Spectrochimica Acta Part B: Atomic Spectroscopy. 2007 Dec 1;62(12):1582–9.

34. Cuney M, Marignac C, Weisbrod A. The Beauvoir topaz-lepidolite albite granite (Massif Central, France); the disseminated magmatic Sn-Li-Ta-Nb-Be mineralization. Economic Geology. 1992 Nov 1;87(7):1766–94.

35. G.Monnier, B.Charoy, M.Cuney, D.Ohnenstetter, J.L.Robert. Evolution spatiale et temporelle de la composition des micas du granite albitique à topaze-lépidolite de Beauvoir. Géologie de la france. n°2-3. 1987;179–88.

36. D. Ohnenstetter, P. Piantone. Caractérisation et étude des substitutions dans les minéraux du groupe des columbo-tantalites et des pyrochlores du granite de Beauvoir. 1987.

37. Mezoued N, Fabre C, Cauzid J, Kim Y, Jatteau M. Analysis of Minerals Using Handheld Laser-Induced Breakdown Spectroscopy Technology. Data. 2025 Mar;10(3):40.

38. Johnstone IM, Titterington DM. Statistical challenges of high-dimensional data. Philosophical Transactions of the Royal Society A: Mathematical, Physical and Engineering Sciences. 2009 Nov 13;367(1906):4237–53.

39. Ray P, Reddy SS, Banerjee T. Various dimension reduction techniques for high dimensional data analysis: a review. Artif Intell Rev. 2021 Jun 1;54(5):3473–515.

Discussion
Conclusion and perspectives

General discussion

The versatility of handheld LIBS, from its multi-scale analytical capabilities to the wide range of information it generates, confirms the advantages of the technique in the mining sector to provide onsite geochemical data throughout the different stages of a mining project.

In the context of quantitative analysis, using unprocessed rock as target samples was guided by the need to align with field conditions and the operational constraints of exploration campaigns. While powdered pellets are typically used in handheld LIBS rock analysis, results from unprocessed samples have shown prediction accuracies within acceptable error margins, comparable to those of homogenized powders. Therefore the choice of sample type and analytical protocol, specifically in field operations when time and infrastructure limit the ability to prepare samples extensively, should prioritize the specific analytical needs and acceptable error margin, rather than default protocols.

The high sensitivity of LIBS technique to chemical and physical matrix effects often implies the development of customized calibration models for each deposit. Although some LIBS-based quantification models are available in the analyzer software, specifically for lithium, they present some challenges for broader applications: (i) lack of diversity, typically designed for a single deposit type (ii) lack of transparency regarding acquisition parameters and preprocessing steps, both crucial factors affecting predictive accuracy on new data, and (iii) tend to be highly misleading when applied to different matrix types. Despite significant demand, current industrial solutions only partially satisfy the demand for standard quantitative assessments. This raised an important question during the Beauvoir granite study: to what extent can the developed calibration models be transferred to other, geologically similar deposits? When tested on granite samples from different locations, the models produced acceptable prediction errors when the test samples exhibited comparable textural characteristics to the reference samples, highlighting the crucial influence of physical properties in determining the accuracy and reliability of LIBS model across deposits. In fact, the distribution of prediction errors within and outside the Beauvoir deposit, revealed the critical importance of textural consistency, such as grain size and degree of alteration, for achieving reliable model performance. Consequently, incorporating textural characteristics as variables in the multivariate models developed could substantially enhance model robustness, whether the objective is to account for lithological variability when generalizing a model across a deposit or to extend its application to different geological settings.

For automated mineral recognition machine learning models demonstrated excellent performance in classifying pure mineral data. This indicates that LIBS data effectively captures the distinct spectral signatures of mineral phases, even when relying on a limited subset of spectral variables, corresponding to major and minor emission lines. The models successfully differentiate chemically similar minerals, such as muscovite and lepidolite or albite and orthoclase. However, when applied to granite samples, the classification models showed mixed performance, with absolute prediction errors in mineral proportions ranging from moderate to high values. Several areas for improvement were identified to enhance mineral identification in complex geological systems. While training models on pure mineral spectra proves effective for pattern recognition, the chemical variability observed across different deposits underscores the need for deposit-specific training datasets to ensure representative and reliable classification. Furthermore, classification performance was found to depend significantly on rock texture. Coarse-grained rocks, such as pegmatites, consistently yielded better results than fine-grained rocks, highlighting grain size as a key factor influencing prediction accuracy. Therefore, developing tailored acquisition protocols that account for the textural characteristics of the target rocks is essential for improving the robustness and accuracy of LIBS-based mineral classification models.

Finally, field campaigns have provided valuable insights about the application of LIBS analyzers under various environmental conditions. Data acquisition missions at the logging department of the Beauvoir granite (Echassière, France), along with field campaigns in Spain (NEXT project) and Greece (Artemis Project) for pure mineral spectra, revealed several key considerations when using the handheld LIBS outside laboratory settings:

The performance of LIBS instruments is affected by external temperatures. At high temperatures, above 35°C, argon consumption increases notably and regular breaks are required to allow the system to cool to acceptable operating temperatures (< 42°). Whereas at temperatures below 0°C, the laser must be maintained in a warmer environment to ensure proper functioning.

Although LIBS is inherently a very fast analytical method, analyzing large volumes of rock samples can significantly extend overall analysis time. For instance, acquiring a representative signal in a 4m drill core section for quantitative analysis require at least 40 minutes, while obtaining map data for mineral identification may take around 20 minutes. Therefore, acquisition time for LIBS data must be carefully considered to ensure operational efficiency in large-scale exploration campaigns.

During active drilling operations, the volume of rock extracted can be substantial, and acquiring systematic LIBS analysis would require extensive resources in terms of time and operators. thus, implementing a benchmark LIBS would optimize time and resource allocation by enabling automatic analysis acquisition. Additionally, the analysis timeline should be carefully structured to occur either before or after the visual logging of core samples. Since core samples are often soaked before visual description to ensure proper examination, a hydrated surface alters LIBS signal acquisition. Therefore, understanding how to effectively and practically integrate handheld LIBS analysis in large-scale mining operations is crucial for standardizing procedures, ensuring best practices, and achieving reliable results.

Conclusion and perspectives

1 Conclusion

This thesis explores the input of handheld LIBS for providing on-site geochemical information to enhance mining operations. Handheld LIBS analyses were used to address two major challenges encountered during exploration campaigns: i) access to on-site and reliable quantitative analysis on unprepared rock samples, and ii) an alternative solution for mineral identification, especially when minerals present similar macroscopic features. Although this thesis primarily focused on addressing these challenges in the context of the Beauvoir granite exploration project, the methodologies developed can be adapted to other geological deposits. The protocols were designed to align with the operational constraints of field operations: i) minimal sample preparation, and ii) balancing between result quality, optimized acquisition time, and resources management.

Conventionally, access to quantitative data can take up to six months from drillcore extraction to laboratory results. Such delays can significantly impact the planning of drilling campaigns, which often require adaptive strategies based on the evolving understanding of ore distribution. To address this limitation, calibration models for lithium and rubidium were developed using reference samples from the Beauvoir granite. Particular attention was given to the use of unprocessed drill core portions to align with the operational conditions during explorative drilling campaigns. Optimization efforts significantly reduced acquisition time, allowing access to quantitative values within 1h for a 4m drill core section. Although the error margins were higher than those associated with laboratory techniques, the predicted values remained within the expected error ranges for LIBS quantitative models and acceptable thresholds for guiding decision-making processes. Furthermore, the potential to generalize pre-established models to different deposits of a similar type was explored. The sensitivity of the LIBS technique to matrix effects often necessitates the development of individual models for each deposit, which

is commonly viewed as a limitation of the broader application of handheld LIBS in the mining industry. To address this, the quantitative models developed for the Beauvoir granite were tested on rare-metal granite samples sourced from different geographical areas. The prediction errors obtained were consistent with those observed for the Beauvoir granite samples, confirming the potential for transferring pre-established handheld LIBS models to similar geological contexts. However, in both settings, the results emphasized the importance of ensuring the textural consistency of the analyzed samples to guarantee accurate and reliable predictions.

Mineral identification during field operations is commonly conducted through visual observations. However, this method can be challenging when minerals display similar macroscopic features. To address this, machine learning algorithms were applied to process LIBS data to automate mineral identification in granite samples. A database of 12,000 reference spectra of different minerals, including silicates, phosphates, oxides, and carbonates, was built to provide reference input data for training the machine learning models to classify unlabeled LIBS spectra in different mineral classes. To account for the inherent variability of geological materials, reference spectra were acquired from multiple samples, ensuring that the geochemical diversity observed in nature was adequately represented. Machine learning models of varying computational complexity (i.e., LDA, PLS-DA, Random Forest, ANN, SVM) were trained using the reference mineral database to classify LIBS spectra acquired on the Beauvoir granite samples into distinct mineral classes. Combining the LIBS high-dimensional spectral data with the pattern recognition capabilities of classification algorithms allows to translate LIBS elemental signals into mineralogical information, including identifying the mineral composition of a given sample and determining the relative abundance of different mineral phases. The results demonstrated excellent performance in classifying pure mineral data, however, variable outcomes were observed when applied to rock samples from the Beauvoir granite. Overall, model performance on rock samples could be significantly improved by optimizing three key factors: adopting tailored data acquisition strategies aligned with sample properties, using deposit-specific reference datasets, and accounting for the textural characteristics of the rocks.

Handheld LIBS ability to acquire geochemical data on-site and in near real-time offers geologists new perspective in field invetsigation. However, several operational and methodological challenges must still be addressed to enable the broader and more systematic implementation of this approach within large-scale exploration workflows. In terms of acquisition times, the large volume and scale of rock samples involved make data collection significantly time-consuming. Furthermore, the error margins of handheld LIBS predictions are larger than those of laboratory-based techniques and are significantly influenced by the

physical properties of the analyzed samples, both for quantitative and mineralogical analysis. This emphasizes the need to interpret LIBS results in conjunction with geological knowledge of the deposit. Therefore, it is essential to recognize that, at present, portable analytical techniques, although extremely valuable, serve as complementary tools for onsite preliminary analysis, rather than as substitutes for traditional laboratory methods.

2 Perspectives

Using the analytical protocols developed during this work, implies multiple steps across independent software, each requiring specialized knowledge. Developing a user-friendly interface that simplifies data extraction and organization, modelization, and results visualization, complemented by preliminary interpretations, would facilitate the practical implementation of both quantitative and automated mineral identification models within mining operations workflows, without extensive operator training.

The application of handheld LIBS for automated mineral identification has the potential to significantly enhance geochemical exploration, particularly in early stages when the focus is on detecting pathfinder towards mineralization by i) determining the mineralogical composition of the host rock at multiple locations to identify potential proxy mineral phases towards mineralization. The classified LIBS spectra can also be processed using qualitative or quantitative values to trace the spatial distribution of key elements in different minerals. This can be particularly valuable when targeting accessory and minor mineral phases, as whole-rock analyses can potentially dilute the compositional variations, concealing meaningful information. Such information can play a critical role in guiding sampling strategies by prioritizing high-potential areas and efforts to be focused on well-supported geological leads.

Additionally, as it has been demonstrated that the high dimensionality of LIBS data can effectively capture the complexity of geological materials, it would be interesting to explore its potential contribution to raw materials traceability. The question of regulated sourcing is strategic in the commodity market, as the uneven global distribution of critical resources can lead to supply chain vulnerabilities, and in some cases, contribute to regional conflicts and instability. In response, international organizations work to establish regulatory policies, such as the EU Conflict Minerals Regulation, to promote transparency and ethical sourcing practices. In this context, handheld LIBS emerges as a particularly effective tool to support the implementation of such policies. Its ability to capture the chemical complexity of geological materials makes it well-suited for distinguishing ore sources based on their unique spectral signatures, both at the deposit and processing levels.

References

1. Fabre C, Ourti NE, Ballouard C, Mercadier J, Cauzid J. Handheld LIBS analysis for in situ quantification of Li and detection of the trace elements (Be, Rb and Cs). Journal of Geochemical Exploration. 2022 May 1;236:106979.

2. Harmon RS, Wise MA, Curry AC, Mistele JS, Mason MS, Grimac Z. Rapid Analysis of Muscovites on a Lithium Pegmatite Prospect by Handheld LIBS. Minerals. 2023 May;13(5):697.

3. Fontana FF, Tassios S, Stromberg J, Tiddy C, van der Hoek B, Uvarova YA. Integrated Laser-Induced Breakdown Spectroscopy (LIBS) and Multivariate Wavelet Tessellation: A New, Rapid Approach for Lithogeochemical Analysis and Interpretation. Minerals. 2021 Mar;11(3):312.

4. Foucaud Y, Fabre C, Demeusy B, Filippova IV, Filippov LO. Optimisation of fast quantification of fluorine content using handheld laser induced breakdown spectroscopy. Spectrochimica Acta Part B: Atomic Spectroscopy. 2019 Aug 1;158:105628.

5. Korbel C, Mezoued N, Demeusy B, Fabre C, Cauzid J, Filippova IV, et al. Quantification of lithium using handheld instruments: application of LIBS and XRF spectroscopy to assay the lithium content of mineral processing products. J Anal At Spectrom. 2024 Jul 3;39(7):1838–53.

6. Wise MA, Harmon RS, Curry A, Jennings M, Grimac Z, Khashchevskaya D. Handheld LIBS for Li Exploration: An Example from the Carolina Tin-Spodumene Belt, USA. Minerals. 2022 Jan;12(1):77.

7. Chen M, Yuan T, Hou Z, Wang Z, Wang Y. Effects of moisture content on coal analysis using laser-induced breakdown spectroscopy. Spectrochimica Acta Part B: Atomic Spectroscopy. 2015 Oct 1;112:23–33.

List of figures

Introduction

4 Figure 1. Organization of the Ph.D. thesis.

Chapter I **The LIBS technique**

9 Figure 1. Handheld libs analyzers: from early commercialized models (LIBSCAN 25+ and StellarCASE-LIBS) to recent designs (Z-300 and Z900).

15 Figure 2. Handheld libs in geological applications for quantitative analysis: a) distribution of target elements, b) sample types, and c) development contexts.

Chapter II **Case study : The Beauvoir granite**

22 Figure 1. The western european variscan belt including variscan granitoids, LCT pegmatites, rare-metal granites and rhyolites outcrops (from Rocher et al. (2024) modified from Ballouard et al. (2024)).

24 Figure 2. a.Satellite view of the Echassières mining site, highlighting the visible open-pit kaolin mine. (b) 3D representation of the Beauvoir granite magmatic body. (c) Schematic illustration of the underground mine (B1) and associated infrastructure planned for lithium extraction. Modified from Imerys documentation.

27 Figure 3. Logging data analysis: (a) Distribution of soft and hard rock facies; (b) Repartition of observed lithological facies, with facies abbreviations following Imerys nomenclature; (c, d) Vertical distribution of altered zones (kaolin and greisen); (e) Vertical distribution of soft rock (highly altered material); (f) Proportion of fresh, moderately altered, and highly altered boreholes based on logging descriptions, categorized by the percentage of altered intervals within each borehole (<25%, 25–50%, and >50%).

28 Figure 4. Vertical evolution of major elements (Al, Si, K, Na, and Li) composing the primary mineral matrix in the Beauvoir granite. The graph shows the variation in their concentrations as a function of depth, reflecting changes in lithology and alteration state

.

Chapter III Handheld LIBS contribution to quantify critical elements during mining operations: the Beauvoir granite case study

38 Figure 1. The analytical protocol followed to build and test the LIBS quantification models for Li and Rb on the Beauvoir granite samples.

39 Figure 2. An example of handheld LIBS spectra (190-950nm) for low and high-concentration samples from the Beauvoir granite deposit.

41 Figure 3. Visual representation illustrating the results obtained while comparing the different LIBS quantification models built for Li using a two-step statistical procedure based on (a) Bias and (b) Standard Error of Prediction (SEP).

43 Figure 4. Visual representation illustrating the results obtained while comparing the different LIBS quantification models built for Rb using a two-step statistical procedure based on (a) Bias and (b) Standard Error of Prediction (SEP).

44 Figure 5. A radar chart displaying the results of Bias, SEP, and MAE obtained on the test dataset to compare the different Li quantification models built and select the optimal solution for the Beauvoir granite deposit. (1) Raw spectra, (2) SNV normalized spectra, (3) Total spectrum normalized spectra.

45 Figure 6. A radar chart displaying the results of Bias, SEP, and MAE obtained on the test dataset to compare the different Rb quantification models built and select the optimal solution for the Beauvoir granite deposit. (1) Raw spectra, (2) SNV normalized spectra, (3) Total spectrum normalized spectra.

46 Figure 7. The mean absolute error (MAE) of predictions calculated under different conditions. (a) varying the proportion of LIBS data used to obtain the average signal per sample. (b)

modifying acquisition parameters: 1- Initial parameters, 2- Reducing the number of shots per point, 3- Reducing the total surface area of analysis point. Lithium (Grey), and rubidium (Black).

47 Figure 8. Handheld LIBS quantification model selected to quantify Li in the Beauvoir granite drill core sections.

48 Figure 9. Photographs of reference samples used for LIBS quantification models: typical unaltered B1 facies (C30, C42), and presenting textural anomalies (C39).

Chapter IV **Quantitative Analysis Using Handheld LIBS: Assessing Model Transferability Across Similar Deposits.**

62 Figure 1. Photographies illustrating the textural features of the granite samples used in this study. Upper panels: Blond granite samples, including microgranular facies (indicated by a star) and predominant very fine-grained rhyolitic textures. Lower panels: Beauvoir granite samples used to develop the lithium calibration model.

64 Figure 2. a) Schematic geological map of the northern French Massif Central (FMC), highlighting the locations of major rare-metal granites, including the Beauvoir granite (Modified from Harlaux et al.2017) (B) in the east and the Blond granite (R) in the west.

b) Simplified geological map of the Blond granite (Modified from Alexandrov et al. 2000).

66 Figure 3. Average LIBS signal for two primary lithium emission lines at 610 and 670 nm for the Richemont dyke sample (green) and Beauvoir granite sample (red), both with comparable lithium concentrations (2781 ppm - 2775 ppm)

68 Figure 4. Comparative analysis of lithium LIBS signal intensities at 610 nm and 670 nm for samples from the Richemont Dyke (a. CB120, c. CB95, e. M13) and Beauvoir Granite Deposit (b. C73 d. C123, f. SK_S18_74)

69 Figure 5. Comparative LIBS analysis of lithium signals at 610 nm and 670 nm for samples with comparable lithium concentrations (ppm). Groups with similar lithium content are marked by the same geometric symbol.

71 Figure 6. Lithium predictions in Richemont dyke samples using the Beauvoir granite quantitative model: a) Linear regression of the reference geochemical values and the predicted values, and b) Distribution of the absolute error based on the textural characteristics of the analyzed samples. The color gradient represents the magnitude of the absolute error for each sample, from highest (red) to lowest (blue).

72 Figure 7. Evolution of the absolute prediction error for rhyolite samples from the Blond Massif using LIBS analysis. Results are shown for both the initial acquisition parameters (4 laser shots per zone) and the optimized parameters (1 laser shot per zone).

Chapter V **Spectral Analysis of Minerals with Handheld Laser-Induced Breakdown Spectroscopy Technology**

83 Figure 1. Mineral LIBS spectra: (a) baseline variation based on mineral composition, showing a higher-density plasma for pyrite due to metallic elements presence, compared to a flat baseline for Li-rich micas; (b) signal intensity variation for quartz analyzed as powder samples exhibiting stronger signals compared to crystal phases.

33 Figure 2. Variation in the LIBS signal intensity for different elements: (a) Li, an element with low ionization energy, is a major component of spodumene; (b) Si, an element with moderate ionization energy, is a primary constituent of topaz; and (c) S, an element with high ionization energy, is a key component of chalcopyrite.

Chapter VI **Automated mineral recognition combining handheld LIBS spectra and machine learning: assessing ore mineral abundance in the Beauvoir granite.**

93 Figure 1. Schematic representation of handheld LIBS data acquisition on Beauvoir granite samples: a) Granite slab with 10 organized LIBS analysis zones arranged vertically from top to bottom of the sample; b) Zoomed-in view of a single analysis zone, representing 90 analysis points organized in a grid; c) Illustration of the LIBS spectrum obtained at each analysis point (900 spectra per sample).

99 Figure 2. Workflow for implementing machine learning models for automated mineral recognition using libs data : (a) phase 1: model training and testing, (b) phase 2: application to the case study.

102 Figure 3. Multivariate Analysis of Reference Mineral Data—(a, b) PCA Score and Loading Plots for Raw (Top) and SNV-Normalized (Bottom) Data; (c) PLS Score Plots for Raw (Left) and SNV-Normalized (Right) Data.

103 Figure 4. Comparison of LDA, SVM, Random Forest, and PLS-DA Model Performance for multi-class classification.

104 Figure 5. Comparison of LDA, SVM, Random Forest, and PLS-DA Model Performance for multi-class classification.

106 Figure 6. Distribution of Prediction Errors for Lepidolite Class**:** a) Comparative analysis of the absolute prediction errors obtained by each model for each Beauvoir granite sample. b) Comparison of the mean absolute prediction error averaged across Beauvoir granite samples.

107 Figure 7. Comparative analysis of mineral abundance predictions and reference values for the Beauvoir granite samples.

108 Figure 8. prediction error distribution across mineral classes and machine learning models: (a-d) error distribution per mineral class, (e) mean absolute error averaged across beauvoir granite samples.

110 Figure 9. LIBS data distribution for pure minerals and beauvoir granite samples: color-coded signal intensity diagram for Si and Li.

111 Figure 10. Petrographical images of an altered granite sample (top, C117) and a relatively fresh granite sample (bottom, C42), a) the distribution of absolute prediction error for the lepidolite class, and b) the mean absolute prediction error for multi-class classification across granite samples, both color-coded according to the degree of alteration.

Chapter VII **Artificial neural network for handheld LIBS data processing: application to automated mineral identification in granite samples**

131 Figure 1. Summary of the 12 ANN models developed for handheld libs data classification.

133 Figure 2. Distribution of the absolute prediction errors obtained from the classification results of lepidolite (a) and multi-class proportion predictions (b) using ann models. The models parameters and configurations are detailed in Figure 1.

134 Figure 3. a) Distribution of the absolute prediction error across different input datasets tested. b) Distribution of the absolute prediction error for different learning rates (0.001, 0.01, and 0.1).

135 Figure 4. Results of ANN Model 1 for the Beauvoir samples. a) AEP for lepidolite classification. (b) AEP for multi-class classification. c) Error distribution for each mineral class, categorized by sample, demonstrating the variation in prediction accuracy for different mineral classes.

136 Figure 5. a) Prediction error for lepidolite classification using ANN Model 2. b) Comparative analysis of the absolute error of prediction (AEP) between visual identification and the LIBS-ANN-based approach for automated mineral recognition.

List of tables

Chapter I **The Handheld LIBS technique**

8 Table 1. Summary of the Design Characteristics, Analytical Capabilities, and elemental detection of Handheld LIBS analyzers currently available (2024).

Chapter III **Handheld LIBS contribution to quantify critical elements during mining operations: the Beauvoir granite case study**

40 Table 1. The Li and Rb emission lines observed in the LIBS spectra, including their specific locations, the spectral ranges determined for signal extraction and the Pearson coefficient calculated using the reference geochemical data.

40 Table 2. The calculated values of Mean Absolute Error (MAE), Root Mean Squared Error (RMSE), and R-squared (R^2) to assess the predictive power of the different LIBS quantification models developed for Li and Rb.

45 Table 3. The results of the Student test comparing the Mean Absolute Errors (MAE) of prediction for successive LIBS measurements on reference granite samples to assess reproducibility.

Chapter IV **Quantitative Analysis Using Handheld LIBS: Assessing Model Transferability Across Similar Deposits.**

66 Table 1. The geographic location and textural, petrographic, and geochemical characteristics of the analyzed samples from the Richemont dyke.

Chapter V **Spectral Analysis of Minerals with Handheld Laser-Induced Breakdown Spectroscopy Technology**

80 Table 1. Summary of the mineral samples analyzed: the mineral species, chemical formulas, number of samples analyzed, and total spectra acquired. Detailed metadata are available in the database.

Chapter VI **Automated mineral recognition combining handheld LIBS spectra and machine learning: assessing ore mineral abundance in the Beauvoir granite.**

94 Table 1. Summary of the reference mineral LIBS spectra selected to mimic the Beauvoir granite mineral composition for training machine learning models: mineral species, chemical formulas, number of samples analyzed, and total spectra acquired.

96 Table 2. Emission line positions and spectral ranges for libs signal extraction of major, minor, and trace elements in targeted minerals (albite, orthose, quartz, topaz, phosphates, lepidolite, and muscovite).

98 Table 3. Comparative Analysis of Machine Learning Models for LIBS data classification: SVM, Random Forest, LDA, and PLS-DA through Mathematical features, Computational Complexity, Hyperparameters, and Limitations.

105 Table 4. Reference values of mineral abundances in beauvoir granite samples.

List of appendix

51 Appendix.1 **Handheld LIBS contribution to quantify critical elements during mining operations: the Beauvoir granite case study**

77 Appendix.2 **Quantitative Analysis Using Handheld LIBS: Assessing Model Transferability Across Similar Deposits.**

120 Appendix.3 **Automated mineral recognition combining handheld LIBS spectra and machine learning: assessing ore mineral abundance in the Beauvoir granite.**